University of Kentucky Doctoral Dissertations   Graduate School

2010

EXPLORATIONS IN HOMEOVISCOUS ADAPTATION AND MASS SPECTRAL ANALYSIS OF MEMBRANE LIPIDS

Michael Douglas Timmons
University of Kentucky, michael.timmons@uky.edu

Right click to open a feedback form in a new tab to let us know how this document benefits you.

ABSTRACT OF DISSERTATION

MICHAEL DOUGLAS TIMMONS

The Graduate School
University of Kentucky
2010

EXPLORATIONS IN HOMEOVISCOUS ADAPTATION AND MASS SPECTRAL ANALYSIS OF MEMBRANE LIPIDS

ABSTRACT OF DISSERTATION

A dissertation submitted in partial fulfillment of the
requirements for the degree of Doctor of Philosophy in the
College of Arts and Sciences
at the University of Kentucky

By
Michael Douglas Timmons

Lexington, KY

Director: Dr. Bert C. Lynn, Professor of Chemistry

Lexington, KY

2010

ABSTRACT OF DISSERTATION

EXPLORATIONS IN HOMEOVISCOUS ADAPTATION AND MASS SPECTRAL
ANALYSIS OF MEMBRANE LIPIDS

The focus of this dissertation is centered on the mass spectral analysis of lipids and changes occurring in keeping with the concept of homeoviscous adaptation [1]. Homeoviscous adaptation is the process of modification of membrane lipids in response to environmental stimuli [1]. Dissertation investigations applied this concept to prokaryotic and eukaryotic organisms, and expanded the perception of environmental factors from exogenous organic solvents to intracellular environment.

The field of lipidomics deals with the analysis of phospholipid and fatty acid components of membranes the changes that occur due to environmental stimuli and their biological significance [2-6]. The high sensitivity of mass spectrometry (MS) is an ideal tool for lipidomics allowing detection, quantification and structural elucidation [6]. Coupling of a mass spectrometer to a chromatographic system, such as gas chromatograph (GC), allows the separation of fatty acid methyl esters analytes prior to analysis [7].

The research investigations that comprise this dissertation are divided into three interrelated projects. The first project involved the analysis of composition and structure of *Clostridium thermocellum* membranes from wild-type and ethanol-adapted strains in response to adaptation of cultures to growth in ethanol. The hypothesis being that adaptation of cultures to growth in ethanol would result in compensatory change to the membrane composition.

Rat mitochondrial fatty acid profiles isolated from brain, liver, kidney and heart tissues were compared. The hypothesis being that differences in cellular environments found among various tissues would be reflected in the mitochondrial membrane composition. These data support the concept that variations to the lipid content of neurological mitochondria may increase susceptibility to the products of oxidative stress.

Lastly, changes in neurological mitochondria as a function of Alzheimer's disease progression were studied. The hypothesis being that changes to the mitochondrial lipidome would be significantly reflected during advanced stages of AD, in addition to being more prevalent in regions displaying greater pathology.

The three interrelated projects increased our understanding of the boundaries established by the concept of homeoviscous adaptation. Project specific hypotheses were supported by data obtained from these investigations.

Michael Douglas Timmons

2010

EXPLORATIONS IN HOMEOVISCOUS ADAPTATION AND MASS SPECTRAL
ANALYSIS OF MEMBRANE LIPIDS

By

Michael Douglas Timmons

Dr. Bert C. Lynn
_____
Director of Dissertation

Dr. Mark Meier
_____
Director of Graduate Studies

_____
Date

RULES FOR THE USE OF DISSERTATIONS

Unpublished dissertations submitted for the Doctor's degree and deposited in the University of Kentucky Library are as a rule open for inspection, but are to be used only with due regard to the rights of the authors. Bibliographical references may be noted, but quotations or summaries of parts may be published only with the permission of the author, and with the usual scholarly acknowledgments.

Extensive copying or publication of the dissertation in whole or in part also requires the consent of the Dean of the Graduate School of the University of Kentucky.

A library that borrows this dissertation for use by its patrons is expected to secure the signature of each user.

<u>Name</u>   <u>Date</u>

_____

_____

_____

_____

_____

_____

DISSERTATION

MICHAEL DOUGLAS TIMMONS

The Graduate School

University of Kentucky

2010

EXPLORATIONS IN HOMEOVISCOUS ADAPTATION AND MASS SPECTRAL
ANALYSIS OF MEMBRANE LIPIDS

DISSERTATION

A dissertation submitted in partial fulfillment of the
requirements for the degree of Doctor of Philosophy in the
College of Arts and Sciences
at the University of Kentucky

By
Michael Douglas Timmons

Lexington, KY

Director: Dr. Bert C. Lynn, Professor of Chemistry

Lexington, KY

2010

Dedicated to

my wife and family whose support and encouragement guided me through the dark times

Acknowledgements

TABLE OF CONTENTS

LIST OF TABLES

LIST OF FIGURES

LIST OF ABBREVIATIONS AND SYMBOLS

ACP	Acyl carrier protein
AD	Alzheimer's disease
aka	Also known as
α-Syn	Alpha-synuclein
amu	Atomic mass unit
AOCS	American Oil Chemists' Society
APP	Amyloid precursor protein
ATCC	American Type Culture Collection
ATP	Adenosine triphosphate
Aβ	Amyloid beta peptide
CACI	Covalent-adduct chemical ionization
CER	Cerebellum
CI	Chemical ionization
CID	Collision-induced dissociation
CoA	Coenzyme A
CSF	Cerebrospinal fluid
DC	Disease control
DCW	Dry cell weight
DHAP	Dihydroxyacetone phosphate
DLB	Dementia with Lewy body
DPH	1,6-Diphenyl-1,3,5-hexatriene
EA	Ethanol-adapted
EI	Electron-impact ionization
ESI	Electrospray ionization
ETC	Electron transport chain
FAMEs	Fatty acid methyl esters
FAs	Fatty acids
FTD	Frontotemporal dementia
hr/hrs	Hour/hours
IB	Isolation buffer
IPL	Inferior parietal lobule
IUPAC	International Union of Pure and Applied Chemistry
LAD	Late-stage Alzheimer's disease
LC	Liquid chromatography
LMCO	Low-mass cut-off
LMCO	Low-mass cut-off
M	Molecular ion
m/z	Mass-to-charge
$M^{+\cdot}$	Molecular radical cation
MCI	Mild cognitive impairment
MHz	Megahertz
MMSE	Mini-mental state examination
MS/MS	Tandem mass spectrometry
mTorr	milliTorr

MUFAs	Monounsaturated fatty acids
N	Number of theoretical plates
NADPH	Nicotinamide adenine dinucleotide phosphate
NC	Age-matched normal control
NFT	Neurofibrillary tangles
P	Plasmalogen
PBS	Phosphate Buffered saline
PCAD	Preclinical Alzheimer's disease
PHG	Polar head group
PMI	Post-mortem interval
PUFAs	Polyunsaturated fatty acids
QIT	Quadrupole ion trap
r	Anisotropy
R	Resolution
rf	Radio frequency
ROS	Reactive oxygen species
SECI	Selected-ejection chemical ionization
SMTG	Superior and middle temporal gyri
sn	Stereospecific numbering
SP	Senile plaques
T_d	Temperature down
T_m	Transition temperature
t_r	Retention time
TTBS	Tween-20/tris-buffered saline
T_{up}	Temperature up
$\bar{u}$	Average linear velocity
u.i.	Unsaturation index
UK-ADC	University of Kentucky Alzheimer's disease center
$\bar{u}_{opt}$	Optimal average linear velocity
V_{0-p}	Voltage (zero-to-peak)
W_h	Peak width at half-height
WT	Wild-type
yrs	Years

LIST OF FILES

MDTimmonsDissertation.pdf

PART I. LIPIDOMICS AND MASS SPECTROMETRY

Chapter 1.1. Background

The analysis of lipids and lipid derivatives has been firmly established in the literature since Folch et al. developed a procedure to extract lipids from animal tissue. From these early days, the evolution of lipid analysis has kept pace with improvements in instrumentation [8-10]. Mass spectrometry (MS) is an ideal tool for lipid analysis allowing quantification and structural identification of components. For studies based on the analysis of biological samples, where analytes might be at µg or ng/µL concentrations, mass spectrometry permits small-volume sample injections and low limits of detection [6]. Mass spectrometry coupled to a separation technique, such as gas chromatography (GC), facilitates the separation of isomers and relative quantitation can be achieved by area count comparisons with an internal standard.

Not being immune from the -omics revolution, the traditional discipline of lipid analysis has evolved into lipidomics. With previously established -omics based disciplines for the study of proteins, nucleic acids and metabolites, lipidomics was a natural scientific step in high-throughput analysis [4-5, 11-13]. The field of lipidomics originated as an area of study centered on the characterization of lipid molecular species and their roles with regard to cellular processes [4-5]. Lipids are linked to numerous cellular pathways by functioning mutually as end-products of metabolism and as substrates for the generation of signaling molecules [4-5, 11-13]. Each of the studies included in this dissertation will be focused on the investigation of derivatizied lipid acyl chains followed by analysis using GC/MS.

Chapter 1.2. Introduction

Lipids

Glycerophospholipids or phospholipids are classified as complex lipids, meaning they can be divided into simpler components through hydrolysis.   The glycerophospholipid units can be divided into two general regions: (1) a polar head group (PHG), typically a derivatized phosphoric acid group, and (2) a hydrophobic portion consisting of long-chain fatty acids esterified to a glycerol backbone (Figure 1.1) [14].

Aggregates of phospholipid monomers associate together through non-covalent interactions to form membrane layers. Due to the nature of the two hydrophobic tails phospholipids interact in order to maximize van der Waals forces between acyl chains. The result is a lipid bilayer formed from the hydrophobic interaction of the acyl chains on opposing phospholipid monomers (Figure 1.2). The associated hydrophilic polar head groups end-capping the chains with the inner leaflet PHG interacting with the cytosol and the outer leaflet PHG exposed to the extracellular matrix [14]. Biological membranes have various proteins and carbohydrates associated with the membrane integrated among the glycerophospholipid units.

The phosphoric acid group is generally modified by a head group bonded through a phosphoester to the phosphate group. The modifying substituent provides the polar head group with unique functionally allowing recognition by signaling molecules (Figure 1.3). The chemical structure of the various head groups range from amine, sugar, amino acid, glycerol, hydroxyl or an additional glycerophospholipid as in the case of cardiolipin [14].

Biological membranes in their native form have two fatty acid chains esterified to the glycerol backbone of each glycerophospholipid moiety. The acyl chains are generally attached to the glycerol backbone on carbons 1 & 2, also known as stereospecific numbering (sn). For the most part acyl chains are attached to the glycerol backbone by an ester linkage (Figure 1.4a). Chains that are attached in this manner are known as fatty acids (FAs), in reference to their carboxylic acid functionality. Replacement of the ester bond with an α,β-unsaturated ether, or vinyl ether linkage results in a lipid species known as plasmalogens (P) (Figure 1.4b) [14-16].
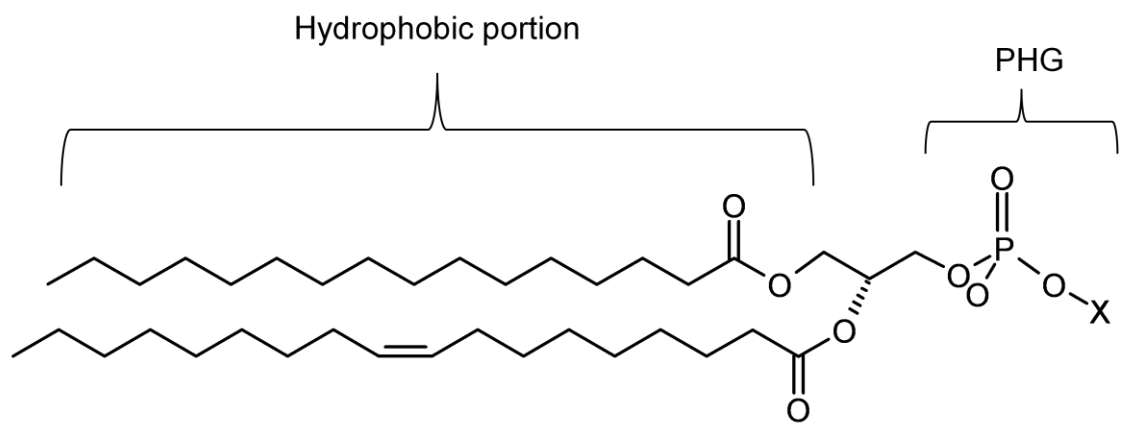
Figure 1.1. Phospholipid structure.
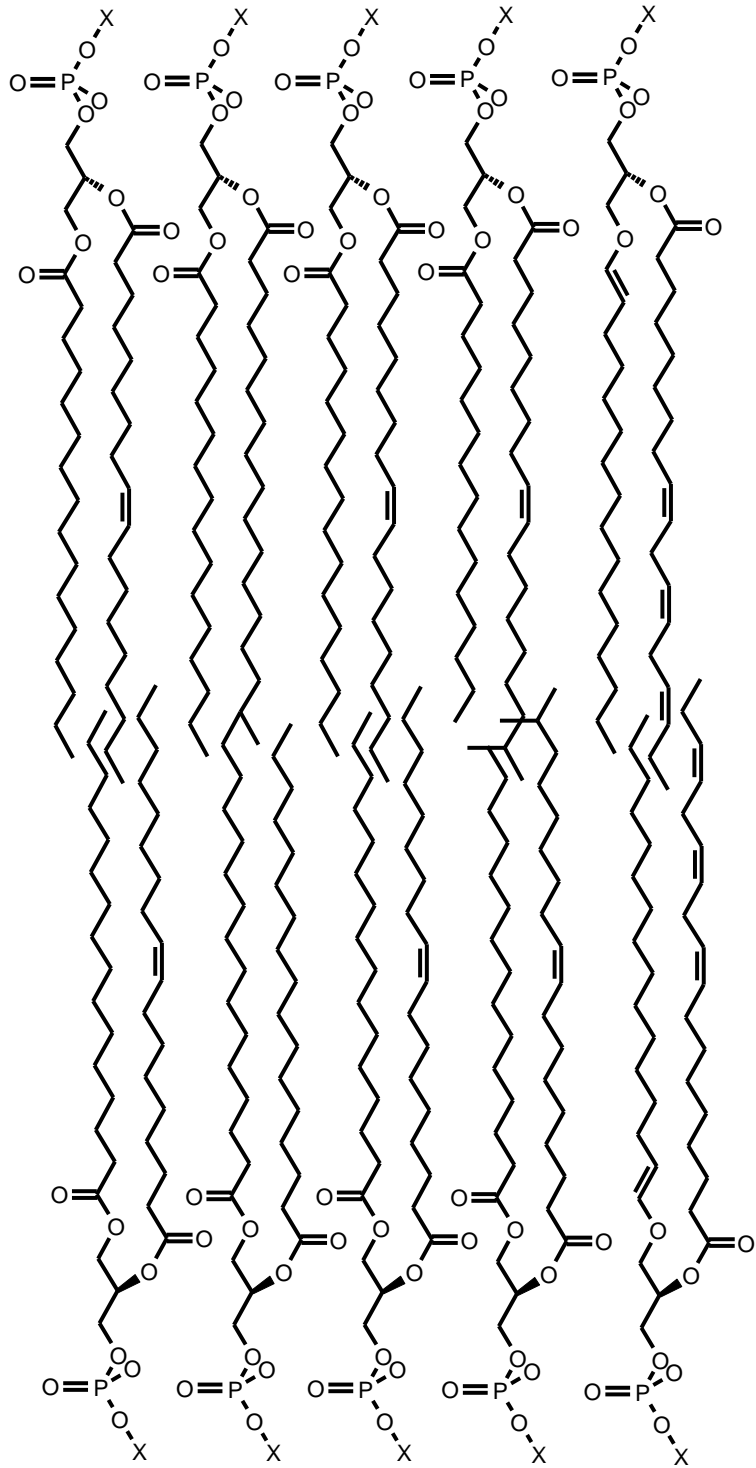
Figure 1.2. Phospholipid bilayer.
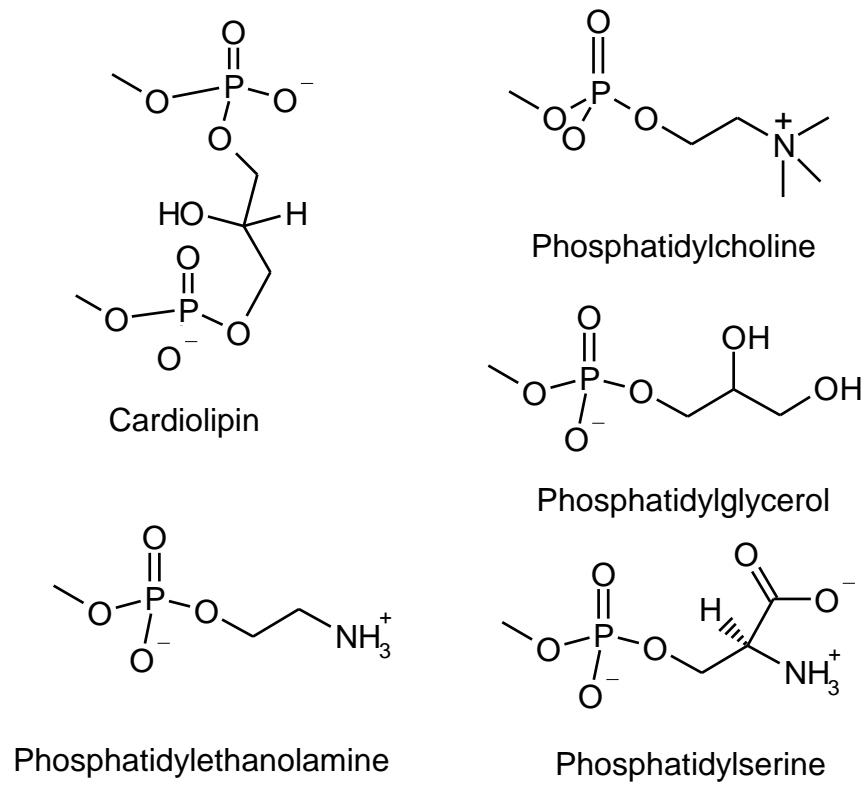
Figure 1.3. Phospholipid polar head groups.

a

R₁ structure (diester phospholipid)

b

R₁ structure (plasmalogen phospholipid)
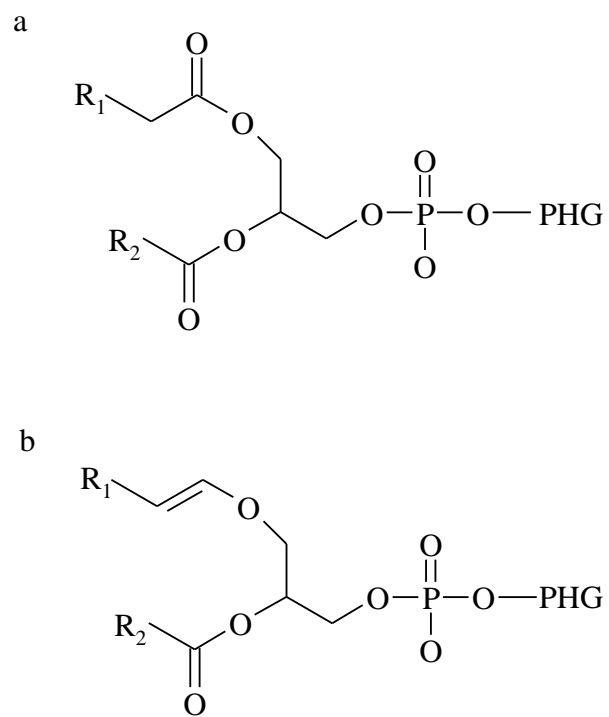
Figure 1.4. Diester (a) and plasmalogen (b) phospholipids.

Since the projects contained herein were focused on analysis of FAs and plasmalogen chain species obtained from phospholipids, the discussion of lipid synthesis and analysis will be targeted to these species.

It is important to cover a brief background on the synthesis of fatty acids and plasmalogens species. The multienzyme complex involved in FA synthesis, fatty acid synthetase, is similar in eukaryotes and bacteria. Overall the synthesis of fatty chains progresses through a series of reactions that serves to lengthen the chain in two carbon units (Figure 1.5) [17]. The initial steps involve the formation of acetyl-acyl carrier protein (ACP) and malonyl-ACP with dissociation of coenzyme A (CoA) from both acetyl and malonyl. The first condensation step combines acetyl-ACP and malonyl-ACP, with the loss of ACP from the acetyl group. This is followed by a reduction of the acetyl carbonyl group by nicotinamide adenine dinucleotide phosphate (NADPH). Dehydration forms a double bond between the acetyl and malonyl bonding carbons. This is followed by a NADPH catalyzed reduction across the double bond [14, 17]. The steps are repeated beginning with the synthesized butyryl-ACP condensing with malonyl-ACP then are repeated in a polymeric fashion beginning with reduction, dehydration then reduction. The elongation reaction proceeds until the chain is sixteen carbons long and no longer a substrate for the fatty acid synthetase enzyme [17]. The C_{16} is then cleaved from the ACP portion. Fatty acids with odd-chain length are formed with propionyl-ACP replacing the acetyl-ACP [14]. Unsaturated FA are the result of oxidase enzyme complexes that consume NADH and O_2 in a oxidation dehydration reaction [17].

Much like the synthesis of FA the synthesis of plasmalogens occurs by a multistep process (Figure 1.6) [16]. The first step is the esterification of dihydroxyacetone phosphate (DHAP) with an acyl CoA molecule. The enzyme alkyl-DHAP synthase forms an ether bond by replacement of the fatty acid chain with a long chain alcohol species. Reduction of the carbonyl group forms a hydroxyl group. The next step is the transfer of an acyl fatty acid chain onto the hydroxyl group. Following this the desaturation of the ether bond by the enzyme Δ1'-desaturase completes plasmalogen synthesis [16].
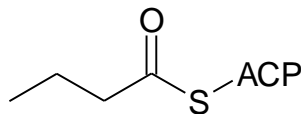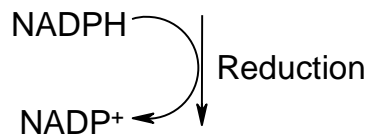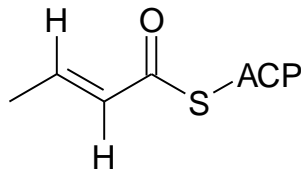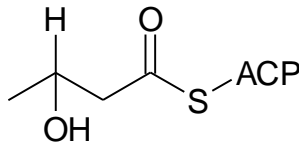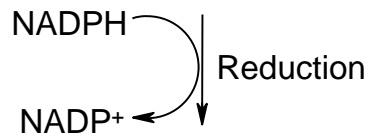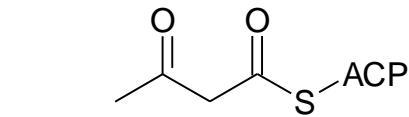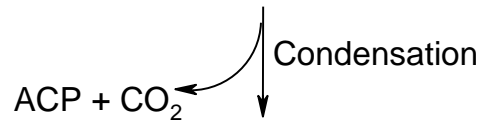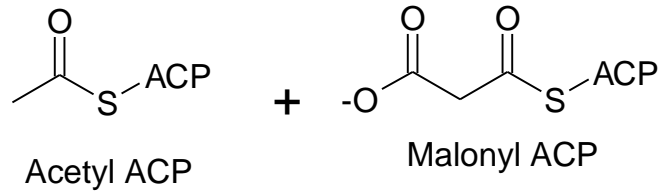
Figure 1.5. Fatty acid synthesis.
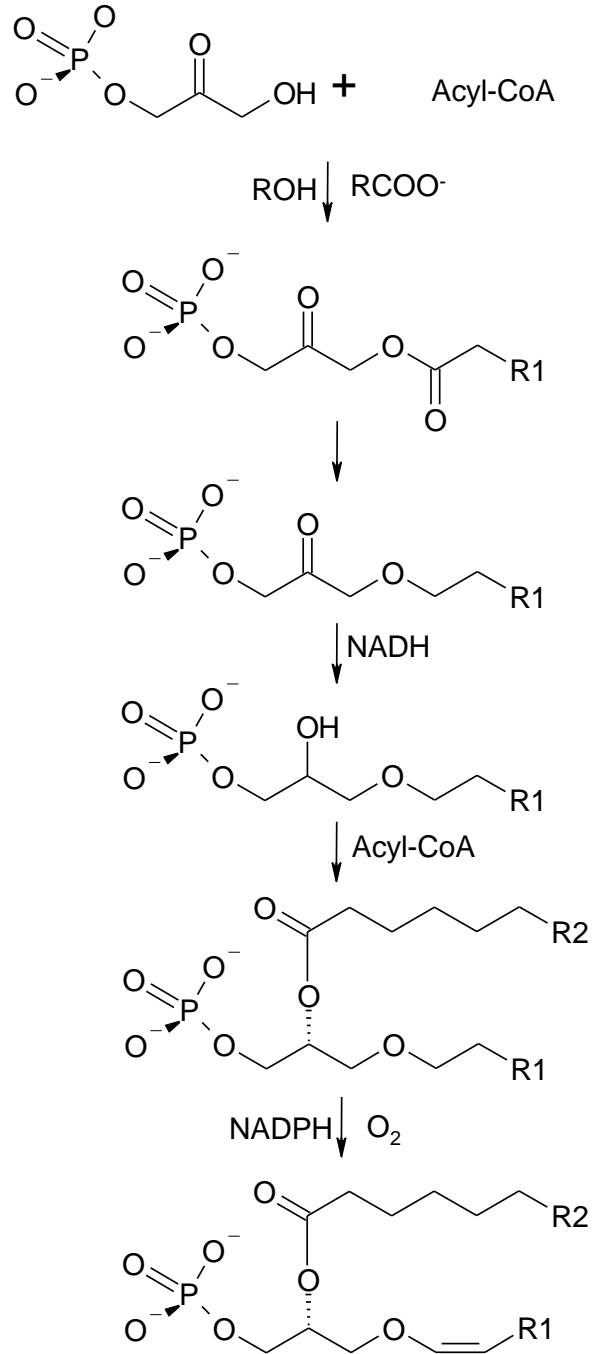
Figure 1.6. Plasmalogen synthesis.

The nomenclature of FAs used throughout this dissertation will be important for understanding background information and later during research projects. The naming system employed followed rules established by the International Union of Pure and Applied Chemistry (IUPAC) nomenclature for carboxylic acid and esters when discussing derivatizied species [18]. In brief, saturated or substituted carboxylic acids were named by modifying the IUPAC name of the root alkane compound by removing the final "-e" and replacing it with "-oic acid". The carbon chain is numbered starting with carbonyl carbon identified as 1. Substituents along the chain are identified by their respective IUPAC nomenclature and named according to the carbon which they are attached. Esters derivatives are again named according to their IUPAC rules. First the substituent group that replaced the hydroxyl of the free acid is identified, (i.e. methyl) followed by replacement of the "-oic acid" suffix with "-oate" (Figure 1.7) [19].

Unsaturated FAs were named in a similar manner, however instead of using the root alkane, the alkene was modified to denote sites of unsaturation. Conversion of the root alkene involves removing the terminal "-e" and replacing it with "-oic acid" for naming the free acid [19]. Multiple double bonds along the chain, as in case with polyunsaturated fatty acids (PUFAs), are denoted by adding a Greek modifier directly before the alkene "-ene" suffix. This follows the same systematic rules as naming alkenes with multiple double bonds. As with substituents along the chain, sites of unsaturation are identified by the number of the initial carbon containing the double bond, when counting from the carbonyl carbon (Figure 1.8) [19].

Shorthand nomenclature is commonly used during the reporting of results. This abbreviated representation takes the form: x:y; where x denotes the number of carbons comprising the chain and y signifies the number of double bonds. The chain is considered carbons from the carbonyl to the terminal methyl group. For esterified species the number of carbons within the chain does not include the substituent added to the carbonyl group. Additional information of double bond location is supplied by adding the Greek uppercase delta (Δ) followed the carbon number at which the double bond is initiated. An example of this would be 10-octadecenoic acid, written in shorthand translates to 18:1Δ10 [19-20]. Another abbreviation commonly used with PUFAs is omega (ω). The ω denotes the number of carbons from the further double

octadecane

octadecanoic acid

methyl octadecanoate
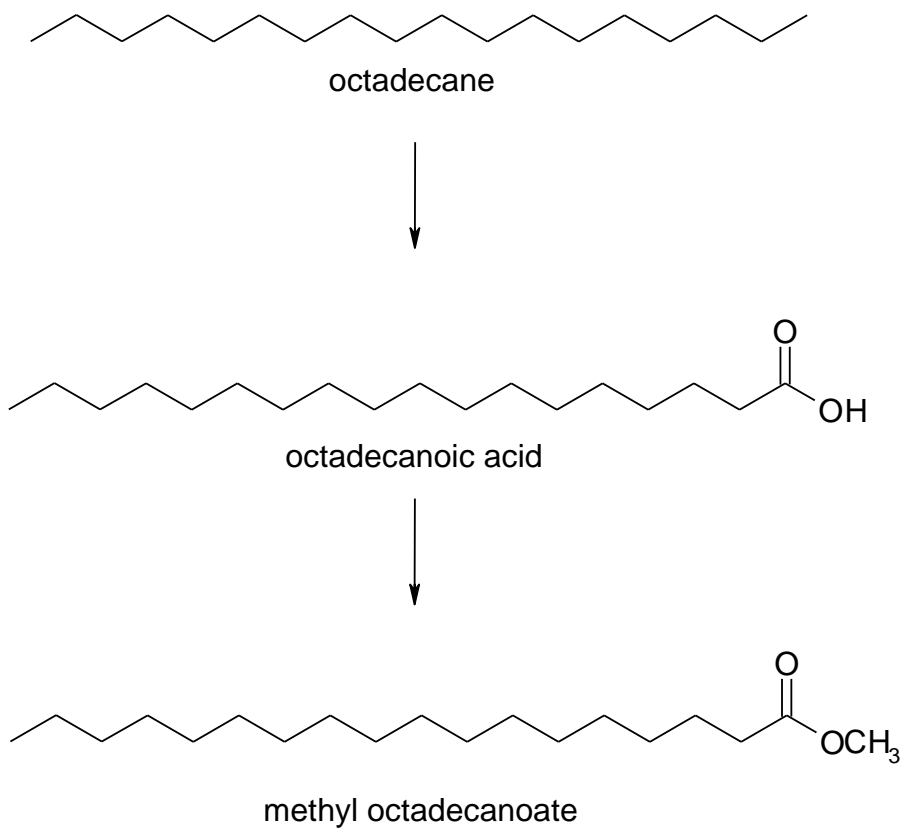
Figure 1.7. Saturated fatty acid nomenclature.

octadecene

10-octadecenoic acid

methyl 10-octadecanoate

18:1Δ10
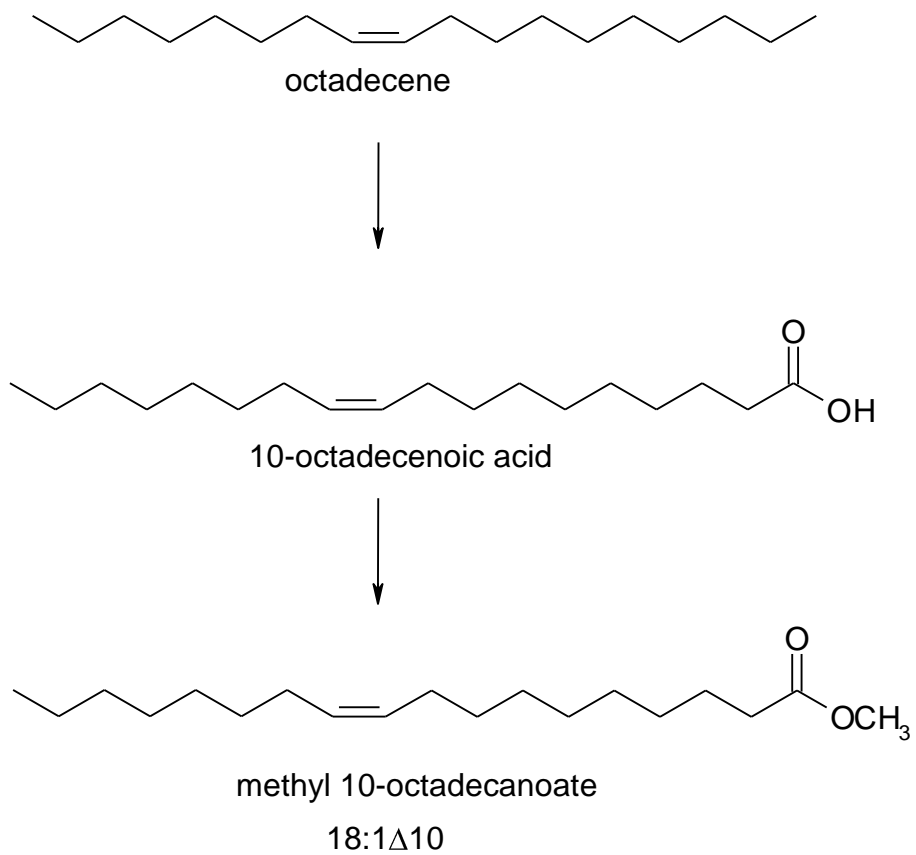
Figure 1.8. Unsaturated fatty acid nomenclature.

bond, relative to the carbonyl, to the terminal methyl group. Therefore, a fatty acid with six carbons from the terminal methyl group to the first double bond would be symbolized in shorthand as ω-6, otherwise known as an omega six fatty acid. At times within the text common names for fatty acids have been used for particular fatty acids as these names are more popular than the systematic names. In these cases the common name is given with the IUPAC systematic name [18, 20].

Analysis of the fatty acid species was achieved by the traditional base-catalyzed saponification reaction to break the bonds between the acyl chains and the glycerol backbone. Intact membrane glycerophospholipids were reacted with sodium hydroxide forming sodium carboxylates [19-20]. Protonation of the free acid was achieved by addition of hydrochloric acid (Figure 1.9). Following extraction of the free acid an esterification reaction converts the free acid to an ester. Methylation of free acids through esterification with acetyl chloride and methanol results in formation of fatty acid methyl esters (FAMEs) (Figure 1.10) [19-20]. Although esterification reactions can be conducted with a number of reagents, reaction with acetyl chloride was preferred for small-scale preparation and mild reaction conditions.

Derivatization of the fatty acids to an ester increases the volatility and removes functionality from the carboxylic acid end improving the amenability to GC analysis [20-21]. Of course analysis of free acids can be conducted without conversion to esters. However, conversion to the ester by reaction with excess alcohol pushes the free acid reagents to form predictable derivatives and generates a stable product. Although nearly any reagent with a hydroxyl group would suffice for esterification, methanol was chosen because the addition of a methyl group minimally increases the molecular weight of the final ester. This is important when considering GC analysis, as higher molecular weight compounds often require increased temperatures for volatility and column elution. On the detection end methyl addition was advantageous because mass analyzers often have mass limits, this is generally not a problem except for extreme cases, such as long-chain FAs and benzyl-type derivatives. The other advantage is that fatty acid methyl esters are the most common researched derivatives, making results comparable to published mass spectra and mass spectral libraries [20].
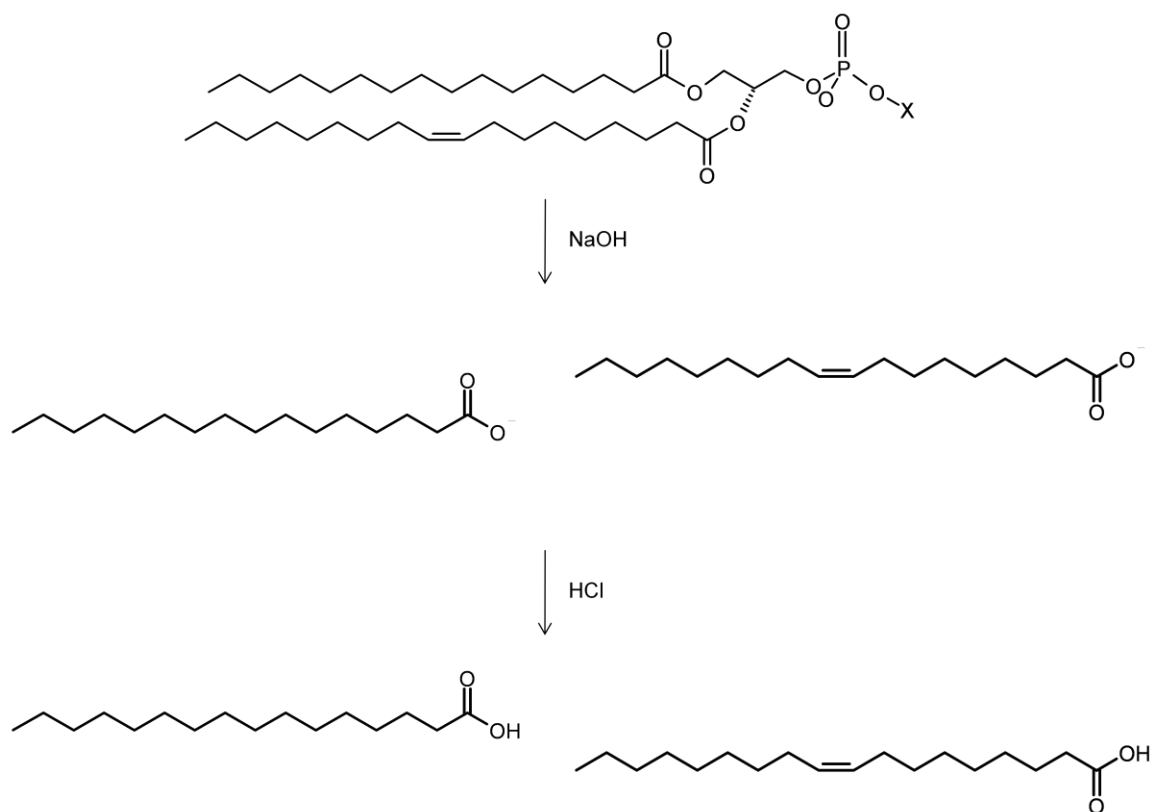
Figure 1.9. Saponification reaction scheme.
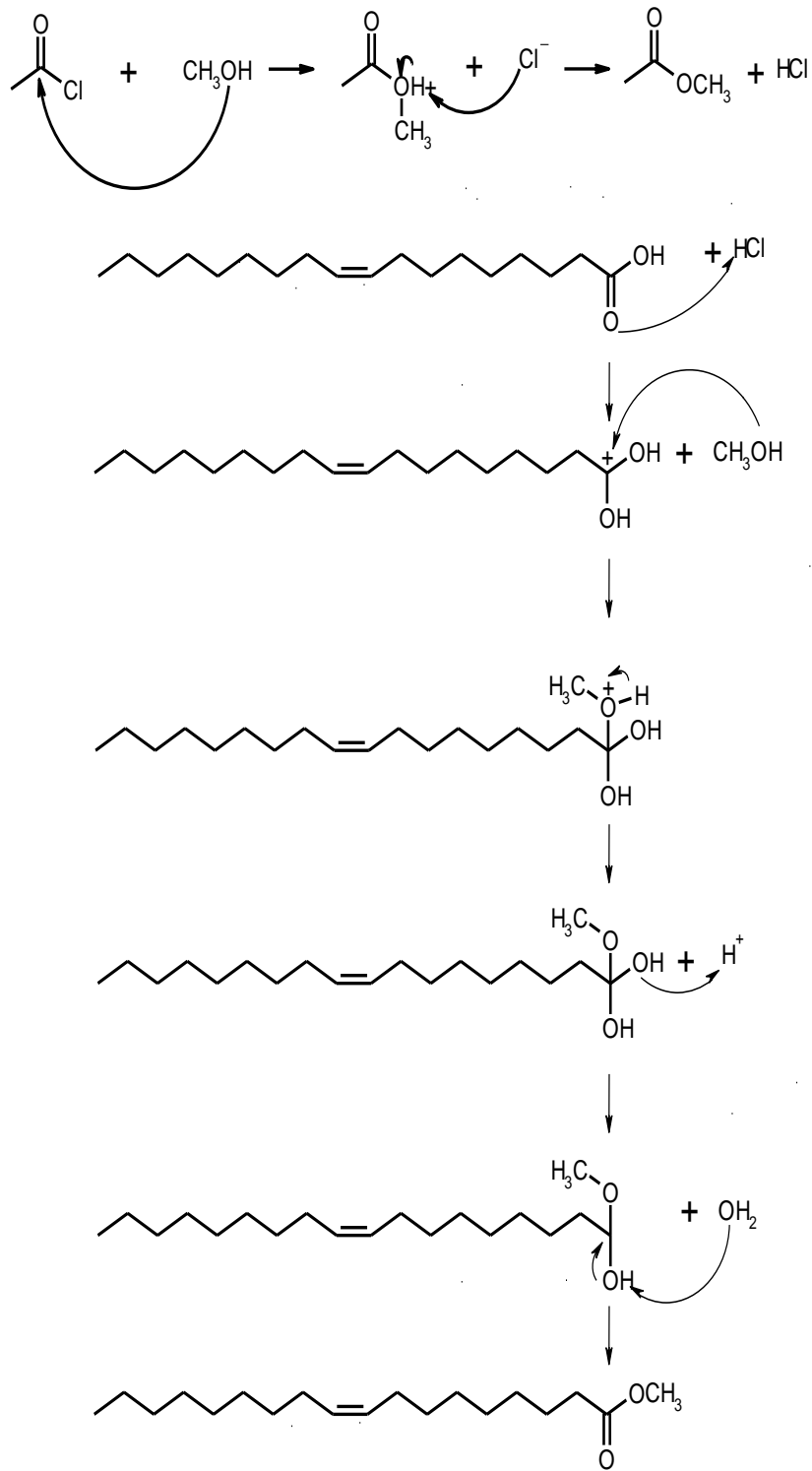
Figure 1.10. Methylation reaction scheme.

During the FA esterification reaction, the vinyl ether bond from the plasmalogen is cleaved generating an aldehyde. Reaction of the aldehyde with methylation reagents converts the aldehydes into dimethyl acetals (Figure 1.11) [19-20]. Following saponification the vinyl ether bond is converted to an aldehyde. Due to the acidic nature of the esterification reaction the carbonyl group of the aldehyde is protonated. Nucleophilic attack by methanol on the activated carbonyl carbon generates formation hemiacetal. Subsequent protonation of the hemiacetal hydroxyl group generates water as a leaving group. The loss of water forms a carbocation that is attacked by another nucleophilic methanol. The result is formation of a dimethyl acetal [19-20]. The nomenclature for these compounds follows the IUPAC rules for naming acetals [18-19].

Instrumentation

The analysis of all derivatizied species were preformed on a Varian Saturn 3 GC/MS system (Figures 1.12 & 1.13). Discussion on instrumentation will first involve the theory and brief background on gas chromatography followed by mass spectrometry theory and operation.

Gas chromatography

A gas chromatograph (GC) is an instrument that separates compounds based on volatility and structure [21]. A gas chromatograph in general has three main components: an injector, a column housed inside an oven and a detector. For GC/MS the detector is a mass analyzer, therefore the GC detector is replaced by a transfer line leading to the mass spectrometer.

The chemical composition of the column's stationary phase is central to the analytical performance of the experiment and interaction with the stationary phase has the greatest single influence on analyte separation [21]. Differential interaction of analytes with the stationary phase is the basis for chromatographic separation in any GC experiment. The column resides within a GC oven and during a chromatographic experiment the oven temperature is increased to elute analytes (Figure 1.14). Heating of the column increases the vapor pressure of analytes, so that compounds with a high vapor
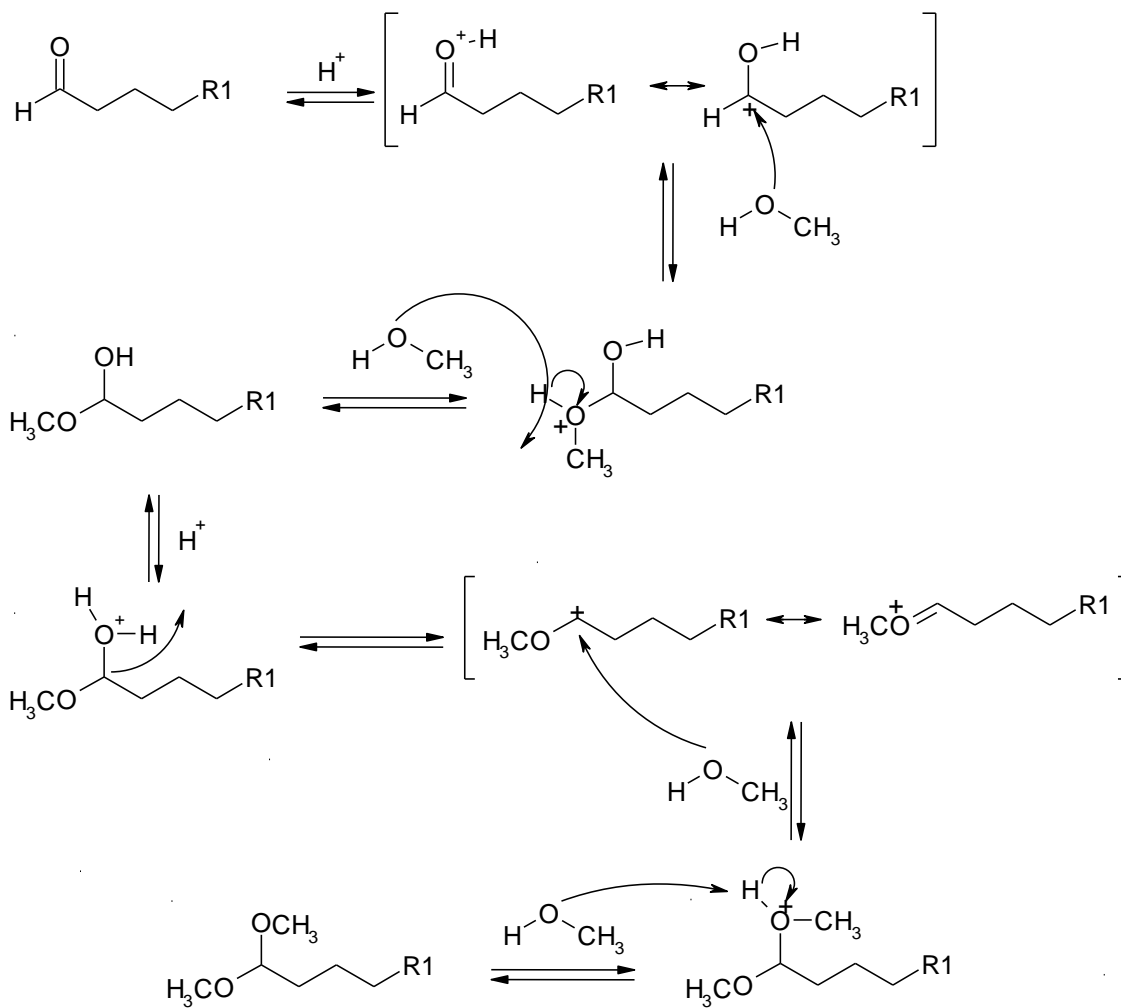
Figure 1.11. Dimethyl acetal derivatization scheme.

Figure 1.12. Varian gas chromatograph.
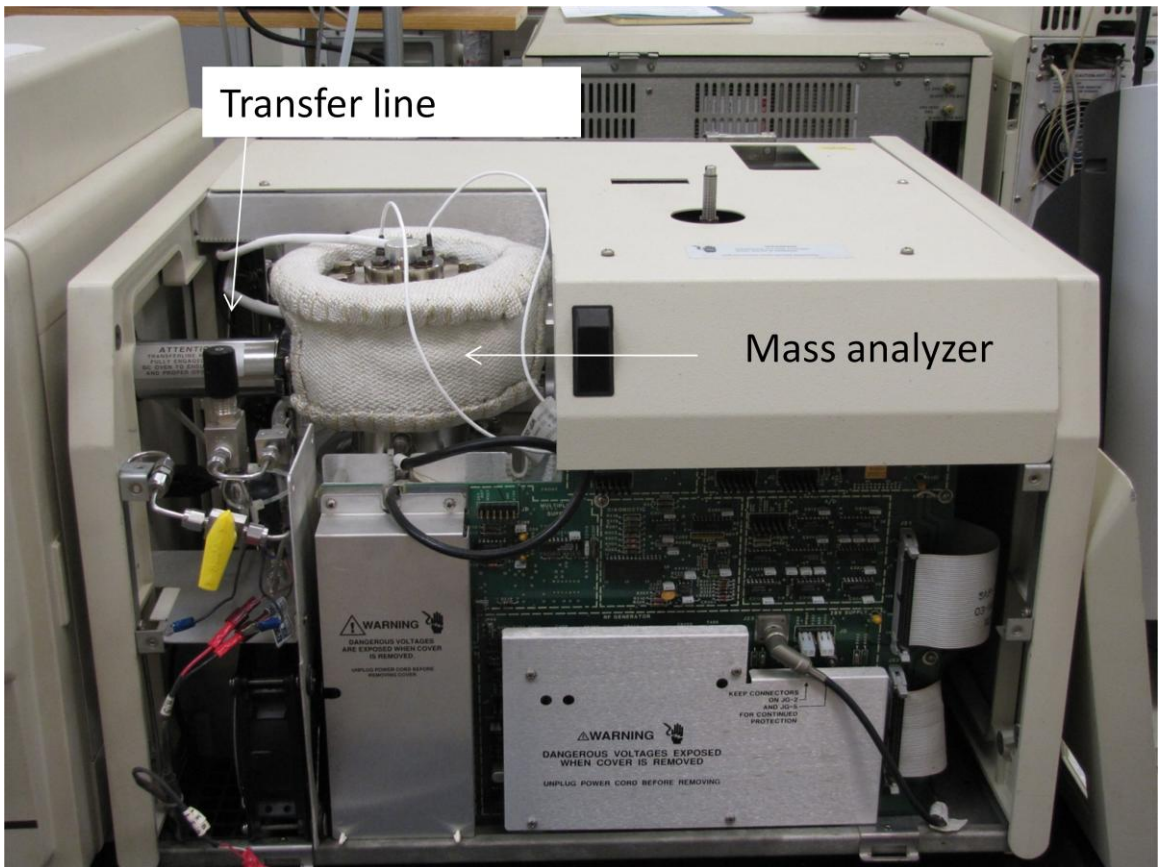
Figure 1.13. Varian Saturn QIT mass spectrometer.
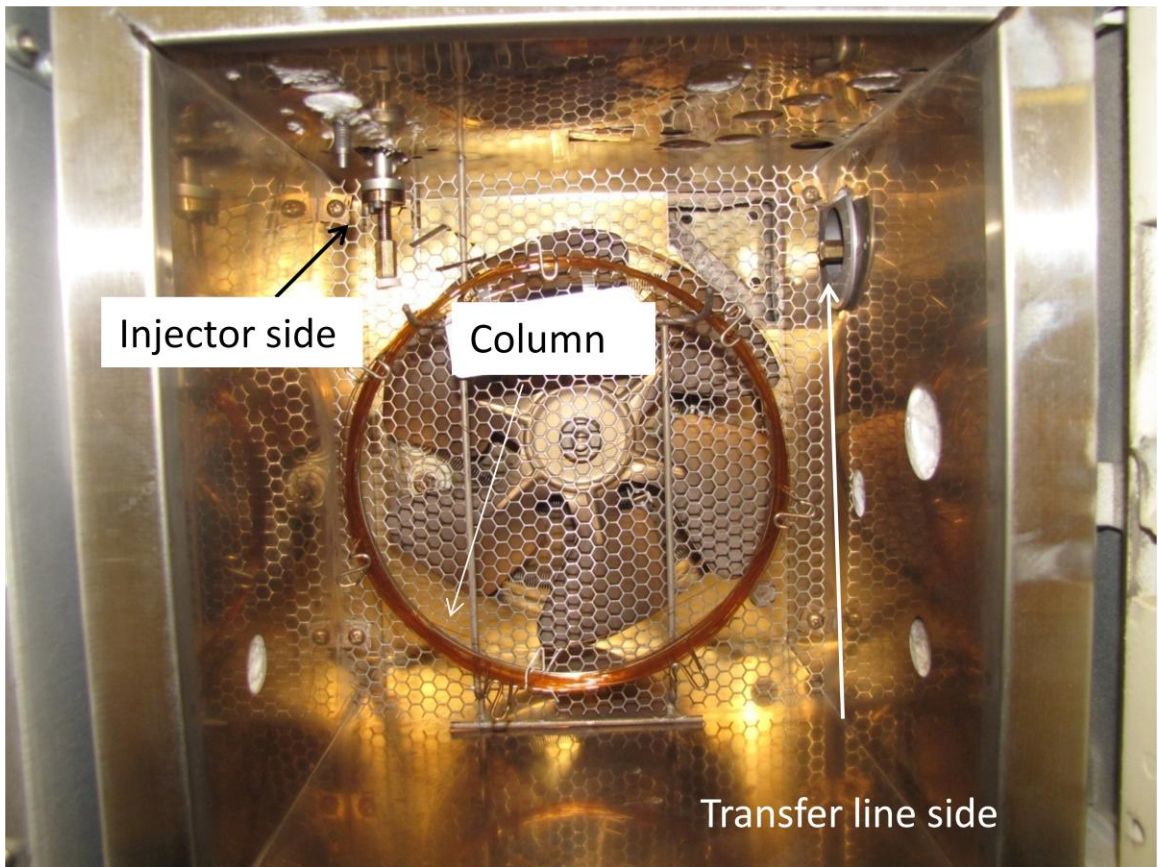
Figure 1.14. Capillary column inside GC oven.

pressure are eluted first. The slope of the temperature ramp in part determines retention time and the separation between peaks.

Gas chromatography is an analytical separation technique that uses a gas, typically He or N_2, as the mobile phase and a substituted polysiloxane stationary phase [21]. Analyte separation for GC is primarily a factor of column stationary phase, column temperature and the compound itself. Unlike liquid chromatography (LC) analyte affinity for the mobile phase is not a factor affecting separation [22]. Helium was used for all GC operations because of the large $\bar{u}_{opt}$ working temperature range and because it presents additional benefits which are important during MS operation [21].

Mass spectrometry

Following chromatographic separation based on the selective retention by the stationary phase the carrier gas transfers the analytes to the detector. In this case the detector will be a mass spectrometer (MS) and the interface between the GC and the MS is made via a transfer line (Figure 1.15). The transfer line is little more than a heated partition that houses a section of the chromatographic column (Figure 1.). Usually transfer lines are at isothermal temperatures, above the final temperature ramp of the column, to prevent condensing the separated analytes back onto the stationary phase, which would be counter-productive to the chromatographic phase. The transfer line should function in the background allowing analyte introduction into the mass analyzer without compromising peak resolution.

The instrumental design used throughout the ensuing studies has elution of analytes entering directly into the MS detector from the transfer line. The mass spectrometer (MS) has three general components: ionization source, detector and mass analyzer. Prior to separation of molecules, by a mass analyzer based on m/z, ionization must occur. Projects conducted in this dissertation employed two types of ionization: electron-impact (EI) ionization and chemical ionization (CI). Both of these techniques involve different ionization mechanisms producing unique ions that are ultimately manifested as distinctive mass spectra. Although the outcomes are different both processes begin with the emission of high-energy electrons, approximately 70 eV, from the heating of a tungsten filament (Figure 1.16) [23]. Electrons are directed toward the column eluent by means of a negatively charged repeller plate situated behind
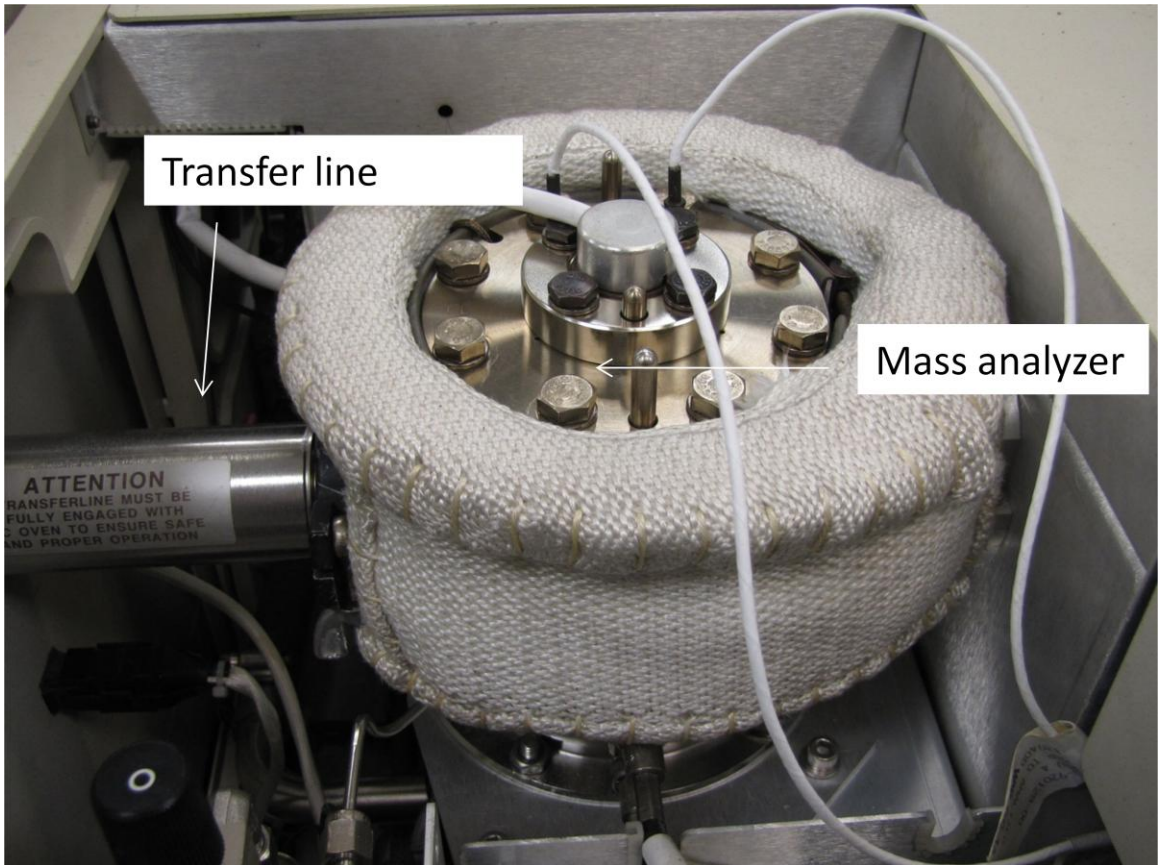
Figure 1.15. GC/MS Transfer line.
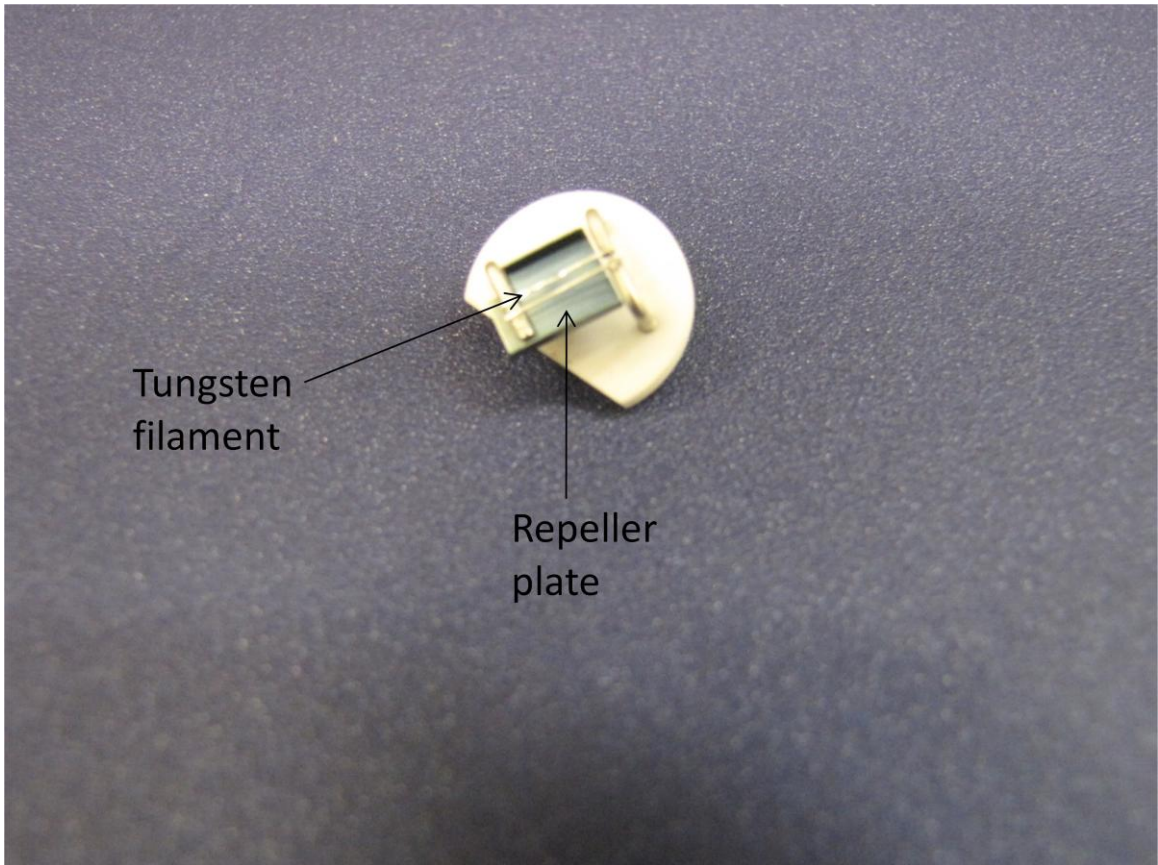
Figure 1.16. Ionization filament.

the filament. It is at this stage the EI and CI process diverge. Electron-impact will be covered first since many of the same principles are encountered during CI. In EI, a high-energy electron will "impact" with an analyte molecule causing ionization. The term "impact" is a misnomer as no actual physical collision occurs. Ionization is the result of the high-energy electron interacting with a resonant electron from the analyte molecule [23]. A portion of energy is transferred to the molecule resulting in ejection of an electron. The overall EI process yields a radical cation ($M^{+\cdot}$) and two electrons, one ejected from the initial molecule and one the ionizing electron (Figure 1.17).

The minimum amount of energy absorbed by an analyte to cause ejection of an electron, or ionization energy, is molecule dependent, however most ionization energies are on the range of 7 to 15 eV [23-24]. The ejection of an electron is a rapid process resulting in a Frank-Condon vertical transition [24]. Essentially electron ejection is faster that molecular bond vibration, so that when ejection occurs atoms and bonds are static. Following ejection the molecule redistributes energy to account for the weakened bond. This redistribution is manifest as vibrational energy that results in bond dissociation releasing a portion of the incurred internal energy.

The nature of EI is a "hard" ionization technique, meaning that the process imparts a significant amount of energy to the analyte causing excessive bond dissociation. Formation of an odd-electron species, $M^{+\cdot}$, consequentially leads to an unstable molecular ion that readily undergoes fragmentation and bond rearrangement. Fragmentation from the molecular ion, $M^{+\cdot}$, occurs two ways; producing either an even-electron ion and a radical, or an odd-electron ion and an even-electron neutral [23-24]. Spectra generated from EI represent statistical distributions of fragments from the molecular ion with the most stable fragments having greater abundance [19].

The most prominent diagnostic ion for fatty acid methyl esters is the McLafferty rearrangement (Figure 1.18). The McLafferty rearrangement is a cyclic hydrogen transfer process occurring between a carbonyl and gamma methyl group [19, 23]. Rearrangement is a two step process, first generating the enol intermediate. In the second step the hydrogen transfer is completed and the bond between the β and γ carbons is broken to produce a cation radical and an alkene. The radical cation is the diagnostic ion.

M + e⁻ ⟶ M⁺· + e⁻ + e⁻
   (70 ev)   (Ionizing)   (Ejected)
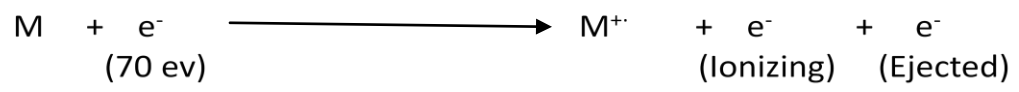
Figure 1.17. Electron-impact ionization scheme.
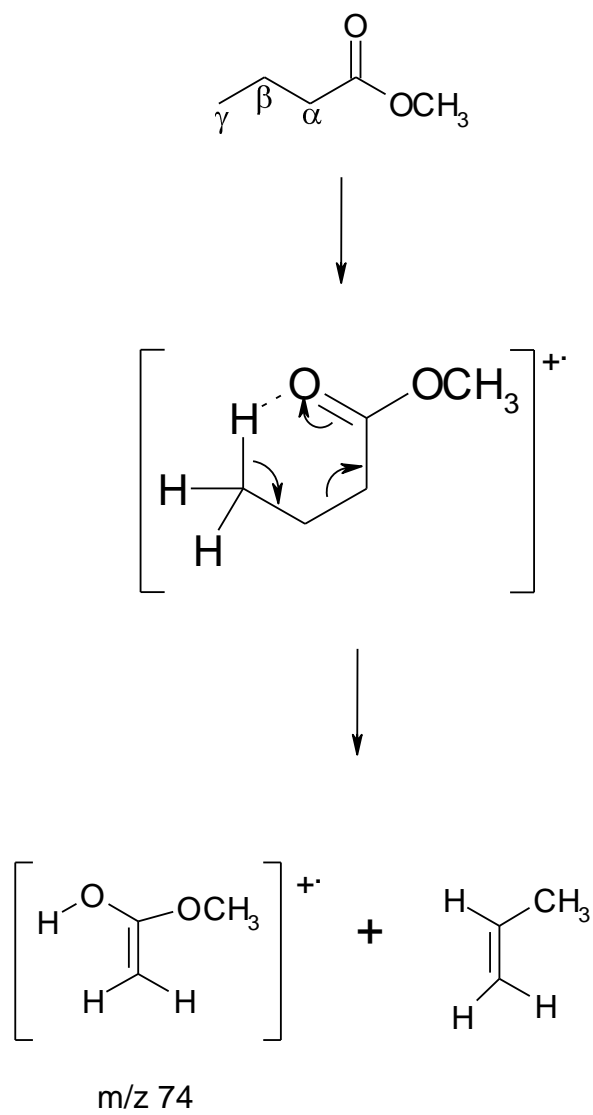
Figure 1.17. McLafferty rearrangement.

For methyl ester species this results in the m/z 74 ion. Other diagnostic ions for fatty acid methyl esters would include: m/z 87, [M-31]$^+$ and [M-74]$^+$ [19, 23].

In contrast to EI, the process of chemical ionization (CI) is a gentle "soft" ionization technique [19, 23]. As with EI a high-energy electron is used to initiate ionization, however instead of impacting with an analyte molecule, ionization first occurs with a reagent gas. The secondary reaction of reagent gas with analyte molecules provides further ionization. The abundance of reagent gas molecules must be significantly higher than analyte molecules to ensure CI and not the competing EI process.

The CI process is highly dependent on the eventual interaction between reagent gas and analyte. Interactions between the two generally involve transfer of a hydrogen, hydride or other charged species. Therefore, the acid/base or proton affinity relationship between the charged reagent gas and analyte is critical to the CI process [19, 23-24]. This relationship determines the eventually molecular species formed. To this end, a variety of reagent gases have been employed depending on the analyte under investigation. Studies contained herein were conducted with acetonitrile as a reagent gas (Figure 2.2), however methane is probably the most frequent reagent gas utilized (Figure 1.19) [23].

Chemical ionization experiments conducted during the course of studies used the selected-ejection CI (SECI) technique [25]. Due to features of the particular mass analyzer utilized, discussed below, CI reactions occur at low pressure instead of high reagent gas pressure usually required. The SECI process allows reagent gas to fill the mass analyzer for a period of time, termed the automatic-reaction control time. Ionization of the reagent gas then occurs followed by reaction of the reagent gas with the analyte molecules. The selected-ejection refers to the process that removes all ions with m/z lower than the background mass prior to an analytical scan [25]. The advantage is that during mass analysis only ions from the predetermined experimental mass range are analyzed.

The contrast of CI to EI is that the secondary ionization process results in less energy transferred to the analyte and the eventual molecular ion, [M+H]$^+$, is an even-electron cation which in intrinsically more stable than the odd-electron radical

$$CH_4 \quad + \quad e^- \longrightarrow \quad {}^{+}_{\cdot}CH_4 \quad + \quad 2e^-$$

$$^{+}_{\cdot}CH_2 + H_2 \quad \text{and} \quad {}^{+}CH_3 \quad + \quad {}^{\cdot}H$$

$$^{+}_{\cdot}CH_4 \quad + \quad CH_4 \longrightarrow \quad CH_5{}^+ \quad + \quad {}^{\cdot}CH_3$$

$$^{+}CH_3 \quad + \quad CH_4 \longrightarrow \quad C_2H_5{}^+ \quad + \quad H_2$$

$$^{+}_{\cdot}CH_2 \quad + \quad 2CH_4 \longrightarrow \quad C_3H_5{}^+ \quad + \quad 2H_2 \quad + {}^{\cdot}H$$
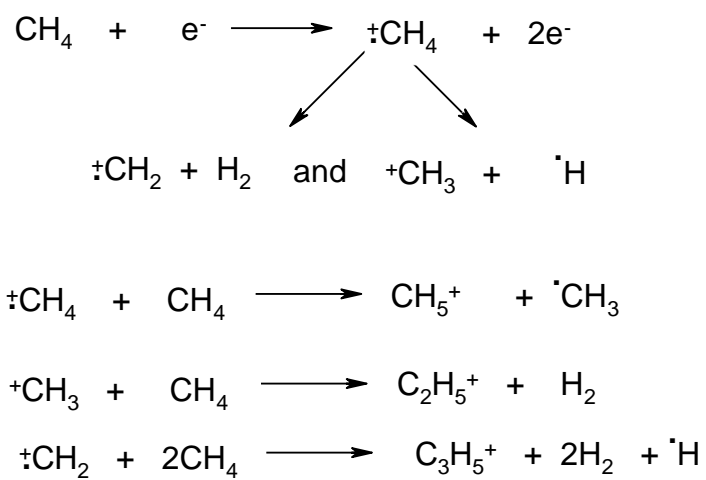
Figure 1.19. Chemical ionization scheme.

28

cation [23-24]. As a consequence CI spectra exhibit a greater relative abundance of molecular ion. However, the trade-off is CI leads to less fragmentation which can be used for structural identification.

Electron-impact and CI are ion forming pathways that can be employed complimentary during analysis. The nature of EI is largely analyte independent, making it applicable to quantitation. Chemical ionization on the other hand is highly analyte and reagent gas dependent, therefore quantitation with CI can be difficult for unknowns. The stability of the molecular ion in CI permits identification of the parent molecule, which is sometimes absent from EI spectra. Whichever ionization method is employed the formation of ions is critical to analysis with a mass analyzer.

Discussion of mass analyzers will focus on the particular analyzer used throughout each of the projects, a quadrupole ion trap (QIT). The QIT, sometimes called a Paul trap in honor of it's inventor Wolfgang Paul, is composed of three main parts: a ring electrode and two endcap electrodes (Figure 1.20) [26]. When assembled the three hyperbolic electrodes are electrically isolated from one another which is vital for operation (Figure 1.21). As the name implies the QIT is a trapping mass analyzer presenting several advantages during analysis, such as tandem mass spectrometry (MS/MS) and low pressure CI as previously discussed.

The arrangement of the QIT electrodes creates a trapping volume that is twice as wide along the horizontal axis, r_0, as the vertical axis, z_0 (eq. 1.5).

$$r_0{}^2 = 2z_0{}^2$$ eq. 1.5

A fundamental radio frequency (rf) is applied to the ring electrode creating the trapping field. For current commercial instruments the fundamental rf is applied at a frequency of 1 megahertz (MHz) [26-29]. In response to this fundamental rf, ions within the trap assume cyclic oscillations that have a frequency based on their particular m/z, otherwise known as a secular frequency. It should be noted that during normal operation the trap is filled with a buffer gas, normally He, to a pressure of 1 mTorr that assists in reducing the kinetic energy of the ions following ionization. The buffer gas aids in focusing the ions to the center of the trap so that they assume predictable movements with the fundamental rf [22]. The buffer gas will also be important later during tandem mass spectrometry (MS/MS).
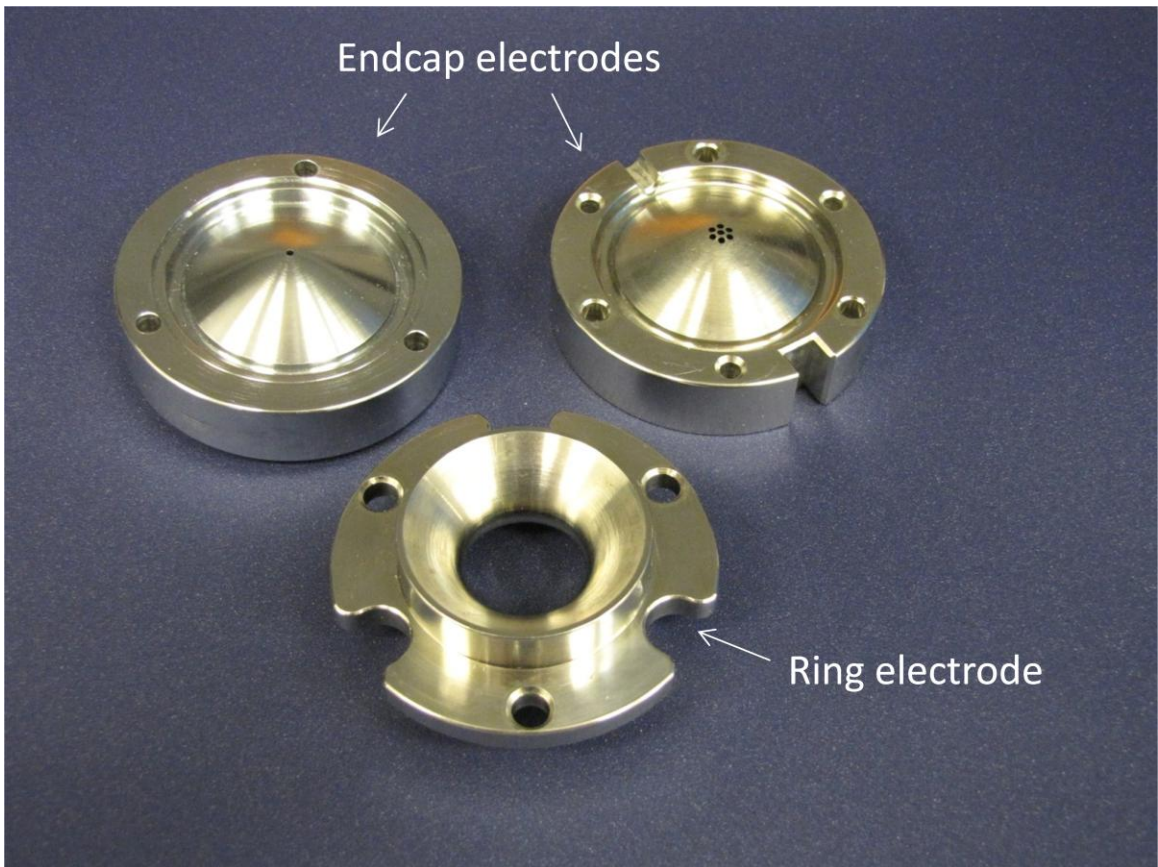
Figure 1.20. Quadrupole ion trap anatomy.
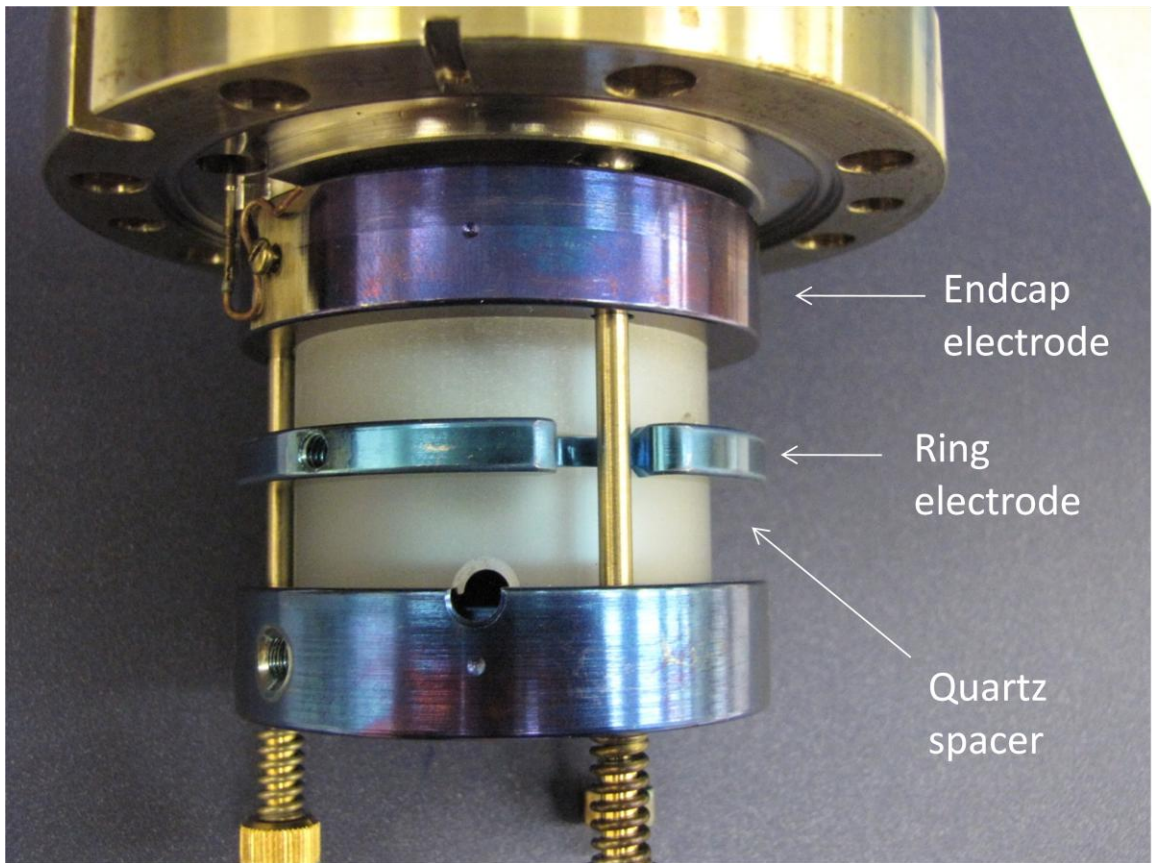
Figure 1.21. Quadrupole ion trap assembly.

The motion of ions within this quadrupolar field is described by the Mathieu equation [26-29]. There are two general solution categories for the Mathieu equation: (1) periodic and stable and (2) periodic but unstable. Together these represent the Mathieu stability diagram (Figure 1.22). Ions adopting a periodic and stable trajectory are successfully trapped within the QIT, whereas the periodic but unstable solutions form the boundaries. In order for an ion to be successfully trapped the trajectory must be stable in the radial (eq. 1.6 & 1.7) and axial planes (eq. 1.8 & 1.9). The stable solutions to the Mathieu equations describing these boundaries are [26-29]:

$$a_r = \frac{8eU}{m\left(r_0^2 + 2z_0^2\right)\Omega^2}$$ eq. 1.6

$$q_r = \frac{-4eV}{m\left(r_0^2 + 2z_0^2\right)\Omega^2}$$ eq. 1.7

Where a_r and q_r are radial space within the trap, m is the mass of a particular ion, e is the charge of an electron, r_0 is the radius of the ring electrode, z_0 is the distance between the endcap electrodes, Ω is the frequency of the fundamental rf, V is the amplitude of the rf and U is the DC potential applied to the ring electrode.

$$a_z = \frac{-16eU}{m\left(r_0^2 + 2z_0^2\right)\Omega^2}$$ eq. 1.8

$$q_z = \frac{8eV}{m\left(r_0^2 + 2z_0^2\right)\Omega^2}$$ eq. 1.9

Where a_z and q_z are axial space within the trap, all other symbols are the same in eq. 1.6 and 1.8. Current commercial QIT mass analyzers do not provide the option of applying a DC potential to the ring electrode. The implications of this are that the U term is always zero, making eq. 1.5 and 1.7 equal to zero, and ion positioning within the Mathieu stability diagram is always at zero along the a_z axis.

The operation of a QIT during a mass analysis experiment involves trapping ions, as discussed above, and then ejecting those ions in a mass dependent manner. The ejection of ions is accomplished by increasing the amplitude, V, of the fundamental rf.
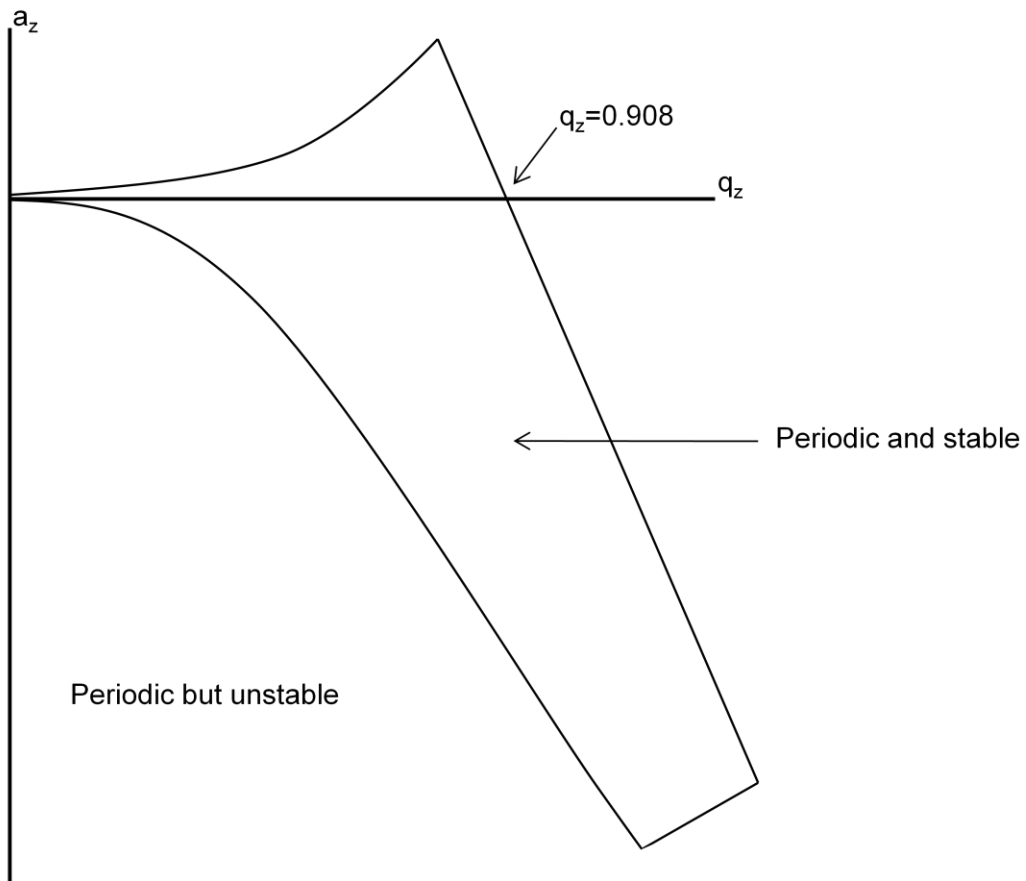
Figure 1.22. Mathieu stability diagram.

Ion movement in the trap is a function of the fundamental rf and an ions m/z ratio. Interaction with the fundamental rf causes ions to adopt regular oscillations, known as secular frequency. An ion's secular frequency is dependent on its m/z ratio, small ions will have a larger secular trajectory than larger ions [26-29]. As the rf amplitude increases the secular frequency of the ions increases causing the trajectory to expand along the axial plane. A graphical representation of this increased oscillation would be an ion moving to the right along the y-axis in the Mathieu stability diagram (Figure 1.). The trajectory of an ion increases until it becomes unstable and is ejected from the trap. This point of instability occurs at approximately a $q_z = 0.908$, which is where the stability boundary intersects the q_z axis [26-29]. This type of scanning is known as a mass-selective instability scan.

The mass-selective nature of ion ejection is due to the relationship between secular frequencies and m/z of ions. Ions with a small m/z will have greater secular frequency, therefore when the rf amplitude is ramped their oscillations increase to the ejection boundary faster than larger ions with lower secular frequencies. The slope of the rf amplitude ramp determines the number of oscillation cycles an ion makes before reaching the critical ejection boundary [26-29]. The ramping of the fundamental rf from low to high amplitude, and the subsequent ejection of ions in a mass dependent manner from low m/z to high m/z, is termed an analytical scan. Data collected from the analytical scan produces a mass spectrum.

The endcaps assist during the mass-selective instability scan in supplying a supplemental rf potential to an ions secular frequency [26-29]. As the secular oscillations of ions increase during the rf ramp their trajectory places them incrementally closer to the endcap electrodes. At a critical point an ion's trajectory will place them close enough to an endcap electrode that the ion will come into resonance with the supplemental rf potential. This process, known as resonance ejection or axial modulation, increases the kinetic energy of the ion and causes prompt ejection. Generally, the frequency of the supplemental rf is approximately half that of the fundamental rf, or 500 kHz [26-29].

One of the advantages with a QIT is the ability to perform tandem mass spectrometry (MS/MS). This is the process where after trapping ions, all ions are ejected except for one m/z ratio. This isolated m/z ratio, also called a parent or precursor ion, is

then fragmented a second time in a process known as collisionally-induced dissociation (CID) to provide further structural or chemical data on the particular m/z [26-29]. Because the m/z is isolated prior to fragmentation the product ions should provide unique data relevant to the parent molecule.

Tandem mass spectrometry in a QIT is a tandem-in-time process meaning the events occur within the same space, the trap, during discrete times [23]. The events leading to a MS/MS experiment are the same as a MS experiment. Following ionization the trap is full of ions with various m/z ratios. Isolation of the parent ion for Varian Saturn QIT occurs via a two step process. Ions with m/z lower that the parent ion are ejected by ramping the supplemental rf on the endcap electrodes. Next a broadband waveform is applied to the endcap electrodes to eject ions with m/z greater that the parent ion. The two events work together to isolate a particular m/z ratio. After isolation the amplitude of the fundamental rf is decreased in order to "place" the parent ion at a particular point along the a_z axis in the stability diagram. There are two main reasons for doing this: the first is to restrain the kinetic energy of the parent ion so that fragmentation can occur under a controlled process; the second is to manage the product ions formed. For organic molecules CID is usually performed at a $q_z = 0.4$, because this is the deepest point in the pseudo-potential well along the stability diagram [26-29]. Usually organic molecules require greater CID voltages to fragment, thus at lower points in the well greater voltages would result in immediate ejection without fragmentation.

The CID process is conducted by applying a low-energy rf waveform across the endcaps, this is known as an excitation or tickle voltage [26-29]. There are two types of CID waveform that can be applied: resonant and non-resonant. A resonant waveform is applied at a frequency that is resonance with the parent ion's secular frequency. The advantage is that only the parent ion is excited to undergo the CID process and not the resulting fragment ions. A non-resonant waveform is a broadband waveform with a range of frequencies. This procedure excites the parent ion and the resulting fragments. The disadvantage with non-resonant CID is that spectra are complicated due to fragments of fragments. All experiments contained herein use resonant CID methods.

With the excitation voltage applied to the endcaps the motion of the parent molecule is increased so that it collides with the He buffer gas. The low-energy CID

process causes multiple collisions between the parent ion and the buffer gas. With each collision the translational kinetic energy of the parent molecule is transferred into vibrational energy [26-29]. As the vibrational energy of the parent ion increases fragmentation occurs. Collision-induced dissociation excitation occurs for a period of time, usually on the order of milliseconds, then the product ions are scanned out the QIT in a typical analytical scan.

One potential disadvantage with performing MS/MS in a QIT is the limited mass range of trapped product ions, because of the low-mass cut-off (LMCO) [26-29]. The low-mass cut-off is the lowest mass that can be successfully trapped at a given q_z value (eq. 1.10).

$$LMCO = \frac{(m/z)q_z}{0.908} \qquad \text{eq. 1.10}$$

Where m/z is the parent ion m/z ratio, q_z fundamental rf amplitude at which CID occurs and 0.908 is the stability boundary along the q_z axis. Of course the mass range can be extended by performing CID at a q_z value, however this limits the CID voltage that can be applied without causing parent ion ejection. Generally, the LMCO does not present a problem during analysis of volatile lipid species by GC/MS.

Following ion ejection through the endcap electrode during the analytical scan, the ion strikes the detector. The type of detector employed throughout studies was an electron multiplier, which was located directly below the bottom endcap electrode (Figure 1.23). The advantage of the electron multiplier is that it provides amplification of the incident ion [23]. The result of amplification is an increased signal per incidence which in turn translates to greater sensitivity.

The analysis of methyl derivatizied species by GC/MS allowed the separation, quantification and structural elucidation of geometric isomers. The QIT mass analyzer provided versatility during analysis that allowed identification of unknown lipid analytes. Mass analysis techniques, such as MS/MS and low-pressure CI, were developed to take advantage of the unique features provided by the QIT. Analytical and biological procedures developed during the course of investigations aided in directing subsequent projects. Projects conducted for this dissertation are linked by the foundation
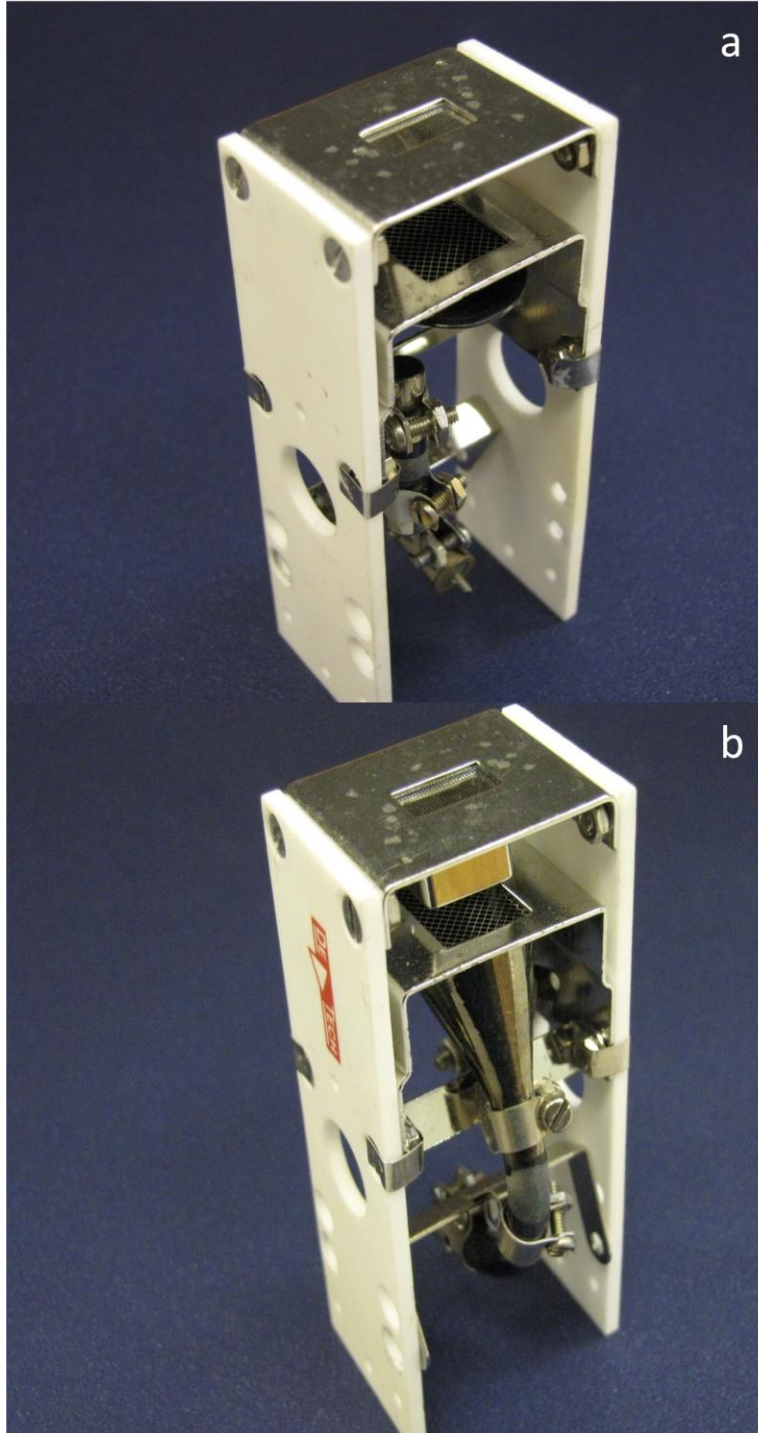
Figure 1.23. Electron multiplier ((a) front, (b) back).

of lipid modification to environmental stimuli. Gas chromatography coupled with MS demonstrated to be the instrument of choice for the analysis of volatile methyl derivatizied lipid species.

PART II. PROKARYOTIC LIPIDOMICS

Chapter 2. The Analysis of Composition and Structure of *Clostridium thermocellum* Membranes from Wild-type and Ethanol-adapted Strains

Chapter 2.1. Introduction

Ethanol derived from fermentation of lignocellulosic biomass is a renewable alternative to petroleum-based transportation fuels. Virtually all bio-ethanol is currently produced from fermentation of starch by yeast, but these organisms are unable to directly degrade saccharify lignocellulosic feedstocks. Enzymatic, chemical, and physical pre-treatments are needed to saccharify the structural carbohydrates and this increases the complexity and expense of the overall process. Consolidated bioprocessing by celluloytic bacteria has been proposed as an alternative technological platform for bio-conversion of lignocellulose to ethanol [30].

Fermentation with microbes that produce ethanol from cellulose reduces the raw material cost. However, most microbes are unable to directly metabolize cellulose. Conventional enzymatic saccharification uses enzymes to break down cellulose and hemi-cellulose into sugars which yeast can then metabolize, producing ethanol [31]. Consolidated bioprocessing by cellulytic microorganisms for the production of ethanol has advantages over conventional methods [31]. However, in order to be commercially viable, strains with high ethanol-tolerance are required.

Clostridium thermocellum is an anaerobic, thermophilic bacterium that metabolizes cellulose to ethanol and has been proposed for use in consolidated bio-processing [30-31]. There are many potential advantages to such a strategy. The optimal growth temperature for *C. thermocellum* is between 55°C to 60°C, and these temperatures provide a convenient means for removal of ethanol. Issues of fermentor contamination by ubiquitous microbes is also lessened at higher temperatures. However, a current limitation is the relatively low ethanol tolerance of cellulolytic bacteria. Most strains tolerate less than 1% (w/v) ethanol while yeast tolerate concentrations that are up to 20% (w/v) [32-33].

Although the wild-type strain is sensitive to ethanol concentrations greater than 1% (w/v), certain ethanol-adapted cultures tolerate concentrations as high as 8% (w/v)

[30-32]. Herrero et al. described membrane lipid changes in an alcohol tolerant strain and showed an increased percentage of shorter (<C14) chain fatty acids and monounsaturated fatty acids when compared to the ethanol-sensitive wild-type [34]. In addition, n- and anteiso-branching was higher in the ethanol-adapted strain at the expense of iso- branching. However, there is little detailed information beyond this earlier work concerning the mechanism of ethanol tolerance in *C. thermocellum*.

The membrane functions as a protective barrier for the cell and serves a vital role in energy-generating pathways. It should not be surprising that regulation of membrane properties is essential to cell proliferation. The volume of literature concerned with membrane adaptation is vast, covering a variety of strains and different modes of perturbation. For instance, studies conducted on *Saccharomyces cerevisiae* found that the degree of monounsaturation and fatty acid chain length increased with ethanol exposure [32]. Experiments with *Kloeckera apiculata* showed an increase in 18:1 with a concurrent decrease in 16:1, thus the unsaturation index remained unchanged when grown in the presence of ethanol [32]. On the other hand, bacterial studies with *Bacillus subtilis* and *Clostridium acetobutylicum* revealed an increase in long-chain fatty acids as a response to ethanol treatment [35]. The entire body of literature concerned with the process of lipid adaptation varies between different genera of bacteria and is therefore beyond the scope of this dissertation, however there are reviews dedicated to this topic [35-38]. As shown by the given examples, discrepancies in the result of adaptation have led to different models for explaining ethanol tolerance. Models of adaptation to various insults usually speculate on changes to the membrane physical properties such as membrane fluidity [32, 35].

The concept of homeoviscous adaptation popularized by Sinensky, established a relationship between membrane fatty acid composition and growth temperature [1]. The theory was based on the belief that bacteria alter their lipids to maintain an optimum level of fluidity. Bacteria have been shown to alter the degree of unsaturation, position of branching, and chain length of their fatty acids in response to environmental stimuli. As a general rule, increasing the unsaturation index and decreasing the average fatty acid chain length both serve to increase fluidity of the membranes. Methyl branching of the alkyl chain is another modification that bacteria use to modify the fluidity of the

membrane. The most frequent branch points encountered are anteiso- (ω-3) and iso- (ω - 2), with the latter imparting a greater degree of fluidity [38]. McElhaney proposed that changes within the membrane are the result of a desire to maintain lipid phases, rather than a specific fluidity [39]. Both theories propose that alterations in membrane composition and structure change the physical properties of the membrane, fluidity and phase transitions respectively [32].

It is widely accepted that ethanol has an effect on increasing membrane fluidity [40]. Previously conducted studies on ethanol-adapted strains have concluded that membrane fluidity increases as a result of the adaptation process [40-41]. Chu-Ky *et al.* conducted fluorescence anisotropy studies on *Oenococcus oeni* and reported that ethanol produced an immediate increase in membrane fluidization that was concentration dependent. The study also reported that anisotropy numbers returned to previous values following incubation with ethanol [42]. Studies with *Schizsosaccharomyces pombe* and *Saccharomyces cerevisiae* reported that anisotropy values decreased, corresponding to an increase in membrane fluidity, proportionally with increasing concentrations of ethanol [43].

In order to gain a more direct understanding of the relationship between fatty acid profiles and membrane fluidity, steady-state fluorescence anisotropy experiments were conducted as part of this study. Anisotropy is a measure of rotation by comparing the ratio of fluorescent emission in parallel and perpendicular polarizations. Within the context of this study, anisotropy correlates to the order of the fatty acid alkyl chains which is inversely related to fluidity, thus as the anisotropy value decreases the fluidity of the membrane increases [44]. The rotation is a function of the fatty acid phase transition temperature, T_m. Longer saturated-chain fatty acids have a higher T_m, as a result of greater Van der Waals interactions between acyl chains. Unsaturated fatty acids have lower transition temperatures, than saturated fatty acids of similar length, as a result of the strained geometry caused by the double bond [45]. Below the T_m the alkyl chains are in an ordered state and rotation of the DPH probe is restricted. With increased temperature the alkyl chains become disordered allowing rotation. Rotation of the fluorescent probe lowers the ratio of horizontal and vertical intensities, translating to a lower anisotropy [40]. Above the T_m of fatty acids a phase transition occurs which is

reflected by a sudden increase in membrane fluidity [46]. Due to non-discriminate integration between acyl chains, a decrease in anisotropy represents an increase in bulk flow across the bilayer [44, 46-47].

Membrane fluidity is highly regulated by the fatty acid composition of the bilayer. Fatty acids have a distinct phase transition temperature (T_m) that is characteristic of their chain length and degree of unsaturation. The T_m signifies the temperature at which the alkyl chains transition from an ordered, less fluid, state to a disordered, more fluid, state, and it is a function of the non-covalent interactions between alkyl chains. Therefore, longer fatty acid chains have a higher T_m due to more non-covalent interactions. Unsaturation decreases the T_m due to the bend introduced into the alkyl chain by the double bond [45].

The molecular probe, 1,6-diphenyl-1,3,5-hexatriene (DPH), is an extremely hydrophobic molecule that will insert itself among the fatty acid acyl chains of the membrane bilayer. The DPH probe is excited with polarized light and the anisotropy is a ratio of emission intensities between the horizontal (0°) and vertical (90°) polarizations. Anisotropy is the inverse of fluidity, thus as the anisotropy value decreases the fluidity of the membrane increases [44].

The main objective of this project was to compare the membrane composition of *C. thermocellum* wild-type and an ethanol-adapted strains. Quantitative lipid analysis was achieved by analysis of fatty acid methyl esters and structural analysis was obtained through derivatization to picolinyl esters. Mass spectrometry was used to determine fatty acid structure and a quantitative lipid profile. In addition, functional aspects of the membrane were measured using steady-state fluorescence anisotropy. These experiments showed that ethanol adaptation was the result of fatty acid changes that increased membrane rigidity and counter-acted the fluidizing effect of ethanol.

Chapter 2.2. Experimental

Reagents

Potassium t-butoxide (1.0 M) in tetrahydrofuran (THF), 3-hydroxymethyl pyridine, tridecanal, and hexane were purchased from Sigma (St. Louis, MO, USA). Methanol, methylene chloride, and hydrochloric acid were obtained from Fisher (Pittsburg, PA, USA). Acetyl chloride was obtained from Fluka (Buchs, Switzerland). Sodium hydroxide, sodium bicarbonate, and potassium carbonate were purchased from J.T. Baker (Phillipsburg, NJ, USA). Ethyl ether was obtained from EMD (San Diego, CA, USA). Anthracene was purchased from Acros (Morris Plains, NJ, USA). Ethanol was purchased from Decon Laboratories, Inc. (King of Prussia, PA, USA). GLC-411 lipid standard, 5,8,11,14-eicosatetraenoic acid, and 4,7,10,13,16,19-docosahexaenoic acid was purchased from Nu-Chek Prep, Inc. (Elysian, MN, USA), and 1,6-diphenyl-1,3,5-hexatriene (DPH) was purchased from Molecular Probes (Eugene, OR, USA).

Equipment and supplies

Savant instruments (Holbrook, NY, USA) speedvac concentrator (model SC110A) with refrigerated condensation trap (model RT490). Eppendorf (Hauppauge, NY, USA) centrifuge (model 5415A) with a F45-24-11 fixed angle rotor. Fisherbrand 2.0 mL polypropylene microcentrifuge tubes (Thermo Fisher Scientific Inc., Waltham, MA, USA). Eppendorf (Hauppauge, NY, USA) Research Adjustable-volume pipettes.

Bacterial cultures and growth

Clostridium thermocellum ATCC 27405 was obtained from the American Type Culture Collection. The wild-type (ethanol-sensitive) strain was adapted to ethanol as previously described [48]. Cultures of wild-type and ethanol-adapted cells (13 L each) were grown in a basal medium as previously described [48]. Briefly, the media consisted of the following ingredients: 10.8 mM Na_2HPO_4, 11.05 mM KH_2PO_4, 9.35 mM NH_4Cl, 3.79 mM $(NH_4)_2SO_4$, 0.44 mM $MgCl_2 \cdot 6H_2O$, 0.27 mM $CaCl_2$, 2.0 g/L yeast extract, 0.5 g cysteine, 1 mg resazurin, 10 mL vitamin standard mixture, and 5 mL of modified micromineral mixture stock supplemented with 10 mg of $Na_2WO_4 \cdot 2H_2O$ and 1 mg Na_2SeO_4 L^{-1} stock. The media was adjusted with 10% NaOH to pH 6.7, then autoclaved for 10 minutes. The solution was sparged with CO_2 until reaching room temperature. An anaerobic solution of Na_2CO_3 was added for a final concentration of 4 gL^{-1}. The solution

was autoclaved for an additional 20 minutes then supplemented with cellobiose for a final concentration of 4 gL^{-1}. Both strains were harvested during their respective growth phases, washed with 50 mM Tris (pH 7.5) and stored at -80°C until analysis.

Saponification of fatty acids

Aliquots (approximately 15 mg cell dry weight) of *C. thermocellum* whole cells were washed three times with 1 mL portions of diH$_2$O, centrifuged (16,100x*g*, 5 min, 25°C) and the supernatants discarded. The cell pellets were placed at 0°C overnight and then vacuum-dried for 24 hrs at 25°C. The saponification methods were based on a previous description [49]. Sodium hydroxide (1 mL of 3 M) was added to the dried cells. The mixture was vortexed and heated to 90°C for 1 hr, cooled to room temperature, and 2 mL of 3.25 M HCl was added and reheated at 90°C for 10 min. After cooling to room temperature, the lipids were extracted three times with 1 mL portions of 1:1 (v/v) hexane:diethyl ether. The organic phases were combined and evaporated to dryness under a stream of N$_2$ at room temperature.

Fatty acid derivatization methods

Fatty acid methyl ester (FAME) procedures were adapted from previous studies [50]. Methanol:acetyl chloride (50:1 (v/v), 5 mL total) was added to the extracted free fatty acids. The solution was mixed and heated at 60°C for 1 hr. After heating, 3 mL of 6% K$_2$CO$_3$ was added, and the FAME products were extracted 1 mL of hexane containing 0.1 mg anthracene (internal standard). Extracted material (1 μL) was used for GC/MS analysis. An overview for fatty acid analysis is provided as a work-flow diagram (Figure 2.1).

Fatty acids were trans-esterified to picolinyl esters using a method adapted from Destaillats et al. [51]. The hexane phase from the FAME procedure was evaporated to dryness under a stream of N$_2$ at room temperature and 1 mL of methylene chloride was added to resolvate the methyl esters. A mixture of 200 μL 3-hydroxymethylpyridine and 100 μL of 1.0 M potassium tert-butoxide in THF were allowed to react for 2 min. This mixture was then added to the FAME methylene chloride solution. The reaction was mixed and heated at 45°C for 1 hr. After cooling to room temperature, 1 mL of 2.5%

C. thermocellum whole cells

↓ saponification

Free fatty acids

↓ methylation

Fatty acid methyl esters
(FAMEs)

GC/MS ↓   transesterification ↓

Fatty acid profiles   Picolinyl esters

↓   ↓ GC/MS

Quantification   Fatty acid profiles

↓

Structure identification
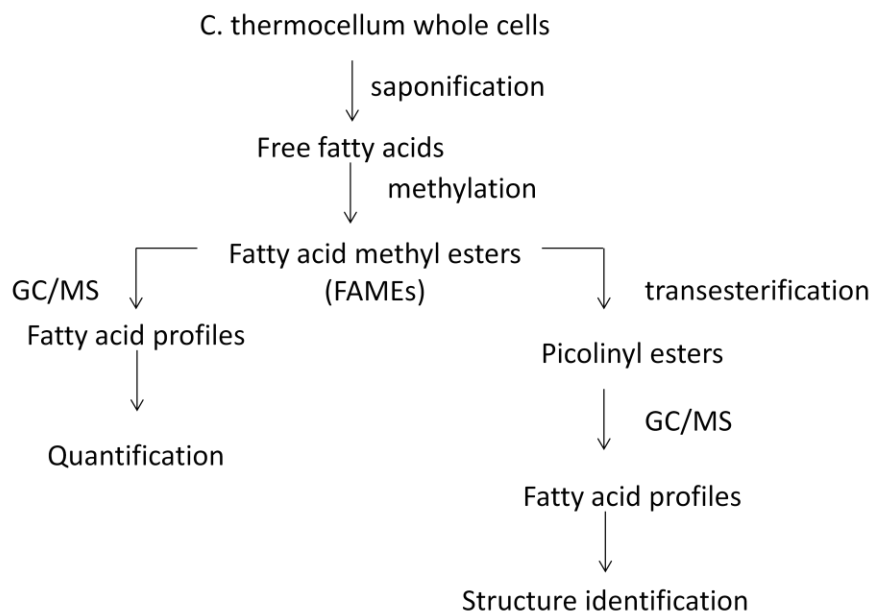
Figure 2.1. Schematic representation of derivatization procedures.

45

NaHCO$_3$ was added and the methylene chloride layer removed. The organic layer was reduced to approximately one-quarter original volume under a stream of N$_2$ at room temperature and 1 μL was injected for analysis. All derivatization methods were validated by analysis of 5,8,11,14-eicosatetraenoic acid (arachidonic acid), 4,7,10,13,16,19-docosahexaenoic acid, and *Escherichia coli (E. coli)* whole cells.

Gas chromatography/mass spectrometry

Fatty acid methyl and ethyl ester derivatives were analyzed using a Varian Saturn 3 GC/MS system equipped with a ZB-5ms capillary column 30 m x 0.25 mm i.d., 0.25 μm film (Phenomenex USA, Torrance, CA). The temperature program was: 130°C to 170°C at 4°C/min, 170°C to 215°C at 2.7°C/min, 215°C for 3.34 min, with a total analysis time of 30 min. Carrier gas head-pressure was set to give a flow rate of 1 mL/min, with a 50:1 split. The injector and transfer line were maintained at 240°C and the manifold temperature was 210°C. Ionization was accomplished by electron impact (EI) at 70 eV, with a 3 minute filament delay. Spectra were generated from full scans m/z 50 to 650, at a scan rate of 1 analytical scan per second and the background mass was set at m/z 49. The GC/MS method was optimized to provide peak resolution for FAMEs from the GLC-411 standard.

Fatty acid picolinyl ester derivatives were analyzed on the same instrument with the following temperature program: 150°C for 4 min., 150°C to 280°C at 20°C/min, 280°C for 19.5 min with a total analysis time of 30 min. All other parameters were as described above except that the filament delay was 10 min and spectra were generated from full scans from m/z 50 to 500.

Chemical ionization (CI) experiments were conducted on the same instrument using the FAME GC/MS program, except the manifold temperature was reduced to 160°C. The MS parameters were as follows: selected-ejection chemical ionization (SECI) mode with acetonitrile as the reagent gas (Figure 2.2)[52], 100 μsec automatic-reaction control (ARC) time, 1000 μsec ionization time, 128 msec reaction time, m/z 15 ionization storage level, 7.5 V$_{0-p}$ reagent gas ion ejection amplitude, m/z 37.0 CI reaction storage level. Spectra were generated by full scans from m/z 80 to 650. All chromatograms were analyzed using Wsearch32 2005 software (version 1.6.2005; Melbourne, Australia).

$$CH_3CN + e^- \longrightarrow CH_3CN^+ + 2e^-$$

$$CH_3CN^{+\bullet} \longrightarrow [CH_2CN]^+ + H^\bullet$$

$$CH_3CN^{+\bullet} + CH_3CN \longrightarrow [CH_3CNH]^+ + [CH_2CN]^\bullet$$

$$[CH_2CN]^+ + CH_3CN \longrightarrow [C_3H_4N]^+ + HCN$$
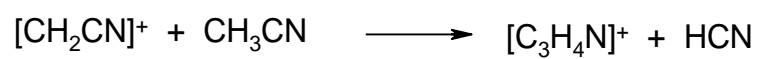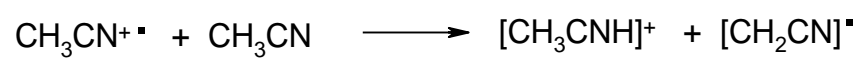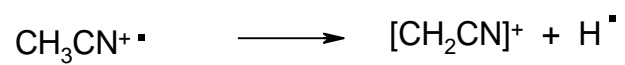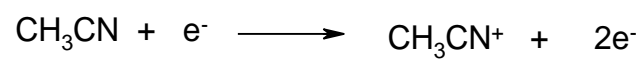
Figure 2.2. Chemical ionization of acetonitrile.

Calculations

Average ($\bar{x}$)

$$<\bar{x}>= \frac{\sum n_1 + n_2 + n_3 + ... + n_k}{n_k}$$

eq. 2.1

Standard deviation (s)

The standard deviation represents the difference between replicate measurements.

$$s = \sqrt{\frac{\sum (x_i - \bar{x})^2}{n-1}}$$

eq. 2.2

Average deviation ($\bar{d}$)

$$\bar{d} = \frac{\sum |d_i|}{n}$$

eq. 2.3

Relative average standard deviation (d_{rel})

$$d_{rel} = \frac{\bar{d}}{\bar{x}}$$

eq. 2.4

F-test for comparison of two variances

The null hypothesis is stated that there is no significant difference between the two variances. If $F_{calc} > F_{table}$, p, v_1, v_2 then the null hypothesis is rejected and there is a significant difference between the two populations. $F_{calc} > 1$, $v_1 = n_1-1$, $v_2 = n_2-1$

$$F_{calc} = \frac{v_1}{v_2} = \frac{s_1^2}{s_2^2}$$

eq. 2.5

Pooled standard deviation (sp)

$$sp = \sqrt{\frac{(n_1 - 1)s_1^2 + (n_2 - 1)s_2^2 + ... + (n_k - 1)s_k^2)}{n_1 + n_2 + ... + n_k - k}}$$

eq. 2.6

t-Test for comparison of two experimental means

$$\pm t_{calc} = \frac{(\overline{X}_1 - \overline{X}_2)}{sp}\sqrt{\frac{n_1 n_2}{n_1 + n_2}}$$ eq. 2.7

Quantification of FAMEs (Conc.$_{FAME}$) was performed by comparing the area counts of the various fatty acid species (Area$_{FAME}$) with that of the internal standard, anthracene (Area$_{IS}$):

$$Conc._{FAME} = \frac{Area_{FAME} \times Conc._{IS}}{Area_{IS}}$$ eq. 2.8

The calculated Conc.$_{FAME}$ value is then divided by the dry cell weight (DCW) to obtain a concentration of FAME species normalized to the starting concentration of cells.

$$Conc._{FAME/DCW} = \frac{mgFAME}{DCW}$$ eq. 2.9

The distribution of FAMEs per *C. thermocellum* strain was determined by dividing area counts for each FAME species by the total observed FAME area count:

$$\% FAME = \frac{Area_{FAME}}{\sum .FAME_{Area}} \times 100$$ eq. 2.10

Statistical analysis for comparison of fatty acids between the two strains employed the paired t-test. Comparisons were limited to equivalent fatty acids between the two species, i.e. WT n-14:0 vs. EA n-14:0. If $t_{calc} > t_{table}$ (p<0.05, two-tailed), then the null hypothesis (HO), HO = μ$_1$ + μ$_2$, was rejected and there was a significant difference between the means of the two fatty acid species (Table 2.1).

DPH-labeling of whole cells and anisotropy

The anisotropy method was adapted from a previously described procedure [53]. Approximately 15 mg of concentrated whole cells were washed with three 1 mL aliquots of 50 mM Tris-HCl (pH 7.5) by centrifugation (16,100x*g*, 5 min, 25°C) and the supernatants discarded. After the final washing, the cells were resuspended in 1.5 mL of 50 mM Tris (pH 7.5) and 100 μL 0.1 mM 1,6-diphenyl-1,3,5-hexatriene (DPH) in THF. The mixture was incubated at 65°C for 1 hr and then at 4°C overnight. The cells were

Table 2.1. Fatty acid composition and distribution of *C. thermocellum* cells.

Species (Structure)[a]	FAME (μg/mg DCW)[c]		FAME (%)[c]		Percent Change[d,e]
	WT	EA	WT	EA	
13-Methyl-tridecanoic acid (i-14:0)	1.02±0.1	0.46±0.2	1.06±0.3	0.46±0.1	44.04*
Tetradecanoic acid (n-14:0)	1.26±0.2	0.68±0.4	1.38±0.4	0.65±0.2	47.09*
Plasmalogen i-14:0 (P i-14:0)	1.06±0.02	0.49±0.1	1.10±0.3	0.60±0.3	54.69*
Plasmalogen n-14:0 (P n-14:0)	1.16±0.2	0.38±0.2	1.29±0.3	0.66±0.2	50.88*
Plasmalogen 15:0 (P 15:0)	1.01±0.2	0.84±0.3	1.11±0.4	1.00±0.2	90.43
14-Methyl-pentadecanoic acid (i-16:0)	23.99±1.7	13.28±1.2	28.21 ±1.9	20.98 ±1.3	74.38*
Hexadecanoic acid (n-16:0)	18.73±3.2	9.69±0.6	21.77 ±0.6	16.22 ±1.2	74.51*
Plasmalogen i-16:0 (P i-16:0)	12.65±2.4	10.99±1.0	14.540.4	18.75 ±3.5	128.98
Plasmalogen n-16:0 (P n-16:0)	8.70±1.8	8.37±0.7	9.94±0.4	13.46 ±1.2	135.53*
15-Methyl-hexadecanoic acid (i-17:0)	3.89±0.6	4.46±0.3	4.43±0.4	7.61±0.9	171.91*
Heptadecanoic acid (n-17:0)	2.52±1.0	2.02±0.4	2.93±0.6	2.98±0.5	101.68
Plasmalogen i-17:0 (P i-17:0)	1.29±0.3	1.55±0.4	1.51±0.3	2.22±0.5	147.17
Plasmalogen n-17:0 (P n-17:0)	1.03±0.4	0.90±0.3	1.19±0.2	1.45±0.3	122.36
16-Methyl-heptadecanoic acid (i-18:0)	6.62±3.0	5.47±0.5	7.38±2.29	9.42±0.4	127.62
Octadecanoic acid (n-18:0)	1.91±0.5	1.73±0.1	2.17±0.5	3.52±0.7	162.40
Total lipid (μg/mg DCW)[b]	86.84±2.1	61.32±0.8			

[a] Number of carbons:degree of unsaturation. i- denotes iso-branching and n- denotes normal or straight chain.

[b] Comparisons made on % FAME basis due to differences in μg/mg DCW between WT and EA.

[c] Values are averages of four replicates ± SEM.

[d] Values represent change in EA relative to WT cells.

[e] Values with asterisks (*) are statistically significantly different ($p \leq 0.05$, n=4).

then centrifuged (16,100xg, 5 min, 25°C) and the supernatant discarded to remove any residual DPH. The pellet was resuspended in 10 mL of 50 mM Tris (pH 7.5) or 10 mL of 50 mM Tris (pH 7.5) with 5% (w/v) ethanol.

The fluorescence anisotropy of DPH-labeled cells was measured with a Varian Cary Eclipse fluorescence spectrophotometer (Walnut Creek, CA, USA), equipped with a custom view cell (Thar Technologies, Pittsburg, PA, USA) and manual polarizer accessory (part #00-100761-00) for both excitation (350 nm, slit width of 5 nm) and emission (452 nm, slit width of 10 nm) (Figure 2.3) [54]. The source was a Xenon pulse lamp (200-900 nm operating wavelength range with ±1.5 nm accuracy and ±0.2 nm reproducibility) and one second average sampling time was employed. Temperature of the view cell was modulated with heating tape and an Omega controller (model CN9000A). Each sample was heated from 24°C to 70°C with five readings taken every 2°C over the temperature ramp cycle. These five readings were averaged together to represent the average anisotropy ($<r>$) for the corresponding temperature. The reported data are the average and relative standard deviation from the average of three analytical replicate samples. The anisotropy (r) was calculated:

$$r = \frac{\left(I_{VV} - gI_{VH} \right)}{\left(I_{VV} + 2gI_{VH} \right)} \qquad\qquad \text{eq. 2.11}$$

where I_{VV} is the intensity when excitation and emission are polarized vertical, I_{VH} is the intensity when excitation is polarized vertical and emission is polarized horizontal, g is the grating factor.

The grating factor (g) was determined for each sample prior to heating:

$$g = \frac{I_{HV}}{I_{HH}} \qquad\qquad \text{eq. 2.12}$$

where I_{HV} is the intensity when excitation is polarized horizontal and emission is polarized vertical, I_{HH} is the intensity when excitation and emission are polarized horizontal. Essentially the g factor is a correction for the monochromator transmission efficiency [41]. The g factor is a function of sample and view cell alignment, therefore it was determined prior to analysis of each sample.
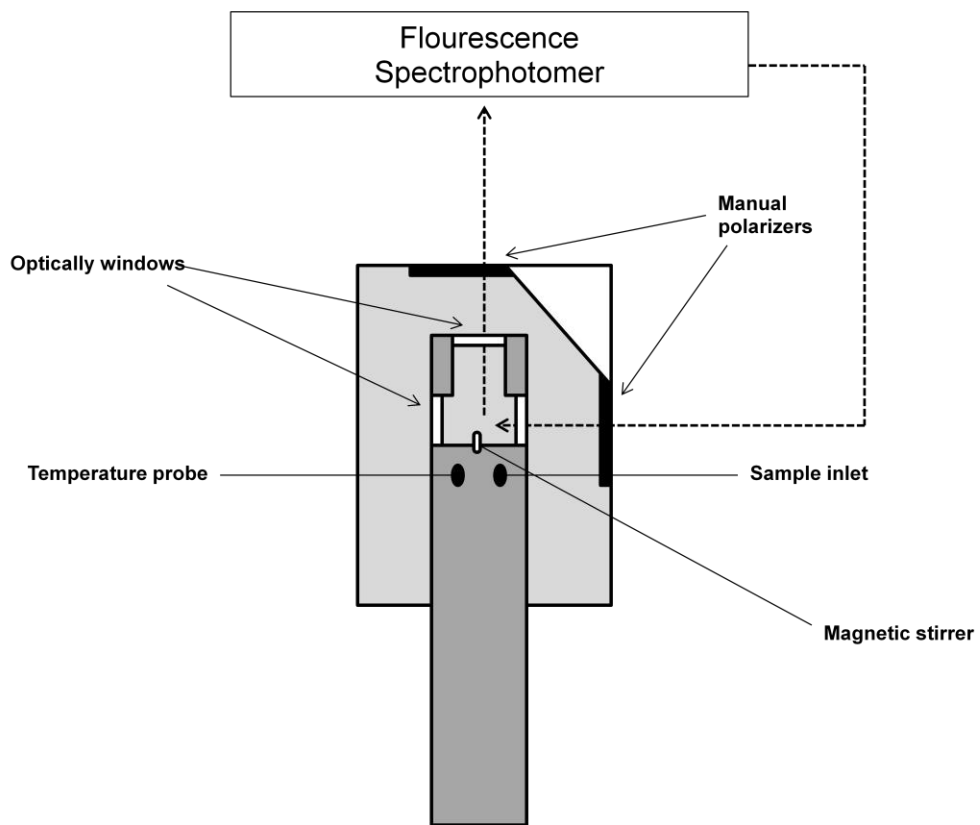
Figure 2.3. Schematic of anisotropy apparatus.

Chapter 2.3. Results

GLC-411 standard

Previous fatty acid studies with *C. thermocellum* used packed columns which resulted in co-eluting peaks that hindered quantification and species identification [34]. The development of a GC method that provided resolution of a broad range of fatty acid species was critical. The GLC-411 standard was chosen to give a wide range of FAMEs both in chain length, saturation and unsaturation (Table 2.2). The objective was to develop a method that could provide resolution of the thirty-one FAMEs contained in the GLC-411 standard. A number of published GC methods were tested, however independently none of these methods provided resolution over the entire FAME spectrum [7, 55-57]. However, two established methods provided superior resolution over a portion of the GLC-411 standard range. A method published by the American Oil Chemists' Society (AOCS) [58] gave separation of FAMEs C_8 to C_{18}, however the later compounds had poor peak shape. A FAME method (application 1774-GC) published by Varian (Varian, Inc., Lake Forest, CA, USA) gave poor results with short chain fatty acids, but worked well for longer chain fatty acids. The AOCS and Varian methods had a common temperature profile around 215°C, therefore the two methods were coupled at this temperature to provide resolution over the entire FAME spectrum. Although the developed GC method provided greater resolution than those previously evaluated, the separation of some geometric isomers was not possible (Figure 2.4). The three geometric isomers of 18:1 (methyl oleate (18:1Δ9), methyl petroselinate (18:1Δ6), and methyl vaccinate (18:1Δ7); two isomers of 20:3 (methyl eicosatrienoate (20:3Δ11,14,17) and methyl homogamma linolenate (20:3Δ8,11,14); and three isomers of 20:1 (methyl 5-eicosenoate (20:1Δ5), methyl 8-eicosenoate (20:1Δ8) and methyl 11-eicosenoate (20:1Δ11) each co-eluted. Further improvement of the temperature ramp to fully resolve these isomers was not undertaken.

***C. thermocellum* dry cell weights**

A specific goal of this project was the direct comparison of fatty acids composition between WT and EA strains, therefore it was necessary to normalize the cellular concentrations for successive reactions. Reaction standardization based on

Table 2.2. List of FAMEs within GLC-411 standard.

Common Name	Chain	FAME Derivative (MW)
Methyl Octanoate	8:0	158
Methyl Decanoate	10:0	186
Methyl 11-Dodecenoate	12:1	212
Methyl Laurate	12:0	214
Methyl Myristoleate	14:1	240
Methyl Myristate	14:0	242
Methyl Palmitoleate	16:1	268
Methyl Palmitate	16:0	270
Methyl Linolenate	18:3	292
Methyl Gamma Linolenate	18:3	292
Methyl Linoleate	18:2	294
Methyl Oleate	18:1	296
Methyl Petroselinate	18:1	296
Methyl Vaccenate	18:1	296
Methyl Stearate	18:0	298
Methyl Arachidonate	20:4	318
Methyl 11,14,17-Eicosatrienoate	20:3	320
Methyl Homogamma Linolenate	20:3	320
Methyl 11,14-Eicosadienoate	20:2	322
Methyl 5-Eicosenoate	20:1	324
Methyl 8-Eicosenoate	20:1	324
Methyl 11-Eicosenoate	20:1	324
Methyl Arachidate	20:0	326
Methyl Docosahexaenoate	22:6	342
Methyl 7,10,13,16-Doscosatetraenoate	22:4	346
Methyl 13,16,19-Docosatrienoate	22:3	348
Methyl 13,16-Docosadienoate	22:2	350
Methyl Erucate	22:1	352
Methyl Behenate	22:0	354
Methyl Nervonate	24:1	380
Methyl Lignocerate	24:0	382
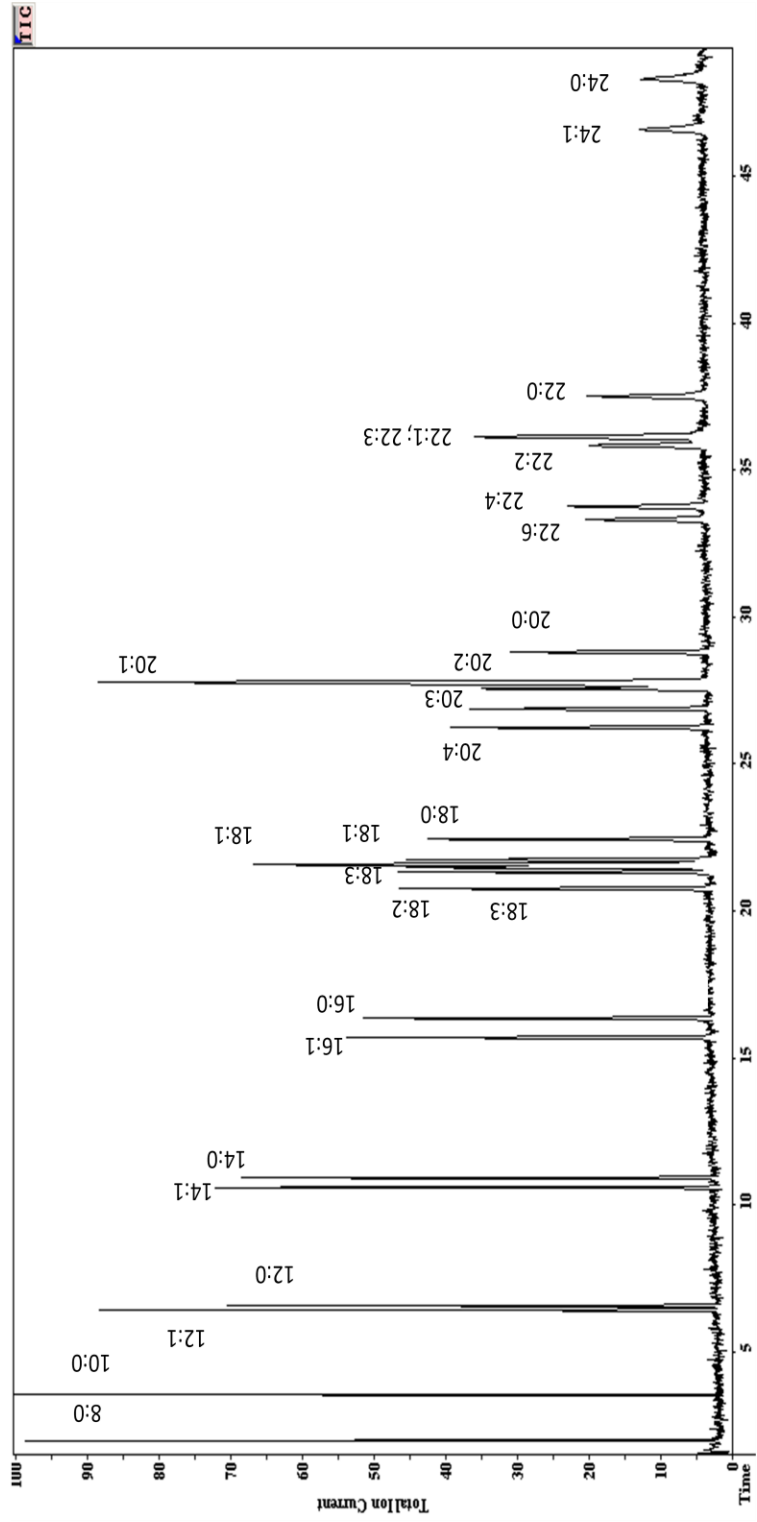
Figure 2.4. Chromtogram of GLC-411 std.

volume was not possible, due to the two strains growing at different rates and the final cellular concentration per volume, as measured by optical density at 600 nm (OD_{600}), varied at the time of harvest. Therefore, reactions based on addition of a standard volume might lead to erroneous differences, since the number of initial cells in the reaction would vary depending on the strain.

The solution was to normalize each reaction based on a dry cell weight. The first step was to examine the time frame needed to fully dry an aliquot of cells. The experiment consisted of freeze drying a fixed volume of cells for a period of time and measuring the weight loss every 12 hrs. The cells were deemed fully dry when the weight loss between successive measurements decreased to a minimum. Each weighing was done in triplicate, the averages minus the empty tube weight subtracted and standard deviations for each set are shown in Tables 2.3, 2.4 and 2.5.

Micro-centrifuge tubes were set-up with the following contents: tubes 1-3 contained 100 μL of 50 mM Tris-HCl buffer (pH 7.5), tubes 4-6 had 100 μL of *C. thermocellum* WT whole cells, and 100 μL of *C. thermocellum* EA whole cells were in tubes 7-9. The dry weight of 50 mM Tris-HCl was required since the cells were solvated in this solution. Thus after drying the buffer salts, would remain on the cells and therefore need to be subtracted from the dry cell weight. The following two tables would have the total average Tris-HCl weight subtracted.

During sampling it was observed that as a result of cell clumping the aliquots could contain an unequal distribution of cells and thus Tris-HCl. This could introduce errors during replicate reactions since it was assumed that the concentration of cells and Tris-HCl would be constant in a measured volume. The solution was to remove the Tris-HCl washing with diH_2O before drying the cells. Subtraction of Tris salts from the dry cell weights was therefore abandoned after cells underwent washings in diH_2O.

Fatty acid structural determination

Earlier *C. thermocellum* studies used analytical approaches with limited capabilities [34]. To enhance these previous studies, we used mass spectrometry to identify and quantify membrane lipids. Upon analysis of *C. thermocellum* WT and EA strains the developed GC temperature ramp provided separation of FAME analytes,

Table 2.3. 50 mM Tris-HCl dry weight (mg) per 100 μL.

Tube #	12 hr	24 hr	36 hr
1	0.577±0.133	0.467±0.074	0.520±0.061
2	0.640±0.082	0.480±0.053	0.483±0.067
3	0.847±0.095	0.613±0.040	0.550±0.071

Table 2.4. *C. thermocellum* WT dry weight (mg) per 100 μL.

Tube #	12 hr	24 hr	36 hr
4	2.450±0.140	2.337±0.133	2.240±0.020
5	2.880±0.030	2.677±0.192	2.677±0.080
6	3.290±0.106	2.807±0.076	2.850±0.065

Table 2.5. *C. thermocellum* EA dry weight (mg) per 100 μL.

Tube #	12 hr	24 hr	36 hr
7	5.340±0.032	5.130±0.081	5.193±0.012
8	6.140±0.072	5.750±0.12	5.853±0.046
9	4.273±0.115	3.940±0.075	3.977±0.010
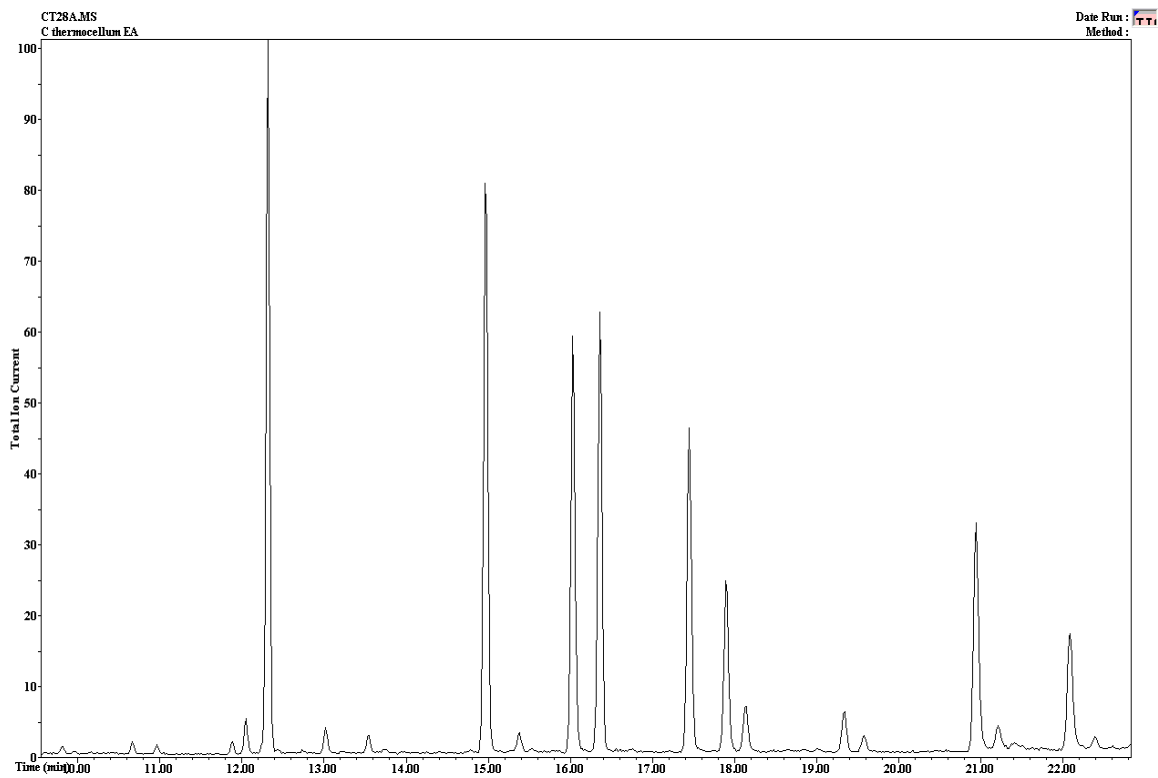
Figure 2.5. Chromatogram of *C. thermocellum* FAMEs.

facilitating accurate quantification the each species (Figure 2.5). Fatty acid structural identification for *C. thermocellum* was complicated by the presence of multiple pairs of peaks that contained nearly indistinguishable mass spectra. Due to the fact that these peaks were chromatographically separated, but displayed identical molecular ions masses, they were believed to be geometric isomers of 14:0, 16:0, 17:0, and 18:0 alkyl chains.

Electron-impact (EI) ionization of FAMEs fails to provide characteristic fragmentation patterns that provide structural elucidation, because EI spectra that are dominated by low molecular weight fragments and contain relatively modest amounts of intact molecular ion. Fragmentation by EI provides a statistical distribution of ions based on the stability of the resulting fragments. Highly stable fragments are represented more frequently in mass spectra. In addition, bond rearrangement regularly occurs to produce stable products. For these reasons alternative methods of derivatization were necessary for structural identification.

A variety of derivatization reagents are available that provide characteristic fragmentation patterns [59-63]. Since no prior mass spectral data about the structure of the *C. thermocellum* fatty acids was available, a derivatization method applicable to a broad range of compounds was necessary. Transesterification with 3-hydroxymethylpyridine, to form picolinyl esters, was chosen for derivatization in the hopes that it might provide insight into the structure of the punitive plasmalogen compounds, in addition it provided a simple method for derivatization and the mild reaction conditions helped minimize fatty acid degradation. The nature of the picolinyl ester resulted in charge remote fragmentation products allowing structure elucidation of the fatty acid alkyl chains.

Mass spectra for the picolinyl ester products from the 16:0 FAME reactants (Figures 2.6 & 2.8). Each mass spectrum gives a moderately abundant molecular ion m/z 347, allowing proper fatty acid identification. Picolinyl fragmentation of straight-chain fatty acids provides a repeating pattern of $[M]^+$-$(CH_2)_n$ mass units, after loss of the terminal methyl group $[M-15]^+$. The spectrum represents the successive loss of methylene groups, 14 atomic mass units (amu) down to the McLafferty ion at m/z 151. Figure 2.7 illustrates common fragmentation pathways for straight-chain picolinyl esters.
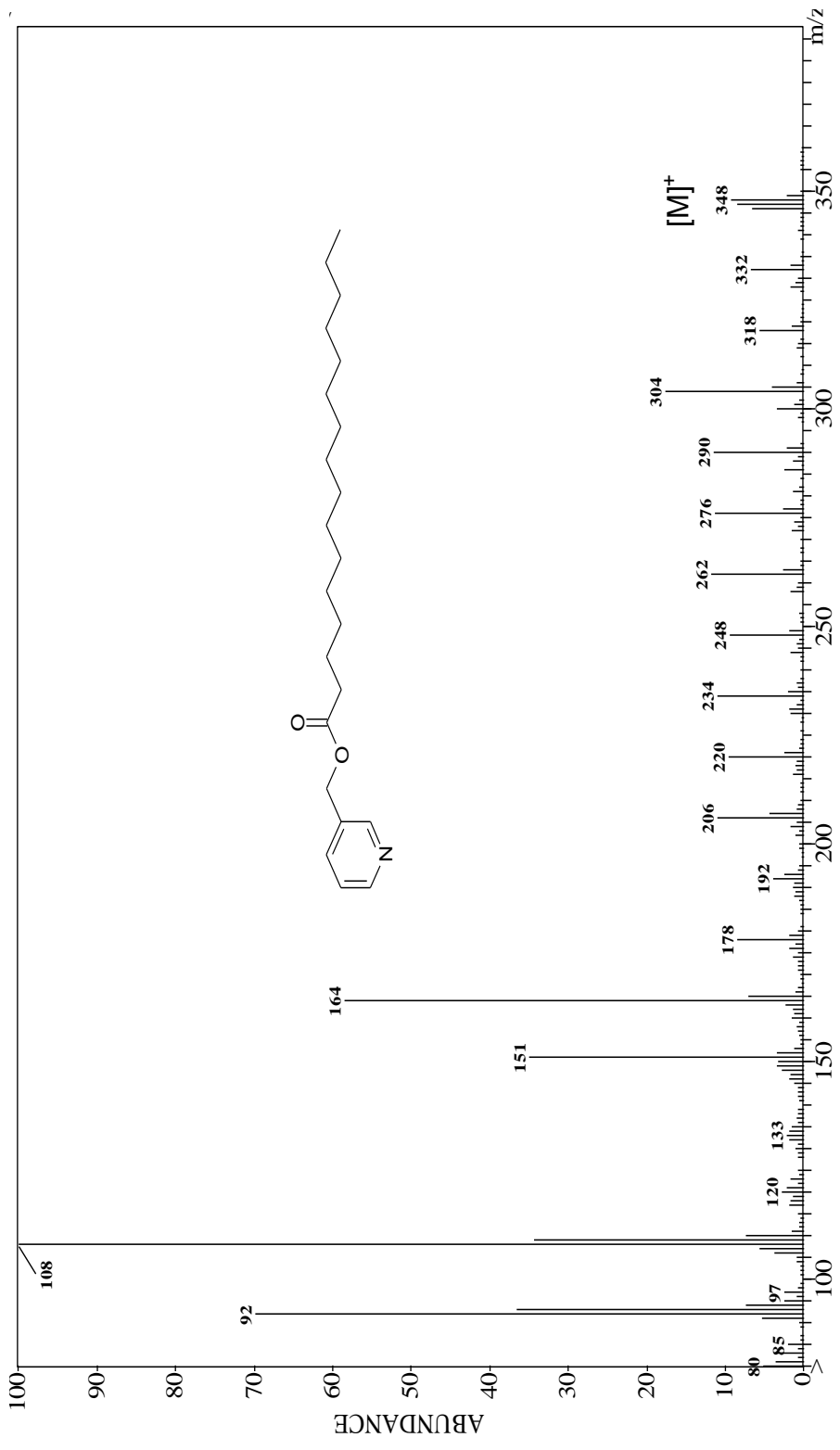
Figure 2.6. Mass spectrum of picolinyl hexadecanoate.
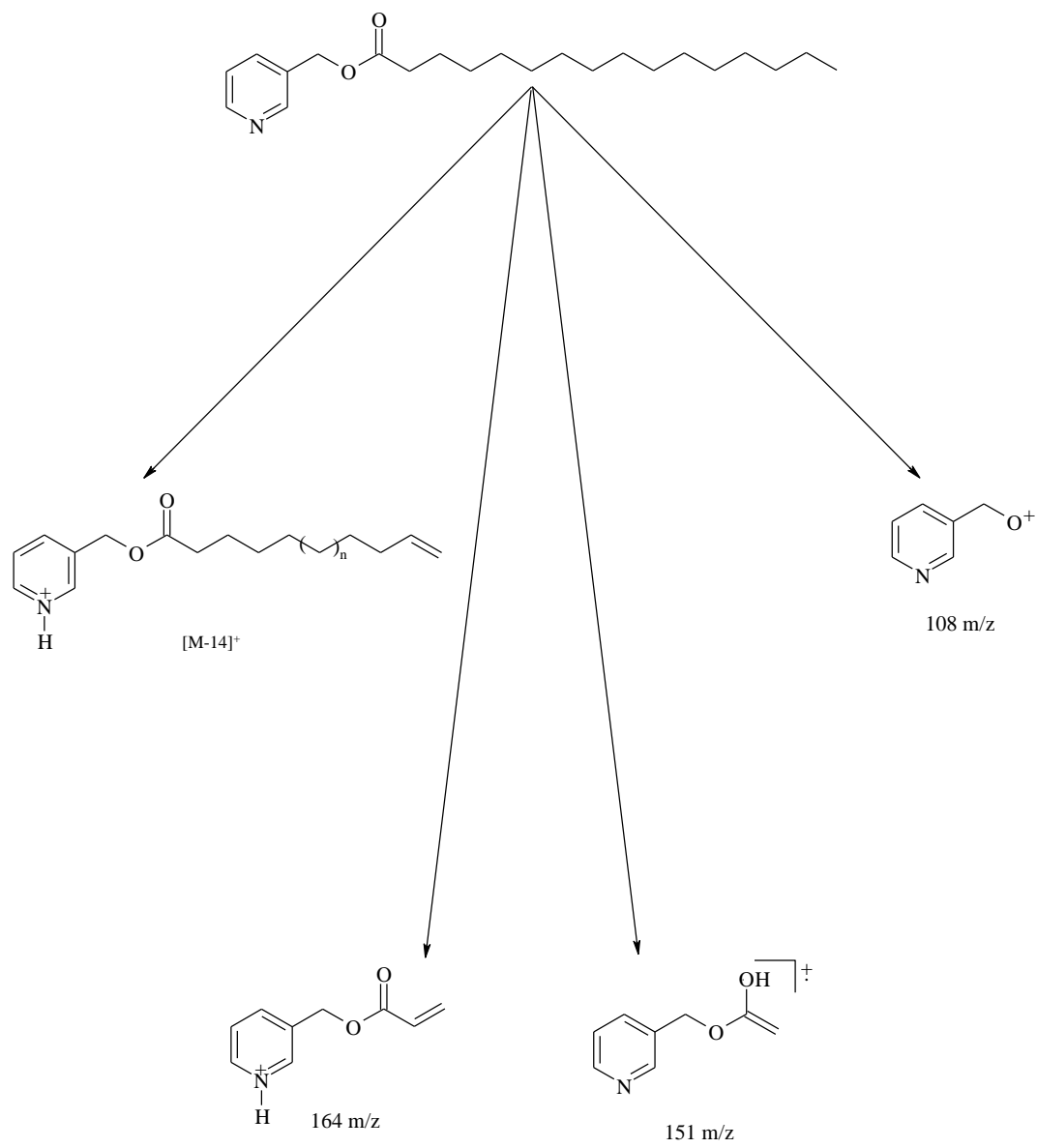
Figure 2.7. Common fragmentation pathways for straight-chain picolinyl esters.
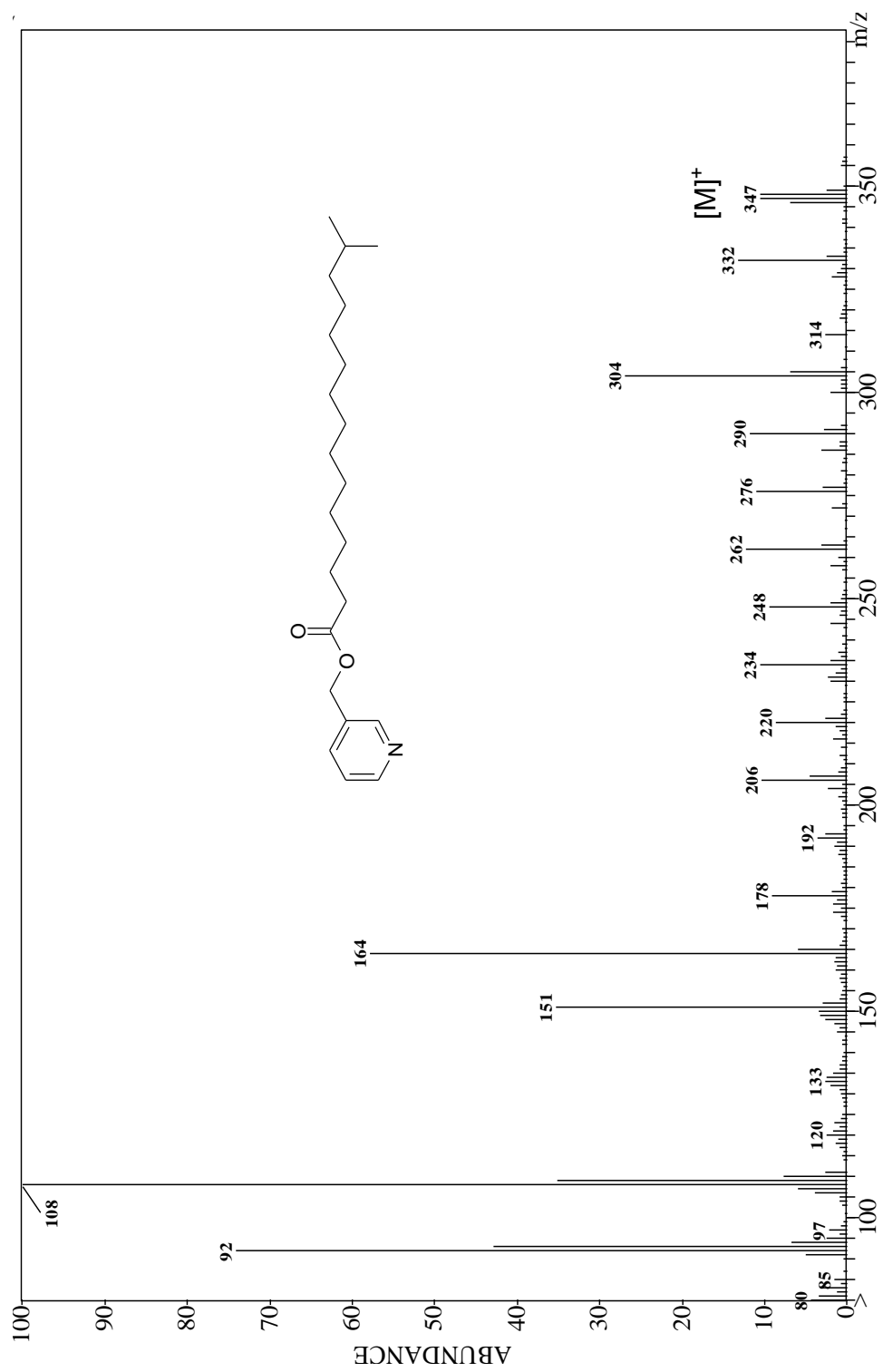
Figure 2.8. Mass spectrum of picolinyl 14-methyl-pentadecanoate.

The mass spectrum for picolinyl 14-methyl-pentadecanoate (Figure 2.8), the iso-methyl is lost to produce m/z 332, however the next mass in the series is m/z 304 which represents a loss of 28 amu. The loss of 28 amu, as opposed to the regular 14 amu, indicates a methyl branch point along the alkyl chain. The absence of an ion at m/z 318 is indicative of an iso- branch point. Fragmentation mechanisms for iso-methyl branched fatty acid picolinyl esters are shown in Figure 2.9. This approach was used to identify the structures of fatty acids with other chain lengths for both WT and EA *C. thermocellum* strains (data not shown). Analysis of both *C. thermocellum* strains through picolinyl transesterification yielded equivalent fatty acid structural profiles, consisting of iso- and normal branched alkyl chains.

In order to confirm the formation of these dimethyl acetals an aldehyde, tridecanal, was reacted through the FAME procedure. Synthesizing a dimethyl acetal standard in this manner should produce mass spectra analogous to those observed from the plasmalogens. The resulting mass spectrum from the dimethyl tridecacetal exhibits a peak at m/z 213, representing [M-31]$^+$ loss of a methoxy group and a base peak at m/z 75, the fragment of the dimethyl head-group (Figure 2.10). Comparison of published mass spectra from dimethyl acetals generated from plasmalogens provided further support for the fragmentation pattern and the presence of plasmalogens within the *C. thermocellum* membrane [64].

To further verify the formation of acetals from plasmalogens, chemical ionization (CI) experiments were conducted using acetonitrile as a reagent gas [65-68]. Comparisons of mass spectra from the punitive plasmalogen (P 16:0) observed from *C. thermocellum* reactions, to those generated from methylation reactions with tridecanal were made. The resulting mass spectra from hexadecan-1-al (P 16:0) and tridecanal provide analogous fragmentation patterns (Figure 2.11). Since CI imparts a softer ionization process to the analyte, than EI, it should facilitate less fragmentation and provide greater structural information. Both spectra contain minor molecular ion peaks, [M+H]$^+$, at m/z 287 and 244 respectively. As with EI generated spectra, fragments generated from the loss of a methoxy group, [M-31]$^+$, are present at m/z 255 and 213. The ion from the dimethyl head-group fragmentation discussed in EI spectra was not
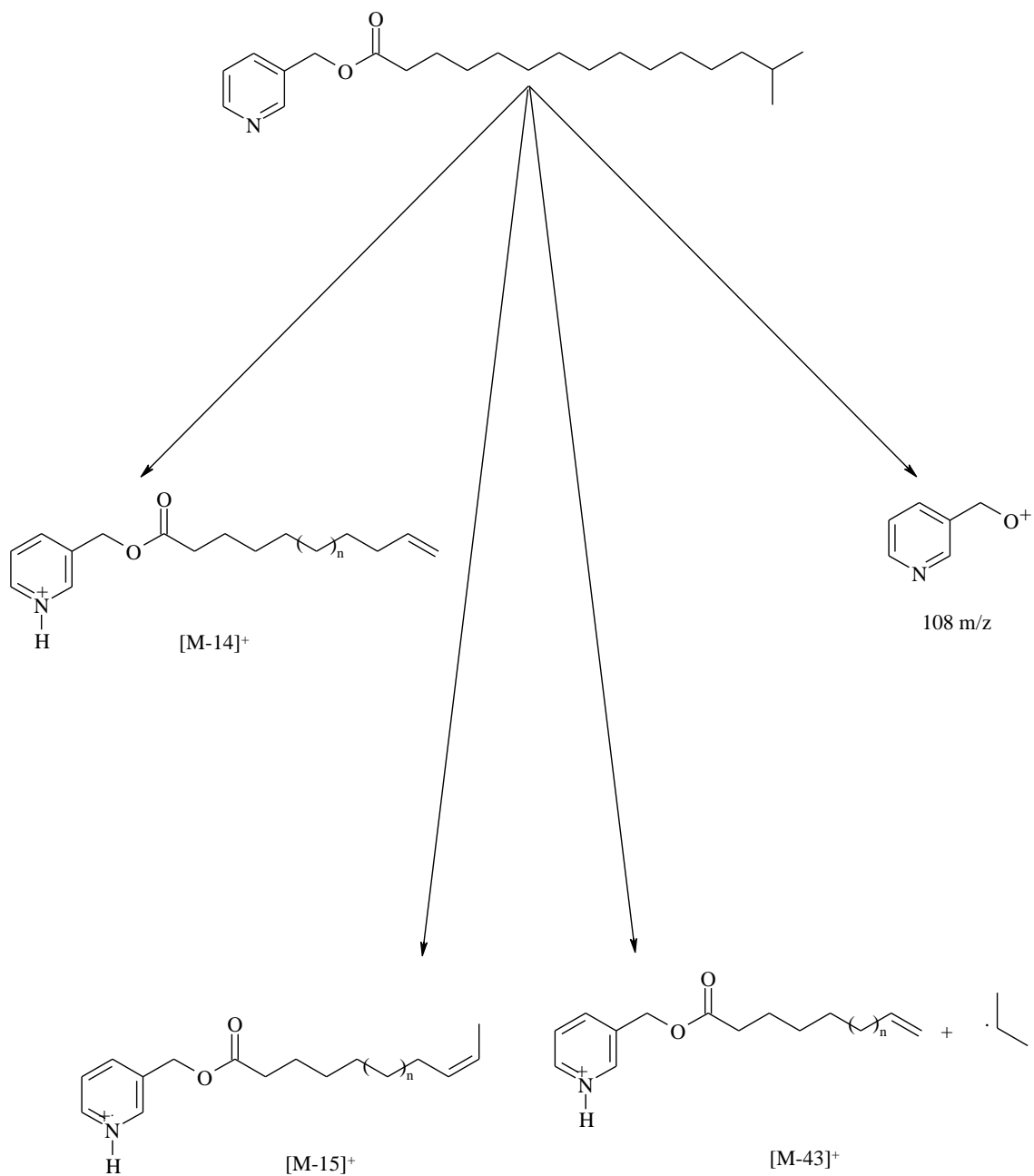
Figure 2.9. Common fragmentation pathways for iso-branched picolinyl esters.
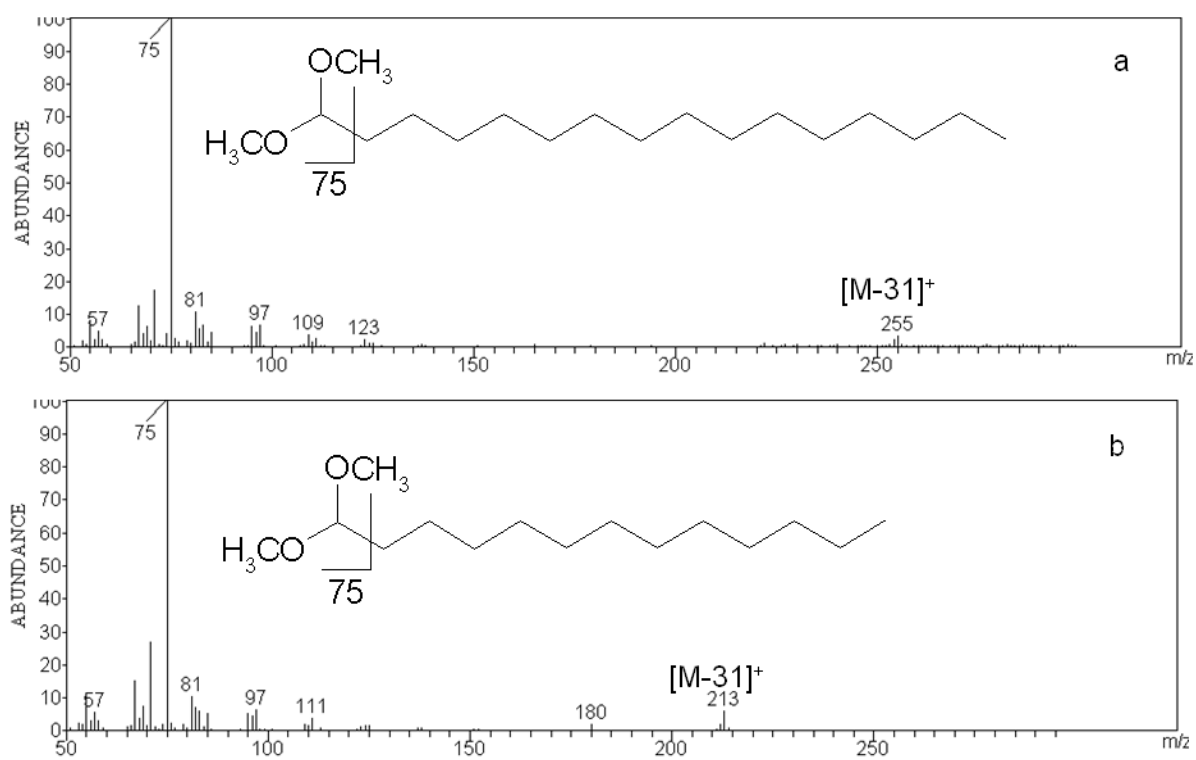
Figure 2.10. Mass spectra from EI experiments from (a) dimethyl acetal of hexadecan-1-al (P 16:0) and (b) dimethyl acetal of tridecanal.
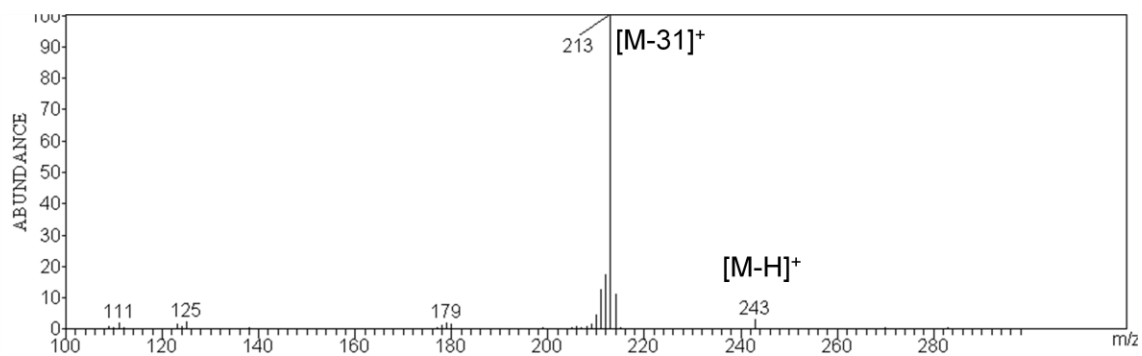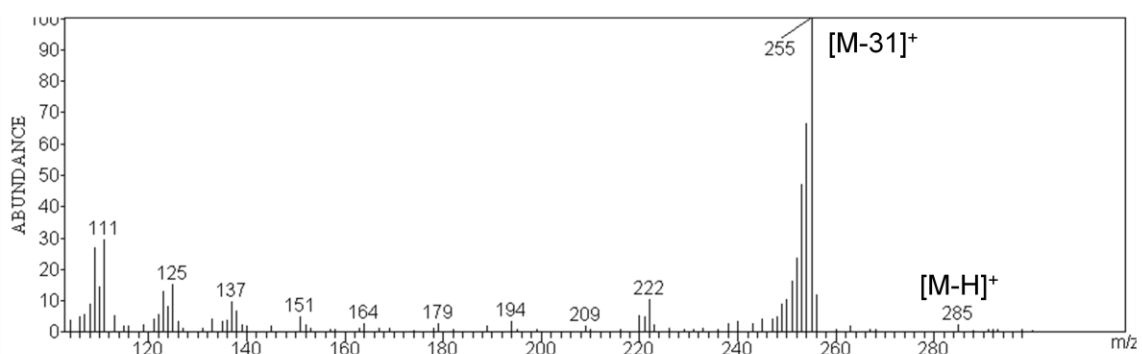
Figure 2.11. Mass spectra from CI experiments from (a) dimethyl acetal of hexadecan-1-al (P 16:0) and (b) dimethyl acetal of tridecanal.

detected due to instrumental constants during CI which requires a higher background m/z cut-off.

Additional validation of dialkyl acetal formation, and by extension plasmalogen detection, was gained by substituting methanol with ethanol during the esterification reaction. The resulting EI mass spectra of diethyl acetals from reactions with hexadecan-1-al (P 16:0) and tridecanal provide spectra where ions are shifted by 28 amu, in comparison to their dimethyl analogs (Figure 2.12). The fragmentation pattern from the diethyl acetals are the equivalent to the dimethyl versions, $[M-45]^+$ representing loss of an ethoxy group and a base peak at m/z 103, from the diethyl head-group fragment.

Fatty acid profiles

Results from the FAME comparison between the two *C. thermocellum* strains are presented in two different arrangements (Table 2.1). Data were first compared on a basis of microgram of FAME species per milligram of dry cell weight. Evaluation of the data in this manner allowed comparison of the fatty acid composition between WT and EA strains based on cellular concentration in each reaction (Figure 2.13).

Data were then compared on a percentage basis of the fatty acids from *C. thermocellum* WT and EA strains (Figure 2.14). These percentages represent the percent area counts of each lipid species compared to the total lipid species detected. This manner of comparison eliminates error resulting from differences in lipid quantities on a dry cell weight basis between the two strains. The t-test established that on a percentage basis, the fatty acid profiles had a significant difference indicated on the graph by "*", at the 95% confidence interval, between the means for i-14:0, n-14:0, P i-14:0, P n-14:0, i-16:0, n-16:0, P n-16:0, and i-17:0.

Anisotropy Results

Utilization of a custom built view cell for anisotropy experiments meant that proper alignment must be maintained in order to reduce variation between experiments. Optimal alignment of the view cell was defined as adjusting the placement so that the xenon excitation source hit the center of the excitation optical window and the center of the emission optical window was aligned with the detector. The Varian Cary Eclipse software package includes an Align feature that runs the xenon lamp and detector

continuously while allowing adjustment of the view cell placement to achieve maximum intensity. The custom design of the viewing cell allowed adjustment at four positions
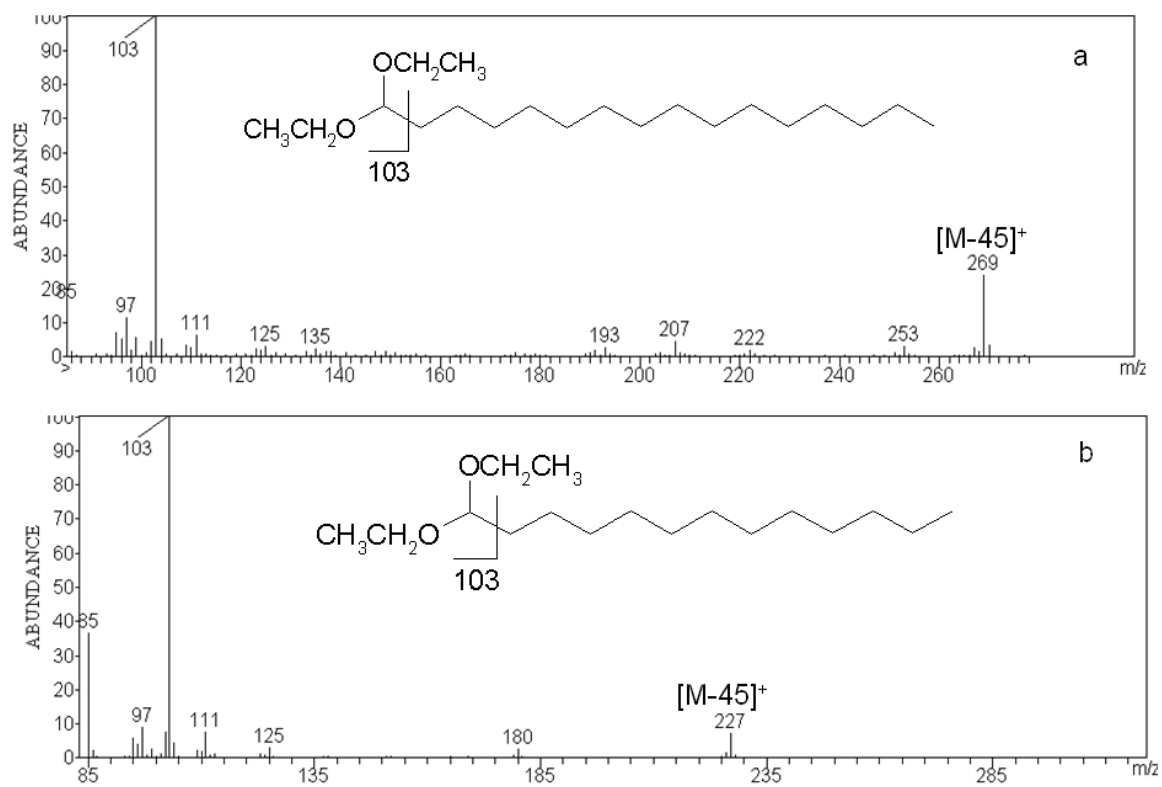
Figure 2.12. Mass spectra from EI experiments from (a) diethyl acetal of hexadecan-1-al (P 16:0) and (b) diethyl acetal of tridecanal.
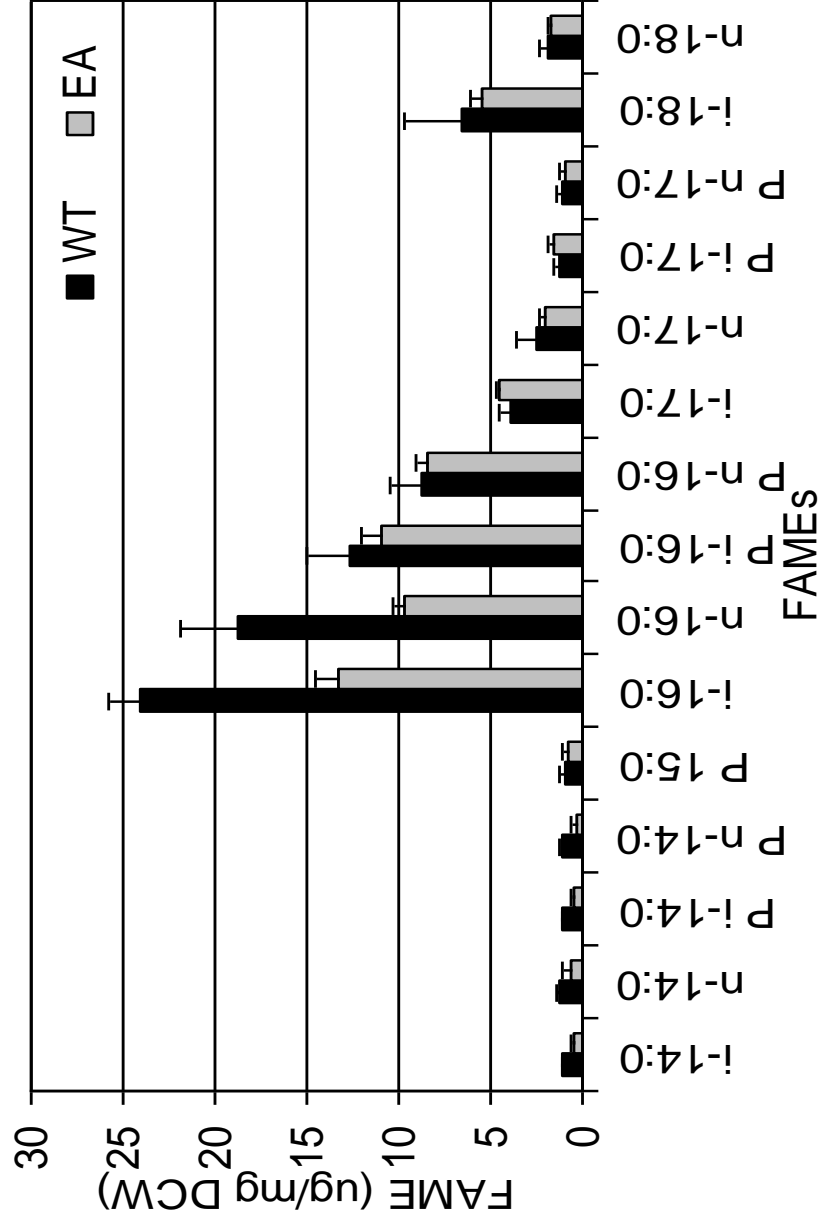
Figure 2.13. Distribution of *C. thermocellum* fatty acids in WT and EA strains based on µg per mg DCW.
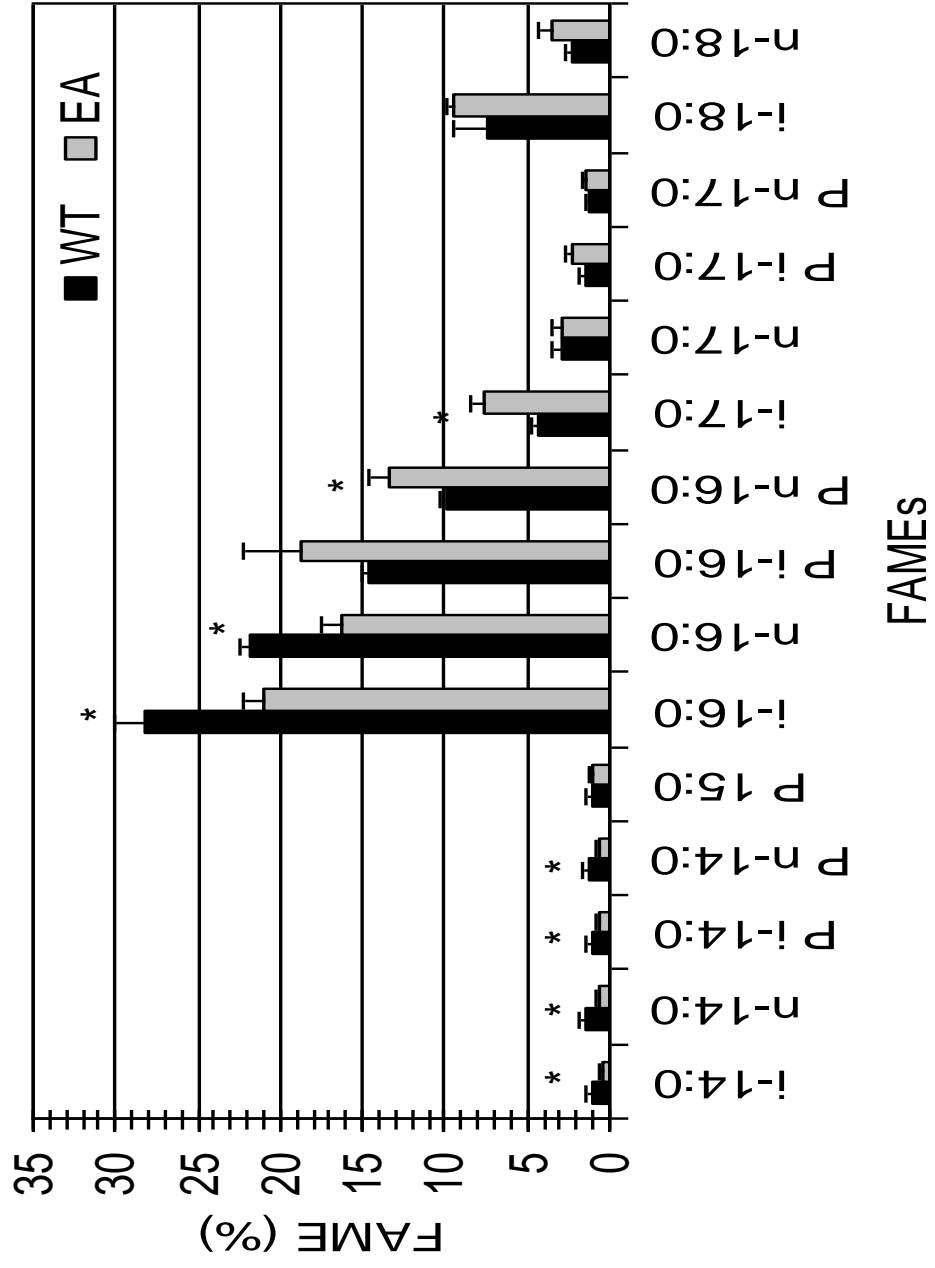
Figure 2.14. Percent distribution of *C. thermocellum* fatty acids in WT and EA strains.

along the excitation and emission planes to achieve a proper 90° orientation. The Align program was utilized prior to the analysis of each sample to ensure maximum sensitivity.

The grating (g) factor, is the ratio of intensity in parallel (I_{HH}) and the intensity in perpendicular (I_{HV}) when excitation is polarized perpendicular. Essentially, the g factor is a correction for molecular probes that are not aligned in the proper orientation to absorb light in the parallel polarization. From the anisotropy equation (eq. 2.11), it is clear that an increase in the g factor will have an impact on the value of I_{VH}, which will subsequently decrease the anisotropy (r) value. Since the g factor is dependent on the alignment of the probe within the sample membrane and the view cell alignment, it was determined prior to analysis of each sample.

The first hurdle in conducting whole-cell anisotropy experiments dealt with incorporation of the DPH into the membrane. Initial studies, conducted by incubating cells with DPH at room temperature, provided sporadic data and lower than expected anisotropy values during the heating phase (Figure 2.15). It was observed that after the sample went through the first heating cycle, T_{up} 1st, the cooling portion, T_d, gave more reproducible numbers and increased anisotropy values. Subsequent heating, T_{up} 2nd, of the sample resulted in an almost identical trend as to that obtained during the cooling cycle.

This reproducible trend was found to be the result of probe integration into the bilayer as the temperature increased. As the DPH probe entered the bilayer and associated with the fatty acid alkyl chains it's rotation was restricted and the absorption in the perpendicular polarization (I_{VH}) decreased, which consequently increased the overall anisotropy. The sample preparation method was modified to incubate the whole cells with 0.1 DPH in THF at 65°C for 1 hr prior to analysis. With the optimization of integrating the DPH probe into the bilayer, the anisotropy changes, from the temperature ramp, were completely reversible when the temperature was decreased from 70°C to 24°C (data not shown).

Following method development for incorporation of the DPH probe into the cells a series of blanks was designed to ensure that no inherent fluorescence emission occurred at 452 nm, by the buffer or cells, as a result of excitation at 350 nm. The first experiments tested *C. thermocellum* WT and EA whole cells in 50 mM Tris-HCl buffer
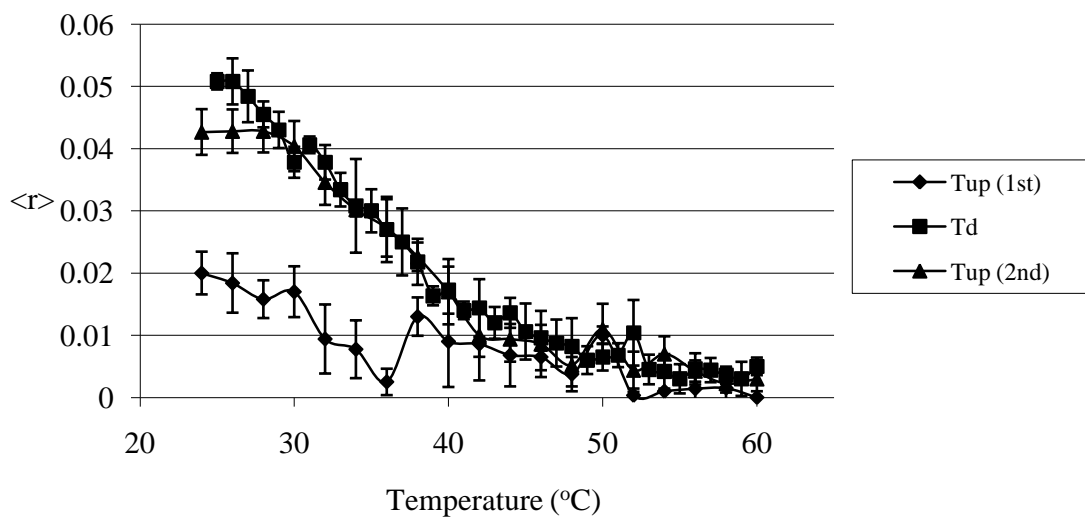
Figure 2.15. Anisotropy method development.

and 50 mM Tris-HCl with 5% (w/v) ethanol for intrinsic fluorescence. Wild-type and ethanol-adapted *C. thermocellum* whole cells were prepared in the same manner as conventional samples, however no DPH probe was added. These cellular samples were excited at 350 nm while the emission detector was scanned from 400 nm to 600 nm without the polarizing lenses applied. The polarizer was removed to ensure maximum transmission of any generated fluorescence. Neat 50 mM Tris-HCl buffer with and without ethanol was also evaluated in this same manner. No detectable signal was generated from any of these samples (data not shown).

Evaluation of unincorporated DPH being transferred into the view cell after cellular incubation was also tested. After DPH incubation the samples were centrifuged and the supernatant discarded, in an attempt to remove any superfluous probe not integrated into the cell membrane. The cell pellet was then dissolved in fresh 50 mM Tris-HCl buffer. Wild-type and ethanol-adapted *C. thermocellum* whole cells were prepared in the same manner as conventional samples, the normally discarded supernatant was tested for fluorescence as well as the cells. These tests were conducted to provide data on whether the DPH remains in solution or associates with the cell. The experiments were excited at 350 nm while the emission detector was scanned from 400 nm to 600 nm without the polarizing lenses applied. The supernatant yielded no detectable signal, however the cells provided an intense signal, at 452 nm, which corresponds to emission by DPH.

Anisotropy experiments were designed to simulate the growth conditions of both WT and EA strains. Since the growth temperature for *C. thermocellum* WT and EA batch cultures was 65°C, measurements were recorded while heating the cells up to 70°C. *C. thermocellum* wild-type and ethanol-adapted whole cells were initially evaluated in a 50 mM Tris-HCl buffer (pH 7.5). However, to accurately reflect growth conditions of EA cultures experiments were conducted with WT and EA whole cells in 50 mM Tris-HCl buffer (pH 7.5) with 5% (w/v) ethanol.

Membrane fluidity was assumed to be lowest at 24°C, and this was arbitrarily set to correspond to 100% anisotropy. Subsequent experimental values were reported as the percentage decrease in anisotropy (i.e., increase in fluidity) as a function of increasing temperature. The normalized steady-state fluorescence anisotropy of *C. thermocellum*

wild-type cells in 50 mM Tris (pH 7.5) as a function of temperature is shown in Figure 2.16. Each data-point (♦) is the average of three analytical replicates and five multiple observations, the standard deviation error bars are concealed by the data-point symbols. A trend line was fit to the data-points using a 2nd order polynomial function. The vertical dashed-line represents the batch growth temperature of 60°C.

The anisotropy experiments conducted without ethanol present, allow a comparison of the two strains in an environment similar to WT batch culture. As the temperature was raised from 24°C to 70°C in 50 mM Tris-HCl buffer, the anisotropy of WT cells decreased by approximately 30% (Figure 2.17). In contrast, there was only a 16% decrease in anisotropy for EA cells over the same temperature range. These results indicate that EA cells have a lower fluidity, greater membrane rigidity, than WT cells in the absence of ethanol [69].

Normalized steady-state anisotropy data from C. thermocellum WT and EA experiments in 50 mM Tris-HCl with 5% (w/v) ethanol provide a comparison of the two strains in an environment similar to EA batch culture (Figure 2.18). The data points, omitted to reduce clutter, are again the average of three analytical replicates and the standard deviation error bars were concealed by the data-point symbols. A trend line was fit to the data-points using a 2nd order polynomial function. The vertical dashed-line represents the batch growth temperature of both strains. When 5% (w/v) ethanol was added to the buffer, WT and EA cells experienced 42% and 30% decreases in anisotropy, respectively (Figure 2.18). In all experiments, the anisotropy changes were completely reversible when the temperature was decreased from 70°C to 24°C (data not shown).
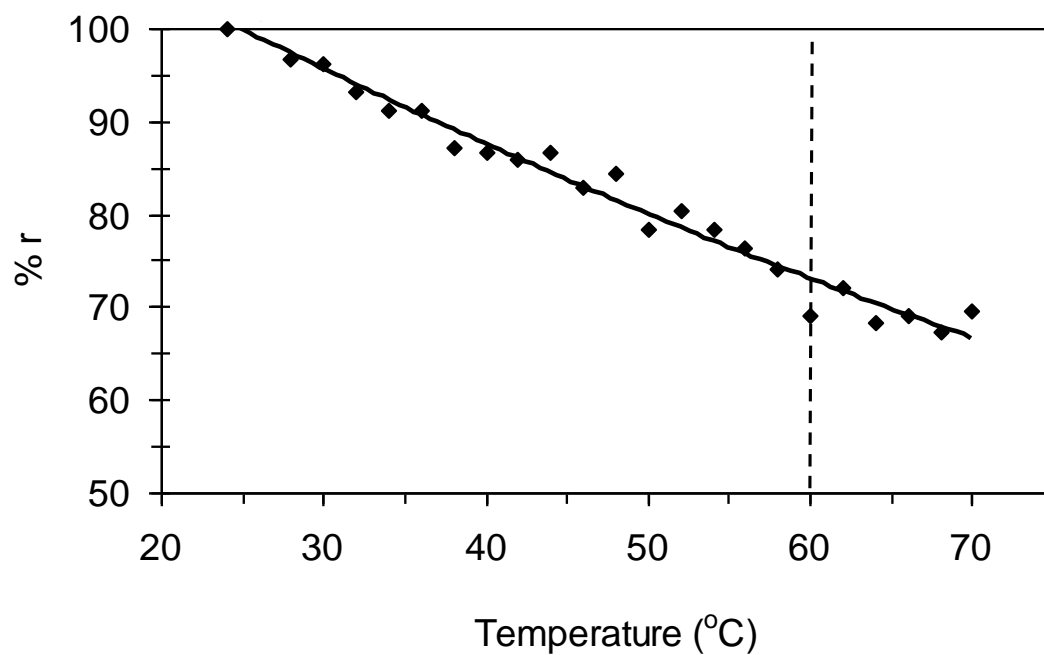
Figure 2.16. Normalized steady-state fluorescence anisotropy with 0% (w/v) ethanol. *C. thermocellum* wild-type cells in 50 mM Tris (pH 7.5) as a function of temperature.
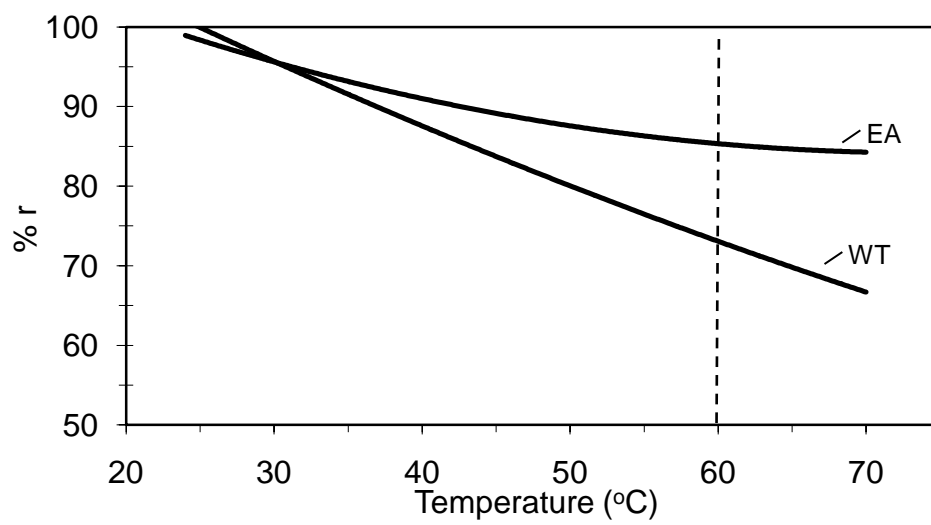
Figure 2.17. Normalized steady-state fluorescence anisotropy with 0% (w/v) ethanol comparison between *C. thermocellum* WT and EA strains.
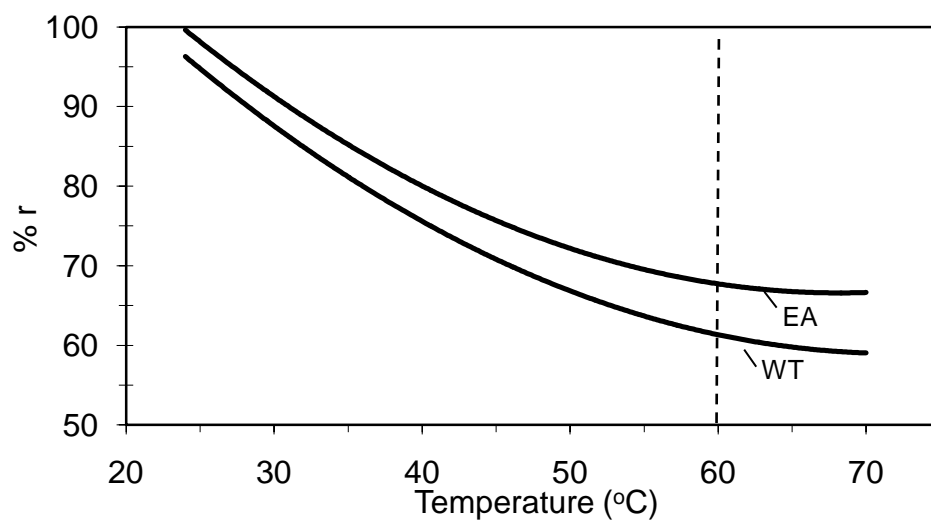
Figure 2.18. Normalized steady-state fluorescence anisotropy with 5% (w/v) ethanol comparison between *C. thermocellum* WT and EA strains.

Chapter 2.4. Discussion

The prokaryotic cell membrane functions as a protective barrier and serves a vital role in energy generating pathways, and so regulation of membrane integrity is essential for microbial survival and growth [70]. The concept that microbes modify their membrane composition in response to environmental stress has been well established [1, 33, 37, 71-72]. The theory of homeoviscous adaptation, that cells modify their membranes in order to maintain an optimal degree of fluidity, has been supported by studies relating fatty acid profiles to temperature changes and solvent insult [35, 71-78]. The accepted model for *C. thermocellum* is that it increases the number of unsaturated and short chain fatty acids in response to ethanol insult. Increasing the percent of unsaturated and shorter chain fatty acids both serve to increase the overall fluidity of the membrane, when compared to longer, saturated alkyl chains. Therefore ethanol-adapted strains increase baseline membrane fluidity in response to selection for alcohol tolerance.

A number of previous fermentation studies with *C. thermocellum* have focused efforts on improving ethanol production [79-82]. Studies concerned with changes to the fatty acid composition during ethanol adaptation, however have been limited [34]. Herrero *et al.* found that their ethanol-adapted strain, C9, had a greater proportion of fatty acids with less than fourteen carbons and more monounsaturated fatty acids. There also appeared to be an increase in n- and anteiso-branching, with a concurrent decrease in iso-branching [34].

Fatty acid study

Mass spectral fragmentation patterns of picolinyl esters allowed definitive identification of fatty acid alkyl chains present within the *C. thermocellum* membrane. Quantification of fatty acids and plasmalogens confirmed changes in cell membrane composition following ethanol treatment. The adaptation process resulted in a shift to longer-chain fatty acids, an increase in iso- to n- branching, but did not increase the unsaturation index; these results were counter to previously published reports [34].

It has been previously documented that members of the *Clostridia* genus and some anaerobic bacteria contain ether-linked alkyl chain lipids [83-84]. The Herrero study also detected the presence of plasmalogen compounds, however due to co-elution with fatty acid methyl esters, plasmalogen quantification was not possible [34]. During

acidic esterification reaction the ether bond is broken and aldehydes are generated. Methylation reagents convert these aldehydes into dimethyl acetals. The spectra for published dimethyl acetals appear remarkably similar to the unknown spectra from *C. thermocellum* reactions [64].

However, picolinyl transesterification failed to provide structural elucidation for the plasmalogen species. The plasmalogen vinyl-ether group forms an aldehyde during the esterification reaction, which immediately converts to a dimethyl acetal. Unfortunately the resulting dimethyl acetals were not amenable to transesterification into picolinyl esters. Mass spectra generated with EI of these dimethyl acetals fail to provide a molecular ion and generally consist of ions with only minor abundances. The only two prominent ions are: m/z 255 representing $[M-31]^+$ loss of a methoxy group and m/z 75 generated by the loss of the dimethyl head-group.

Chemical ionization (CI) with acetonitrile has been used to elucidate double bond location in the analysis of polyunsaturated fatty acids [65-68]. The expectation was that CI could provide a softer ionization mechanism capable of producing structural characteristic ions for the plasmalogen species. Experiments conducted utilizing chemical ionization did provide $[M+H]^+$ ions, which were not observed during EI experiments. The $[M+H]^+$ ions did fragment to produce the $[M-31]^+$ ions as observed during EI, indicating that ions seen during EI were generated from the respective dimethyl acetal species. Data from the diethyl acetal fragmentation patterns corroborated spectra from both EI and CI of dimethyl acetals. The advantage to employing this three-tiered approach was that the chromatographic separation remains intact during each process, allowing peaks to be confidently identified based on mass spectra and retention times. Comparison of spectra generated from reactions with tridecanal via CI and EI lend credibility to the generation of dimethyl acetals and thus the presence of plasmalogens.

The milligram FAME per cell dry weight data (Figure 2.13) were analyzed statistically. However, it was believed that differences between the two strains were exaggerated due to differences in the amount of lipid per DCW between the two strains. The disparity in the lipid to DCW ratio was believed to be a result of variations in size and non-lipid components between the strains. This theory was supported by

experiments that showed total carbohydrate levels in EA cells were five times greater than those of WT cells (data not shown).

Therefore it was necessary to compare the fatty acids as area percents (Figure 2.14). Presenting the data as area percents, the data were normalized with respect to variations due to differences in lipid per DCW.

In contrast to the previous work, our work revealed that adaptation to exogenous ethanol did not change the site of methyl branching or the degree of unsaturation [32, 34, 75]. The absence of unsaturated fatty acids within the *C. thermocellum* membrane raised concerns about the validity of the derivatization methods. In order to confirm that unsaturated fatty acids were not being deteriorated as a result of the saponification and FAME methods, reactions with 5,8,11,14-eicosatetraenoic acid (ARA), 4,7,10,13,16,19-docosahexaenoic acid (DHA) standards, and *Escherichia coli* whole cells were conducted. Reactions with ARA and DHA yielded mass balance recoveries and FAME molecular ions of m/z 318 and m/z 342, respectively. Qualitative analysis of the *E. coli* fatty acid profile was consistent with previously published data, which contained both unsaturated and cyclopropane fatty acids (data not shown) [49]. Concluding that results obtained from our dervitization methods were valid.

The present work found that the ratio of iso- to n- branched was higher in the EA strain for every fatty acid and plasmalogen, with the exception of 14:0 and P 14:0 (Table 2.1). Comparison of the WT and EA strains on a percentage basis revealed that WT had a greater percentage of fatty acids with chain lengths sixteen carbons or less. On the other hand, the EA strain had a larger percentage of fatty acids and plasmalogens with chain lengths sixteen carbons and longer. These data indicate that growth in 5% (w/v) ethanol resulted in the bacteria increasing the chain length of fatty acids. However, ethanol-adaptation did not promote incorporation of unsaturation fatty acids or change the location of methyl branching on the fatty acids.

One plausible reason for differences between the Herrero study and our study could be due to growth conditions after ethanol-adaptation. Both studies selected ethanol-adapted strains by serial transfer of viable cells with successive growth cycles and increasing exogenous ethanol concentration [75]. The Herrero et al. study implied that their ethanol-tolerant strain, C9, after selection was grown in media without ethanol

present [34]. If *C. thermocellum* changes membrane composition in the presence of ethanol, it might be plausible that the membrane is further changed when grown in the absence of ethanol.

Another reason for differences could be due to the method of analysis. Herrero *et al.* used a packed-column GC as the chromatographic method and detection by means of a flame ionization detector (FID). Fatty acid identification was based on retention time comparisons between sample and standards. Therefore, unknown compounds such as plasmalogens could be misinterpreted as fatty acids due to similar retention times. Our study employed capillary-column GC/MS with identification and structural analysis based on molecular weight and fragmentation patterns, thereby distinctly separating plasmalogens and fatty acids.

Anisotropy Study

Previous studies conducted on the effect of exogenous solvents added to *C. thermocellum* batch cultures found that solvents impact bacterial proliferation and metabolism [79]. Growth inhibition caused by solvents dispersed in culture media is known as molecular toxicity, and such toxicity is the result of interactions between the solvent and the membrane or membrane components [85-86]. This solvent interaction disrupts membrane integrity by causing loss of protein function and increased membrane fluidity. Molecular toxicity is theorized to be responsible for growth inhibition of *C. thermocellum* WT cells at low ethanol concentrations [85]. Based on this theory, ethanol-adapted strains of *C. thermocellum* are believed to change their membrane composition in order to counteract the effects of molecular toxicity.

In order to gain a more direct understanding of the relationship between fatty acid profiles and membrane fluidity, steady-state fluorescence anisotropy experiments were conducted as part of this study. Anisotropy is a measure of probe rotation obtained by comparing the ratio of fluorescent emission in parallel and perpendicular polarizations. Within the context of this study, anisotropy correlates to the order of the fatty acid alkyl chains which is inversely related to fluidity, thus as the anisotropy value decreases the fluidity of the membrane increases [44]. The rotation of DPH is a function of the fatty acid phase transition temperature, T_m. Longer saturated-chain fatty acids have a higher T_m, due to a greater number of van der Waals interactions between acyl chains.

Unsaturated fatty acids have lower transition temperatures than saturated fatty acids of similar length, due to reduced van der Waals interactions as a result of the distorted geometry around the double bond [45]. Below the T_m the alkyl chains are in an ordered state and rotation of the DPH probe is restricted. With increasing temperature the alkyl chains become disordered allowing rotation of DPH. Rotation of DPH lowers the ratio of horizontal and vertical intensities, translating to a lower anisotropy [40]. Above the T_m of fatty acids a phase transition occurs which is reflected by a sudden increase in membrane fluidity [46]. Due to the heterogeneity of the *C. thermocellum* membrane and because DPH integrates non-discriminately between hydrocarbon chains, a decrease in anisotropy represents an increase in the average fluidity of the membrane [46].

Numerous papers report relationship between fatty acid chain length, ethanol exposure, and membrane fluidity [32, 69, 87]. Anisotropy experiments with exogenous ethanol provided conformation of the membrane fluidizing effects of exogenous ethanol [88]. We hypothesize that the increased fluidity afforded by exogenous ethanol reduced the membrane rigidity for WT cells below an optimum level. This sub-optimum membrane rigidity occurred because WT cells have a high percentage of short chain length fatty acids. Increased fluidity is believed to result in growth inhibition due to molecular toxicity when in the presence of ethanol. The EA cells adapted to ethanol by producing a higher percentage of longer-chain fatty acids. Therefore, interaction between exogenous ethanol and the more rigid EA membrane together change the fluidity to a level that was consistent to that of WT cells without ethanol. The Herrero et al. concluded that *C. thermocellum* responded to ethanol treatment by increasing membrane fluidization [34]. The assumption was that ethanol had a rigidifying effect on the membrane. This was based on partition coefficient studies conducted with liposomes and branched-chain alcohols [89].

Anisotropy experiments on EA cells without ethanol, displays the smallest % change, 16%, over the experimental temperature range. However the effect of 5% (w/v) ethanol on the fluidity of EA cells, increases the fluidity, lowering the anisotropy approximately 30% over the experimental temperature range. These results are similar to those obtained for WT cells without ethanol. The addition of ethanol to WT cells

increases the membrane fluidity, illustrated by a reduction in anisotropy by more than 40%, presumably resulting in a less than optimum fluidity barrier.

Since the *C. thermocellum* WT and EA membranes were comprised of 28% and 37% plasmalogens, their contribution to membrane structure and fluidity may be significant, as the vinyl-ether bond imparts different characteristics to the phosphatidyl group than the traditional fatty acid ester bond. The plasmalogens' role might be to modify the T_m of the membrane in a similar manner to that of unsaturated fatty acids [16]. Regulating membrane fluidity by means of plasmalogens might provide the cell with a more discrete mechanism of changing membrane properties.

The data from the fatty acid studies combined with the anisotropy data provide strong evidence for a refined model for acquired ethanol tolerance by *C. thermocellum* (Figure 2.19). Adaptation was the result of changes to the fatty acid profile that increased membrane rigidity, allowing the integrity of the membrane to be maintained during growth in the presence of exogenous ethanol. These data presented in this study support the idea that EA cells maintain an optimum level of fluidity by increasing their fatty acid chain lengths in response to the increased fluidity provided by growth in media containing ethanol. This study provided evidence of an alternative description of the route for bacterial survival due to adaptation to exogenous solvent. Understanding the mechanism of membrane adaptation by *C. thermocellum* to acquire ethanol tolerance could be utilized to develop cultures that exhibit resistance to higher concentrations of ethanol. This, in-turn, could lead to more cost-effective ethanol production which would be a step closer to consolidated bioprocessing (CBP).

Previous Model

Wild-type cells

ethanol
exposure ↓

Decreased membrane fluidity

adaptation ↓

Decreased fatty acid chain length
Increased unsaturation index
Decreased i-/n- ratio
Increased a-/ i- ratio

↓

Increased membrane fluidity

↓

Ethanol-adapted cells

Proposed Model

Wild-type cells

↓ ethanol exposure

Increased membrane fluidity

↓ adaptation

Increased fatty acid chain length
No unsaturation
Increased i-/n- ratio
No a-

↓

Decreased membrane fluidity

↓

Ethanol-adapted cells

Figure 2.19. Schematic of ethanol-adaptation mechanism. i- denotes iso-branching, n- denotes normal or straight chain, a- denotes anteiso-branching.

PART III. MITOCHONDRIAL LIPIOMICS

Chapter 3. Comparison of Sprague Dawley Rat Mitochondrial Fatty Acid Profiles Isolated from Various Tissues

Chapter 3.1. Introduction

As shown by the previous study, bacteria alter their membrane composition as a result of adaptation to various environmental stimuli [70, 90-91]. However, modification of membrane content is not relegated to prokaryotic organisms. Mammalian systems have also been shown to exhibit variations in their lipid content on a tissue specific basis and as a function of diet [92-93].

In eukaryotes, biological processes are compartmentalized by membranes, this segregation gives rise to different inter- and intra-cellular biochemical environments. Exposure and interaction of cells, within a macromolecular system, to potential differences in metabolomes (i.e. ions, secondary messengers, and/or signaling molecules) could further stimulate differentiation in cellular composition [94]. Variations in the inter-cellular environments among tissues, has been shown to stimulate changes in the lipid content of the plasma membrane [95-97]. Based on this knowledge, our hypothesis is that alterations in inter-cellular environments could cause tissue specific changes to the fatty acid profiles of sub-cellular organelles such as mitochondria.

Changes to the fatty acid composition will have a significant impact on the physical properties of the membrane [15, 45, 98]. Fluidity is a function of the van der Waals interactions between acyl chains, which is in part determined by the chain length and degree of unsaturation. Short-chain saturated fatty acids will have greater fluidity than longer-chain saturated fatty acids due to the reduced number of van der Waals interactions. Unsaturation along the acyl chain will also decrease the van der Waals interactions as a result of the geometry around the double bond. Double bonds with cis geometry, which comprise the majority of naturally occurring double bonds, result in a $30°$ bend along the acyl backbone. This distortion effectively shortens the fatty acid chain length by one methylene group per incident.

Mitochondrial membranes house many protein complexes involved in the reaction cascade of the electron transport chain (ETC) [99-100]. Therefore electrons leaking from

the ETP are the greatest source of reactive oxygen species (ROS) within a cell. Because of their proximity to these ROS, mitochondria are considered both the cause and a target of oxidative stress [101]. The high oxygen consumption rate of neurological cells and the relatively low abundance of antioxidant counter measures would likely require compensatory changes to the fatty acid profile in order to minimize susceptibility to oxidative damage.

Oxidative stress, a consequence of ROS proliferation, has been suspected to be causal in many neurodegenerative diseases [102-104]. Considerable research is dedicated to monitoring ROS mediated damage to nucleic acids [105], proteins [106], and lipids [107]. Due to the mitochondrial role in the ETP, common targets for these ROS are lipid components of the mitochondrial membrane, namely polyunsaturated fatty acids (PUFAs). Previous studies have shown that neurological plasma membranes contain an abundance of polyunsaturated fatty acids. Enzymes required for mitochondrial fatty acid synthesis are localized within the mitochondria matrix, whereas fatty acid synthesis for other cellular organelles occurs mainly in the cytosol [15]. Therefore mitochondria provide a semi-autonomous organelle when studying changes to the FA profile. Thus, a comparison of the fatty acid profiles from brain mitochondria in comparison to other tissues may provide evidence for the increased neurological susceptibly to ROS.

The focus of the project centered on the analysis and variation of mitochondrial membrane composition from distinctive cellular environments. Tissues selected for this study represent functioning organs with distinctive biochemical processes. Mitochondria isolated from brain, heart, liver and kidneys were chosen because mitochondrial disorders that effect each of these tissues are of interest to researchers [92-94, 108].

In order to gain a better understanding of the distinction between each of the tissues, a brief description for each is necessary. The heart is a muscle that is composed of short, striated fibers. The heart functions to maintain and direct the circulation of blood throughout the body. Mitochondria from cardiac cells usually only respire through an aerobic pathway, however they commonly utilize a variety of carbon sources for raw materials. Permeability across the cellular membrane in cardiac cells results having a biochemistry that vacillates between high concentrations of Ca^{2+}, Na^+ and low K^+ to periods of high K^+ concentrations and low Ca^{2+} and Na^+ levels. Therefore, mitochondria

are regularly exposed to fluctuating levels of divalent cations, which have been linked to the synthesis of cardiolipin [15].

The kidney is responsible for regulating the consistency of fluids throughout an organism's system. The constant supply of blood and fluids to the kidneys results in cells exposed to fluctuating levels of K^+ and Na^+, much like cardiac cells, during the reabsorption process. Similar to the kidneys, the liver functions to process nutrients in the blood. The liver produces bile that aids in the digestion of fats and absorption of fatty acids. Metabolically the liver is probably the most active organ within this study. The liver metabolically processes and detoxifies many of the nutrients from external sources. In addition, the liver stores vitamins and iron removed from red-blood cells.

Lastly, the brain, specifically the cerebral cortex, is the processing center for the organisms motor, sensory and memory functions. Unlike the other organs that comprise this study, the brain is protected from abrupt changes in cellular environment as a result of supplement metabolism. The brain is surrounded by cerebrospinal fluid (CSF) a solution with an abundant concentration of Na^+, Cl^- and Mg^{2+} ions. The CSF contains a reduced amount of Ca^{2+} and K^+ than found in blood serum, which is in constant contact with the heart, liver and kidneys. The blood-brain barrier allows the diffusion of amino acids, electrolytes and fat soluble molecules; while maintaining balanced surroundings for neuronal events.

Comparison of mitochondrial membrane compositions between various tissues may provide evidence for neurological tissues having an increased vulnerability to oxidative damage. Gas chromatography/mass spectrometry (GC/MS) techniques were used to elucidate fatty acid structures and quantify lipid species. Our analysis of mitochondrial lipids showed a significant increase in acyl chain unsaturation from brain mitochondria compared to heart, liver and kidney, perhaps explaining the increased vulnerability of the brain to ROS.

Chapter 3.2. Experimental

Reagents

Potassium t-butoxide (1.0 M) in tetrahydrofuran (THF), 3-hydroxymethyl pyridine, hexane, D-mannitol, sucrose, Triza base, Tween-20, calcium chloride, and ethylenediaminetetraacetic acid disodium were purchased from Sigma (St. Louis, MO, USA). Methanol, methylene chloride, and hydrochloric acid were obtained from Fisher (Pittsburg, PA, USA). Acetyl chloride was obtained from Fluka (Buchs, Switzerland). Sodium hydroxide, sodium bicarbonate, and potassium carbonate were purchased from J.T. Baker (Phillipsburg, NJ, USA). Ethyl ether was obtained from EMD (San Diego, CA, USA). Anthracene was purchased from Acros (Morris Plains, NJ, USA). Percoll™ was obtained from GE Healthcare (Uppsala, Sweeden). Porin antibody was purchased from Calbiochem (Gibbstown, NJ, USA). Lamin B was ordered from Santa Cruz Biotechnology (Santa Cruz, CA, USA). MAP2 was purchased from Abcom Inc. (Cambridge, MA, USA). Isothesia (isoflurene) was obtained from Bulter Animal Health Supply (Dublin, OH, USA). GLC-411 lipid standard, 5,8,11,14-eicosatetraenoic acid (ARA), and 4,7,10,13,16,19-docosahexaenoic acid (DHA) were purchased from Nu-Chek Prep, Inc. (Elysian, MN, USA).

General equipment and supplies

Dounce homogenizer (Wheaton Industries, Millville, NJ, USA). Nalgene brand Oak Ridge polypropylene copolymer centrifuge tubes (Thermo Fisher Scientific Inc., Waltham, MA, USA). Beckman Polyallomer centrifuge tube (Beckman Coulter, Inc., Brea, CA, USA). Fisherbrand 2.0 mL polypropylene microcentrifuge tube (Thermo Fisher Scientific Inc., Waltham, MA, USA). Beckman Coulter (Beckman Coulter, Inc., Brea, CA, USA) Avanti J-25 series centrifuge equipped with a JA-25.50 fixed angle rotor. Beckman Coulter (Beckman Coulter, Inc., Brea, CA, USA) L-80 Ultracentrifuge series equipped with a SW 55 Ti swinging bucket rotor. Thermo IEC Micromax Centrifuge (Thermo Fisher Scientific, Rochester, NY, USA) with a 851 series microtube fixed angle rotor. Eppendorf (Hauppauge, NY, USA) Research Adjustable-volume pipettes.

Animals

Sprague Dawley SD outbred rats were obtained from Harlan Laboratories (Harlan Laboratories, Indianapolis, IN, USA) and were housed at the Sanders-Brown Center on Aging Animal Facility (Lexington, KY, USA). All animals were fed a Teklad Global 18% Protein Rodent Diet (Harlan Laboratories Inc., Indianapolis, IN, USA) and had access to food and water *ad libitum*. Animals were kept in plastic cages with wire tops containing Sani-Chip bedding (P.J. Murphy Forest Products Corp., Montville, NJ, USA). At four months of age rats were euthanized by exposure to Isothesia (isoflurene) followed by cervical dislocation. Necropsies were performed by trained laboratory personnel and harvested tissue was flash frozen in liquid nitrogen and stored at -80˚C until processed. All animal procedures were in accordance with Institutional Animal Care and Use Committee (IACUC) regulations at the University of Kentucky under approved protocol number 2009-0548.

Rat mitochondria isolation

Mitochondria were isolated using a procedure (Figure 3.1) adapted from previous studies [109]. Throughout the procedure all reagents were kept at 4°C, samples and equipment were placed on ice. Tissue samples were homogenized via a manual Dounce homogenizer in isolation buffer (IB) (10 mM Tris, 0.32 M sucrose, 0.25 mM Na_2EDTA, pH 7.4). The total volume of isolation buffer used during homogenization gave a tissue to buffer ratio of approximately 0.1 g/mL (wt/vol). The tissue was homogenized with approximately 8 to 10 up-and-down strokes or until the tissue was completely liquefied. The homogenate was centrifuged (2,000xg, 3 min, 4°C). The supernatant was collected and the pellet was dissolved in approximately half the original volume of isolation buffer then centrifuged (2,000xg, 3 min, 4°C). The supernatants were combined and the pellet discarded. The combined supernatants were centrifuged (21,000xg, 10 min, 4°C). The supernatant was discarded and the pellet, containing the crude mitochondria isolate, was resuspended in 3 mL 19% Percoll solution. The crude mitochondria solution was carefully layered atop two discrete Percoll concentrations (30% over 50%, 1:1 by vol, 7 mL total). The mixture was centrifuged (16,900xg, 30 min, 4°C). Three bands were discernible following centrifugation. The bottom most band, containing the enriched

Tissue homogenization

Centrifuge (2000xg, 3 min, 4°C)

Nuclear pellet   **Supernatant**

Centrifuge (2000xg, 3 min, 4°C)

Nuclear pellet   **Supernatant**

Centrifuge (21000xg, 10 min, 4°C)

Crude mitochondria pellet

Percoll gradient

Centrifuge (16900xg, 30 min, 4°C)

Enriched mitochondria band (4x vol PBS)

Centrifuge (17500xg, 30 min, 4°C)

Mitochondria (3 mL PBS)

Centrifuge (17500xg, 30 min, 4°C)

Mitochondria (1 mL PBS)

Centrifuge (21000xg, 10 min, 4°C)

Purified mitochondria

Figure 3.1. Mitochondria isolation scheme.

free-mitochondria, was extracted with a Pasteur pipette and dissolved in 4 volumes of PBS buffer and centrifuged (17,500xg, 30 min, 4°C). The mitochondrial pellet was washed two additional times with 1 mL aliquots of PBS, each washing was centrifuged (21,000xg, 30 min, 4°C). The final pellet was resuspended in deionized H_2O and stored at -80°C until further analysis.

Quantification of mitochondrial proteins

Quantification of mitochondrial proteins was carried out on a Thermo Labsystems Multiskan MCC/3340 spectrometer (Pittsburgh, PA, USA) using a Pierce Bicinchoninic acid (BCA) assay (Rockford, IL, USA) [105]. A calibration curve was prepared by addition of 0, 1, 5, 10, 15, 20 μg BSA standard into separate wells; each concentration in duplicate. Aliquots of isolated mitochondria (5 μL) were added to separate wells; each sample in duplicate. Wells were adjusted to a final volume of 100 μL by addition of deionized H_2O. Lastly, 100 μL of a 10 μL/mL $CuSO_4$ in bicinchoninic acid solution was pipetted into each well. The plate was incubated at 37°C for 30 min prior to reading. The mitochondrial protein concentration was determined by absorbance at 620 nm. The concentration (μg/μL) was calculated by averaging the sample replicates and dividing by the addition volume (eq. 3.1):

$$\text{Protein}\left(\mu g / \mu L\right) = \frac{\left(\dfrac{A_1 + A_2}{2}\right)}{5 \mu L} \qquad\qquad \text{eq. 3.1}$$

Western blot analysis

Mitochondrial isolations were evaluated for purity by western blot (Figure 3.2). Isolated mitochondria (20 μg) were separated on a 4-15% SDS-PAGE gradient gel. Protein bands were transferred to a nitrocellulose membrane and incubated with 5% milk in 0.5% Tween-20/Tris-buffered saline (TTBS) plus goat serum (1:30, 2 hrs, 25°C). The membrane was incubated with primary antibodies: anti-porin (1:5000) specific for mitochondria; anti-lamin B (1:3750) a marker specific for nuclei; and anti-MAP2 (1:3750) a cytosolic specific marker (12 hrs, 4°C). The membrane was washed three times with 0.5% Tween-20/Tris-buffered saline then incubated with horseradish peroxidase (1:7500 for lamin B and MAP2; 1:10000 for porin) conjugated secondary antibody (1 hr, 25°C). Following three washings with 0.5% Tween-20/Tris-buffered

92

	TH	Nuc	Cyto	Mito	a
Lamin B (nuc)					
MAP2 (cyto)					
Porin (mito)					

	Brain	Heart	Liver	Kidney	b
Porin (mito)					
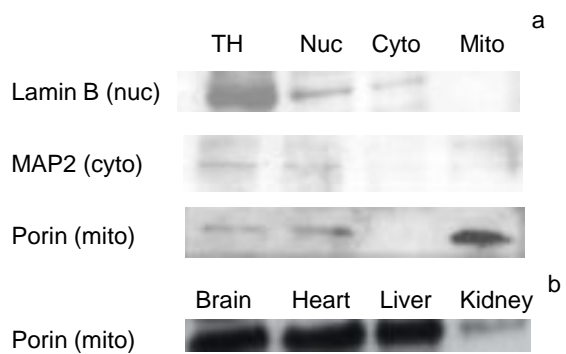
Figure 3.2. Mitochondria western blot results. Protein markers (a) for total homogenate (TH), nuclear (Nuc), cytoplasmic (Cyto), and mitochondria isolates (Mito) from rat brain and mitochondria protein marker (b) from each tissue.

saline, the bands were visualized with enhanced chemiluminescence (Amersham Pharmacia Biotech, Piscataway, NJ, USA) as per manufacturer's instructions.

Saponification of fatty acids

Aliquots (250 μg) of isolated mitochondrial protein were used for each reaction. Saponification methods were based on a previous description by Kurkiewicz et al [49]. Sodium hydroxide (1 mL of 3 M) was added to the mitochondria solution. The mixture was vortexed and heated to 90°C for 1 h, cooled to room temperature, and 2 mL of 3.25 M HCl was added and reheated at 90°C for 10 min. After cooling to room temperature, the lipids were extracted three times with 1 mL portions of hexane/diethyl ether (1:1, by vol). The organic phases were combined and evaporated to dryness under a stream of N_2 at room temperature.

Fatty acid derivatization methods

Fatty acid methyl ester (FAME) procedures were adapted from Lepage and Roy [50]. Methanol:acetyl chloride (50:1 (v/v), 5 mL total) was added to the extracted free fatty acids. The solution was vortexed and heated at 60°C for 1 h. After heating, 3 mL of 6% K_2CO_3 was added, and the FAME products were extracted 1 mL of hexane containing 50 ng/μL anthracene. Extracted material (1 μL) was used for GC/MS analysis.

An aliquot of the FAME solution was transesterified to picolinyl esters using an adapted method [51]. The hexane phase from the FAME procedure was evaporated to dryness under a stream of N_2 at room temperature and 1 mL of methylene chloride was added to resolvate the methyl esters. In a separate vial a mixture of 200 μL 3-hydroxymethylpyridine and 100 μL of 1.0 M potassium tert-butoxide in THF were allowed to react for 2 min. This mixture was then added to the FAME methylene chloride solution. The reaction was mixed and heated at 45°C for 1 h. After cooling to room temperature, 1 mL of 2.5% $NaHCO_3$ was added and the methylene chloride layer removed. The organic layer was reduced to approximately one-quarter original volume under a stream of N_2 at room temperature and 1 μL was injected for analysis. All derivatization methods were validated by analysis of 20:4 (arachidonic acid) and 22:6 (docosahexaenoic acid).

Gas chromatography/mass spectrometry

Fatty acid methyl ester derivatives were analyzed using a Varian Saturn 3 GC/MS system equipped with a ZB-5ms capillary column 30 m x 0.25 mm i.d., 0.25 μm film (Phenomenex USA, Torrance, CA). The temperature program was: 130°C to 170°C at 4°C/min, 170°C to 215°C at 2.7°C/min, 215°C for 3.34 min, with a total analysis time of 30 min. Carrier gas head-pressure was set to give a flow rate of 1 mL/min, with a 50:1 split. The injector and transfer line were maintained at 240°C and the manifold temperature was 210°C. Ionization was accomplished by electron impact (EI) at 70 eV, with a 3 minute filament delay. Full scan spectra (m/z 50 to 650) were acquired at a scan rate of 1 analytical scan per second with a background mass set at m/z 49. The GC/MS method was optimized to provide peak resolution for FAMEs from the GLC-411 standard.

Fatty acid picolinyl ester derivatives were analyzed on the same instrument with the following temperature program: 150°C for 4 min., 150°C to 280°C at 20°C/min, 280°C for 19.5 min with a total analysis time of 30 min. All other parameters were as described above except that the filament delay was 10 min and spectra were generated from full scans from m/z 50 to 500.

Chemical ionization (CI) experiments were conducted on the same instrument using the FAME GC/MS program, except the manifold temperature was reduced to 160°C. The MS parameters were as follows: selected-ejection chemical ionization (SECI) mode with acetonitrile as the reagent gas (Figure 2.2) [52], 100 μsec automatic-reaction control (ARC) time, 1000 μsec ionization time, 128 msec reaction time, m/z 15 ionization storage level, 7.5 V_{0-p} reagent gas ion ejection amplitude, m/z 37.0 CI reaction storage level. Spectra were generated by full scans from m/z 80 to 650. All GC/MS data were analyzed using the Wsearch32 2005 Software (version 1.6.2005; Melbourne, Australia).

Calculations

The distribution of FAMEs per tissue was determined by dividing area counts for each FAME species by the total observed FAME area count (eq. 3.2):

$$\%FAME = \frac{Area_{FAME}}{\sum FAME_{Area}} \times 100 \qquad\qquad \text{eq. 3.2}$$

The unsaturation index (u.i.) was calculated by dividing the number of double bonds by the total number of bonds on the fatty acid chain (eq. 3.3):

$$\% \, u.i. = \frac{\sum double \, bonds}{\sum total \, bonds} \times 100$$

eq. 3.3

Plasmalogens were not included in the number of double bonds or total fatty acid chain bonds.

Average ($\bar{x}$)

$$< \bar{x} > = \frac{\sum n_1 + n_2 + n_3 + ... + n_n}{n_n}$$

eq. 3.4

Standard deviation (s)

The standard deviation represents the difference between replicate measurements.

$$s = \sqrt{\frac{\sum (x_i - \bar{x})^2}{n-1}}$$

eq. 3.5

F-test for comparison of two variances

The null hypothesis is stated that there is no significant difference between the two variances. If $F_{calc} > F_{table}$, p, v_1, v_2 then the null hypothesis is rejected and there is a significant difference between the two populations. $F_{calc} > 1$, $v_1 = n_1-1$, $v_2 = n_2-1$

$$F_{calc} = \frac{v_1}{v_2} = \frac{s_1^2}{s_2^2}$$

eq. 3.6

t-Test for comparison of two experimental means

$$\pm t_{calc} = \frac{(\bar{X}_1 - \bar{X}_2)}{sp} \sqrt{\frac{n_1 n_2}{n_1 + n_2}}$$

eq. 3.7

Analysis of Variance (ANOVA)

$$F_{calc} = \frac{V_1}{V_2}$$

eq. 3.8

Where V_1 equals the mean square error between the classes and V_2 represents the mean square error within the classes. If $F_{calc} > F_{table}$ then the HO is rejected and there is some systematic difference among the classes.

Statistical analysis for comparison of fatty acids between classes employed commercially available ABstat software (AndersonBell Corp, Arvada, CO, USA). Averages of the fatty acids were compared using a one-way ANOVA and Tukey post hoc test (p<0.05, n=3). Comparisons were limited to equivalent fatty acids between each of the tissues compared to brain, i.e. brain 14:0 vs. heart, kidney and liver 14:0 (Table 3.1).

Table 3.1. Mitochondrial fatty acid composition and distribution between various tissues.

Species (Structure)[a]	FAME (%)[c,d]			
	Brain[b]	Heart	Kidney	Liver
Dodecanoic acid (12:0)	0.48±0.13	0.66±0.15	0.74±0.07	0.43±0.04
Tetradecanoic acid (14:0)	0.67±0.12[*,≠]	1.03±0.11	1.35±0.12	0.93±0.03
Pentadecanoic acid (15:0)	0.47±0.12[≠]	0.57±0.06	0.94±0.05	0.62±0.08
9-Hexadecenoic acid (16:1Δ9)	1.49±0.61[*]	0	1.89±0.94	1.17±0.15
Hexadecanoic acid (16:0)	30.49±0.58[*]	15.12±1.3	32.14±0.04	30.01±0.49
Plasmalogen 16:0 (P 16:0)	2.09±0.34[‡]	2.20±0.14	1.59±0.71	0.31±0.27
Heptadecanoic acid (17:0)	0.66±0.11[≠]	0.89±0.13	0.97±0.06	0.59±0.01
9,12-Octadecadienoic acid (18:2Δ9,12)	1.08±0.33[*,≠,‡]	23.92±0.62	10.40±1.2	11.19±0.68
9-Octadecenoic acid (18:1Δ9)	16.18±0.82[*,≠,‡]	6.49±0.36	8.36±0.34	7.16±0.78
10-Octadecenoic acid (18:1Δ10)	5.57±0.90[‡]	6.79±0.76	4.16±0.46	3.81±0.15
Octadecanoic acid (18:0)	21.28±1.1[‡]	25.33±1.1	22.06±1.22	29.77±0.88
Plasmalogen 18:1a (P 18:1a)	0.87±0.19	0	0	0
Plasmalogen 18:1b (P 18:1b)	0.86±0.18	0	0	0
Plasmalogen 18:0 (P 18:0)	2.69±0.92	1.74±0.18	0	0
5,8,11,14-Eicosatetraenoic acid (20:4)	9.28±0.81[*,≠,‡]	15.25±0.39	15.39±1.4	14.02±0.39
4,7,10,13,16,19-Docosahexaenoic acid (22:6)	3.79±1.4	0	0	0
7,10,13,16-Docosatetraenoic acid (22:4)	2.13±0.44	0	0	0

[a] Number of carbons:degree of unsaturation
[b] Significant differences between brain fatty acids (p<0.05, n = 3) indicated by [*] for heart, [≠] for kidney, and [‡] for liver
[c] Comparisons made on % FAME basis due to differences in μg fatty acid per mitochondrial protein concentration between tissues
[d] Values are averages of three replicates ± sd

Chapter 3.3. Results

The objective of this project was a membrane composition comparison between mitochondria originating from various tissues from Sprague Dawley rats. An impediment in the analysis of sub-cellular organelles is the necessity for high-purity isolation from biological samples. There are numerous procedures for the isolation of mitochondria [105, 109-114]. The methods share a common foundation in the isolation through differential centrifugation, however they differ in the isolation buffer, centrifugation times, speeds, and in the density gradient. The chosen isolation procedure was comparable to a previously employed procedure, therefore little optimization was required [105, 109].   The modification in the use of a discontinuous Percoll gradient provided greater mitochondria separation from the myelin layer than the previously used continuous gradient [115]. The discontinuous gradient also allowed separation of free mitochondria from those trapped in lipid vesicles, such as synaptosomes from brain tissue. The results of mitochondrial isolations are represented by western blot analysis (Figure 3.2). The intense porin band signifies an increased concentration of mitochondria over the total homogenate. The absence of MAP2 and lamin B bands verify the purity of mitochondrial isolation.

Fatty acid structure analysis

A complete description of the fatty acid profile requires structural analysis of the acyl chains. Unfortunately electron-impact ionization, used during quantification of FAMEs, fails to provide characteristic fragmentation patterns that provide structural elucidation of double-bond or chain-branching locations. Spectra obtained by EI are dominated by low molecular weight fragments and ions generated from fragmentation pathways that produce statistical stable products.   Representative EI spectra for mitochondrial FAME products, not discussed in detail below, are shown in Figures 3.3 to 3.9. Spectra generated through CI provide an abundant $[M+H]^+$ ion for proper fatty acid recognition, but as with EI fragments for conclusive structural identification are not generated due to rearrangement around bond breakage sites.

For these reasons alternative methods of derivatization were necessary for structural identification. A variety of derivatization reagents are available that provide characteristic fragmentation patterns [62].   Derivatization of methyl esters through

transesterification with 3-hydroxymethylpyridine, to form picolinyl esters, allowed charge remote fragmentation along the fatty acid backbone facilitating structural elucidation.

The process of remote charge fragmentation allows separation of the cation charge from the site of fragmentation [51, 60, 63]. The result for straight-chain saturated fatty acids is an equal distribution of ions originating from each site along the fatty acid chain length. Picolinyl fragmentation of straight-chain fatty acids provides a repeating pattern of $[M]^+$-$(CH_2)_n$ mass units, after the loss of the terminal methyl group [60, 63]. Examination of the mass spectrum for the picolinyl ester of octadecanoic acid (18:0), the presence of the molecular ion, m/z 375, permits conclusive identification of the particular fatty acid derivative (Figure 3.11). The ion at m/z 360 is generated by loss of the terminal methyl group, followed by successive loss of 14 amu to m/z 151. The EI spectrum for the methyl ester of octadecanoic acid is provided for comparison (Figure 3.10)

The lack of diagnostic fragment ions creates difficultly in determining sites of unsaturation along the acyl chain, as seen with the EI spectra of methyl 9,12-octadecadienate (Figure 3.12). However, fragmentation of picolinyl fatty acids with double bonds have a distinctive pattern indicating the site of the unsaturation, as illustrated by 9,12-octadecadienic acid (18:2Δ9,12) (Figure 3.13). As with the saturated fatty acid the molecular ion, m/z 371, loses the terminal methyl group to produce m/z 356, then the repeating pattern of $[M]^+$-$(CH_2)_n$ mass units is present except for locations of double bonds. Cleavage at the methylene group alpha to the double bond results in a 26 amu gap between m/z 300 and m/z 274, indicated by * (Figure 3.13). There is a loss of 14 amu from m/z 274 to m/z 260, then a second 26 amu gap from m/z 260 to m/z 234. This type of fragmentation pattern is indicative of a methylene interrupted diene acyl chain. The double bond location indicator ions can also be seen by a gap of 40 amu from m/z 314 to m/z 274 and m/z 260 to m/z 220 [60, 63-64]. Mechanisms for fragmentation of unsaturation fatty acids are shown in Figure 3.14.
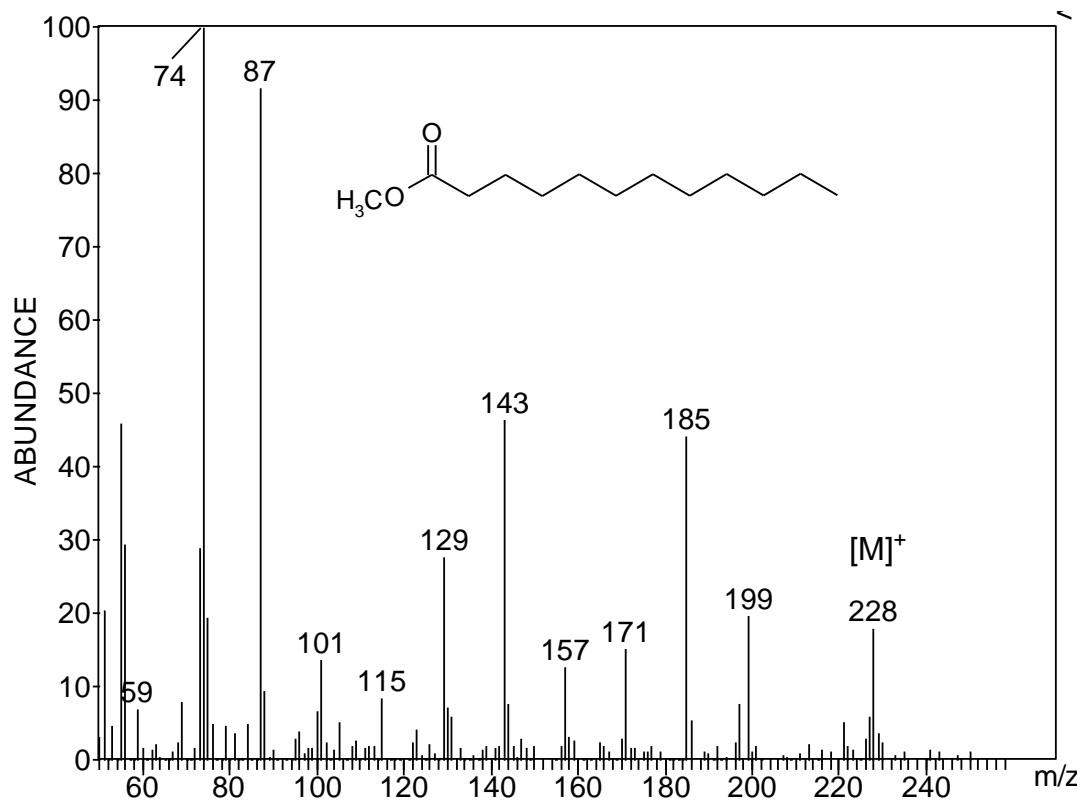
Figure 3.3. Mass spectrum of methyl dodecanoate (12:0).
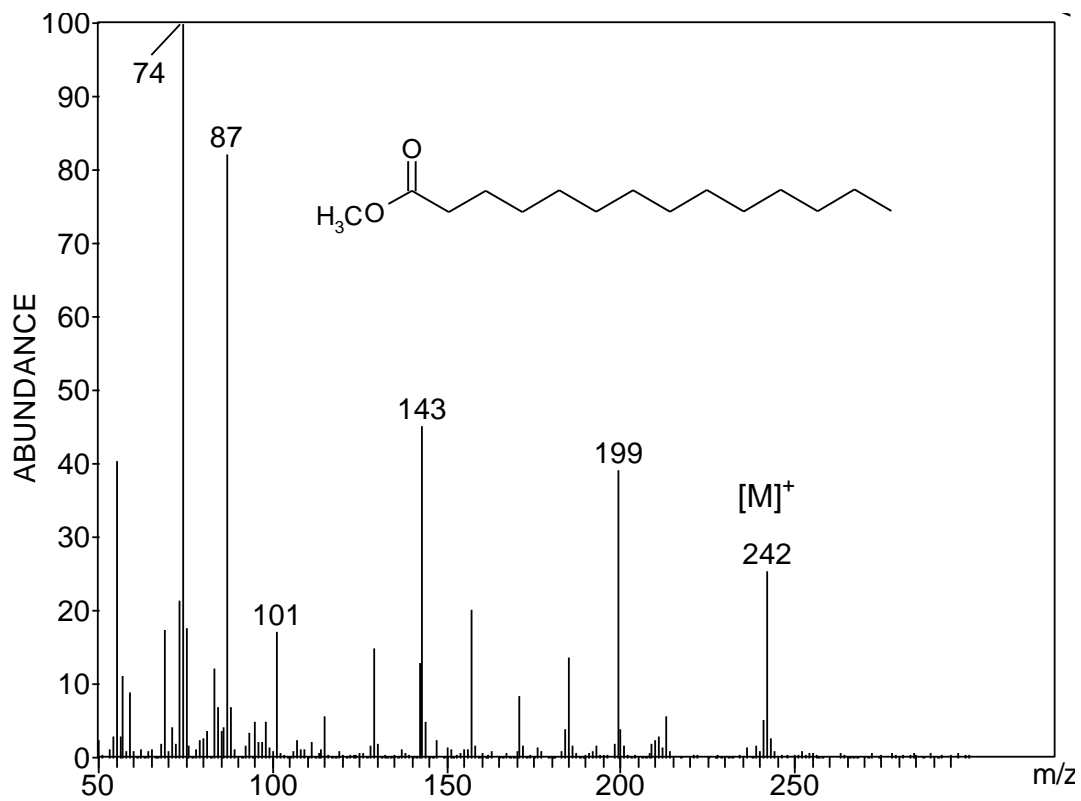
Figure 3.4. Mass spectrum of methyl tetradecanoate (14:0).
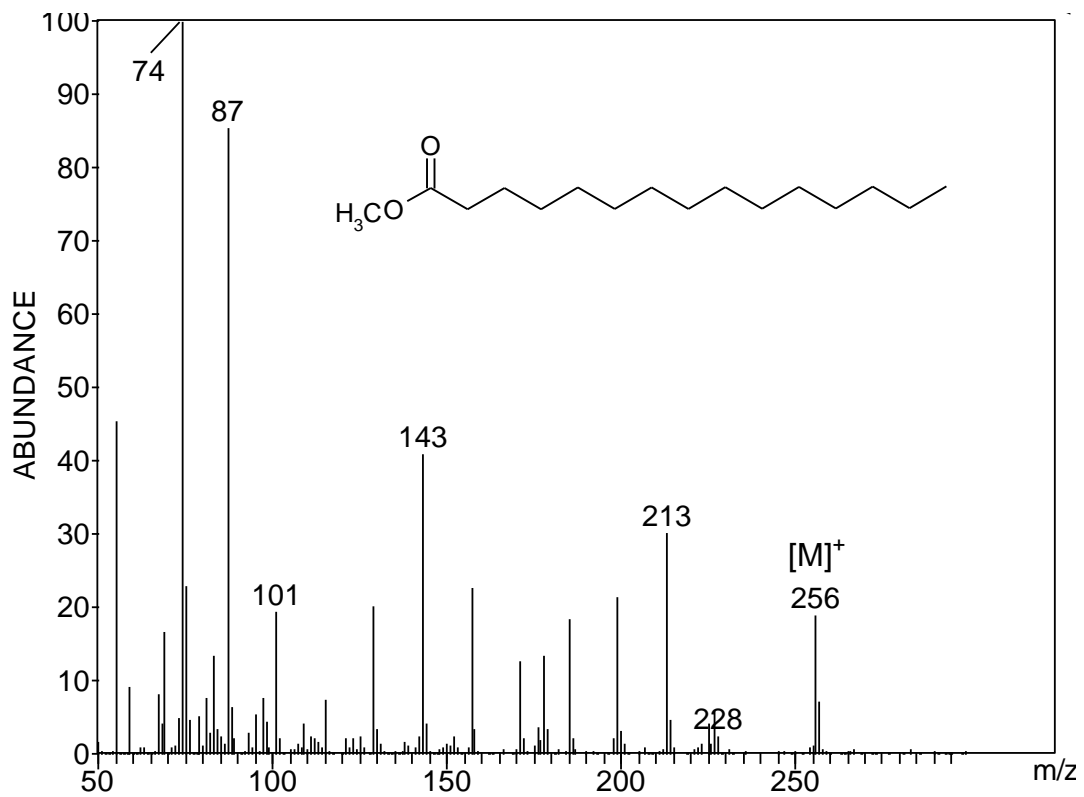
Figure 3.5. Mass spectrum of methyl pentadecanoate (15:0).
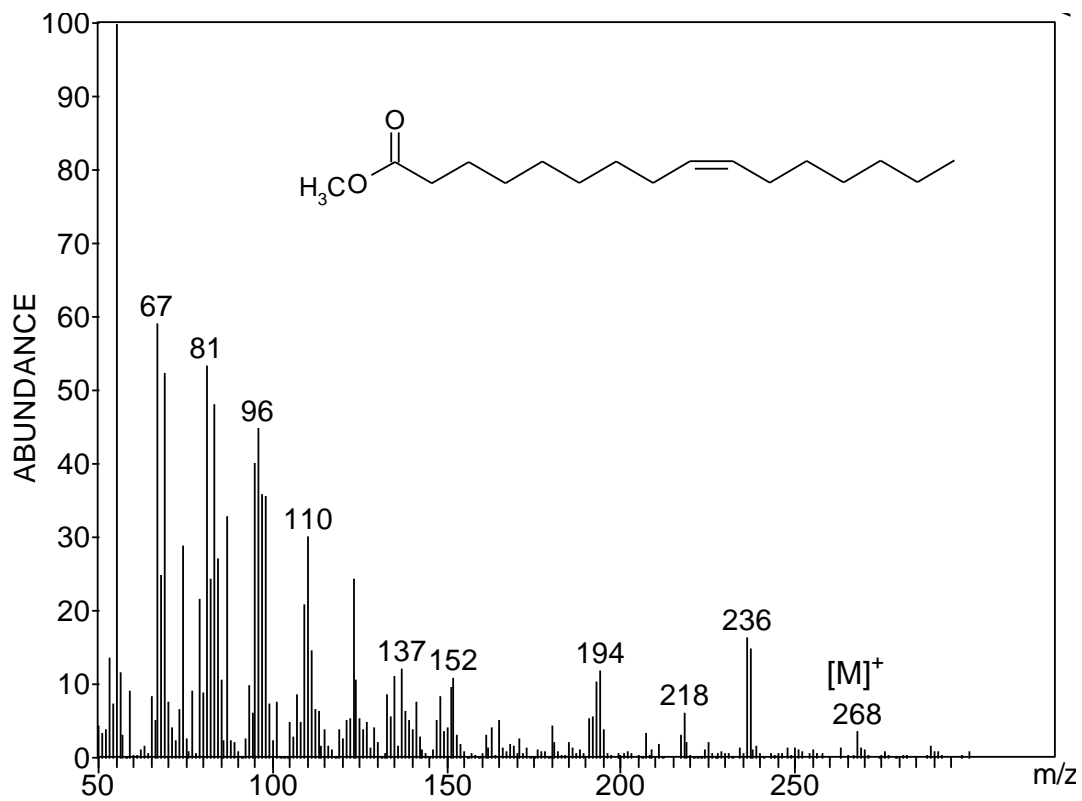
Figure 3.6. Mass spectrum of methyl 9-hexadecenoate (16:1Δ9).
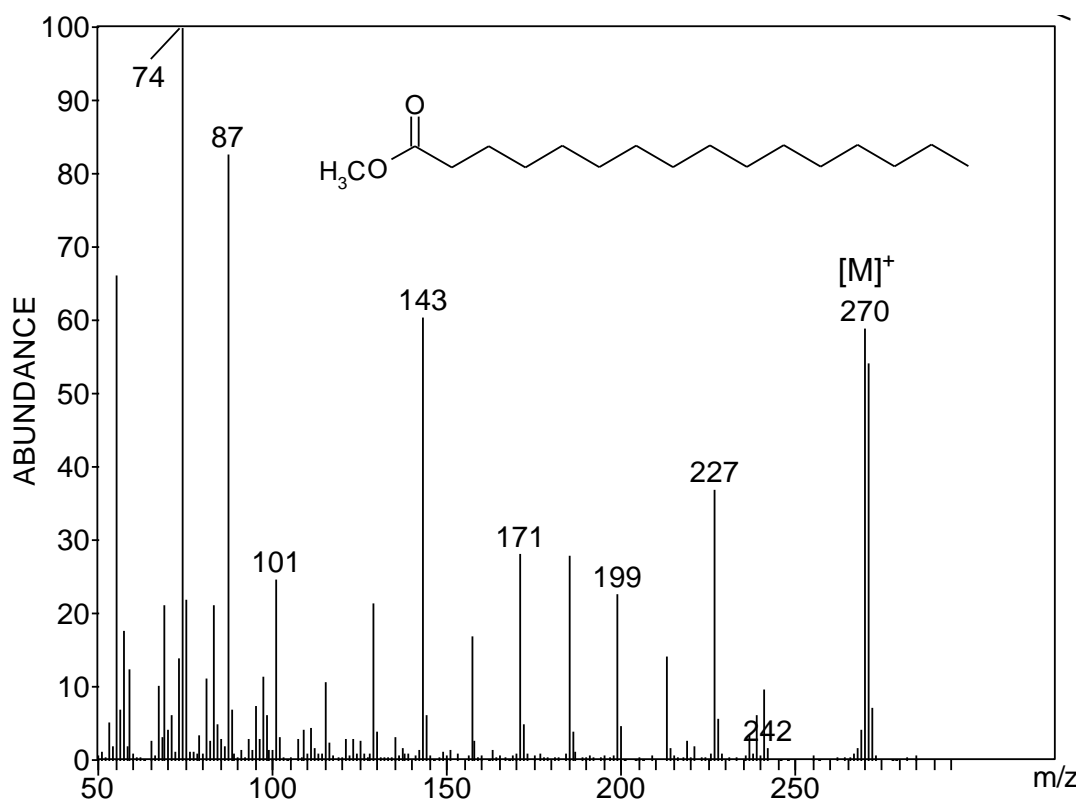
Figure 3.7. Mass spectrum of methyl hexadecanoate (16:0).
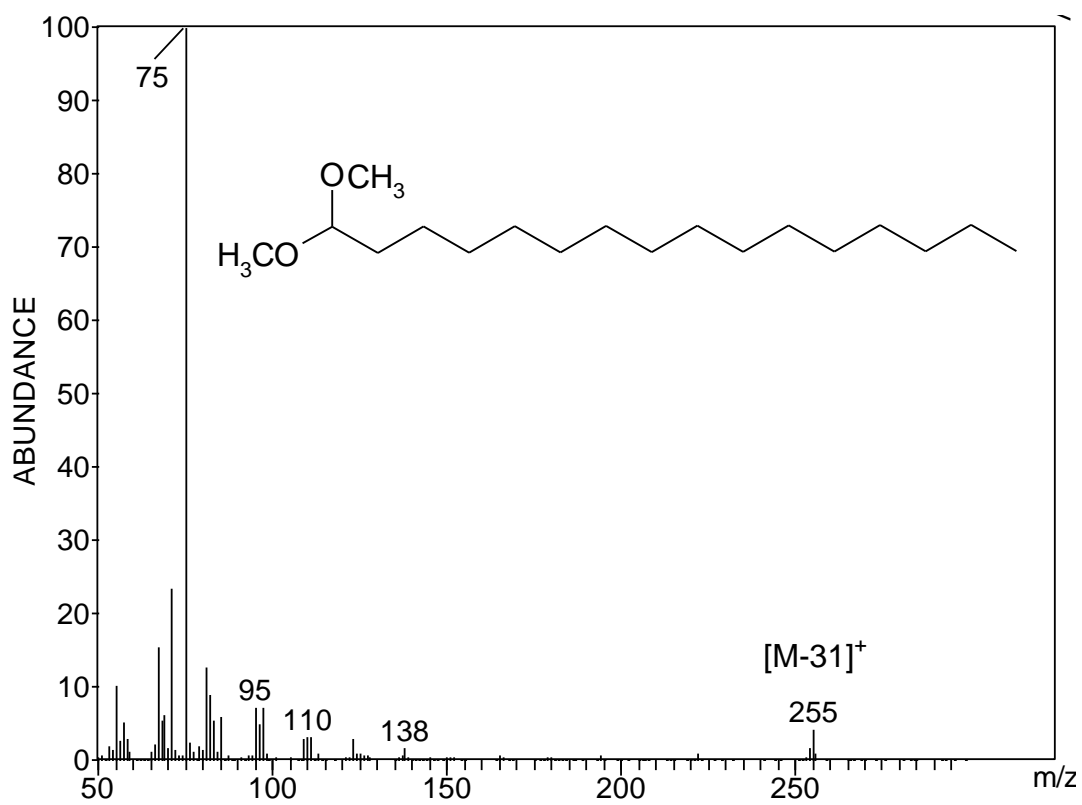
Figure 3.8. Mass spectrum of dimethyl acetal of hexadecan-1-al (P 16:0).
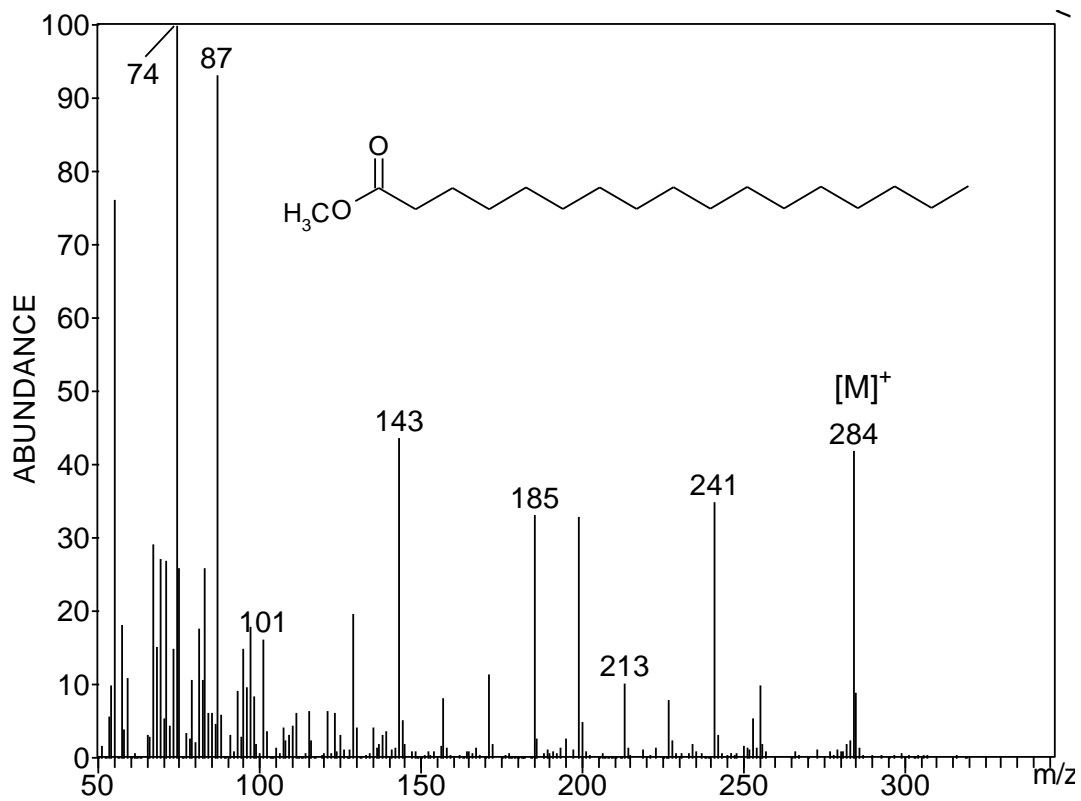
Figure 3.9. Mass spectrum of methyl heptadecanoate (17:0).
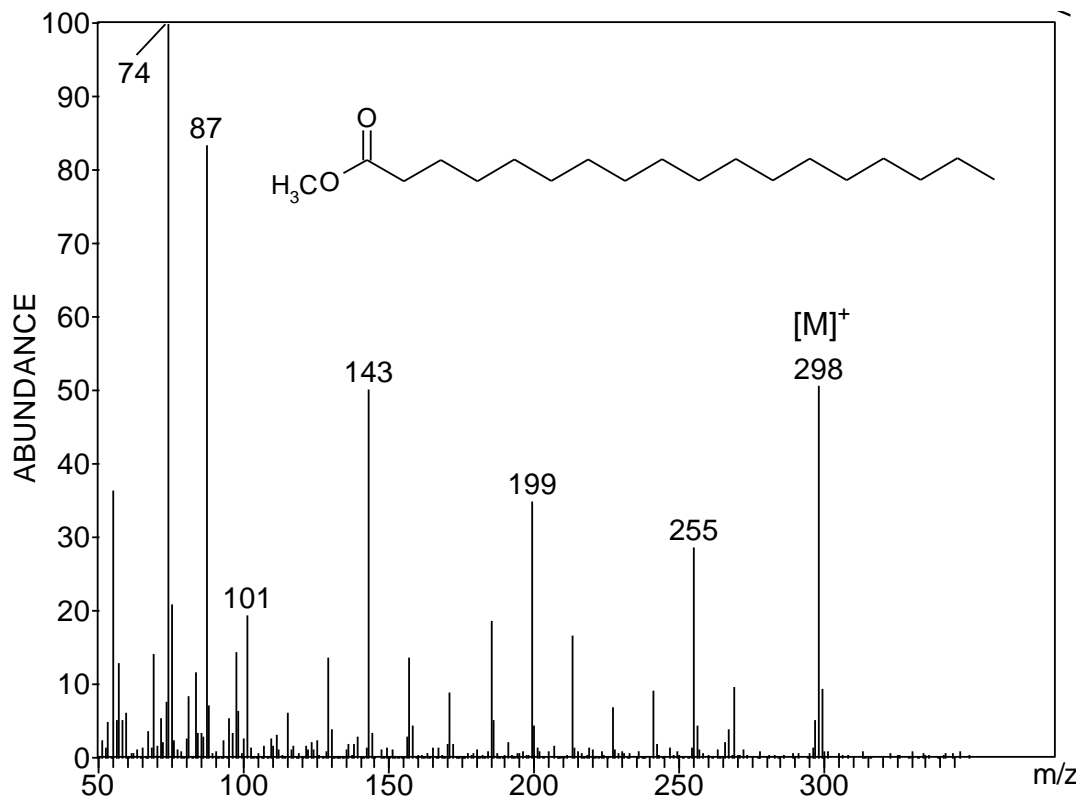
Figure 3.10. Mass spectrum of methyl octadecanoate (18:0).
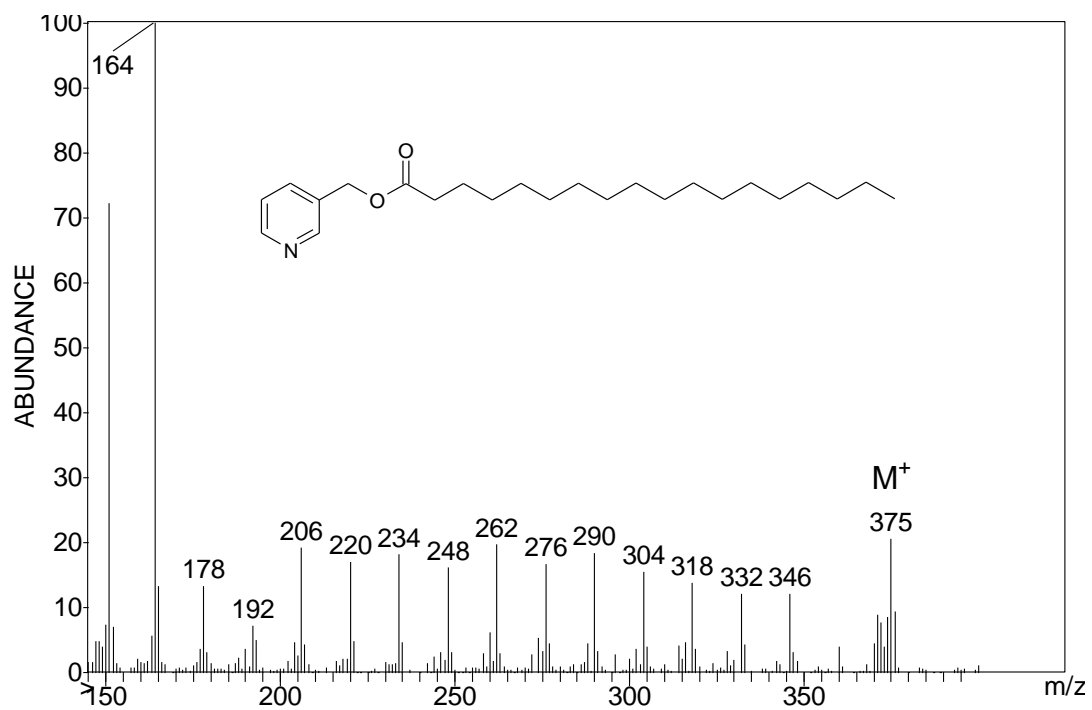
Figure 3.11. Mass spectrum of picolinyl octadecanoate (18:0).
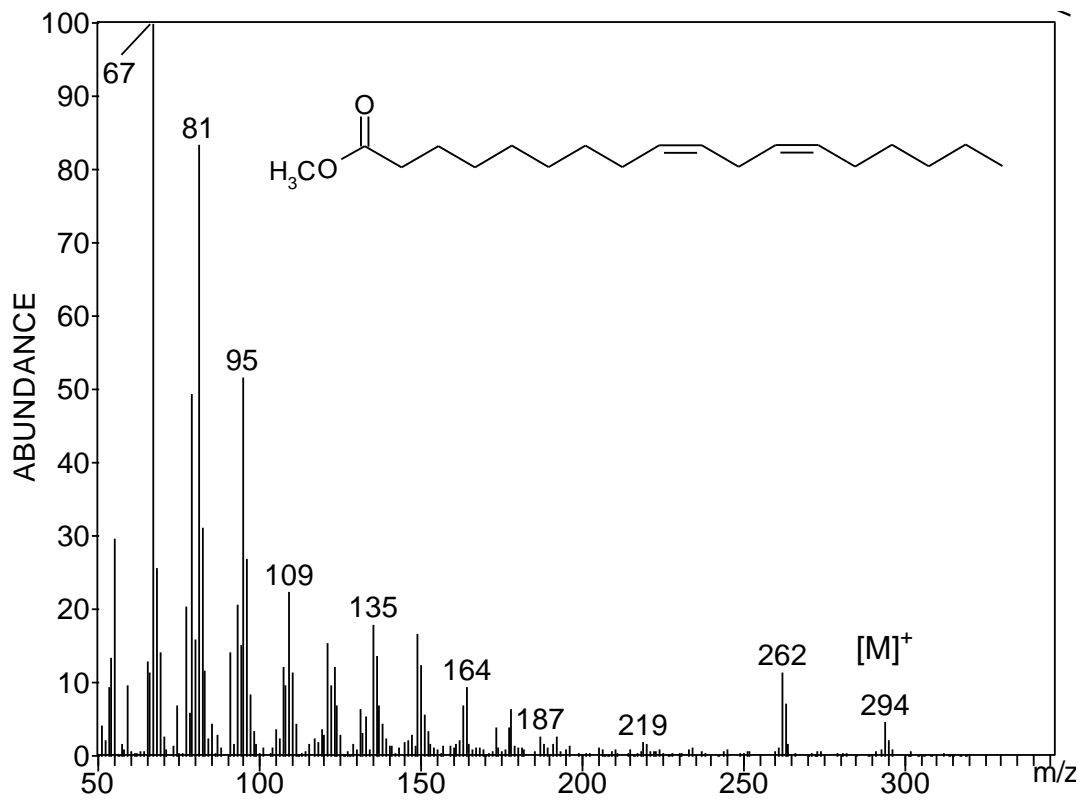
Figure 3.12. Mass spectrum of methyl 9,12-octadecadienoate (18:2Δ9,12).
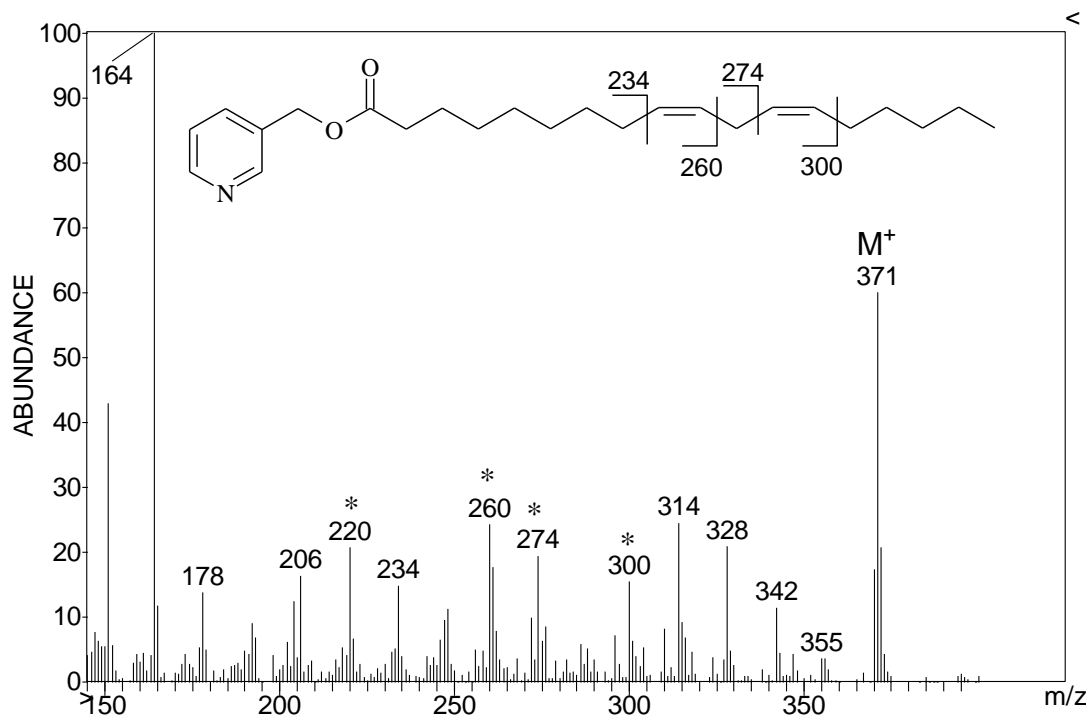
Figure 3.13. Mass spectrum of picolinyl 9,12-octadecadienoate (18:2Δ9,12).

The EI spectra from the methyl ester derivatives of the two octadecenoic acids (18:1) are shown in Figures 3.15 & 3.16. Spectra from EI of the two octadecenoic acid picolinyl esters, reveal the site of unsaturated through the fragmentation patterns (Figures 3.17 & 3.18). As with the other two previous examples the molecular ion, m/z 373, loses the terminal methyl group to produce m/z 358, and the $[M]^+$-$(CH_2)_n$ mass units trend repeats except at the double bond site. The spectrum for 9-octadecanic acid (18:1Δ9) displays a difference of 26 amu between m/z 246 and m/z 220, signifying the double bond position (Figure 3.17) [60, 63-64]. The spectrum for 10-octadecanic acid (18:1Δ10) has a 26 amu difference between m/z 274 and m/z 248, indicative of a distal shift in the double bond position by one methylene unit (Figure 3.18) [60, 63-64].

This approach was used to identify the structures of fatty acids with other chain lengths. Analysis of mitochondria from all four tissues through picolinyl transesterification indicates that double bond positions are consistent for all tissues.

Fatty acid profile analysis

Methylation reactions were conducted with approximately equal mitochondrial protein concentrations as determined by BCA assay. The fatty acids from brain, heart, kidney and liver mitochondria were compared on a percent area count basis (individual FAME area count divided by total FAME area count, Figure 3.19). A significant increase in the percentage of 18:1Δ9 was noted in the FA profile between brain compared to heart, kidney or liver mitochondria. Concurrently, significant decreases in the percentages of 18:2Δ9,12 and 20:4 were evident between brain FA profiles and the other mitochondrial profiles. Additionally, brain mitochondria contained several FA species not present in other tissues: P18:1s, 22:6 and 22:4.

The total percentage of saturated fatty acids across brain, kidney and liver showed minor variation (Table 3.1). The lower percentage of saturated FAs in brain mitochondria was compensated for by an increase in plasmalogen species (Table 3.2). In keeping with this trend, the percentage of unsaturated fatty acids (both mono- and polyunsaturated) was comparable across brain, liver and kidney. However, heart had
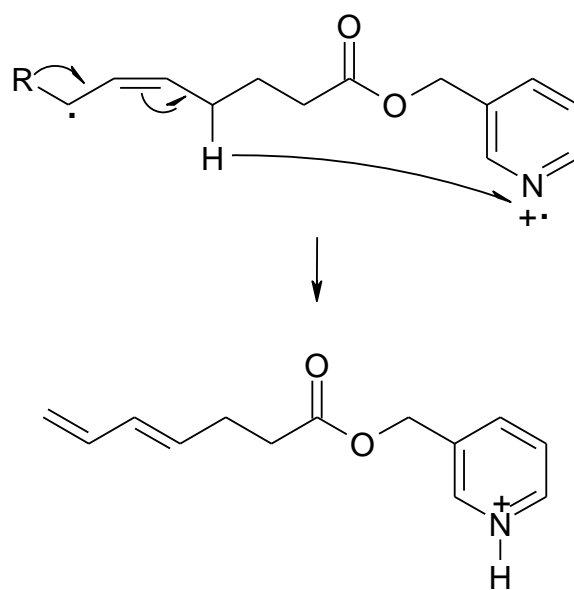
Figure 3.14. Fragmentation pathways for unsaturated picolinyl esters.
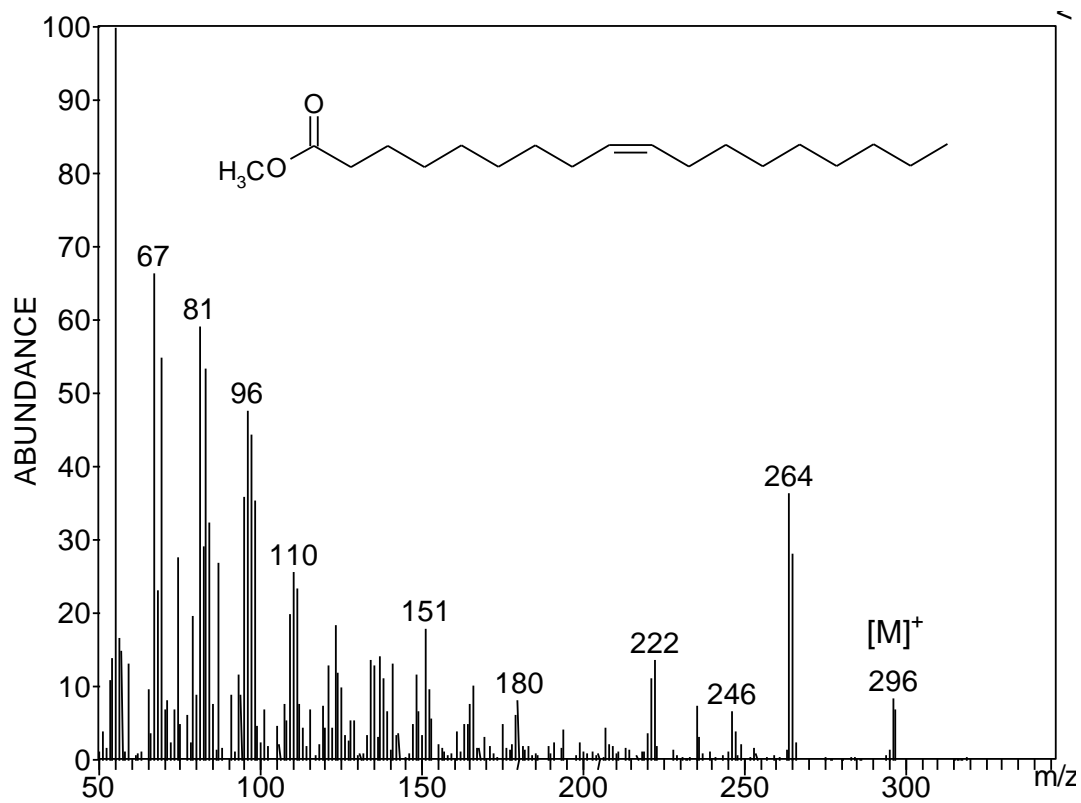
Figure 3.15. Mass spectrum of methyl 9-octadecenoate (18:1Δ9).
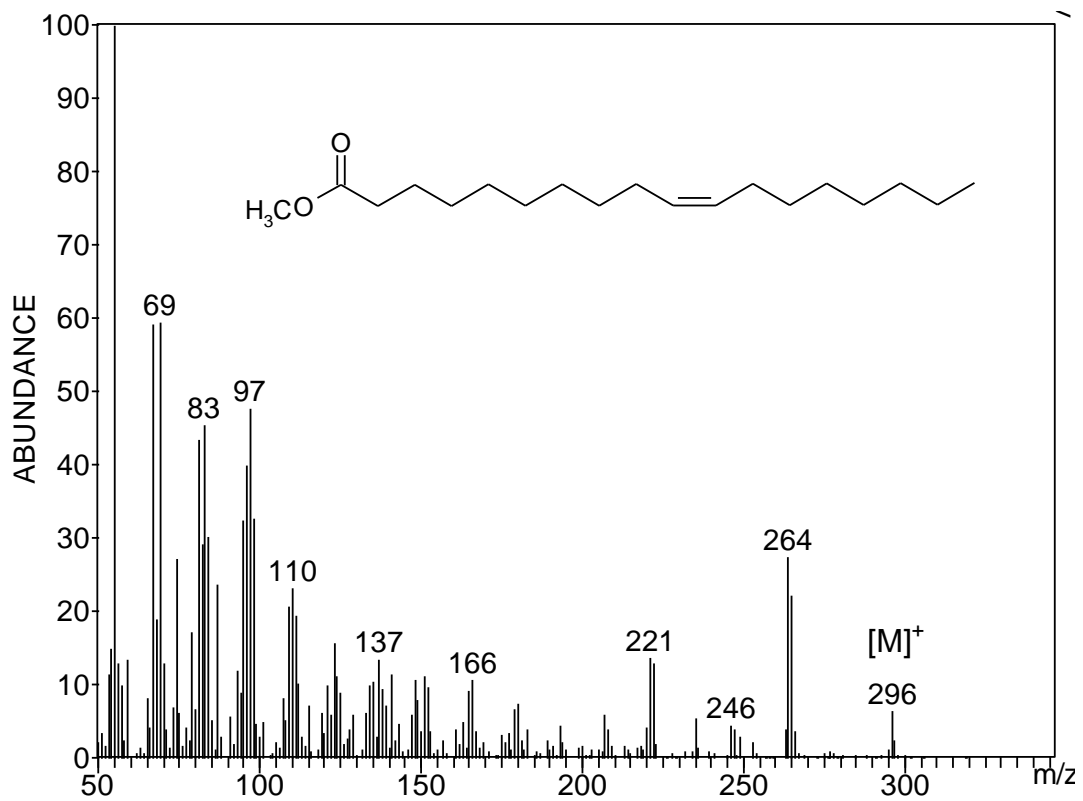
Figure 3.16. Mass spectrum of methyl 10-octadecenoate (18:1Δ10).
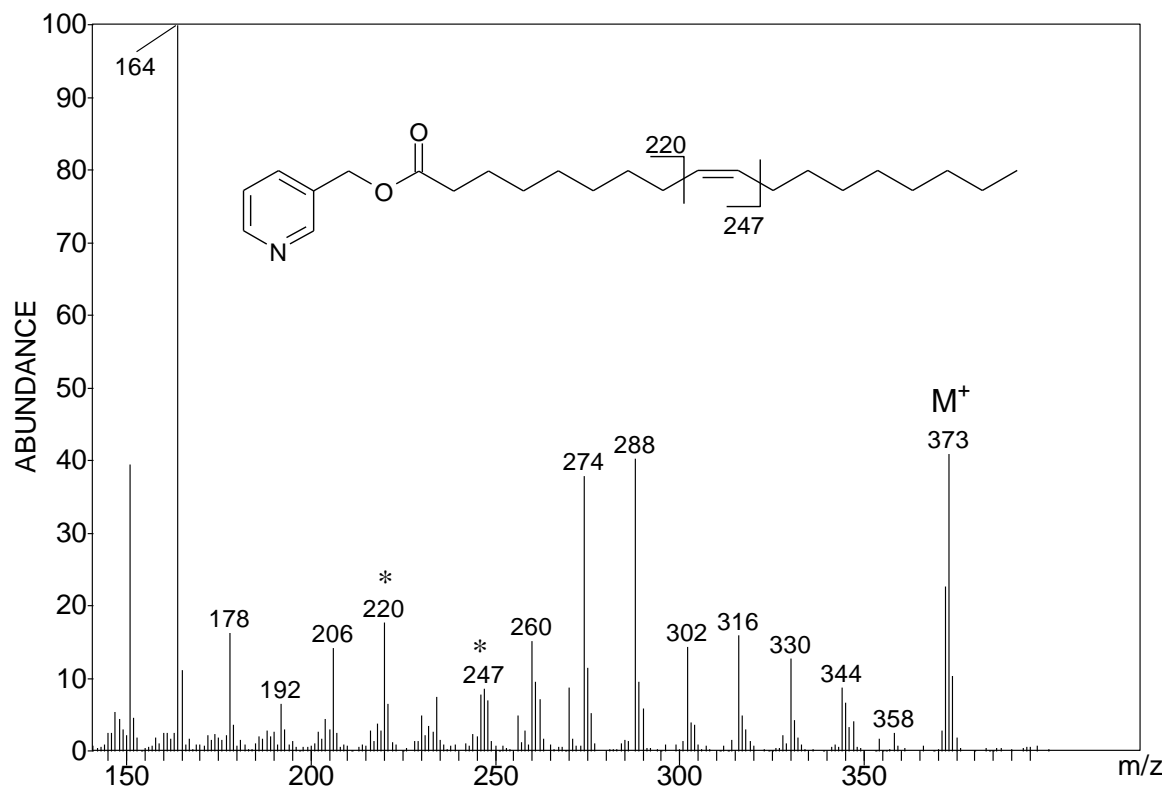
Figure 3.17. Mass spectrum of picolinyl 9-octadecenoate (18:1Δ9).
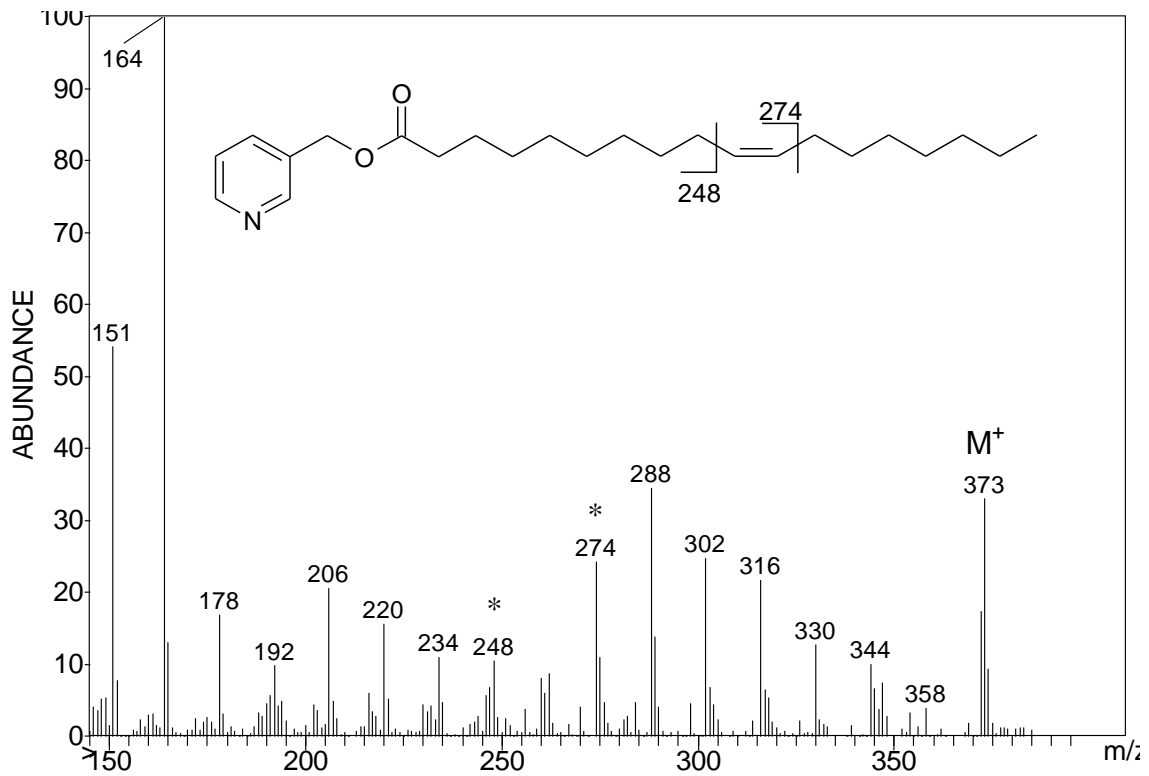
Figure 3.18. Mass spectrum of picolinyl 10-octadecenoate (18:1Δ10).
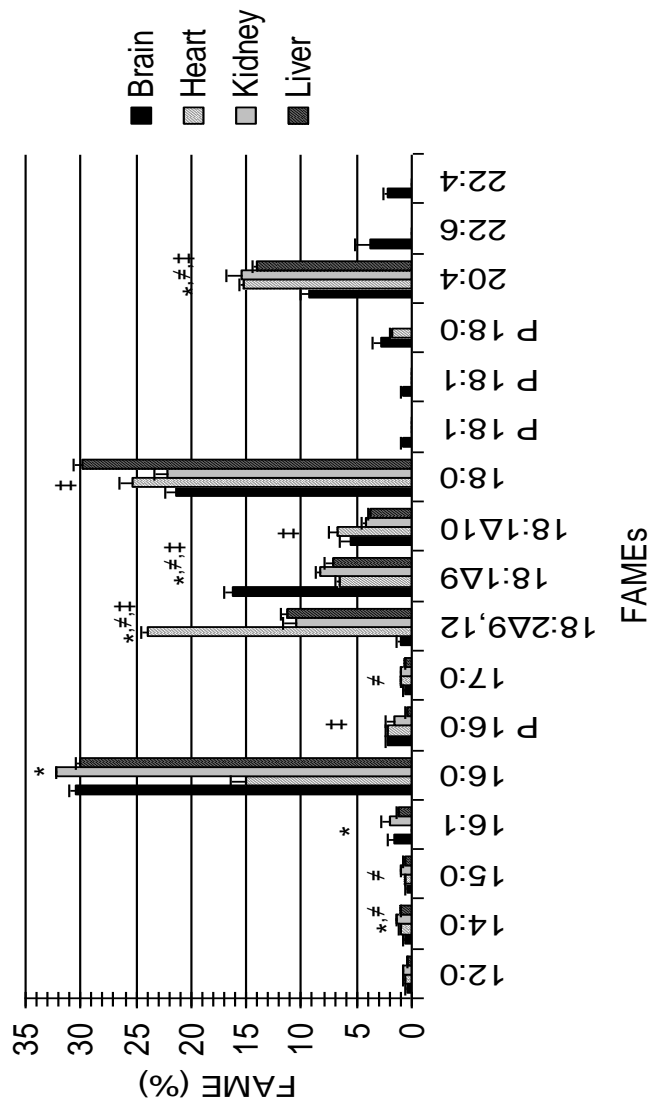
Figure 3.19. Distribution of mitochondrial fatty acids per tissue.

Table 3.2. Percent comparison of saturated to unsaturated fatty acids between various tissues.

Tissue	SFA[a]	MUFA; PUFA[b]	SFA/UFA ratio[c]	Unsaturation index (%)[d]	Plasmalogens
Brain	53.94	23.25; 16.29	1.36	8.41	6.52
Heart	43.60	13.29; 39.17	0.83	4.81	3.94
Kidney	58.20	14.42; 25.79	1.45	4.94	1.59
Liver	62.34	12.14; 25.21	1.67	4.94	0.31

[a] Saturated fatty acids

[b] Monounsatured fatty acids; Polyunsaturated fatty acids

[c] Values represent ratio of saturated/total unsaturated fatty acids

[d] Number of double bonds divided by total number of bonds in the fatty acid chain (calculation does not include unsaturation contributions from plasmalogen species)

approximately 12% lower saturated FAs percentage than the other tissues. As expected the percentage of unsaturated fatty acids (both mono- and polyunsaturated) increased for heart, as a result of an appreciable higher 18:2Δ9,12 level.

The distribution of mono- and polyunsaturated FAs provided greater distinction between mitochondria from the various tissues (Table 3.2). Heart mitochondria had the largest percentage of polyunsaturated FAs (a total of 39%), due to a disproportionate excess of 18:2Δ9,12 (Figure 3.19). In fact, the percentage of 18:2Δ9,12 from heart mitochondria was significantly higher (p<0.01) than the other three tissues. The percentage of monounsaturated FAs in brain was approximately doubles that of kidney and liver. However the polyunsaturated FA percentage from brain was roughly half than in kidney and liver, despite the presence of several PUFA species not incorporated in the other mitochondrial samples (Figure 3.19). The percentage of monounsaturated FAs in brain was approximately double that of kidney and liver. However the polyunsaturated FA percentage from brain was roughly half than in kidney and liver, despite the presence of several PUFA species not incorporated in the other mitochondrial samples (Figure 3.19).

Differences in the fatty acid species from brain, heart and kidney were also evaluated on a log scale as normalized to the corresponding liver FAME species (Figure 3.20). Normalizing the data to liver, illustrates the change in the brain lipid profile when compared to the other three tissues and also emphasizes the homogeneity among the heart, kidney and liver mitochondrial profiles. Positive deviation from the baseline, such as 18:1Δ9, signify an increase in relative abundance of FAME species for brain in relation to liver. Negative deviation, as in the case of 18:2Δ9,12 and 20:4, signify a reduction in relative abundance of FAME species relative to liver. Only FAME species present in all four tissues have been shown.
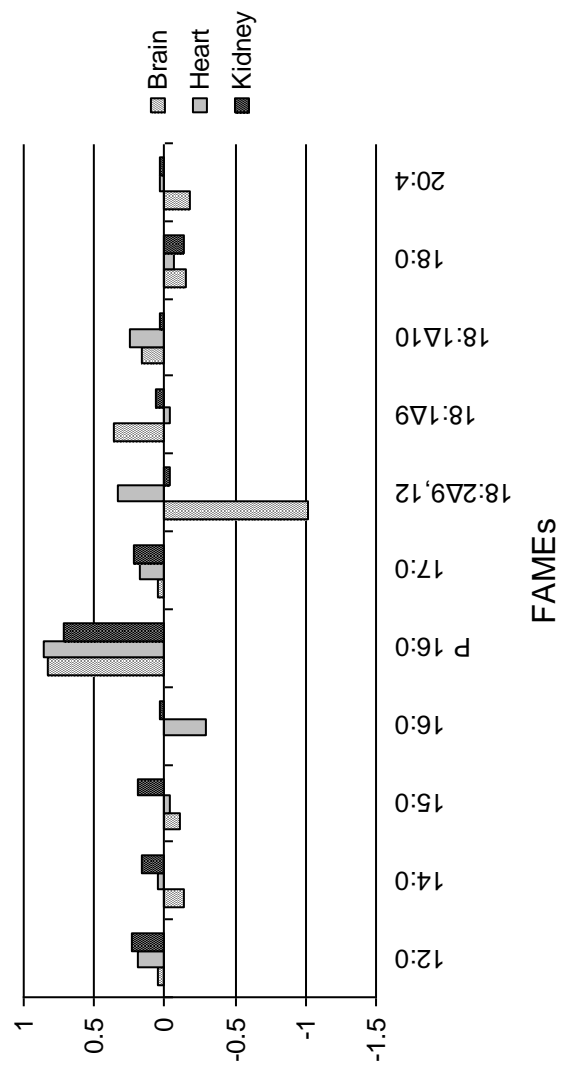
Figure 3.20. Relative distribution of brain, heart and kidney mitochondrial fatty acids compared to liver.

Chapter 3.4. Discussion

Since lipids serve a dual function as membrane components and as secondary messengers, changes in the mitochondrial membrane composition might be the result of distinctive cellular environments between various tissues. Diversity in the lipid profile, as a function of tissue, could lead to a variety of innate responses as a consequence of detrimental species generated in vivo. Specifically, neurological tissue has an increased potential for oxidative stress due to a higher oxygen consumption rate and comparatively low level of antioxidant capacity.   Oxidative stress, a hallmark of many neurodegenerative diseases, leads to the development of ROS [116]. Common targets for ROS are lipid components, namely polyunsaturated fatty acids (PUFAs) [103, 117-119]. Previous studies have shown that neurological plasma membranes contain an abundance of PUFAs. Most notably, grey matter is highly enriched with docosahexaenoic acid (22:6ω3) [118, 120]. The susceptibility of PUFAs to oxidation is theoretically reduced by the presence of plasmalogens (P) [121-123]. Plasmalogens are commonly associated with PUFAs in the sn-1 position along the glycerol backbone of phospholipids. They are believed to act as endogenous anti-oxidants, providing preferential cleavage sites for ROS thus protecting PUFAs [121-123].

The current study was successful in identifying deviations in the fatty acid profile of neurological mitochondria compared to mitochondria from other tissues from Sprague Dawley rats. Data support the premise that variations in brain mitochondrial lipids may increase the susceptibility to the products of oxidative stress. Several researchers have linked changes in the proportion of PUFAs to membrane stability as measured by life expectancy [124-125].   Pamplona et al. compared the mitochondria membrane compositions from liver of rats and pigeons [125]. Their data supported the theory that reduced incorporation of PUFAs in the mitochondria from pigeons contributed to an increased life expectancy. Similar conclusions were drawn by Mitchell et al. who conducted studies with the naked mole-rat and found a reduction in DHA and an increase in plasmalogen content [124]. Their results were believed to contribute to a longer life expectancy, inferring that mitochondria containing lower levels of PUFAs will have a considerable reduced susceptibility to oxidative damage [124]. Studies conducted by Tahin et al. found the fatty acid profiles of rat brain mitochondria were less influenced to

dietary changes than the fatty acid profiles of heart and liver mitochondria [126]. It was hypothesized that the resilient nature neurological mitochondria to modify their membrane composition in response to dietary changes might be the result of the blood-brain barrier [126]. This pseudo-insulation for the brain may result in long-term health implementations.

Fatty acid structure analysis

The true measure of membrane variations with the potential to affect the susceptibility of lipids to oxidation by ROS would be changes in unsaturation. The ratio of mono- to polyunsaturated fatty acids for the brain mitochondria samples was significantly higher than that of the other three tissues (Table 3.2). The major contributor for the increased ratio of monounsaturated over polyunsaturated FAs in brain mitochondria stems from the lower abundance of $18:2\Delta9,12$. This decrease in $18:2\Delta9,12$ may be the result of increased long chain PUFAs synthesis that utilizes $18:2\Delta9,12$ as a precursor. Conversely, the significant increase in the polyunsaturated FAs in heart mitochondria is probably the result of a greater abundance of cardiolipin, which has been shown to predominately consist of $18:2\Delta9,12$ fatty acids [127-128]. Cardiolipin has been shown to be highly abundant in the inner mitochondrial membrane and plays a critical role in the electron transport chain [129]. This is a noteworthy finding of our study, since brain mitochondria had a significantly lower percentage of $18:2\Delta9,12$ than mitochondrial from the other tissues (Table 3.1). This alteration in fatty acid composition, may impart unique physical properties to the membrane of neurological mitochondria [128].

The attribute with the greatest potential to increase the susceptibility of lipid oxidation by ROS would be changes in the unsaturation index. The percent of double bonds per total methylene moieties, unsaturation index (u.i.), presents an interesting comparison between the tissues (Table 3.2). The u.i. associated with brain mitochondria was approximately twice that of other tissues. This increase in u.i. was the result of two FAs, 22:4 and 22:6, which were unique FAs to brain samples. These two PUFAs, encompassing ten double bonds between them, more than doubled the number of double bonds in brain mitochondria. In essence, this represents an increased potential for susceptibility to ROS. In addition to greatly increasing the potential targets for ROS, the higher percentage of double bonds would significantly alter membrane dynamics [44].

Fatty acid profile analysis

Results from the current study found that the percentage of total saturated FAs was nearly equivalent within brain, kidney and liver mitochondria. This similarity in fatty acid profiles across three of the four tissues studied lends credence to the theory that preservation of membrane physical properties are essential for functionality, as changes to the fatty acid species will have a significant impact on the physical properties of the membrane [2, 15]. The homogeneity of fatty acid saturation echoes results obtained by Pamplona et al. in their study of liver mitochondria between species [125].

Neurological tissue has been reported to have an increased abundance of polyunsaturated fatty acids, therefore, it is interesting that brain mitochondria would display a greater abundance of monounsaturated fatty acids [130-132]. In fact, the distribution of arachidonic acid (ARA; 20:4ω6), showed that brain mitochondria contained approximately 5% lower abundance than the other tissues. However, this deficiency in ARA was in essence offset by the presence of two other long-chain PUFAs, 22:6 and 22:4.

The presence of plasmalogens (vinyl-ether lipids) in neurological membranes has been well documented [133-135]. Plasmalogens are distinguished by a vinyl ether bond to the glycerol backbone as opposed to the ester linkage of traditional fatty acids [133-135]. It has long since been recognized that PUFAs and plasmalogens are commonly associated along the same phosphoglyceride backbone. The detection of plasmalogens in brain mitochondria that were absent from other tissues would certainly impart unique physical characteristics and functionality to the membrane [16]. Since the initial steps of plasmalogen synthesis occurs in peroxisomes, their existence within the mitochondrial membrane is the result of importation [15-16]. Plasmalogens function within the membrane and their role with regard to ROS has been the focus of extensive investigation [16, 121-123, 136]. The proposed functionality of plasmalogens as an endogenous anti-oxidant arises from the preferential oxidation of the vinyl-ether bond [121-123]. These unique plasmalogens (P18:0 and P18:1) increase the percentage of ether-linked lipids in brain to twice that of heart mitochondria, and four to six times that of liver and kidney, respectively (Table 3.2). The increased proportion of plasmalogens in brain

mitochondria might be a compensatory response to the higher unsaturation index and relatively low abundance of antioxidant counter measures [128].

Elucidation of the double bond location for the unique plasmalogens found in brain mitochondria and the bonding geometry along the glycerol backbone may provide insight into the nature of the mitochondria membrane and provide further differences between tissue specimens. The methylation reaction used in forming the FAMEs converts the vinyl-ether group to a dimethyl acetal. Unfortunately, these functional groups were not amenable to transesterification to picolinyl esters, and therefore alternative structural analysis methods were necessary. Chemical ionization experiments using acetonitrile as a reagent gas has been used for lipidomic structural analysis studies [65-66, 137]. Regrettably, these plasmalogens were also not amenable to structural elucidation by acetonitrile covalent-adduct CI (CACI), nevertheless isolation and MS/MS techniques on the molecular ions provided confidence in molecular classification (Figures 3.21 & 3.22) [138].

The appearance of unique PUFAs and plasmalogen species in brain mitochondria may provide the membrane with a greater susceptibility and protection from ROS. Differences in the mitochondria fatty acid profiles among the tissues may also reflect generational life spans of the mitochondria which might vary depending on the tissue [139]. Previous lipid studies from brain mitochondria have shown an increased turnover rate for phosphatidylethanolamine compared to other phospholipids [139]. The significance of phosphatidylethanolamine might be due to the fact that PUFAs and plasmalogens are commonly associated this polar head group and mitochondria serve as the site of synthesis for this polar head group [15]. This phospholipid species has also been shown to decrease in abundance with progression of neurodegenerative disease [140].

This study presents data on the elucidation of tissue specific variations in mitochondrial lipid profiles that support the theory of increased susceptibly of neurological mitochondria to oxidative stress. The relative pattern of abundance amongst $18:2\Delta9,12$ and $18:1\Delta9$ fatty acids gave a significantly different FA profile for brain
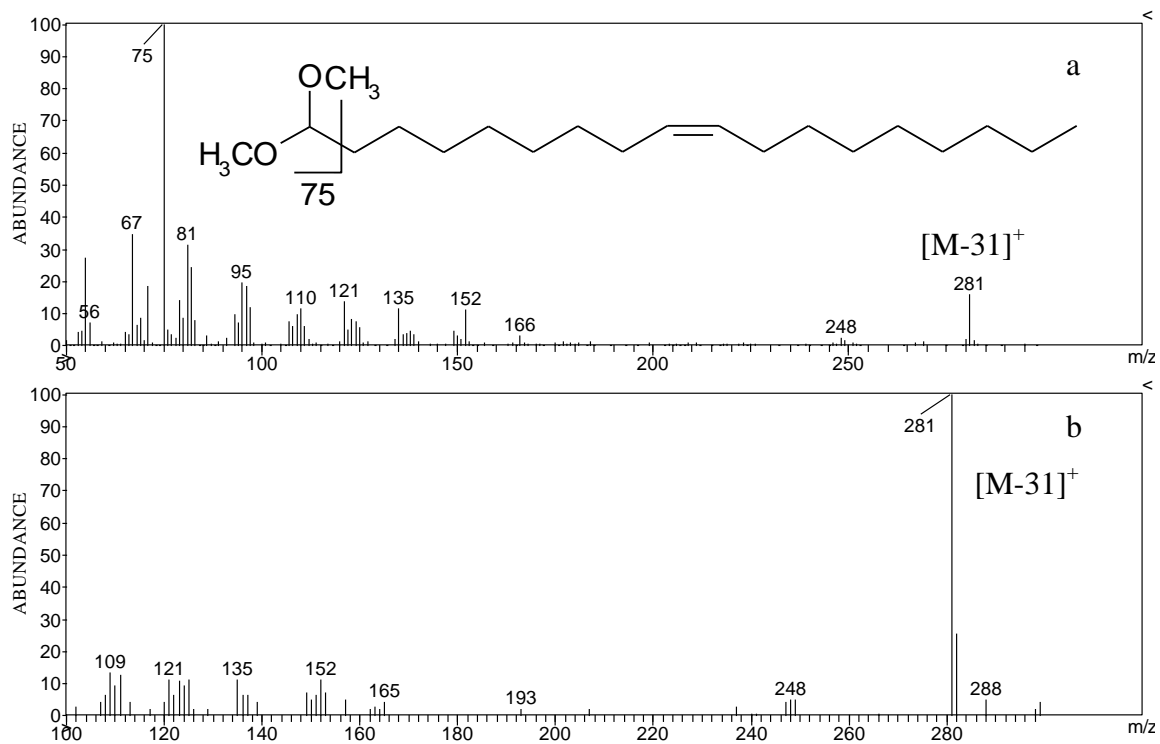
Figure 3.21. Mass spectra from (a) EI experiments and (b) CI experiments from dimethyl acetal of octadecen-1-al (P 18:1).
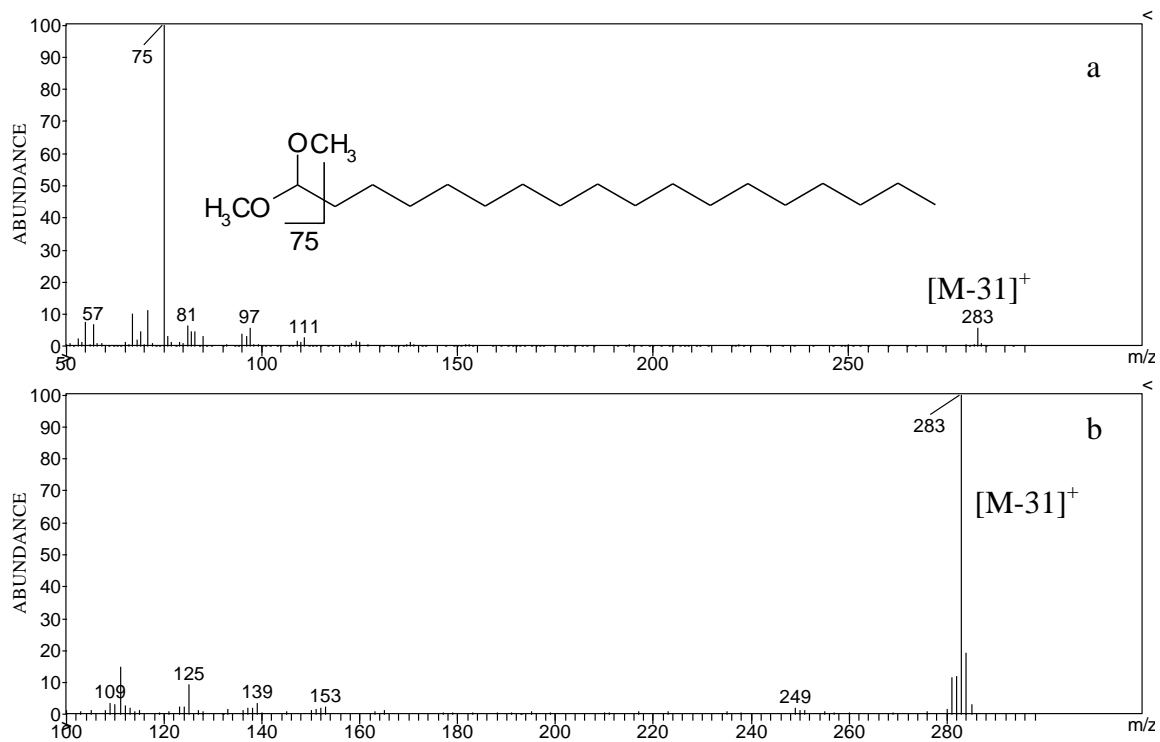
Figure 3.22. Mass spectra from (a) EI experiments and (b) CI experiments from dimethyl acetal of octadecan-1-al (P 18:0).

mitochondria compared to liver, kidney and heart. Even though the total percentage of unsaturated fatty acids was lower for brain, the appearance of unique PUFAs led to an unsaturation index double that of other tissues. The appearance of unique PUFAs in brain mitochondria increases the potential susceptibility to ROS. Diversity in the lipid profile, as a function of a tissue environment, could lead to a variety of detrimental responses as a consequence of the type of ROS generated in vivo. The characteristic fatty acid profile found in brain mitochondrial membranes will be used as a biological template for the exploration of changes that occur in the mitochondrial membrane during the progression of Alzheimer's disease.

Chapter 4. Study of Changes in the Mitochondrial Fatty Acids as a Function of Alzheimer's Disease Progression

Chapter 4.1. Introduction

The electron transport chain (ETC), which is vital for cellular energy production, is located on the inner mitochondrial membrane. The ETP is comprised of a multi-protein transmembrane complex that functions to oxidize hydrogen atoms which in turn drives the synthesis of adenosine triphosphate (ATP). Electron leakage from the ETP results in the generation of reactive oxygen species (ROS) and subsequent, ROS mediated oxidative damage [141-142]. Increased oxidative damage of cellular biomacromolecules has been shown in normal aging and is thought to play a role in the pathogenesis of numerous neurodegenerative diseases such as, Alzheimer's disease (AD) [103-104, 141]. Numerous studies report increased ROS mediated damage to nucleic acids [105], proteins [106], and lipids [107] during the pathogenesis of AD.

Oxidative stress, a hallmark of neurodegenerative disease, leads to the development of reactive oxygen species (ROS) [103]. Electrons leaking from mitochondria are the greatest source of ROS, thus mitochondria are a likely source and a target of oxidative stress. The high oxygen consumption rate and comparatively low levels of antioxidant capacity in neurological tissue would be expected to cause compensatory changes to the lipidome in order to minimize susceptibility to oxidative damage. A common target for these reactive oxygen species are lipid components, namely polyunsaturated fatty acids (PUFAs) [143-144]. Previous studies have shown that neurological plasma membranes contain an abundance of polyunsaturated fatty acids [145]. Most notably, grey matter is highly enriched with docosahexaenoic acid (22:6ω3). The susceptibility of PUFAs to oxidation is theoretically reduced by the presence of plasmalogens (P). Plasmalogens are commonly associated with PUFAs in the sn-1 position along the glycerol backbone of phospholipids. The vinyl-ether bonds are believed to act as endogenous anti-oxidants, providing preferential cleavage sites for ROS thus protecting PUFAs [134, 143, 146].

A diagnosis of AD requires both a clinical and a neuropathologic examination for proper disease state classification. Alzheimer's disease is diagnosed clinically by progressive decline in cognitive aptitude [103]. Cognitive aptitude is generally evaluated

by administration of the mini-mental status examination. The mini-mental status exam (MMSE) was developed by Folstein and Folstein in 1975 [147]. The MMSE was designed to be an all encompassing exam for neurological disorders including: psychiatric, neurologic and geriatric medical populations. Results from the MMSE are normalized to population factors, including years of formal education, to assess an individual's cognitive decline.

Pathologically, Alzheimer's disease is distinguished by neuronal deterioration that results in widened sulci and contraction of the gyri compared to normal control subjects. The gyri are the elevated crests, these features are most commonly associated with the wrinkle-like appearance of the brain. The sulci separate the gyri and are shallow indentions along the surface. The appearance of neurofibrillary tangles (NFT) and neuritic plaques (NP) are also two characteristic pathological facets of AD [103, 106, 148]. Neurofibrillary tangles are intraneuronal deposits which are enriched in hyperphosphorylated tau [103]. Tau is associated with microtubules which exhibit an increased abundance in neurons. Assembly of multiple hyperphosphorylated tau subunits results in protein aggregations which are believed to be fundamental in the development of neurofibrillary tangles [106]. The frequency of NFT are utilized to categorize a subject to a particular pathological disease state within the AD scale. The benchmark scale of pathological assessment was established by Braak and Braak [149]. Braak scores are based on the quantity and lateral diffusion of NFT across neurological regions [149]. The scale established by Braak and Braak ranks individuals based on pathology of NFT on a scale of I to VI. Individuals with mild pathology and limited spread of NFT across several areas are ranked either I or II. Prolific expansion of NFT within neuronal tissue, such as that seen in late-stage AD (LAD), are assigned a ranking of V or VI. Assessment of neuropathological degradation requires examination of multiple regions and although end-points may be easily characterized, differentiation between intermediate stages is more difficult [149]. Due to Braak scores being presented as median scores, rather than unambiguous values, statistical analysis required the use of non-parametric Kruskal-Wallis one way ANOVA ranks test with a Dunn's post hoc method to establish significance between disease states.

Plaques are extracellular aggregates composed mainly of amyloid beta peptide (Aβ) resulting from the amyloid precursor protein (APP) [103]. The amyloid beta peptide is formed as a result of proteolytic cleavage from the membrane bound amyloid precursor protein [142]. The APP is a transmembrane protein associated with synapses, APP is believe to be involved in synapse functionality although its exact role has yet to be determined [150].

The purpose of the study was to examine variations in the mitochondrial fatty acids across distinct regions during neuropathological changes associated with Alzheimer's disease. The areas chosen, cerebellum, superior and middle temporal gyri and inferior parietal lobule, represent histological sections functioning in discrete neurological processes (Figure 4.1). Tissue samples from each region were composed of gray matter or the outer most cortex layer from each region. Gray matter is primarily composed of nerve cell bodies and slow-twitch unmyelinated neuronal fibers [151]. The cerebellum (CER) is the region that regulates the integration of sensory perception, coordination and motor control [151]. As with the cerebrum, the cerebellum is symmetrically divided bilaterally. Bodily movement is coordinated across the two hemispheres; hence the cerebellum is more associated with motor functions. Because of the lack of memory and cognitive involvement by the cerebellum it is generally devoid of AD pathological markers compared to the frontal and temporal lobes.

The superior and middle temporal gyri (SMTG) are both sections of the temporal lobe. The superior temporal gyrus contains the primary auditory cortex which is responsible for processing sound, and a region for speech recognition [151]. The middle temporal gyrus is associated with visual processes such as recognition of known faces and accessing word meaning while reading [151]. Of the three regions studied the SMTG displays the most pathology during the progression of AD. Data from this area provides the examination of changes that occur in relation to the pathology of AD during that various stages.

The inferior parietal lobule (IPL) is a section found in approximately the middle portion of the parietal lobe. This domain is involved with integration of a variety of sensory information, including spatial sense, navigation, knowledge of numbers and the manipulation of objects [151-152]. Due to the nature of the multimodal processing that

131
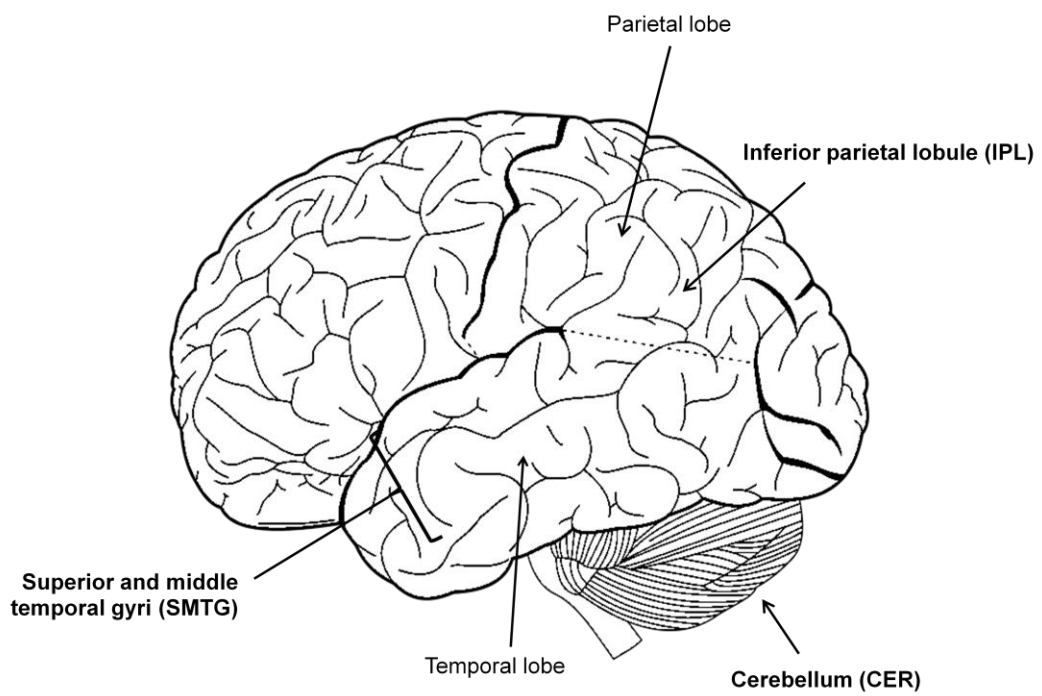
Figure 4.1. Neurological regions under study.

occurs in the IPL, it has been hypothesized to function in direct relationship to other regions [152].

For the analysis of the mitochondrial lipidome as a progression of Alzheimer's disease, tissue was chosen based on patient classification by the University of Kentucky Alzheimer's Disease Center (UK-ADC). Age-matched normal control (NC) are individuals with no cognitive deficits and limited evidence of pathology at time of autopsy. Generally, they have Braak scores of I at the time of autopsy. Mild cognitive impairment (MCI) marks the transition between normal cognitive decline and rapid onset of AD. Patients falling into this category have pathology with evidence of minor plague and neurofibrillary tangle formation. Braak scores for MCI subjects are usually III or IV.

Preclinical AD (PCAD) are individuals that have no record of cognitive decline, however they exhibit a greater degree of pathology compared to NC subjects. The preclinical designation is thought to be a prodromal stage of AD pathology [153].

The final stage of AD is marked behaviorally when individuals lose the ability to respond to their environment, speak and control movement. Late-stage AD (LAD) patients have discernible pathology marked by a significant number of plagues and neurofibrillary tangles (NFTs). Braak scores from LAD patients generally rank V or VI. On a whole neurological tissue from LAD patients exhibit extensive degradation in the form of contracted of gyri and broadening of sulci at the time of autopsy.

An additional subject set was added consisting of frontotemporal dementia (FTD) and dementia with Lewy body (DLB) disease patients. Both of these are neurodegenerative diseases that are linked by a common pathology consisting of protein aggregates [154-157]. For DLB pathology, Lewy bodies are enriched in the protein alpha-synuclein (α-syn) [156, 158]. Alpha-synuclein commonly exists as a soluble, cytoplasmic monomer that is associated with neural tissue [157]. The events of initiating Lewy body formation as a result of α-syn aggregation have not been determined, however a link between oxidative stress has been hypothesized [154, 157]. In contrast, FTD Lewy bodies are enriched in tau, as seen with NFT in AD. Frontotemporal dementia is classified as a tauopathy. The comparison between AD states and these combined pathology groups, aka disease control (DC), provide an evaluation of mitochondrial lipids from comparable neurodegenerative disease pathologies [159].

The objective of this study is to provide a comprehensive examination of mitochondrial fatty acid composition from various brain regions during the progression of AD. We focused on the mitochondrial membrane because electrons leaking from mitochondria are the greatest source of ROS with in a cell, thus mitochondria are a potential cause and a target of oxidative stress. Therefore, compensatory changes to the fatty acid profile would be expected in order to minimize susceptibility to oxidative damage. Comparison of mitochondrial membrane compositions between various regions may provide an understanding of why certain neurological regions have an increased vulnerability to oxidative damage.

Chapter 4.2. Experimental

Reagents

Potassium t-butoxide (1.0 M) in tetrahydrofuran (THF), 3-hydroxymethyl pyridine, tridecanal, cis-4-decenal, trans-2-tridecenal, hexane, D-mannitol, sucrose, Triza base, Tween-20, calcium chloride, and ethylenediaminetetraacetic acid disodium were purchased from Sigma (St. Louis, MO, USA). Methanol, methylene chloride, and hydrochloric acid were obtained from Fisher (Pittsburg, PA, USA). Acetyl chloride was obtained from Fluka (Buchs, Switzerland). Sodium hydroxide, sodium bicarbonate, and potassium carbonate were purchased from J.T. Baker (Phillipsburg, NJ, USA). Ethyl ether was obtained from EMD (San Diego, CA, USA). Anthracene was purchased from Acros (Morris Plains, NJ, USA). Percoll™ was obtained from GE Healthcare (Uppsala, Sweden). Anti-rabbit porin antibody was purchased from Calbiochem (Gibbstown, NJ, USA). Anti-rabbit lamin B was ordered from Santa Cruz Biotechnology (Santa Cruz, CA, USA). Anti-mouse MAP2 and anti-mouse synaptophysin were purchased from Abcom Inc. (Cambridge, MA, USA). 10-20% Tris-HCl SDS-PAGE gradient gels were purchased from BIO-RAD (Hercules, CA, USA). Isothesia (isoflurene) was obtained from Bulter Animal Health Supply (Dublin, OH, USA). GLC-411 lipid standard, 5,8,11,14-eicosatetraenoic acid (ARA), and 4,7,10,13,16,19-docosahexaenoic acid (DHA) were purchased from Nu-Chek Prep, Inc. (Elysian, MN, USA).

General equipment and supplies

Dounce homogenizer (Wheaton Industries, Millville, NJ, USA). Nalgene brand Oak Ridge polypropylene copolymer centrifuge tubes (Thermo Fisher Scientific Inc., Waltham, MA, USA). Beckman Polyallomer centrifuge tube (Beckman Coulter, Inc., Brea, CA, USA). Fisherbrand 2.0 mL polypropylene microcentrifuge tube (Thermo Fisher Scientific Inc., Waltham, MA, USA). Beckman Coulter (Beckman Coulter, Inc., Brea, CA, USA) Avanti J-25 series centrifuge equipped with a JA-25.50 fixed angle rotor. Beckman Coulter (Beckman Coulter, Inc., Brea, CA, USA) L-80 Ultracentrifuge series equipped with a SW 55 Ti swinging bucket rotor. Thermo IEC Micromax Centrifuge (Thermo Fisher Scientific, Rochester, NY, USA) with an 851 series microtube fixed angle rotor. Eppendorf (Hauppauge, NY, USA) Research Adjustable-volume pipettes.

Human subject neuropathological demographics

Tissue specimens from the superior and middle temporal gyri (SMTG), inferior parietal lobule (IPL), and cerebellum (CER) of short post-mortem interval (PMI) autopsies of subjects were obtained through the University of Kentucky Alzheimer's Disease Center (UK-ADC). Samples were flash frozen at autopsy in liquid nitrogen and stored at -80˚C until analysis. Sample demographics consisted of 14 (4 men, 10 women) age-matched normal control (NC) patients; 7 (2 men, 5 women) mild cognitive impairment (MCI) patients; 14 (3 men, 11 women) preclinical Alzheimer's disease (PCAD) patients; 15 (7 men, 8 women) late-stage Alzheimer's disease (LAD) patients and 11 (7 men, 4 women) diseased control (DC) patients (Table 4.1).

Human mitochondria isolation

The method presented here (Figure 4.2) for isolation of enriched mitochondria is based on a series of modifications described in previous studies [109, 111-112, 114]. Throughout the procedure all reagents, samples, and equipment were placed on ice. Isolation buffer, Percoll and digitonin solutions were prepared fresh on the day of isolation.

Tissue samples, approximately 1 g wet tissue weight, were homogenized via a manual Dounce homogenizer in isolation buffer (10 mM Tris, 0.32 M sucrose, 0.25 mM Na$_2$EDTA, pH 7.4). The total volume of IB used during homogenization gave a tissue to buffer ratio of approximately 0.1 g/mL. The tissue was homogenized with approximately 8 to 10 up-and-down strokes or until the sample was completely liquefied. The homogenate was transferred into a Nalgene brand Oak Ridge polypropylene copolymer centrifuge tube with a polypropylene screw closure. The homogenate was centrifuged (2,000xg, 3 min, 4°C), in a Beckman Coulter Avanti J-25 series centrifuge equipped with a JA-25.50 fixed angle rotor set at maximum acceleration and deceleration with the brake activated. The supernatant was collected and the pellet resuspended dissolved in approximately half the original volume of IB, re-homogenized and centrifuged (2,000xg, 3 min, 4°C). The combined the supernatants, consisting of cytosolic material, were centrifuged (20,000xg, 10 min, 4°C). The supernatant was discarded and the pellet, containing the mitochondria, was resuspended in 10 mL isolation buffer and centrifuged (2,000xg, 3 min, 4°C). The pellet was discarded and the supernatant transferred to a new

Table 4.1. Sample demographic information categorized by disease state.

Sample demographic	Normal control (NC)	Mild cognitive impairment (MCI)	Preclinical AD (PCAD)	Late-stage AD (LAD)	Disease control (DC)[a]
n[b]	14	7	14	15	11
Gender (M/W)	4/10	2/5	3/11	7/8	7/4
Avg. age (yrs)	86.4±1.5	91.0±1.9	85.8±1.7	80.8±1.4	71.8±4.2
Avg. PMI (hrs)	2.79±0.20	2.55±0.21	2.78±0.16	3.57±0.42	3.48±0.39
Median Braak score	I	IV*	IV*	VI*	II

[a] Represents a combination of Dementia with Lewy body disease (DLB) and frontotemporal dementia (FTD)
[b] Represents the number of samples for each region (cerebellum (CER), superior and middle temporal gyri (SMTG) and inferior parietal lobule (IPL))

Tissue Homogenization

Centrifigue (2000xg, 3 min, 4˚C)

Pellet (Nuclear)　　　　　　　　　　　　　　　　　**Supernatant**

Resuspend in IB & Centrifigue (2000xg, 3 min, 4˚C)

Pellet (Nuclear)　　　　　　　　　**Supernatant**

Combine Supernatant fraction & Centrifigue
(20,000xg, 10 min, 4˚C)

Pellet　　　　　　　　**Supernatant
(Cytosolic Fraction)**

Resuspend in IB & Centrifigue (2,000xg,
10 min, 4˚C)

Pellet (nuclear)　　　　　　**Supernatant**

Centrifuge 20,000xg, 10 min, 4˚C)

**Pellet (Crude Mitochondia &
Synatosomes)**　　　　**Supernatant**

Resuspend in 19% Precoll:IB & Centrifuge
(19,600xg, 30 min, 4˚C)

Pellet (Mitochondia & Synatosomes)　　　　**Supernatant**

Wash Pellet & Centrifuge (19,600xg, 10 min, 4˚C)

Pellet (Mitochondia & Synatosomes)　　　　**Supernatant**

Resuspend in 1% Digitonin (10 min, 4˚C)

Add 28% Precoll:IB & Centrifuge (19,600xg, 10 min 4˚C)

Mitochondrial Pellet　　　　**Supernatant**

Wash with PBS & Centrifuge (19,600xg, 10 min 4˚C)

Resuspend in PBS

Purified Mitochondira

Figure 4.2. Mitochondria isolation procedure.

tube and centrifuged (20,000xg, 10 min, 4°C). The resulting pellet, containing the crude free and synaptosomal mitochondria isolate, was dissolved in 3 mL of a 19% (vol/vol) Precoll:IB and transferred to a Beckman Polyallomer centrifuge tube. The solution was centrifuged (19,600xg, 30 min, 4°C), in a Beckman Coulter L-80 Ultracentrifuge series equipped with a SW 55 Ti swinging bucket rotor set at maximum acceleration and deceleration with the brake activated. The supernatant was discarded and the pellet, containing both free and synaptosomal mitochondria, was transferred to a Fisherbrand 2.0 mL polypropylene microcentrifuge tube and washed in 1 mL PBS and centrifuged (19,600xg, 10 min, 4°C) in a Thermo IEC Micromax Centrifuge with a 851 series microtube fixed angle rotor set at maximum acceleration and deceleration with the brake activated. The supernatant was discarded and the mitochondrial pellet was dissolved in PBS containing 1% digitonin (wt/vol) and placed on ice for 10 min. Following incubation, 3 mL of 28% (vol/vol) Percoll:IB buffer was added and the samples centrifuged (19,600xg, 10 min, 4°C). The supernatant was discarded and the pellet, consisting of free and synaptic mitochondria, was washed two times with 1 mL aliquots of PBS, each washing was centrifuged (16,900xg, 10 min, 4°C). The final mitochondrial pellet was resuspended in 500 µL PBS and stored at -80°C until further analysis.

Quantification of mitochondrial proteins

Quantification of mitochondrial proteins was carried out on a Thermo Labsystems Multiskan MCC/3340 spectrometer (Pittsburgh, PA, USA) using a Pierre Bicinchoninic acid (BCA) assay (Rockford, IL, USA) [105]. A calibration curve was prepared by addition of 0, 1, 5, 10, 15, 20 µg BSA standard into separate wells; each concentration in duplicate. Aliquots of isolated mitochondria (5 µL) were added to separate wells; each sample in duplicate. Wells were adjusted to a final volume of 100 µL by addition of deionized H_2O. Lastly, 100 µL of a 10 µL/mL $CuSO_4$ in Bicinchoninic acid solution was pipetted into each well. The plate was incubated at 37°C for 30 min prior to reading. The mitochondrial protein concentration was determined by absorbance at 620 nm. The concentration (µg/µL) was calculated by averaging the sample replicates and dividing by the addition volume (eq. 4.1):

$$\text{Protein } (\mu g / \mu L) = \frac{\left(\dfrac{A_1 + A_2}{2}\right)}{5 \mu L}$$

eq. 4.1

Western blot analysis

Mitochondrial isolations were evaluated for purity by western blot (Figure 4.3). Isolated mitochondria (20 μg) were separated on a 10-20% Tris-HCl SDS-PAGE gradient gel. Protein bands were transferred to a nitrocellulose membrane and incubated with 5% milk in 0.5% Tween-20/Tris-buffered saline (TTBS) with 3.3% goat serum (1 hrs, 25°C). The membrane was incubated with primary antibodies (1:3750): anti-porin, specific for a mitochondrial channel protein; anti-lamin B a marker specific for a nuclear envelope protein; anti-MAP2 a microtubular associated protein and anti-synaptophysin (12 hrs, 4°C). The membrane was washed three times with 0.5% Tween-20/Tris-buffered saline then incubated with horseradish peroxidase conjugated secondary antibody goat anti-mouse for MAP2 and synaptophysin at a dilution of 1:7500 and goat anti-rabbit for porin and lamin B at a dilution of 1:7500 (2 hr, 25°C). Following three washings with 0.5% Tween-20/Tris-buffered saline, the bands were visualized with enhanced chemiluminescence (Amersham Pharmacia Biotech, Piscataway, NJ, USA) as per manufacturer's instructions.

Saponification of fatty acids

Aliquots (approximately 100 μg of mitochondrial protein) of isolated mitochondria were used for each reaction. Saponification methods were based on a previous description by Kurkiewicz et al [49]. Sodium hydroxide (1 mL of 3 M) was added to the mitochondria solution. The mixture was vortexed and heated to 90°C for 1 h, cooled to room temperature, and 2 mL of 3.25 M HCl was added and reheated at 90°C for 10 min. After cooling to room temperature, the lipids were extracted three times with 1 mL portions of hexane/diethyl ether (1:1, by vol). The organic phases were combined and evaporated to dryness under a stream of N_2 at room temperature.

Fatty acid derivatization methods

Fatty acid methyl ester (FAME) procedures were adapted from Lepage and Roy [50]. Methanol:acetyl chloride (50:1 (v/v), 5 mL total) was added to the extracted free fatty acids. The solution was vortexed and heated at 60°C for 1 h. After heating, 3 mL

a

	TH	NF	CF	MF
Lamin B (nuc) →				
MAP2 (cyto) →				
Porin (mito) →				
Synaptophysin →				

b

Digitonin (%)

	0.75	1	2
Porin (mito) →			

Figure 4.3. Representative western blot analysis for mitochondrial isolation (a) and digitonin treatment (b). Total homogenate (TH), nuclear fraction (NF), cytosolic fraction (CF), and mitochondrial fraction (MF) from inferior parietal lobule of brain.

of 6% K_2CO_3 was added, and the FAME products were extracted 1 mL of hexane containing 50 ng/μL anthracene. Extracted material (1 μL) was used for GC/MS analysis.

An aliquot of the FAME solution was transesterified to picolinyl esters using an adapted method [51]. The hexane phase from the FAME procedure was evaporated to dryness under a stream of N_2 at room temperature and 1 mL of methylene chloride was added to resolvate the methyl esters. In a separate vial a mixture of 200 μL 3-hydroxymethylpyridine and 100 μL of 1.0 M potassium tert-butoxide in THF were allowed to react for 2 min. This mixture was then added to the FAME methylene chloride solution. The reaction was mixed and heated at 45°C for 1 h. After cooling to room temperature, 1 mL of 2.5% $NaHCO_3$ was added and the methylene chloride layer removed. The organic layer was reduced to approximately one-quarter the original volume under a stream of N_2 at room temperature and 1 μL was injected for analysis. All derivatization methods were validated by analysis of 20:4 (arachidonic acid) and 22:6 (docosahexaenoic acid).

Gas chromatography/mass spectrometry

Fatty acid methyl ester derivatives were analyzed using a Varian Saturn 3 GC/MS system equipped with a ZB-5ms capillary column 30 m x 0.25 mm i.d., 0.25 μm film (Phenomenex USA, Torrance, CA). The temperature program was: 130°C to 170°C at 4°C/min, 170°C to 215°C at 2.7°C/min, 215°C for 3.34 min, with a total analysis time of 30 min. Carrier gas head-pressure was set to give a flow rate of 1 mL/min, with a 50:1 split. The injector and transfer line were maintained at 240°C and the manifold temperature was 210°C. Ionization was accomplished by electron impact (EI) at 70 eV, with a 3 minute filament delay. Full scan spectra (m/z 50 to 650) were acquired at a scan rate of 1 analytical scan per second with a background mass set at m/z 49. The GC/MS method was optimized to provide peak resolution for FAMEs from the GLC-411 standard.

Fatty acid picolinyl ester derivatives were analyzed on the same instrument with the following temperature program: 150°C for 4 min, 150°C to 280°C at 20°C/min, 280°C for 19.5 min with a total analysis time of 30 min. All other parameters were as described above except that the filament delay was 10 min and spectra were generated

from full scans from m/z 50 to 500. All GC/MS data were analyzed using the Wsearch32 2005 Software (version 1.6.2005; Melbourne, Australia).

Calculations

Average ($\bar{x}$)

$$< \bar{x} >= \frac{\sum n_1 + n_2 + n_3 + ... + n_n}{n_n} \qquad \text{eq. 4.2}$$

Standard deviation (s)

The standard deviation represents the difference between replicate measurements.

$$s = \sqrt{\frac{\sum (x_i - \bar{x})^2}{n-1}} \qquad \text{eq. 4.3}$$

Standard error of the mean (SEM)

$$SEM = \frac{s}{\sqrt{n}} \qquad \text{eq. 4.4}$$

Shapiro-Wilk test for normality

$$W = \frac{\left(\sum_{i=1}^{n} a_i x_{(i)} \right)^2}{\sum_{i=1}^{n} \left(x_i - \bar{x} \right)^2} \qquad \text{eq. 4.5}$$

Where W is the Wilk statistic, $x_{(i)}$ is the smallest value for test samples, a_i is a constant based on $x_{(i)}$ and $\bar{x}$ is the samples mean.

Skewness test

$$skewness = \frac{\sum \left(\frac{x_i - \bar{x}}{s} \right)^3}{n} \qquad \text{eq. 4.6}$$

Where x_i are the individual values, $\bar{x}$ is the average of all values, s is the standard deviation and n is the number of samples.

Pearson Product-Moment test for correlation

$$\rho = \sum \left(\frac{((x_i - \bar{x})(y - \bar{y}))}{((n-1) * s_x s_y)} \right)$$

eq. 4.7

Where ρ is the Pearson's coefficient, x and y are variables, x_i is an each value of x, $\bar{x}$ and $\bar{y}$ are the means for and y variables, n is the number of variables and s_x and s_y are the standard deviations for x and y variables.

F-test for comparison of two variances

The null hypothesis is stated that there is no significant difference between the two variances. If $F_{calc} > F_{table}$, p, v_1, v_2 then the null hypothesis is rejected and there is a significant difference between the two populations. $F_{calc} > 1$, $v_1 = n_1 - 1$, $v_2 = n_2 - 1$

$$F_{calc} = \frac{v_1}{v_2} = \frac{s_1^{\,2}}{s_2^{\,2}}$$

eq. 4.8

t-Test for comparison of two experimental means

$$\pm t_{calc} = \frac{(\bar{X}_1 - \bar{X}_2)}{sp} \sqrt{\frac{n_1 n_2}{n_1 + n_2}}$$

eq. 4.9

Analysis of Variance (ANOVA)

$$F_{calc} = \frac{v_1}{v_2}$$

eq. 4.10

Where v_1 equals the mean square error between the classes and v_2 represents the mean square error within the classes. If $F_{calc} > F_{table}$ then the HO is rejected and there is some systematic difference among the classes. The Tukey post hoc test was then employed to compare each group against each other and established significance.

Kruskal-Wallis One Way Analysis of Variance on Ranks

$$H = (N-1)\frac{\sum_{i=1}^{g} n_i (\bar{r}_i - \bar{r})^2}{\sum_{i=1}^{g} \sum_{j=1}^{n_i} (r_{ij} - \bar{r})^2}$$

eq. 4.11

Where N is the total number of observations, n_i is the number of observations in group i, $\bar{r}$ is the average rank, $\bar{r}_i$ is the average for observations from group r_i, r_{ij} is the rank of observation j within group i. If $H_{calc} > H_{critical}$ then the HO is rejected and there is some systematic difference among the ranks. Dunn's or Tukey post hoc tests were then employed to compare each group pairwise and establish significance.

Statistical analysis employed the commercially available SigmaPlot software (Systate Software, Inc, San Jose, CA, USA). Comparisons were limited to equivalent fatty acids between brain regions and/or disease states, i.e. NC vs. MCI vs. PCAD vs. LAD vs. DC. Significant differences ($p<0.05$) across disease states, within a particular brain region, compared to NC are depicted by *. Significant differences ($p<0.05$) within equivalent disease states, across distinct brain regions, are depicted by ‡.

Box-and-whisker plots

Box-and-whisker plots were utilized to graphically represent much of the data acquired. A diagram of a typical box-and-whisker plot is provided to help illustrate the data contained these graphs (Figure 4.4). The gray area of the box represents the upper to lower quartile for the selected data. Within this gray area are the median line (solid) and the mean line (dotted) for the data. The whiskers proved the data range from lowest to highest. Outliers, greater than $5^{th}/95^{th}$ percentile from either the lowest or highest value, are represented by solid circles.
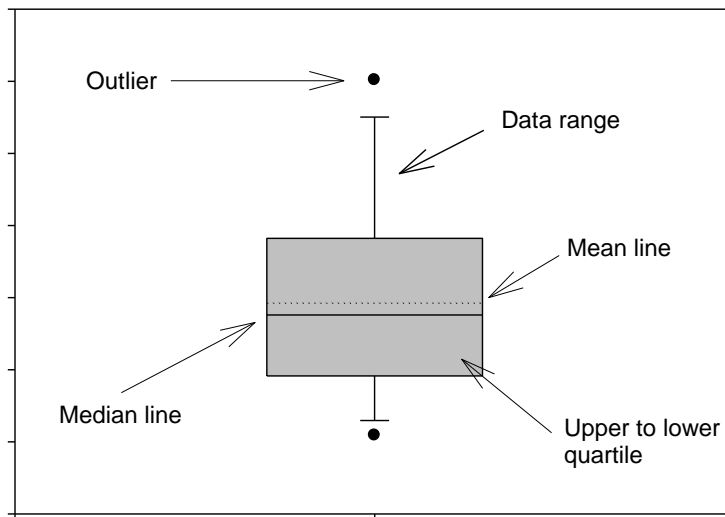
Figure 4.4. Box-and-whisker plot anatomy.

Chapter 4.3. Results

The characteristic fatty acid profile found in brain mitochondrial membranes from experiments with Sprague Dawley rats, was used as a template for the exploration of changes that occur in the mitochondrial membrane during the progression of neurological diseases.   The objective of this study was designed to examine the changes in the mitochondrial lipidome as a function of Alzheimer's disease (AD) progression. Mitochondria isolated from human neurological tissue from three stages of AD progression ranging from preclinical (PCAD), mild cognitive impairment (MCI), through late-stage (LAD) were compared to lipid profiles from age-matched normal (NC) and disease controls (DC). The scope of this study will also map the changes that occur as a function of regional proliferation of AD across three areas of the brain: cerebellum (CER), superior and middle temporal gyri (SMTG), and inferior parietal lobule (IPL). The hypothesis being that changes to the mitochondrial fatty acids will be reflected during advanced stages of AD, in addition to being more prevalent in regions displaying greater pathology.

Subject neuropathological demographics

The patient demographics used in these studies were compared statistically to determine possible differences between the subjects (Table 4.1). The average age was compared by one way ANOVA and showed no statistical differences between AD states compared to NC (Figure 4.5). However, the disease control subjects were found to be significantly younger ($p<0.001$) than all of the other neuropathologic states. Analysis of the post-mortem interval (PMI) data by one way ANOVA indicated there was no statistical difference between the samples (Figure 4.6).

Comparisons of the median Braak scores and neuritic plaque (NP) data among the disease states provided the main distinction between the subjects. The Braak scores were evaluated by the non-parametric Kruskal-Wallis one way ANOVA ranks test with a Dunn's method post hoc test to establish significance. Both NC and DC groups were significantly different ($p<0.05$) than MCI, PCAD and LAD states (Figure 4.7).

The average neuritic plaques (NP) were compared across disease states for IPL and SMTG regions. The plaque counts were compared statistically by one way ANOVA with Tukey post hoc test. Inferior parietal lobule had a significant increase ($P<0.001$) in
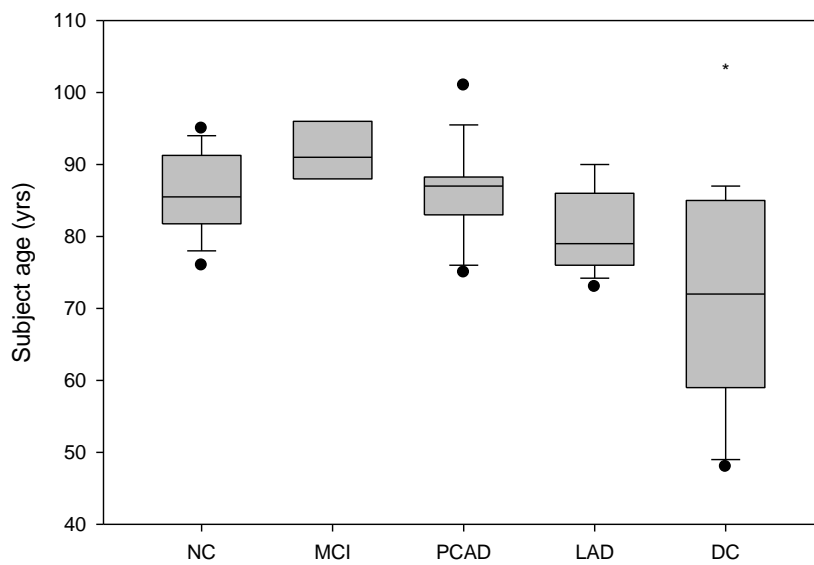
Figure 4.5. Differences in subject age between disease states (normal control (NC), mild cognitive impairment (MCI), preclinical AD (PCAD) late-stage AD (LAD) and disease control (DC)). Significant differences (p<0.05) between disease states, compared to NC are depicted by *.
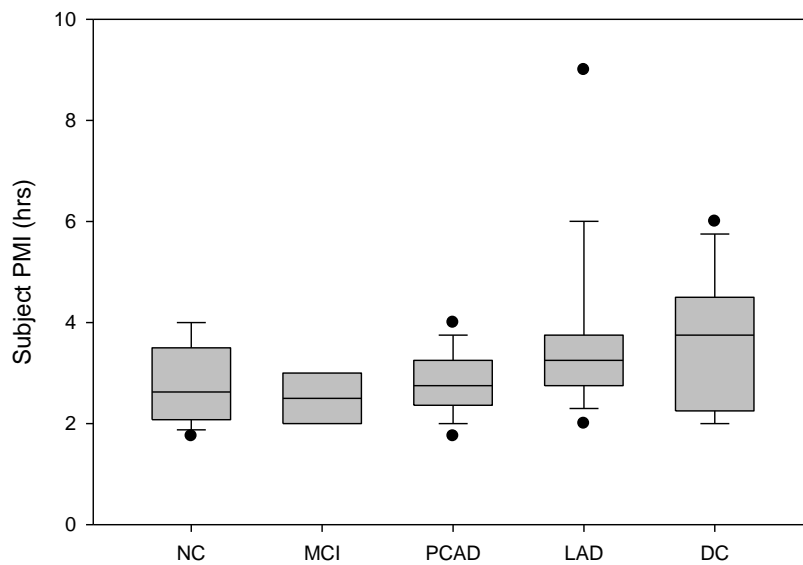
Figure 4.6. Differences in subject post-mortem interval (PMI) between disease states (normal control (NC), mild cognitive impairment (MCI), preclinical AD (PCAD) late-stage AD (LAD) and disease control (DC)). Significant differences (p<0.05) between disease states, compared to NC are depicted by *.
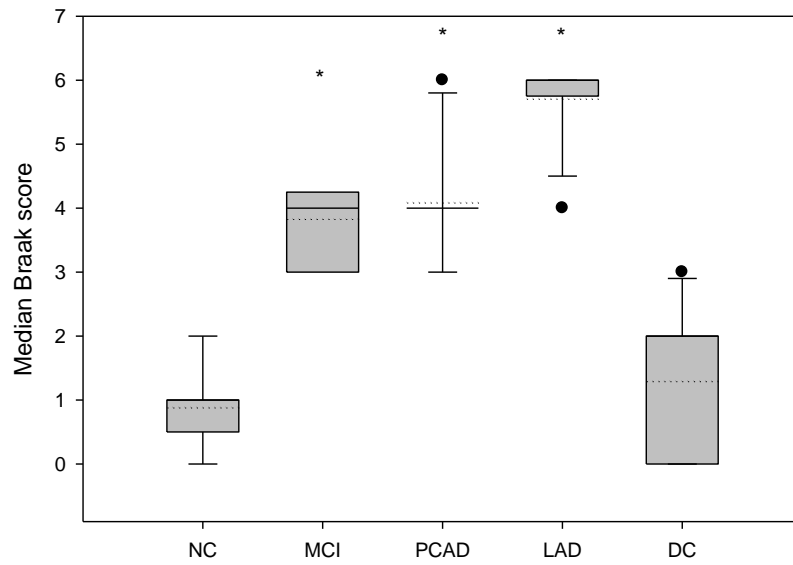
Figure 4.7. Differences in subject median Braak score between disease states (normal control (NC), mild cognitive impairment (MCI), preclinical AD (PCAD) late-stage AD (LAD) and disease control (DC)). Significant differences (p<0.05) between disease states, compared to NC are depicted by *.

NP for LAD compared to all other disease states (Figure 4.8). For SMTG the LAD samples had a significant increase ($p < 0.001$) in NP compared to NC, PCAD and DC; however, the LAD comparison to MCI samples resulted in a $p < 0.05$ significant increase (Figure 4.9).

Mitochondria isolation

The development of a mitochondrial isolation procedure that provided significant purity while maximizing yield, from neurological tissue, was essential for lipidomic analysis (Figure 4.2). Protein markers for total homogenate (TH), nuclear fraction (NF), cytosolic fraction (CF) and mitochondria fraction (MF) as visualized with enhanced chemiluminescence (Figure 4.3a). The western blot result confirms the purity and increased concentration of mitochondria isolation over that of the total homogenate. The absence of MAP2 and lamin B bands verified the purity of mitochondrial isolation.

Quantification of mitochondrial proteins based on bicinchoninic acid (BCA) assay, did not indicate any significant differences in isolation yields across the three brain regions studied for the combined disease states (Figures 4.10). The average mitochondrial protein yield per tissue weight, for the entire sample population was 500 µg/g ± 0.006 (Figure 4.10). When the data of mitochondria protein quantification is separated into individual disease states for the three regions only slight statistical differences are present (Figures 4.11). For inferior parietal lobule there was a significant decrease ($p < 0.05$) in yield for MCI and LAD compared to NC, indicated by *. In addition, there was also a significant increase ($p < 0.05$) in yield for LAD from the inferior parietal lobule compared to LAD from cerebellum, indicated by ‡.

Fatty acid structure analysis

As discussed with the previous project (Chapter 3) a complete description of the fatty acid profile requires structural analysis of the acyl chains. As described previously derivatization to picolinyl esters provided charge remote fragmentation along the fatty acid backbone facilitating structural elucidation [62]. Results for fatty acid structural analysis from human neurological mitochondria yielded equivalent results to fatty acids from the preceding study with Sprague Dawley neurological mitochondria (Chapter 3). Therefore, the presented results will focus on long-chain polyunsaturated fatty acids not
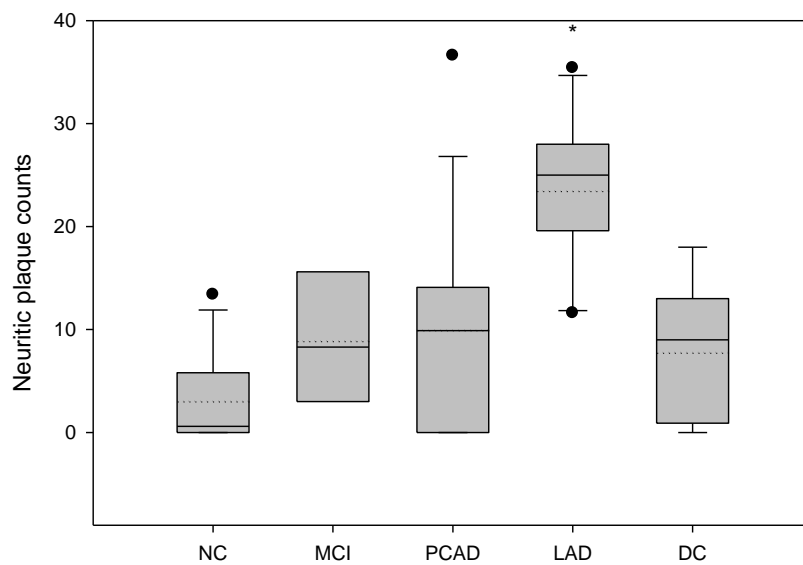
Figure 4.8. Differences in subject neuritic plaques counts within IPL between disease states (normal control (NC), mild cognitive impairment (MCI), preclinical AD (PCAD) late-stage AD (LAD) and disease control (DC)). Significant differences (p<0.05) between disease states, compared to NC are depicted by *.
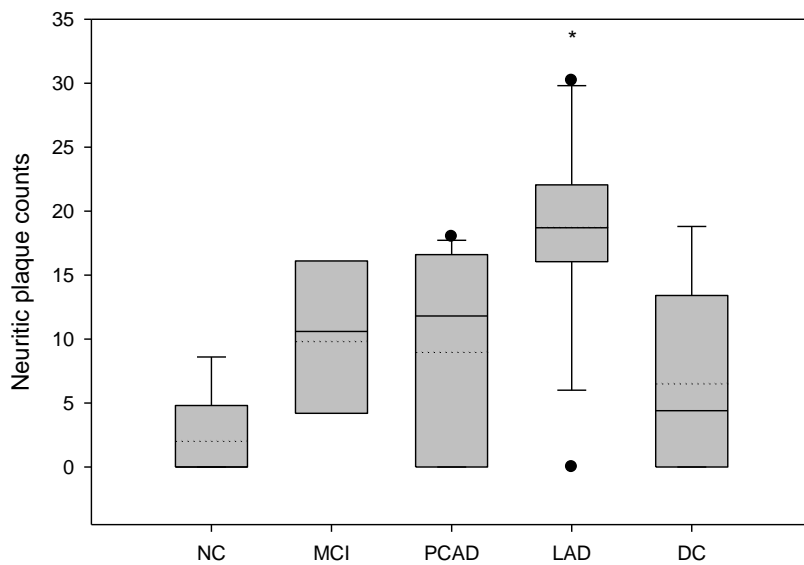
Figure 4.9. Differences in subject neuritic plaques counts within SMTG between disease states (normal control (NC), mild cognitive impairment (MCI), preclinical AD (PCAD) late-stage AD (LAD) and disease control (DC)). Significant differences ($p<0.05$) between disease states, compared to NC are depicted by *.
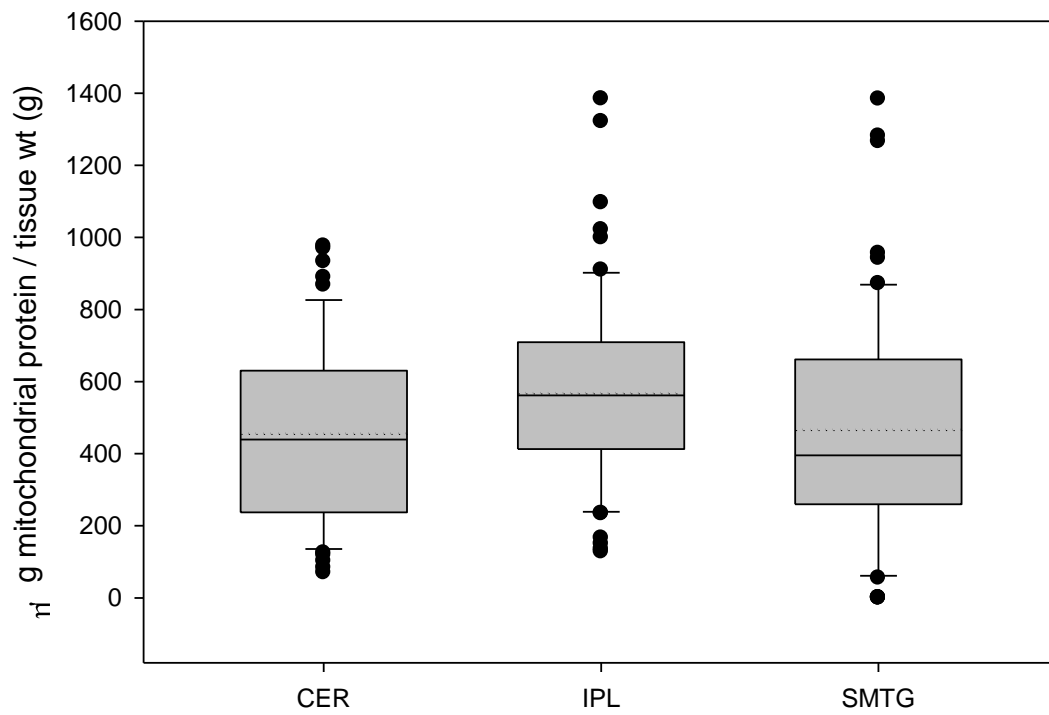
Figure 4.10. Differences in mitochondrial yield across brain regions as measured by BCA assay for combined disease states.
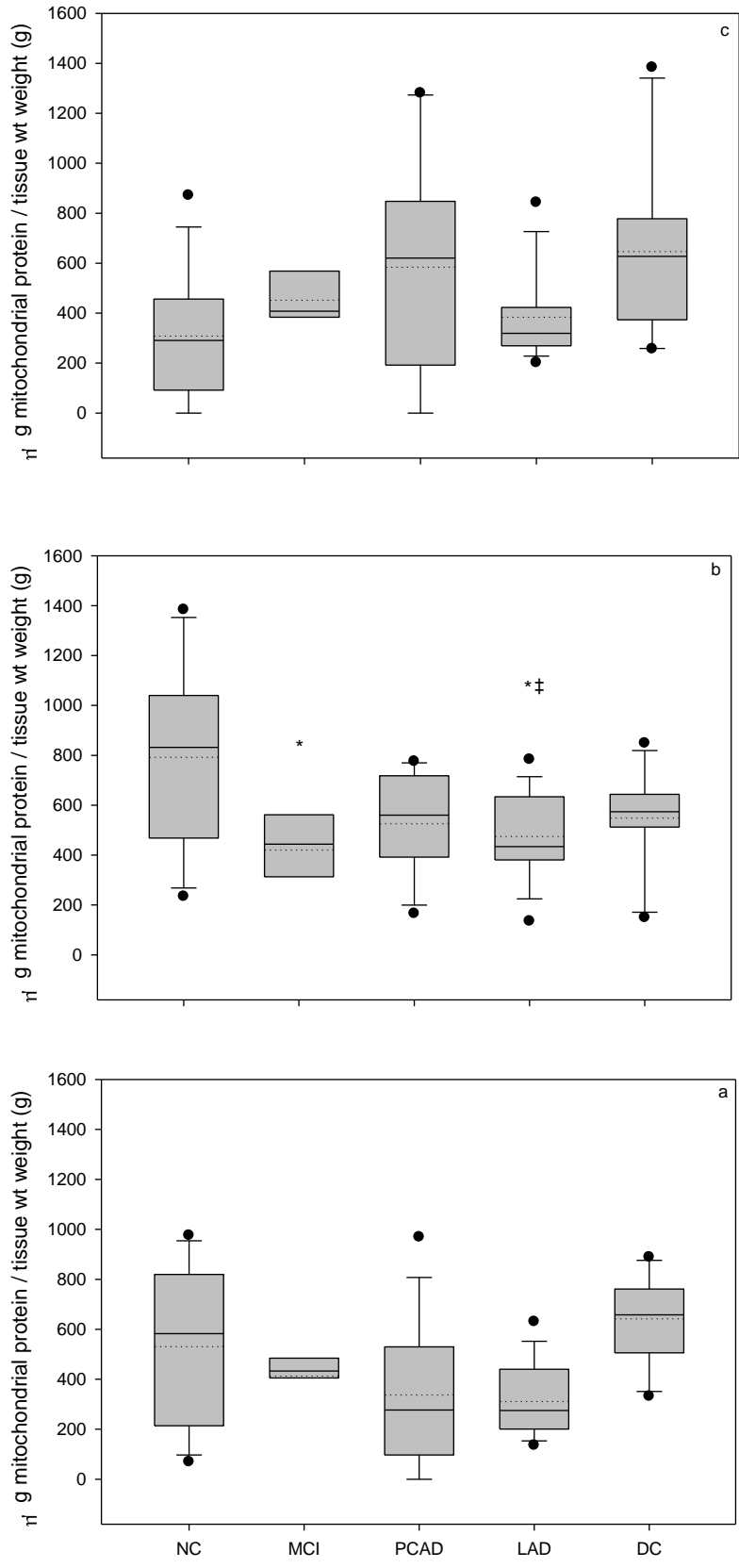
Figure 4.11. Differences in mitochondrial yield based on BCA assay between disease states (normal control (NC), mild cognitive impairment (MCI), preclinical AD (PCAD) late-stage AD (LAD) and disease control (DC), for cerebellum (a), inferior parietal lobule (b) and superior and middle temporal gyri (c)). Significant differences (p<0.05) between disease states, within the same region, compared to NC are depicted by *. Significant differences (p<0.05), within equivalent disease states, across regions are depicted by ‡.

previously discussed. For spectra and discussions concerning other fatty acids, the reader is referred to Chapter 3.3 and Figures 3.3-3.18.

Fragmentation of picolinyl esters with double bonds have a distinctive pattern indicating the site of the unsaturation, although mass intervals are sometimes difficult to determine with long-chain PUFAs. As before, loses of the terminal methyl group produces $[M-15]^+$, then the repeating pattern of $[M]^+-(CH_2)_n$ mass units is present except for locations at double bonds. Cleavage at the methylene group alpha to the double bond results in a 26 amu gap. Usually, following a loss of 26 amu, there is a loss of 14 amu indicating the methylene interrupted site along the chain, prior to another loss of 26 amu for PUFAs. The double bond location indicator ions can also be seen by a gap of 40 amu.

These methodologies were used to determine the structure of each the PUFAs. The EI spectra are presented in two forms, first the methyl ester derivative then the picolinyl ester of 5,8,11,14-arachidonic acid (20:4 Δ5,8,11,14) (Figures 4.12 & 4.13). Increasing the number of conjugated double bonds along the alkyl chain imparts greater difficulty interpreting the spectrum. Still present is the fragmentation to lose the terminal methyl group producing, m/z 380, from the molecular ion, m/z 395. Following the same concept as above the loss of 26 amu from m/z 324 to m/z 298 represents the double bond between carbon fourteen and fifteen, confirming that this is an ω-6 fatty acid. The next double bond corresponds to the loss from m/z 284 to m/z 258. The remaining two double bonds adhere to the same pattern of a 26 amu loss from m/z 244 and m/z 204 to m/z 218 and m/z 178 respectively. Following each loss of 26 amu, indicated by *'s, the subsequent loss of 14 amu before the next 26 amu loss represents the methylene separation between double bonds.

The mass spectrum for the picolinyl ester of 8,11,14-eicosatrienoic acid (20:3Δ8,11,14) is shown in Figure 4.14. The molecular ion, m/z 397, loss of the terminal methyl group yields m/z 368. The ω-6 double bond between carbons 14 and 15, results in the first 26 amu gap in the spectrum. This fragmentation yields m/z 326 to m/z 300, however this paticular unsaturation site is probably better illustrated by the 40 amu loss from m/z 340 to m/z 300. The next double bond, located between carbons 11 and 12, produces the 26 amu loss between m/z 286 to 260 m/z. Finally, m/z 246 to m/z 220 results from the double bond between carbons 8 and 9. Note that between each double
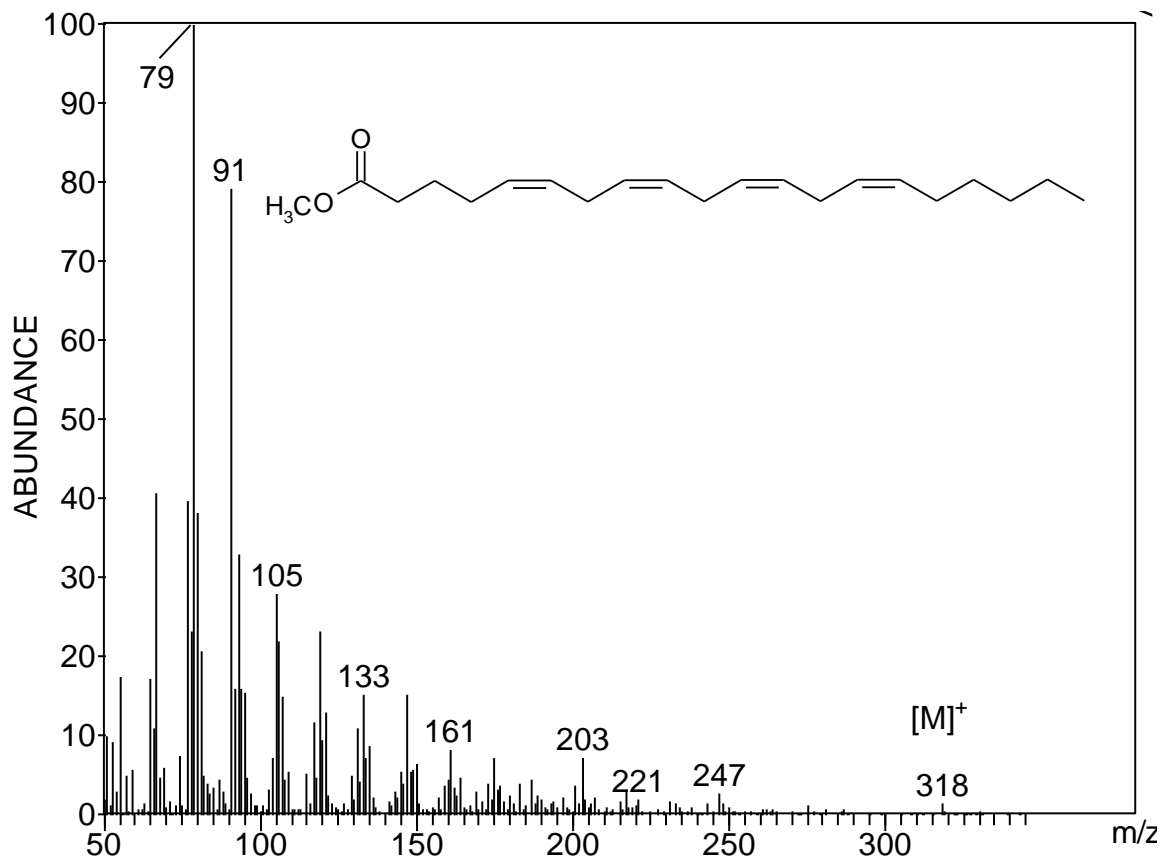
Figure 4.12. Mass spectrum of methyl 5,8,11,14-eicosatetraenoate (20:4Δ5,8,11,14).
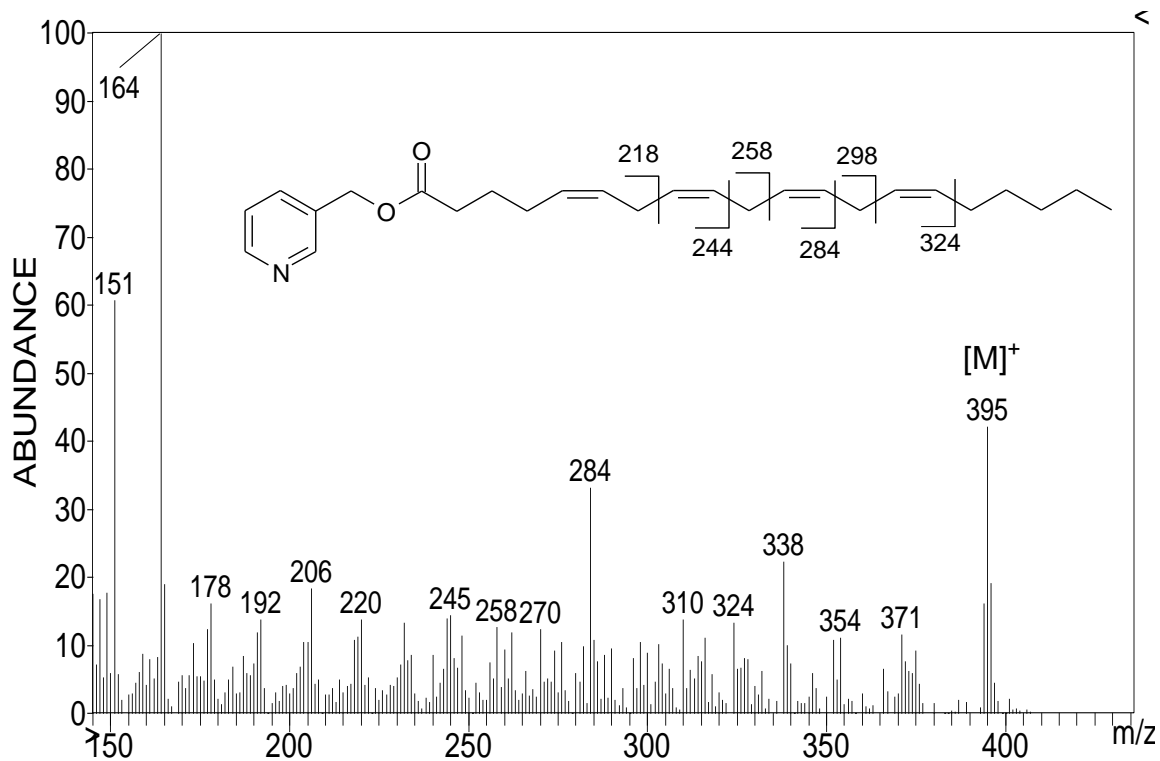
Figure 4.13. Mass spectrum of picolinyl 5,8,11,14-eicosatetraenoate (20:4Δ5,8,11,14).
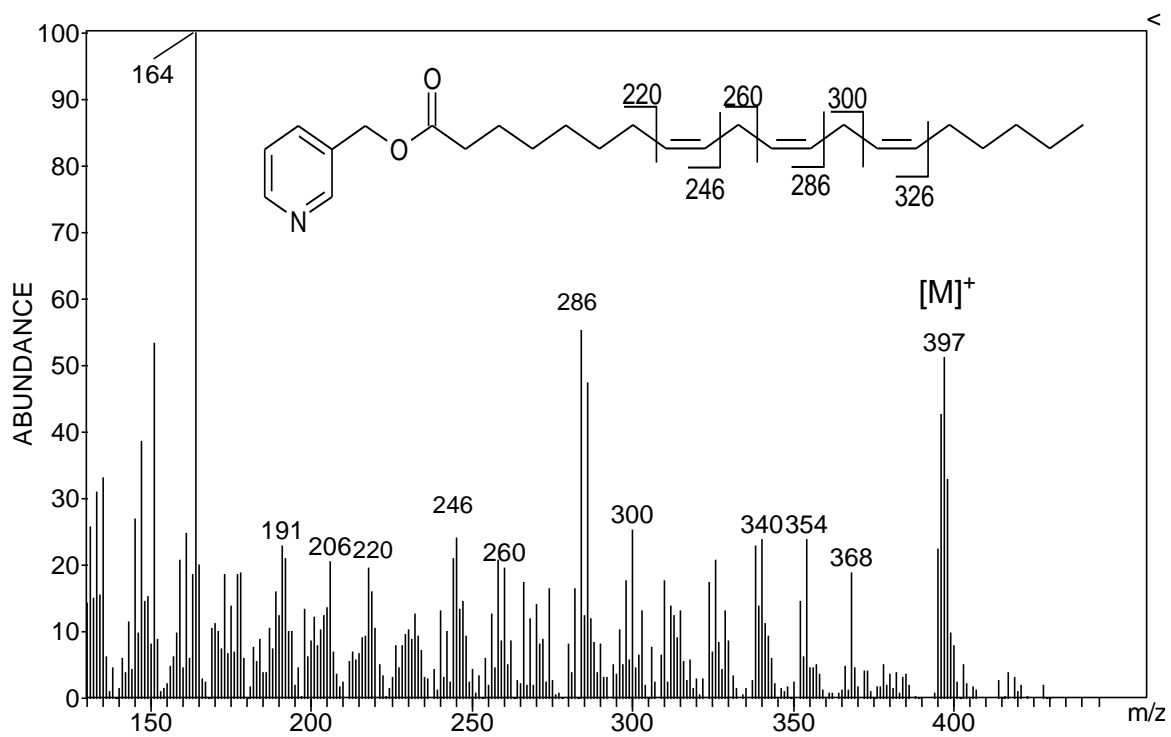
Figure 4.14. Mass spectrum of picolinyl 8,11,14-eicosatrienoate (20:3Δ8,11,14).

bond is a 14 amu gap, indicating a conjugated triene systems. For comparison the methyl ester EI spectrum of 8,11,14-eicosatrienoic acid is provided (Figure 4.15).

The mass spectrum for the methyl ester of 4,7,10,13,16,19-docosahexaenoic acid ($22:6\Delta4,7,10,13,16,19$) provides little to no molecular ion and is dominated by low molecular weight fragments (Figure 4.16). In addition the picolinyl ester, is difficult to interpret due to the increased number of double bonds (Figure 4.17). Once again the $[M]^+$ ion, m/z 419, is prominent however the $[M-15]^+$ ion is minor compared to other spectra. The ω-3 double bond at carbon 19, results in m/z 390 minus 26 amu to m/z 364. The double bond at carbon 16 is indicated by the 40 amu gap between m/z 350 and m/z 310. This pattern is also present for the double bond at carbon 7, m/z 244 to m/z 204. The remaining double bond locations are indicated by 26 amu breaks between m/z 310 to 284, m/z 270 to 244 and m/z 204 to 178. Note that each of the double bonds producing -26 amu fragments, is separated by 14 amu indicating a methylene interrupted double bond. The two double bonds distinquished by the 40 amu loss, have the methylene group as part of the fragment.

Finally, the mass spectrum for picolinyl 7,10,13,16-docosatetraenoate ($22:4\Delta7,10,13,16$) is shown in Figure 4.18. As with docosahexaenoic acid the increased carbon length and double bonds complicates interpretation of the spectrum. The ω-6 double bond at carbon 16 is prominently indicated by the loss of 40 amu between m/z 352 and m/z 312. Likewise the next double bond location is revealed m/z 312 to m/z 272, again a difference of 40 amu. The final two sites of unsaturation result in the fragmentation pattern of m/z 272 to m/z 246 and m/z 246 to 220, respectively. The analogous methyl ester derivative spectrum is provided for comparison (Figure 4.19).

Two unsaturated plasmalogen species (P 18:1a&b) were unique to neurological mitochondria. Mass spectra generated with EI of the derivatizied dimethyl acetals fail to provide a molecular ion and generally consist of ions with only minor abundances, as seen with saturated plasmalogen derivatives. The only two prominent ions are: m/z 281 representing $[M-31]^+$ loss of a methoxy group and m/z 75 generated by the loss of the dimethyl head-group (Figure 4.20).

To confirm the formation of these dimethyl acetals and in an attempt to establish the unsaturation sites, three aldehydes (tridecanal, cis-4-decenal and trans-2-tridecenal)
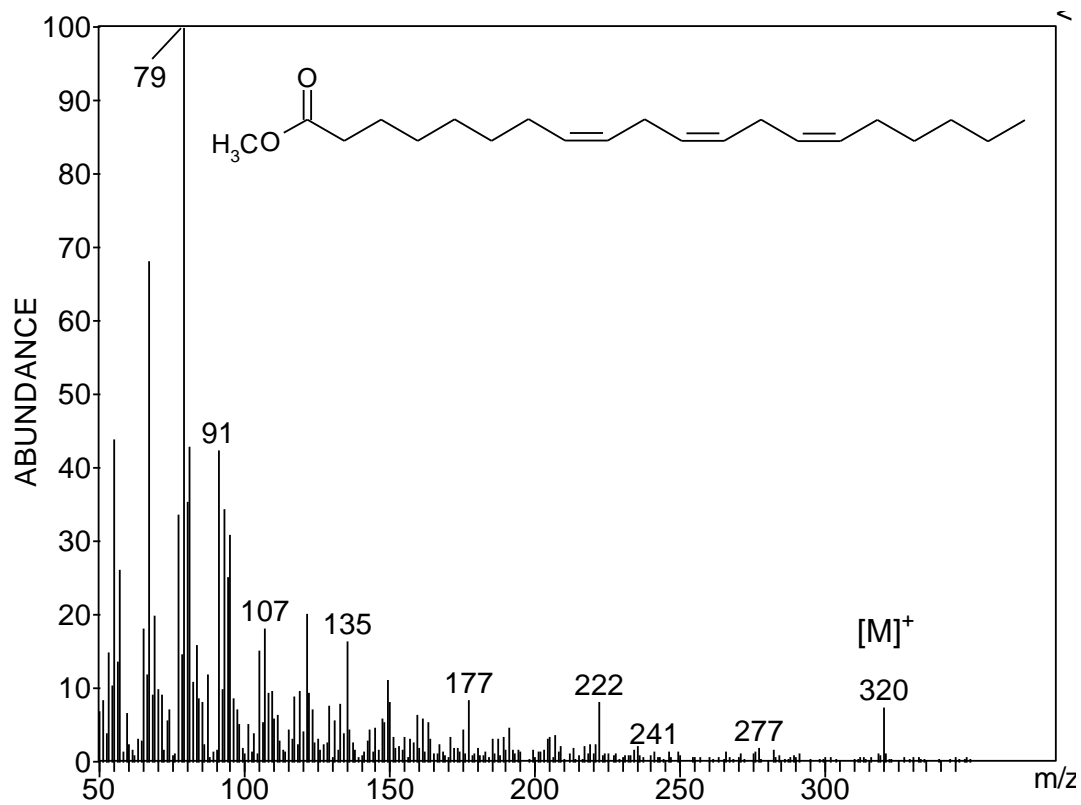
Figure 4.15. Mass spectrum of methyl 8,11,14-eicosatrienoate (20:3Δ8,11,14).
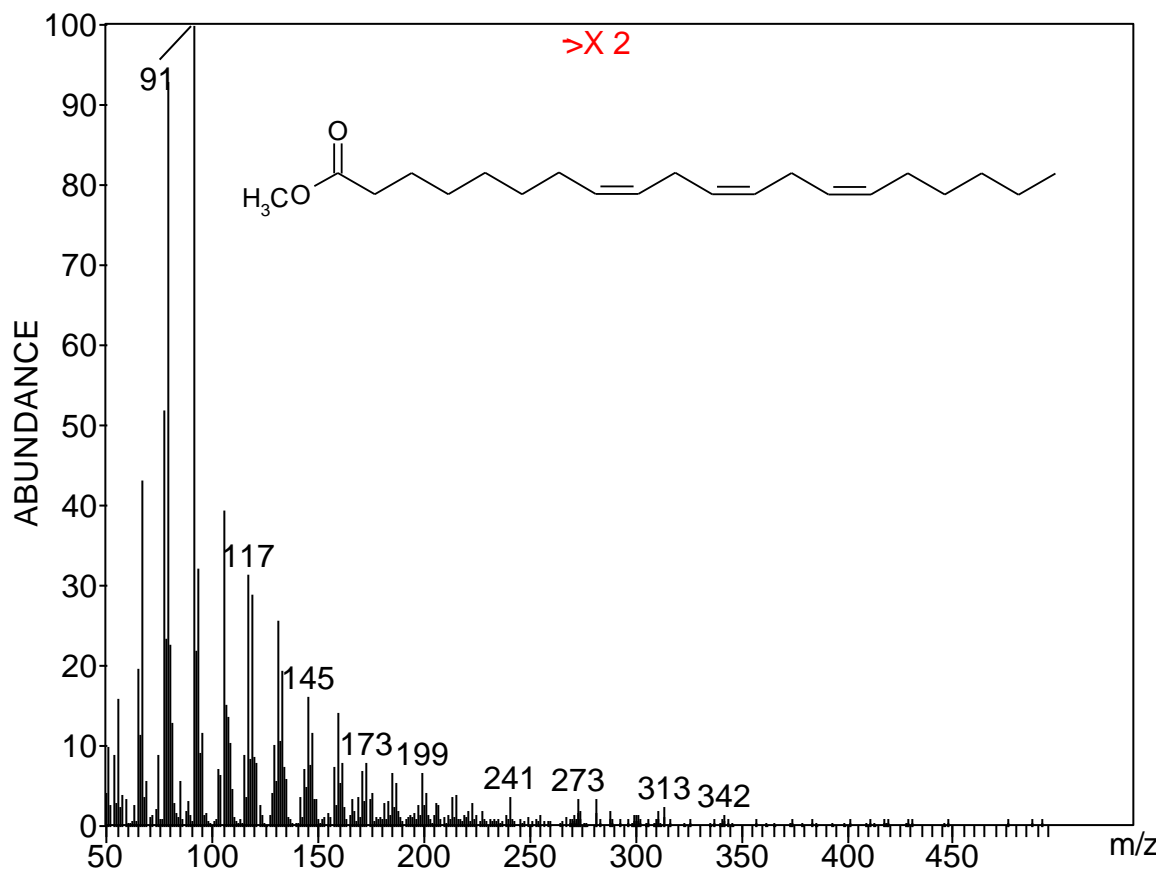
Figure 4.16. Mass spectrum of methyl 4,7,10,13,16,19-docosahexaenoate (22:6Δ4,7,10,13,16,19).
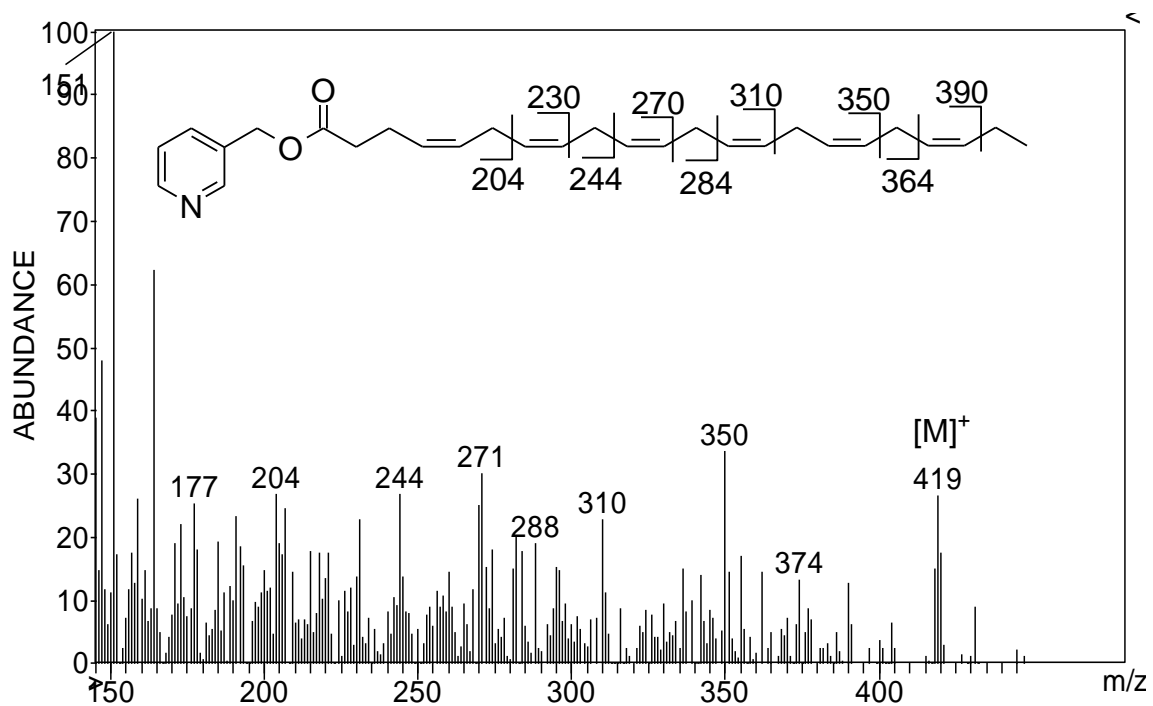
Figure 4.17. Mass spectrum of picolinyl 4,7,10,13,16,19-docosahexaenoate (22:6Δ4,7,10,13,16,19).
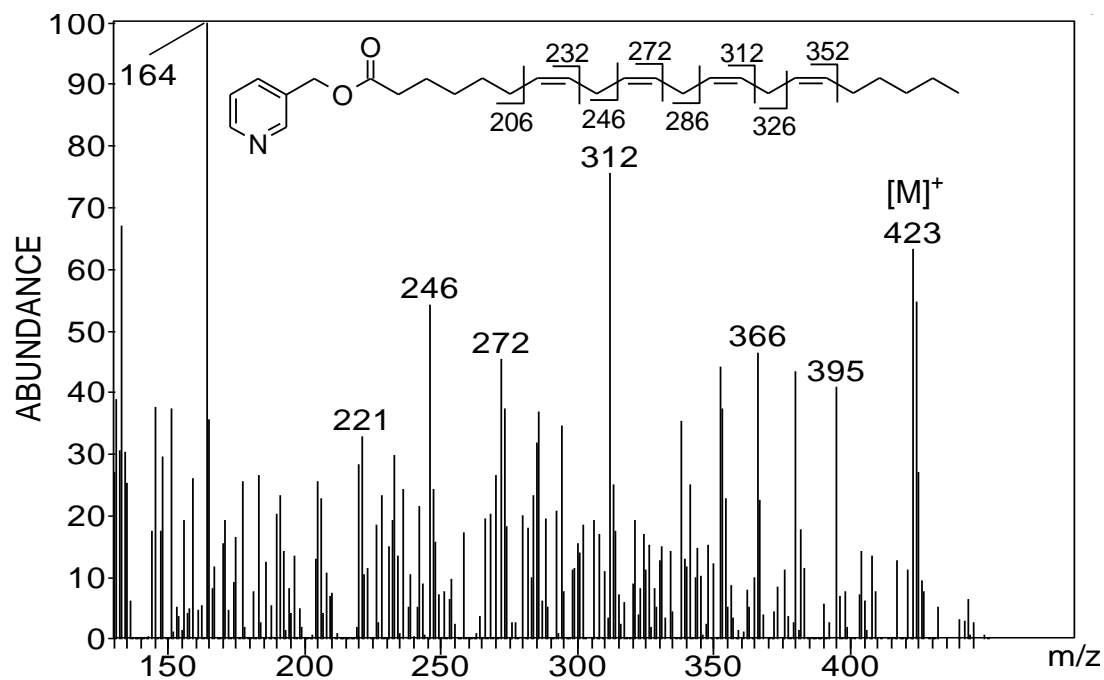
Figure 4.18. Mass spectrum of picolinyl 7,10,13,16-docosatetraenoate (22:4Δ7,10,13,16).

Figure 4.19. Mass spectrum of methyl 7,10,13,16-docosatetraenoate (22:4Δ7,10,13,16).

Figure 4.20. Mass spectra from EI experiments from dimethyl acetals of octadecen-1-al (P 18:1a&b).

were reacted through the FAME procedure. Synthesizing a dimethyl acetal standard in this manner should produce mass spectra analogous to those observed from the plasmalogens. The mass spectrum from the resulting dimethyl tridecacetal exhibits a peak at m/z 213, representing $[M-31]^+$ loss of a methoxy group and a base peak at m/z 75, the fragment of the dimethyl head-group (Figure 4.21). The mass spectrum from the dimethyl acetal of cis-4-decenal displayed a m/z 169 ion from $[M-31]^+$ and the dimethyl head-group, m/z 75 (Figure 4.22). The dimethyl acetal mass spectrum from trans-2-tridecenal, displays an ion at m/z 211 corresponding to $[M-31]^+$, and the ever present dimethyl head-group at m/z 75 (Figure 4.23). Comparison of published mass spectra from unsaturated dimethyl acetals generated from plasmalogens provided further support for the fragmentation pattern of P 18:1a&b [64].

To further verify the formation of acetals and attempt to locate unsaturation sites from plasmalogens, chemical ionization (CI) experiments were conducted using acetonitrile as a reagent gas [65-68]. The resulting mass spectra from the dimethyl acetal of octadecen-1-al (P 18:1a&b) CI experiments are shown in Figure 4.24. Since CI imparts a softer ionization process to the analyte, than EI, it should facilitate less fragmentation and provide greater structural information. Both spectra contain minor $[M+54]^+$ ion peaks, at m/z 366, and a major $[M-31]^+$ ion peak, at m/z 281. The ion from the dimethyl head-group fragmentation discussed in EI spectra was not detected due to instrumental constants during CI which requires a higher background m/z cut-off.

Fatty acid profile analysis

Normality test

Fatty acid methyl esters were evaluated for normality by a Shapiro-Wilk test. The normality test indicates whether the data results from a population with a Gaussian distribution. For the Shapiro-Wilk's test a significance level of $p<0.05$ indicates the sample population was drawn from a non-normally distributed population and therefore non-parametric testing would be required for comparisons. A $p>0.05$ implies a sample population with normal distribution, facilitating the using of parametric testing. Each methyl ester was analyzed for normality based on disease state from combined brain regions (Table 4.2). The data was then further divided based on disease state for each
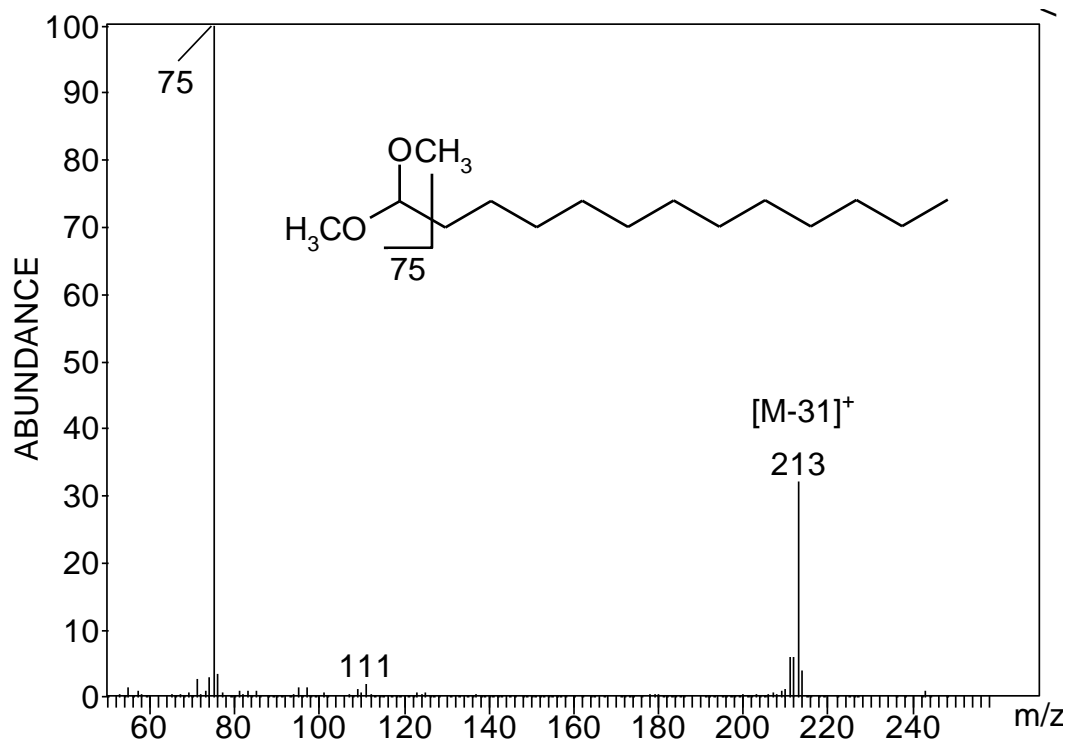
Figure 4.21. Mass spectrum from EI experiments from dimethyl acetal of tridecanal.
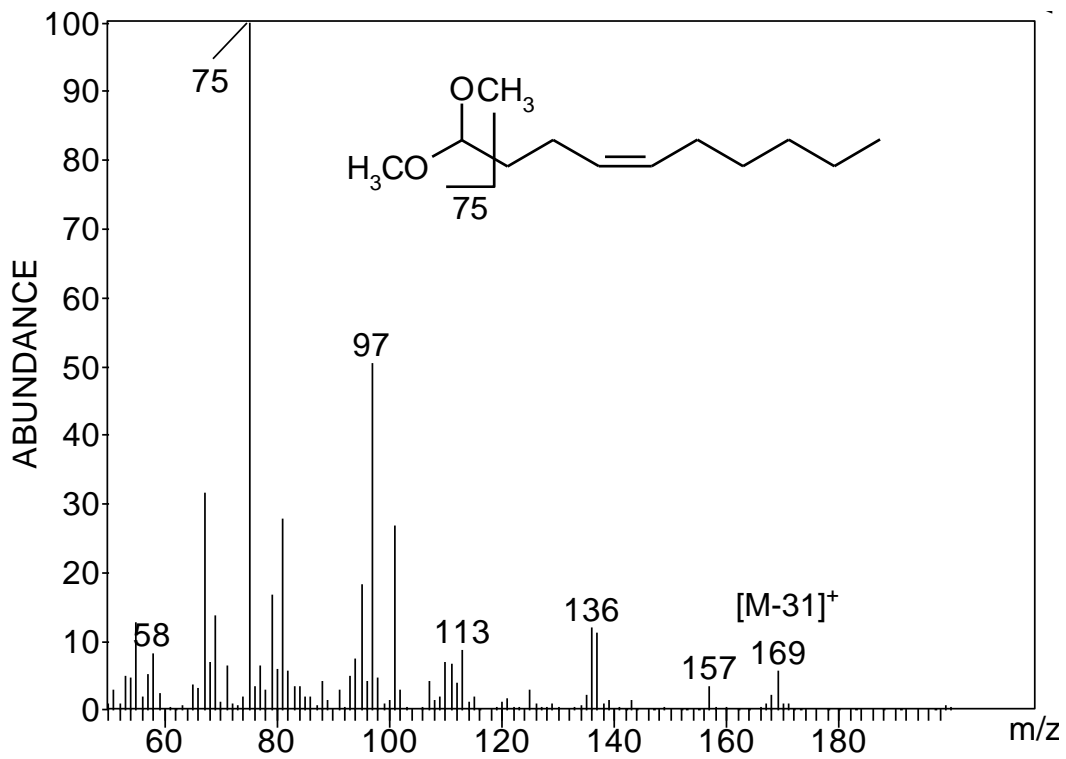
Figure 4.22. Mass spectrum from EI experiments from dimethyl acetal of cis-4-decenal.
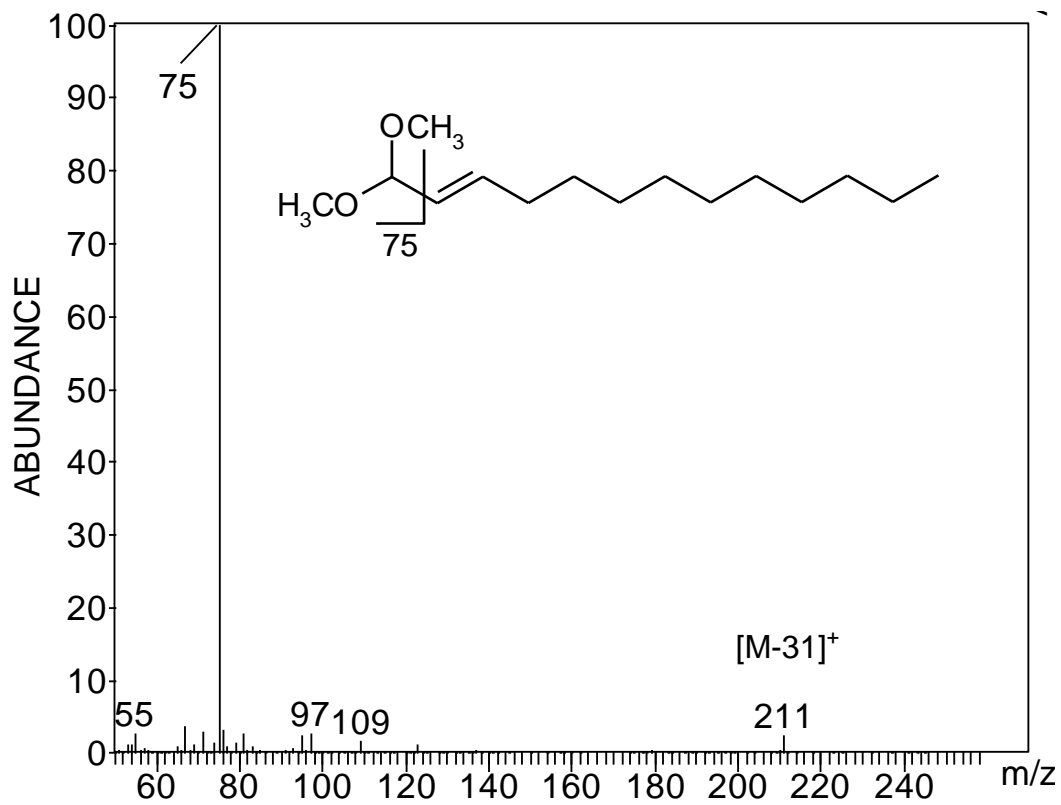
Figure 4.23. Mass spectrum from EI experiments from dimethyl acetal of trans-2-tridecenal.
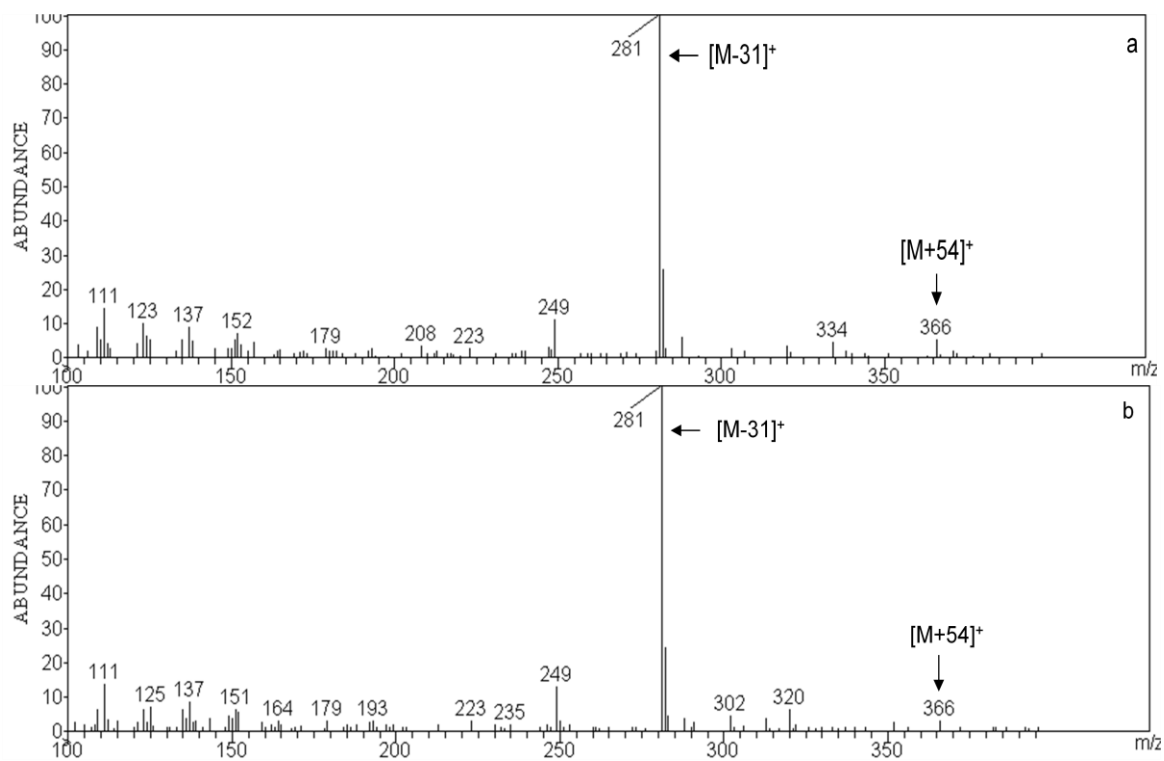
Figure 4.24. Mass spectra from CI experiments from dimethyl acetals of octadecen-1-al (P 18:1a&b).

Table 4.2. Shapiro-Wilk normality test results for mitochondrial fatty acid composition between various disease states.

Species (Structure)[a]	p-value[b]				
	Normal Control (NC)	Mild cognitive impairment (MCI)	Preclinical AD (PCAD)	Late-stage AD (LAD)	Disease Control (DC)[c]
Dodecanoic acid (12:0)	<0.001	<0.001[†]	<0.001	0.085	<0.001[†]
Tetradecanoic acid (14:0)	0.072	0.546	<0.001	0.079	0.038
Pentadecanoic acid (15:0)	0.136	0.011	<0.001	0.033[†]	0.061
9-Hexadecenoic acid (16:1Δ9)	0.094	0.081	0.047	0.111	0.098[#]
Hexadecanoic acid (16:0)	0.068	0.166	0.042[†]	0.398	0.195
Plasmalogen 16:0 (P 16:0)	0.094[#]	0.081	0.047[†]	0.111	0.098
Heptadecanoic acid (17:0)	<0.001	0.010[†]	0.221	0.018[†]	0.323
9,12-Octadecadienoic acid (18:2Δ9,12)	<0.001	0.043	0.042	0.038[†]	0.044[†]
9-Octadecenoic acid (18:1Δ9)	<0.001	0.322	0.548	0.281	0.111[#]
10-Octadecenoic acid (18:1Δ10)	0.056	0.183[#]	0.591	0.348[#]	0.804
Octadecanoic acid (18:0)	<0.001	0.037	0.235[#]	0.486	0.769
Plasmalogen 18:1a (P 18:1a)	0.039	0.726	0.752	0.020[†]	0.029[†]
Plasmalogen 18:1b (P 18:1b)	<0.001	0.920	0.372	0.036	0.034[†]
Plasmalogen 18:0 (P 18:0)	<0.001	0.069	0.918	0.066[#]	0.690[#]
5,8,11,14-Eicosatetraenoic acid (20:4Δ5,8,11,14)	0.001	0.066	0.343	0.791	0.636
8,11,14-Eicosatrienoic acid (20:3Δ8,11,14)	0.291	0.016[†]	0.129	0.017[†]	0.143
4,7,10,13,16,19-Docosahexaenoic acid (22:6Δ4,7,10,13,16,19)	0.123	0.909	0.004	0.011	0.102
7,10,13,16-Docosatetraenoic acid (22:4Δ7,10,13,16)	0.003	0.004[†]	0.218[#]	0.032	0.270

[a] Number of carbons:degree of unsaturation
[b] Values represent data from CER, IPL and SMTG
[c] Represents a combination of dementia with Lewy body disease (DLB) and frontotemporal dementia (FTD)

brain region: CER (Table 4.3), IPL (Table 4.4) and SMTG (Table 4.5). The overall results across each disease state and from each region suggested that the majority of FAs were from normally distributed populations. Although no dominating pattern was present for individual disease states, the greatest abundance of non-normally distributed FAs were found in the inferior parietal lobule.

Skewness test

Fatty acid methyl esters were evaluated for skewness, which provides a measurement of data symmetry around the mean. A population with a Gaussian distribution would have a skewness value equal to zero, indicating perfect symmetry. Positive skewness values result when the distribution of data is heavily concentrated at lower values, the outcome being a population with a long-tailing peak to the right (Figure 4.25). Negative skewness values result from data distributions that are more concentrated at higher values, in this case the sample population curve has a long-fronting peak to the left (Figure 4.26). In both cases a larger deviation from zero, positive or negative, indicates a greater degree of asymmetry from a Gaussian distribution. The data from each methyl ester was initially examined as a function of disease state from the combined brain regions (Table 4.6). The data was then separated into the various regions: CER (Table 4.7), IPL (Table 4.8) and SMTG (Table 4.9) for each disease state.

The evaluation of skewness for the combined regions, did not exhibit any dramatic shifts, positive or negative, in relation to NC values (Table 4.6). A handful of FA species displayed a difference in magnitude between NC and the other demographics. The FA species: 18:2Δ9,12, P18:1b, P18:0 and 20:4 had a large positive skewness value for NC patients, but a substantially lower positive skewness for later AD states.

Evaluation of skewness as a function of disease population for each brain region provided greater disparity between subject demographics, meaning skewness oscillations between positive and negative values. The cerebellum (CER) mitochondrial FA profile imparts a change in positive to negative skewness for 20:3 and 22:4 PUFAs, whereas P18:1b and 22:6 displayed the opposite trend when comparing NC to LAD (Table 4.7). Skewness data from inferior parietal lobule (IPL) was consistent across the disease categories with the only major change involving 20:4 for NC and LAD (Table 4.8).
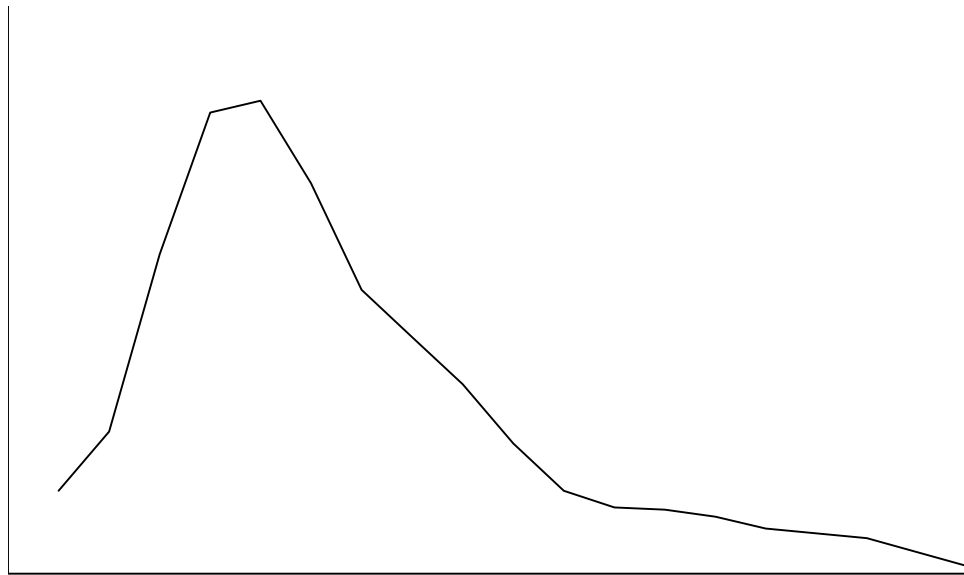
Figure 4.25. Representation of a population with positive skewness.
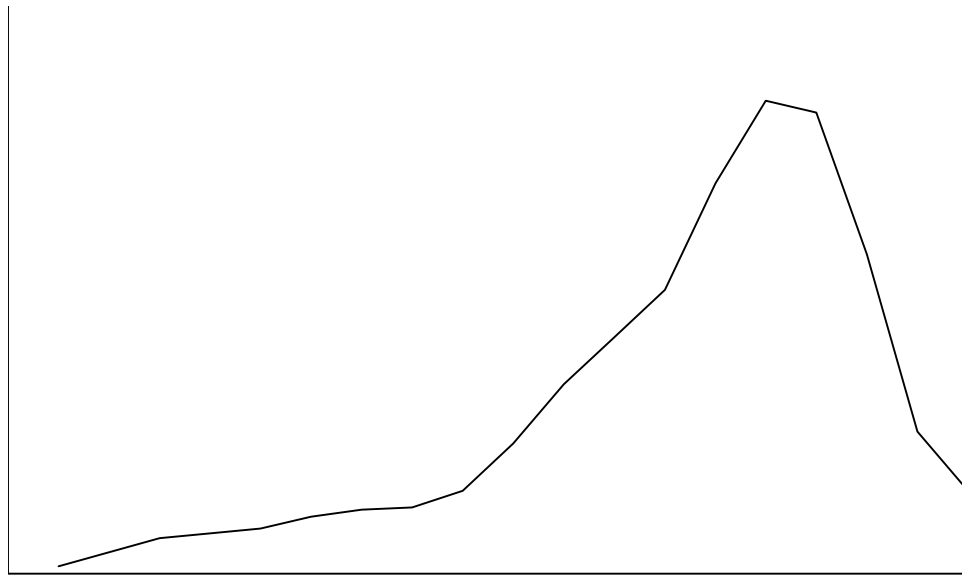
Figure 4.26. Representation of a population with negative skewness.

Table 4.3. Shapiro-Wilk normality test results for mitochondrial fatty acid composition between various disease states for cerebellum (CER).

Species (Structure)[a]	p-value				
	Normal Control (NC)	Mild cognitive impairment (MCI)	Preclinical AD (PCAD)	Late-stage AD (LAD)	Disease Control (DC)[b]
Dodecanoic acid (12:0)	0.003	0.429	0.005	0.227	0.235
Tetradecanoic acid (14:0)	0.145	0.697	0.017	0.831	0.270
Pentadecanoic acid (15:0)	0.545	0.788	0.014	0.379	0.205
9-Hexadecenoic acid (16:1Δ9)	0.595	0.540	0.024	0.492	0.463
Hexadecanoic acid (16:0)	0.853	0.380	0.161	0.737	0.106
Plasmalogen 16:0 (P 16:0)	0.023	0.839	0.510	0.858	0.354
Heptadecanoic acid (17:0)	0.058	0.471	0.836	0.665	0.423
9,12-Octadecadienoic acid (18:2Δ9,12)	0.315	0.485	0.023	0.112	0.187
9-Octadecenoic acid (18:1Δ9)	0.390	0.500	0.698	0.358	0.040
10-Octadecenoic acid (18:1Δ10)	0.102	0.317	0.660	0.601	0.067
Octadecanoic acid (18:0)	0.064	0.444	0.263	0.605	0.085
Plasmalogen 18:1a (P 18:1a)	0.624	0.832	0.423	0.647	0.405
Plasmalogen 18:1b (P 18:1b)	0.495	0.501	0.382	0.026	0.973
Plasmalogen 18:0 (P 18:0)	0.400	0.800	0.850	0.857	0.103
5,8,11,14-Eicosatetraenoic acid (20:4Δ5,8,11,14)	0.135	0.750	0.332	0.486	0.375
8,11,14-Eicosatrienoic acid (20:3Δ8,11,14)	0.349	0.544	0.415	0.093	0.202
4,7,10,13,16,19-Docosahexaenoic acid (22:6Δ4,7,10,13,16,19)	0.592	0.617	0.409	0.341	0.589
7,10,13,16-Docosatetraenoic acid (22:4Δ7,10,13,16)	0.519	0.855	0.592	0.939	0.592

[a] Number of carbons:degree of unsaturation
[b] Represents a combination of dementia with Lewy body disease (DLB) and frontotemporal dementia (FTD)

Table 4.4. Shapiro-Wilk normality test results for mitochondrial fatty acid composition between various disease states for inferior parietal lobule (IPL).

Species (Structure)[a]	p-value				
	Normal Control (NC)	Mild cognitive impairment (MCI)	Preclinical AD (PCAD)	Late-stage AD (LAD)	Disease Control (DC)[b]
Dodecanoic acid (12:0)	0.005	0.528	0.044	0.318	0.259
Tetradecanoic acid (14:0)	0.588	0.509	0.022	0.474	0.796
Pentadecanoic acid (15:0)	0.678	0.337	0.674	0.081	0.098
9-Hexadecenoic acid ($16:1\Delta9$)	0.918	0.248	0.344	0.881	0.018
Hexadecanoic acid (16:0)	0.352	0.764	0.217	0.097	0.265
Plasmalogen 16:0 (P 16:0)	0.435	0.861	0.870	0.050	0.745
Heptadecanoic acid (17:0)	<0.001	0.054	0.255	0.856	0.165
9,12-Octadecadienoic acid ($18:2\Delta9,12$)	<0.001	0.143	0.603	0.933	0.359
9-Octadecenoic acid ($18:1\Delta9$)	0.013	0.203	0.115	0.855	0.289
10-Octadecenoic acid ($18:1\Delta10$)	0.914	0.004	0.181	0.837	0.329
Octadecanoic acid (18:0)	0.785	0.043	0.021	0.749	0.624
Plasmalogen 18:1a (P 18:1a)	0.737	0.109	0.956	0.869	0.810
Plasmalogen 18:1b (P 18:1b)	<0.001	0.905	0.630	0.214	0.579
Plasmalogen 18:0 (P 18:0)	<0.001	0.002	0.593	0.028	0.047
5,8,11,14-Eicosatetraenoic acid ($20:4\Delta5,8,11,14$)	0.420	0.203	0.110	0.819	0.097
8,11,14-Eicosatrienoic acid ($20:3\Delta8,11,14$)	0.402	0.061	0.845	0.127	0.221
4,7,10,13,16,19-Docosahexaenoic acid ($22:6\Delta4,7,10,13,16,19$)	0.086	0.779	0.007	0.249	0.470
7,10,13,16-Docosatetraenoic acid ($22:4\Delta7,10,13,16$)	0.026	0.399	0.011	<0.001	0.078

[a] Number of carbons:degree of unsaturation
[b] Represents a combination of dementia with Lewy body disease (DLB) and frontotemporal dementia (FTD)

177

Table 4.5. Shapiro-Wilk normality test results for mitochondrial fatty acid composition between various disease states for superior and middle temporal gyri (SMTG).

Species (Structure)[a]	p-value				
	Normal Control (NC)	Mild cognitive impairment (MCI)	Preclinical AD (PCAD)	Late-stage AD (LAD)	Disease Control (DC)[b]
Dodecanoic acid (12:0)	0.005	0.700	0.009	0.052	0.166
Tetradecanoic acid (14:0)	0.274	0.456	0.525	0.439	0.348
Pentadecanoic acid (15:0)	0.327	0.104	0.072	0.654	0.898
9-Hexadecenoic acid (16:1Δ9)	0.124	0.415	0.895	0.650	0.598
Hexadecanoic acid (16:0)	0.429	0.430	0.498	0.177	0.572
Plasmalogen 16:0 (P 16:0)	0.661	0.718	0.476	0.803	0.364
Heptadecanoic acid (17:0)	0.408	0.369	0.440	0.090	0.608
9,12-Octadecadienoic acid (18:2Δ9,12)	0.760	0.584	0.948	0.261	0.917
9-Octadecenoic acid (18:1Δ9)	0.530	0.577	0.857	0.253	0.415
10-Octadecenoic acid (18:1Δ10)	0.434	0.292	0.947	0.045	0.365
Octadecanoic acid (18:0)	0.816	0.608	0.350	0.190	0.208
Plasmalogen 18:1a (P 18:1a)	0.425	0.953	0.594	0.135	0.389
Plasmalogen 18:1b (P 18:1b)	0.473	0.382	0.732	0.094	0.612
Plasmalogen 18:0 (P 18:0)	0.876	0.667	0.843	0.730	0.756
5,8,11,14-Eicosatetraenoic acid (20:4Δ5,8,11,14)	0.871	0.514	0.333	0.568	0.501
8,11,14-Eicosatrienoic acid (20:3Δ8,11,14)	0.285	0.629	0.201	0.681	0.123
4,7,10,13,16,19-Docosahexaenoic acid (22:6Δ4,7,10,13,16,19)	0.442	0.556	0.348	0.037	0.167
7,10,13,16-Docosatetraenoic acid (22:4Δ7,10,13,16)	0.820	0.303	0.294	0.287	0.964

[a] Number of carbons:degree of unsaturation
[b] Represents a combination of dementia with Lewy body disease (DLB) and frontotemporal dementia (FTD)

Table 4.6. Skewness test results for mitochondrial fatty acid composition between various disease states.

Species (Structure)[a]	Skewness value[b]				
	Normal Control (NC)	Mild cognitive impairment (MCI)	Preclinical AD (PCAD)	Late-stage AD (LAD)	Disease Control (DC)[c]
Dodecanoic acid (12:0)	1.645	0.839	2.871	0.233	0.851
Tetradecanoic acid (14:0)	0.651	0.209	1.682	0.805	1.124
Pentadecanoic acid (15:0)	0.675	1.721	1.887	0.744	0.504
9-Hexadecenoic acid (16:1Δ9)	0.152	0.0926	1.193	0.0798	1.404
Hexadecanoic acid (16:0)	0.819	0.530	0.448	0.528	-0.222
Plasmalogen 16:0 (P 16:0)	0.217	1.150	0.760	0.438	0.854
Heptadecanoic acid (17:0)	2.478	1.522	0.490	0.688	0.331
9,12-Octadecadienoic acid (18:2Δ9,12)	3.202	1.276	1.045	0.995	0.456
9-Octadecenoic acid (18:1Δ9)	1.473	0.811	0.381	0.431	0.281
10-Octadecenoic acid (18:1Δ10)	0.710	0.524	0.406	0.231	0.134
Octadecanoic acid (18:0)	2.032	0.678	0.562	0.504	0.208
Plasmalogen 18:1a (P 18:1a)	1.009	0.514	0.411	0.802	0.855
Plasmalogen 18:1b (P 18:1b)	2.410	0.448	0.418	0.601	1.156
Plasmalogen 18:0 (P 18:0)	2.583	0.943	0.257	0.619	-0.263
5,8,11,14-Eicosatetraenoic acid (20:4Δ5,8,11,14)	1.262	1.096	0.686	0.314	0.259
8,11,14-Eicosatrienoic acid (20:3Δ8,11,14)	0.111	1.414	0.579	1.105	0.667
4,7,10,13,16,19-Docosahexaenoic acid (22:6Δ4,7,10,13,16,19)	0.741	0.393	0.795	0.948	0.776
7,10,13,16-Docosatetraenoic acid (22:4Δ7,10,13,16)	1.003	1.836	0.723	0.906	0.619

[a] Number of carbons:degree of unsaturation
[b] Values represent data from CER, IPL and SMTG
[c] Represents a combination of dementia with Lewy body disease (DLB) and frontotemporal dementia (FTD)

Table 4.7. Skewness test results for mitochondrial fatty acid composition between various disease states for cerebellum (CER).

Species (Structure)[a]	Skewness value				
	Normal Control (NC)	Mild cognitive impairment (MCI)	Preclinical AD (PCAD)	Late-stage AD (LAD)	Disease Control (DC)[b]
Dodecanoic acid (12:0)	1.749	0.184	0.528	0.797	-1.266
Tetradecanoic acid (14:0)	0.306	-0.475	1.499	0.198	0.394
Pentadecanoic acid (15:0)	0.226	0.453	1.842	0.796	-0.326
9-Hexadecenoic acid (16:1Δ9)	0.0794	0.444	1.681	0.770	-0.547
Hexadecanoic acid (16:0)	-0.0138	0.388	-0.413	-0.0524	0.914
Plasmalogen 16:0 (P 16:0)	1.417	0.0489	0.774	0.0116	1.050
Heptadecanoic acid (17:0)	0.255	0.854	0.153	0.418	0.423
9,12-Octadecadienoic acid (18:2Δ9,12)	0.326	1.096	1.390	1.189	-0.881
9-Octadecenoic acid (18:1Δ9)	0.805	-0.456	0.210	0.0248	1.112
10-Octadecenoic acid (18:1Δ10)	1.383	0.0848	0.571	0.0568	1.261
Octadecanoic acid (18:0)	1.292	-0.0379	-0.189	-0.138	1.161
Plasmalogen 18:1a (P 18:1a)	0.260	-0.0833	0.976	0.208	0.747
Plasmalogen 18:1b (P 18:1b)	0.790	0.0460	0.682	0.234	-0.319
Plasmalogen 18:0 (P 18:0)	-0.666	0.259	0.494	0.368	-0.776
5,8,11,14-Eicosatetraenoic acid (20:4Δ5,8,11,14)	0.970	0.328	-0.551	0.554	0.137
8,11,14-Eicosatrienoic acid (20:3Δ8,11,14)	0.584	0.407	0.790	-0.534	-0.666
4,7,10,13,16,19-Docosahexaenoic acid (22:6Δ4,7,10,13,16,19)	-0.113	0.00404	-0.253	1.040	0.128
7,10,13,16-Docosatetraenoic acid (22:4Δ7,10,13,16)	0.414	0.588	0.497	-0.253	-0.0928

[a] Number of carbons:degree of unsaturation
[b] Represents a combination of dementia with Lewy body disease (DLB) and frontotemporal dementia (FTD)

Table 4.8. Skewness test results for mitochondrial fatty acid composition between various disease states for inferior parietal lobule (IPL).

Species (Structure)[a]	Skewness value				
	Normal Control (NC)	Mild cognitive impairment (MCI)	Preclinical AD (PCAD)	Late-stage AD (LAD)	Disease Control (DC)[b]
Dodecanoic acid (12:0)	2.055	0.392	1.227	-0.0345	0.864
Tetradecanoic acid (14:0)	0.535	-0.000203	1.613	0.207	-0.220
Pentadecanoic acid (15:0)	-0.0720	1.083	-0.277	1.404	0.727
9-Hexadecenoic acid (16:1Δ9)	-0.587	0.565	1.024	-0.186	1.956
Hexadecanoic acid (16:0)	0.0588	0.929	0.960	1.077	-0.141
Plasmalogen 16:0 (P 16:0)	0.624	0.379	-0.364	0.857	0.430
Heptadecanoic acid (17:0)	2.390	1.779	-0.132	0.429	-1.082
9,12-Octadecadienoic acid (18:2Δ9,12)	3.301	-0.119	0.552	0.363	-0.0387
9-Octadecenoic acid (18:1Δ9)	1.896	1.541	0.453	0.230	0.193
10-Octadecenoic acid (18:1Δ10)	0.154	2.162	0.971	0.271	-0.321
Octadecanoic acid (18:0)	0.0539	1.837	1.081	0.260	-0.0547
Plasmalogen 18:1a (P 18:1a)	-0.410	1.579	0.0961	-0.105	0.0394
Plasmalogen 18:1b (P 18:1b)	2.767	0.375	0.642	0.558	0.272
Plasmalogen 18:0 (P 18:0)	3.134	2.298	0.262	0.944	-1.019
5,8,11,14-Eicosatetraenoic acid (20:4Δ5,8,11,14)	1.008	0.623	1.343	-0.398	-0.469
8,11,14-Eicosatrienoic acid (20:3Δ8,11,14)	0.165	0.904	0.238	0.874	-0.720
4,7,10,13,16,19-Docosahexaenoic acid (22:6Δ4,7,10,13,16,19)	1.425	0.190	1.942	0.994	0.0473
7,10,13,16-Docosatetraenoic acid (22:4Δ7,10,13,16)	0.851	0.145	1.901	1.962	-0.925

[a] Number of carbons:degree of unsaturation
[b] Represents a combination of dementia with Lewy body disease (DLB) and frontotemporal dementia (FTD)

Table 4.9. Skewness test results for mitochondrial fatty acid composition between various disease states for superior and middle temporal gyri (SMTG).

Species (Structure)[a]	Skewness value				
	Normal Control (NC)	Mild cognitive impairment (MCI)	Preclinical AD (PCAD)	Late-stage AD (LAD)	Disease Control (DC)[b]
Dodecanoic acid (12:0)	1.998	-0.283	1.217	0.533	1.002
Tetradecanoic acid (14:0)	-0.0870	-0.712	0.913	0.834	1.076
Pentadecanoic acid (15:0)	0.455	1.715	1.405	0.313	-0.409
9-Hexadecenoic acid (16:1Δ9)	-0.790	-0.222	0.394	-0.876	0.343
Hexadecanoic acid (16:0)	-0.288	0.597	0.761	1.013	0.580
Plasmalogen 16:0 (P 16:0)	-0.692	0.727	0.585	-0.324	0.513
Heptadecanoic acid (17:0)	0.363	1.128	0.958	-0.354	0.777
9,12-Octadecadienoic acid (18:2Δ9,12)	0.229	0.649	-0.353	1.039	-0.0367
9-Octadecenoic acid (18:1Δ9)	0.0531	0.469	0.539	0.617	-0.0377
10-Octadecenoic acid (18:1Δ10)	0.496	-0.255	0.243	0.899	0.227
Octadecanoic acid (18:0)	0.612	-0.655	0.757	0.846	1.163
Plasmalogen 18:1a (P 18:1a)	0.480	0.300	0.512	0.130	0.382
Plasmalogen 18:1b (P 18:1b)	0.422	0.653	0.315	-0.0965	0.799
Plasmalogen 18:0 (P 18:0)	-0.269	0.482	0.295	0.618	-0.166
5,8,11,14-Eicosatetraenoic acid (20:4Δ5,8,11,14)	-0.220	0.771	0.980	0.464	0.410
8,11,14-Eicosatrienoic acid (20:3Δ8,11,14)	-0.911	1.094	0.612	0.559	0.430
4,7,10,13,16,19-Docosahexaenoic acid (22:6Δ4,7,10,13,16,19)	-0.0839	1.074	1.023	1.032	1.326
7,10,13,16-Docosatetraenoic acid (22:4Δ7,10,13,16)	0.0738	1.352	0.161	-0.776	-0.131

[a] Number of carbons:degree of unsaturation
[b] Represents a combination of dementia with Lewy body disease (DLB) and frontotemporal dementia (FTD)

The FA profile from the superior and middle temporal gyri (SMTG) exhibited the most change in skewness shifting (Table 4.9). In total four species: P18:0, 20:4, 20:3 and 22:6 altered negative to positive skewness from NC to LAD subjects. Two other species (P18:1b and 22:4) had the reverse trend. As with the IPL, data from SMTG disease states were compared to CER data. Values from SMTG demonstrated less change from CER than with IPL, but again the change in the data population occurred within PCAD and LAD subjects.

Correlation tests

Pearson product-moment tests were employed to determine possible relationships between various subject neuropathological characteristics and fatty acid species. The Pearson correlation test provides a means of evaluating the association between multiple variables, without regard to dependence. The reported data is given in terms of correlation coefficient and significance value (p-value). A positive correlation coefficient and a p<0.050, signifies that the two variables increase together. A negative correlation coefficient and a p<0.050, denotes that the variables decrease concurrently. A p>0.050 indicates that no significant relationship exists between the two variables. Unlike other statistical treatments, for correlation studies, the data from individual disease states were pooled together to provide a single variable. Data relating the subjects' neuropathological demographics were first tested for possible correlations, among the different regions. Age and Braak scores for mitochondria isolated from cerebellum exhibited no significant relationship between the two variables (Table 4.10). For SMTG and IPL age, Braak score and neuritic plagues were compared (Tables 4.11 & 4.12). The results from both regions yielded analogous results. Age showed no relationship to either Braak score or neuritic plaques, however comparison of Braak scores and NP counts displayed a positive correlation.

Next, subject neuropathologic variables were compared to data for each fatty acid species. Overall there seemed to be little correlation between fatty acid species and subject variables among the three brain regions. Data from cerebellum demonstrated a negative correlation between dodecanoic acid (12:0) for age and Braak score (Table 4.13). In contrast, there was a positive correlation between Braak score and 8 of the unsaturated fatty acids, excluding 18:1Δ10, from cerebellum mitochondria.

Table 4.10. Pearson product-moment correlation test for mitochondria from cerebellum (CER).

Variables	Braak score
Age	0.128^a
	0.325^b

^{a} Correlation coefficient
^{b} p-value

Table 4.11. Pearson product-moment correlation test for mitochondria from inferior parietal lobule (IPL).

Variables	Braak score	Neuritic plagues
Age	0.137[a]	-0.243
	0.301[b]	0.0660
Braak score		0.692
		0.00000000173

[a] Correlation coefficient
[b] p-value

Table 4.12. Pearson product-moment correlation test for mitochondria from superior and middle temporal gyri (SMTG).

Variables	Braak score	Neuritic plagues
Age	0.224^a	0.0327
	0.118^b	0.823
Braak score		0.728
		0.00000000297

[a] Correlation coefficient
[b] p-value

Table 4.13. Pearson product-moment correlation test for mitochondrial fatty acids from cerebellum (CER).

Species (Structure)[a]	Variables	
	Age	Braak score
Dodecanoic acid (12:0)	-0.487[b]	-0.418
	0.000120[c]	0.00123
Tetradecanoic acid (14:0)	-0.00120	0.143
	0.993	0.280
Pentadecanoic acid (15:0)	0.0404	0.120
	0.765	0.375
9-Hexadecenoic acid (16:1Δ9)	0.0278	0.325
	0.834	0.0120
Hexadecanoic acid (16:0)	-0.175	0.354
	0.196	0.00740
Plasmalogen 16:0 (P 16:0)	0.0557	0.158
	0.675	0.231
Heptadecanoic acid (17:0)	0.176	0.110
	0.187	0.411
9,12-Octadecadienoic acid (18:2Δ9,12)	0.255	0.267
	0.0536	0.0431
9-Octadecenoic acid (18:1Δ9)	-0.160	0.378
	0.233	0.00372
10-Octadecenoic acid (18:1Δ10)	-0.138	0.360
	0.296	0.00510
Octadecanoic acid (18:0)	-0.167	0.355
	0.219	0.00721
Plasmalogen 18:1a (P 18:1a)	0.0743	0.0670
	0.586	0.624
Plasmalogen 18:1b (P 18:1b)	-0.0774	0.184
	0.560	0.164
Plasmalogen 18:0 (P 18:0)	-0.165	0.398
	0.212	0.00180
5,8,11,14-Eicosatetraenoic acid (20:4Δ5,8,11,14)	-0.00624	0.403
	0.963	0.00153
8,11,14-Eicosatrienoic acid (20:3Δ8,11,14)	0.147	0.321
	0.265	0.0131
4,7,10,13,16,19-Docosahexaenoic acid (22:6Δ4,7,10,13,16,19)	0.128	0.398
	0.335	0.00181
7,10,13,16-Docosatetraenoic acid (22:4Δ7,10,13,16)	0.0205	0.311
	0.879	0.0173

[a] Number of carbons:degree of unsaturation

[b] Correlation coefficient

[c] p-value

The inferior parietal lobule mitochondrial fatty acid profile displayed random correlations between Braak scores and neuritic plaque counts, however no correlations between age and FAs were detected (Table 4.14). Braak scores were found to have negative correlations between pentadecanoic (15:0) and heptadecanoic (17:0) acids, the only odd-carbon chain fatty acid species. A positive correlation was found between 18:1Δ9, 18:0, 20:4, 22:4 and neuritic plaques. In addition, positive correlations were established between hexadecanoic (16:0), 10-octadecanoic (18:1Δ10), Braak scores and neuritic plaques.

The relationship between subject variables and mitochondria fatty acids from SMTG were more sparse than those in the inferior parietal lobule (Table 4.15). Age was found to have a negative correlation with 9-hexadecenoic (16:1Δ9), plasmalogen 16:0, heptadecanoic (17:0) and plasmalogen 18:1a. Neuritic plaques were only found to have a positive correlation with plasmalogen 16:0. No relationship was found between Braak score and any fatty acid species from SMTG.

Fatty acid distribution and disease state analysis

Data on mitochondrial lipid species, cumulative from the three regions (CER, IPL and SMTG) were compared as a function of disease states. Data are graphically represented by box-and-whisker plots (odd-numbered Figures 4.27-4.61). Individual boxes for the five discrete neuropathological classifications, from left-to-right: age-matched normal control (NC), mild cognitive impairment (MCI), preclinical AD (PCAD), late-stage AD (LAD) and disease control (DC).

Fatty acid methyl esters were also analyzed as a function of disease state and region of isolation (even-numbered Figures 4.28-4.62). Data are graphically represented by box-and-whisker plots segmented by region CER (a), IPL (b) and SMTG (c). As with the preceding graphs, each graph consists of individual boxes for the five discrete neuropathologic classifications, from left-to-right: age-matched normal control (NC), mild cognitive impairment (MCI), preclinical AD (PCAD), late-stage AD (LAD) and disease control (DC).

Methyl ester species, 18 total, were evaluated statistically by either a parametric one way ANOVA, for normally distributed data or a non-parametric Kruskal-Wallis one

Table 4.14. Pearson product-moment correlation test for mitochondrial fatty acids from inferior parietal lobule (IPL).

Species (Structure)[a]	Variables		
	Age	Braak score	Neuritic plagues
Dodecanoic acid (12:0)	-0.0790[b]	-0.143	-0.0105
	0.555[c]	0.286	0.938
Tetradecanoic acid (14:0)	0.0944	0.129	0.0688
	0.481	0.339	0.611
Pentadecanoic acid (15:0)	-0.0829	-0.294	-0.169
	0.536	0.0251	0.209
9-Hexadecenoic acid (16:1Δ9)	0.151	0.0148	0.0586
	0.258	0.912	0.665
Hexadecanoic acid (16:0)	-0.0907	0.281	0.367
	0.502	0.0342	0.00538
Plasmalogen 16:0 (P 16:0)	-0.156	0.0211	0.146
	0.242	0.875	0.279
Heptadecanoic acid (17:0)	-0.0775	-0.315	-0.180
	0.563	0.0162	0.180
9,12-Octadecadienoic acid (18:2Δ9,12)	-0.00291	-0.160	-0.116
	0.983	0.226	0.384
9-Octadecenoic acid (18:1Δ9)	-0.152	0.193	0.337
	0.253	0.146	0.0104
10-Octadecenoic acid (18:1Δ10)	0.0594	0.282	0.278
	0.658	0.0318	0.0361
Octadecanoic acid (18:0)	-0.108	0.201	0.307
	0.431	0.142	0.0241
Plasmalogen 18:1a (P 18:1a)	-0.193	-0.00972	0.177
	0.150	0.943	0.192
Plasmalogen 18:1b (P 18:1b)	-0.0666	0.0808	0.154
	0.616	0.543	0.247
Plasmalogen 18:0 (P 18:0)	-0.137	0.224	0.215
	0.302	0.0879	0.105
5,8,11,14-Eicosatetraenoic acid (20:4Δ5,8,11,14)	-0.135	0.189	0.324
	0.316	0.158	0.0150
8,11,14-Eicosatrienoic acid (20:3Δ8,11,14)	-0.0913	0.000380	0.111
	0.500	0.998	0.415
4,7,10,13,16,19-Docosahexaenoic acid (22:6Δ4,7,10,13,16,19)	-0.199	0.0408	0.211
	0.141	0.765	0.121
7,10,13,16-Docosatetraenoic acid (22:4Δ7,10,13,16)	-0.191	0.165	0.285
	0.157	0.224	0.0349

[a] Number of carbons:degree of unsaturation
[b] Correlation coefficient
[c] p-value

Table 4.15. Pearson product-moment correlation test for mitochondrial fatty acids from superior and middle temporal gyri (SMTG).

Species (Structure)[a]	Variables		
	Age	Braak score	Neuritic plagues
Dodecanoic acid (12:0)	-0.288[b]	0.146	0.0781
	0.0610[c]	0.351	0.623
Tetradecanoic acid (14:0)	-0.0804	-0.0701	0.152
	0.583	0.632	0.304
Pentadecanoic acid (15:0)	-0.252	-0.142	0.121
	0.0809	0.329	0.411
9-Hexadecenoic acid (16:1Δ9)	-0.326	-0.0298	0.190
	0.0222	0.839	0.195
Hexadecanoic acid (16:0)	0.0845	0.240	0.173
	0.577	0.108	0.255
Plasmalogen 16:0 (P 16:0)	-0.284	0.0521	0.293
	0.0480	0.722	0.0433
Heptadecanoic acid (17:0)	-0.318	-0.0770	0.181
	0.0292	0.607	0.223
9,12-Octadecadienoic acid (18:2Δ9,12)	0.100	-0.0308	0.0590
	0.492	0.834	0.690
9-Octadecenoic acid (18:1Δ9)	0.0260	0.202	0.131
	0.862	0.173	0.385
10-Octadecenoic acid (18:1Δ10)	-0.137	0.0979	0.129
	0.350	0.503	0.384
Octadecanoic acid (18:0)	0.112	-0.0460	-0.0645
	0.440	0.751	0.660
Plasmalogen 18:1a (P 18:1a)	-0.339	-0.0719	0.123
	0.0173	0.623	0.404
Plasmalogen 18:1b (P 18:1b)	-0.210	-0.0658	0.0696
	0.147	0.653	0.638
Plasmalogen 18:0 (P 18:0)	-0.120	-0.0243	0.109
	0.412	0.868	0.462
5,8,11,14-Eicosatetraenoic acid (20:4Δ5,8,11,14)	0.0303	0.000328	0.0973
	0.838	0.998	0.515
8,11,14-Eicosatrienoic acid (20:3Δ8,11,14)	-0.189	0.00975	0.270
	0.193	0.947	0.0637
4,7,10,13,16,19-Docosahexaenoic acid (22:6Δ4,7,10,13,16,19)	-0.00370	-0.0219	0.0497
	0.980	0.881	0.737
7,10,13,16-Docosatetraenoic acid (22:4Δ7,10,13,16)	0.0294	-0.0725	0.0540
	0.841	0.621	0.715

[a] Number of carbons:degree of unsaturation

[b] Correlation coefficient

[c] p-value

Figure 4.27. Distribution of 12:0 between disease states for combined neurological regions (normal control (NC), mild cognitive impairment (MCI), preclinical AD (PCAD) late-stage AD (LAD) and disease control (DC)). Significant differences ($p<0.05$) between disease states, compared to NC, are depicted by *.

Figure 4.28. Distribution of 12:0 between disease states and regions (normal control (NC), mild cognitive impairment (MCI), preclinical AD (PCAD) late-stage AD (LAD) and disease control (DC), for cerebellum (a), inferior parietal lobule (b) and superior and middle temporal gyri (c)). Significant differences (p<0.05) between disease states, within the same region, compared to NC are depicted by *. Significant differences (p<0.05), within equivalent disease states, across regions are depicted by ‡.

Figure 4.29. Distribution of 14:0 between disease states for combined neurological regions (normal control (NC), mild cognitive impairment (MCI), preclinical AD (PCAD) late-stage AD (LAD) and disease control (DC)). Significant differences (p<0.05) between disease states, compared to NC, are depicted by *.

Figure 4.30. Distribution of 14:0 between disease states and regions (normal control (NC), mild cognitive impairment (MCI), preclinical AD (PCAD) late-stage AD (LAD) and disease control (DC), for cerebellum (a), inferior parietal lobule (b) and superior and middle temporal gyri (c)). Significant differences (p<0.05) between disease states, within the same region, compared to NC are depicted by *. Significant differences (p<0.05), within equivalent disease states, across regions are depicted by ‡.

194

Figure 4.31. Distribution of 15:0 between disease states for combined neurological regions (normal control (NC), mild cognitive impairment (MCI), preclinical AD (PCAD) late-stage AD (LAD) and disease control (DC)). Significant differences (p<0.05) between disease states, compared to NC, are depicted by *.

Figure 4.32. Distribution of 15:0 between disease states and regions (normal control (NC), mild cognitive impairment (MCI), preclinical AD (PCAD) late-stage AD (LAD) and disease control (DC), for cerebellum (a), inferior parietal lobule (b) and superior and middle temporal gyri (c)). Significant differences (p<0.05) between disease states, within the same region, compared to NC are depicted by *. Significant differences (p<0.05), within equivalent disease states, across regions are depicted by ‡.

Figure 4.33. Distribution of 16:1 between disease states for combined neurological regions (normal control (NC), mild cognitive impairment (MCI), preclinical AD (PCAD) late-stage AD (LAD) and disease control (DC)). Significant differences (p<0.05) between disease states, compared to NC, are depicted by *.

Figure 4.34. Distribution of 16:1 between disease states and regions (normal control (NC), mild cognitive impairment (MCI), preclinical AD (PCAD) late-stage AD (LAD) and disease control (DC), for cerebellum (a), inferior parietal lobule (b) and superior and middle temporal gyri (c)). Significant differences (p<0.05) between disease states, within the same region, compared to NC are depicted by *. Significant differences (p<0.05), within equivalent disease states, across regions are depicted by ‡.

Figure 4.35. Distribution of 16:0 between disease states for combined neurological regions (normal control (NC), mild cognitive impairment (MCI), preclinical AD (PCAD) late-stage AD (LAD) and disease control (DC)). Significant differences ($p < 0.05$) between disease states, compared to NC, are depicted by *.

Figure 4.36. Distribution of 16:0 between disease states and regions (normal control (NC), mild cognitive impairment (MCI), preclinical AD (PCAD) late-stage AD (LAD) and disease control (DC), for cerebellum (a), inferior parietal lobule (b) and superior and middle temporal gyri (c)). Significant differences (p<0.05) between disease states, within the same region, compared to NC are depicted by *. Significant differences (p<0.05), within equivalent disease states, across regions are depicted by ‡.
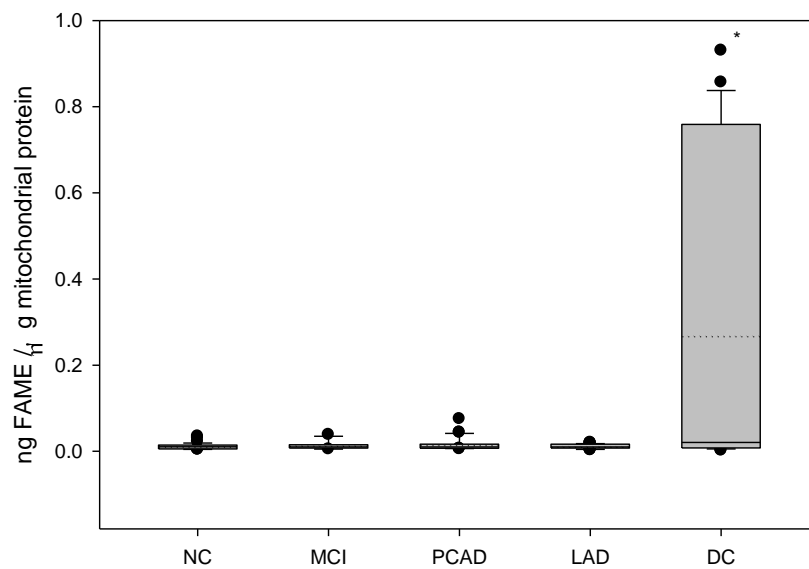
Figure 4.37. Distribution of P 16:0 between disease states for combined neurological regions (normal control (NC), mild cognitive impairment (MCI), preclinical AD (PCAD) late-stage AD (LAD) and disease control (DC)). Significant differences (p<0.05) between disease states, compared to NC, are depicted by *.
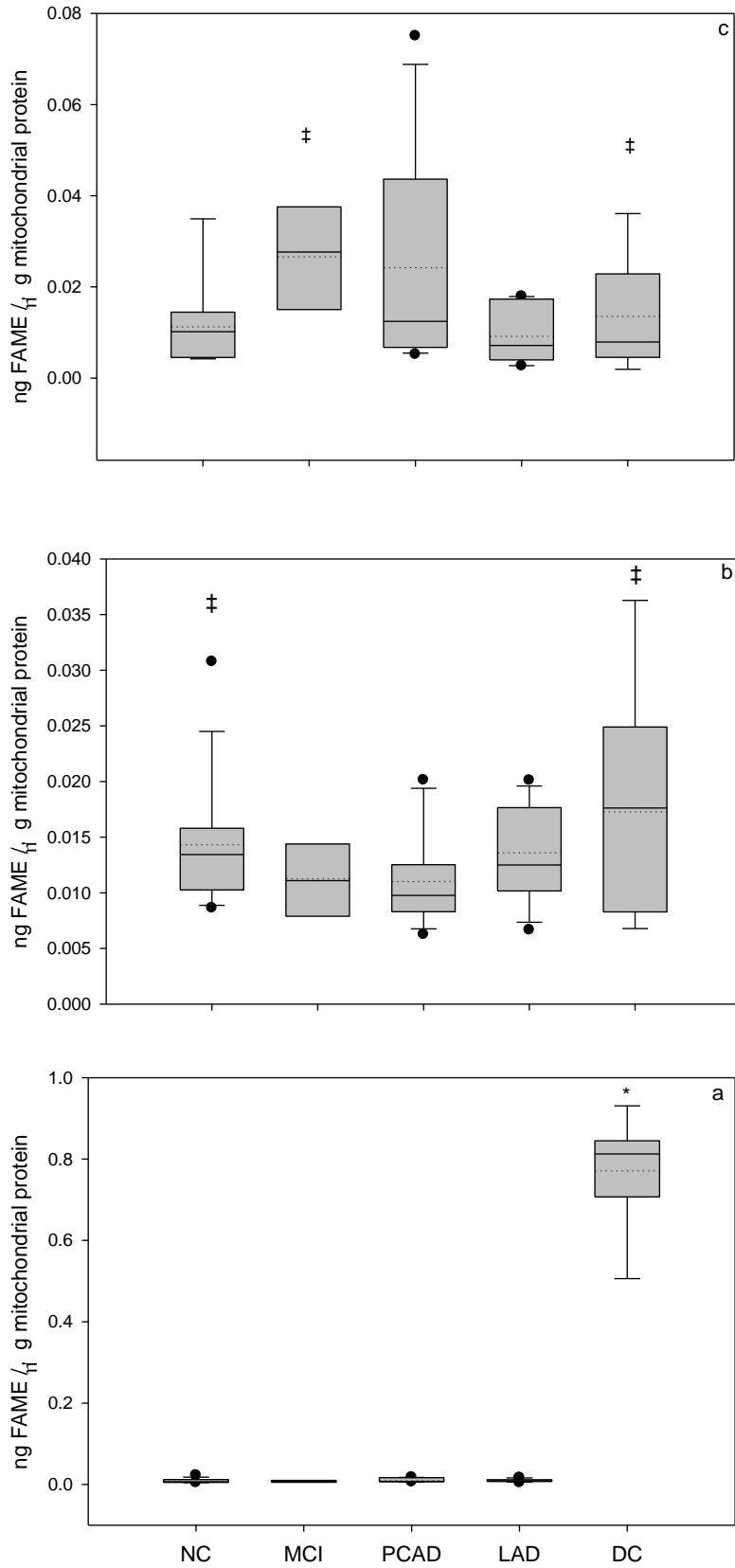
Figure 4.38. Distribution of P 16:0 between disease states and regions (normal control (NC), mild cognitive impairment (MCI), preclinical AD (PCAD) late-stage AD (LAD) and disease control (DC), for cerebellum (a), inferior parietal lobule (b) and superior and middle temporal gyri (c)). Significant differences (p<0.05) between disease states, within the same region, compared to NC are depicted by *. Significant differences (p<0.05), within equivalent disease states, across regions are depicted by ‡.
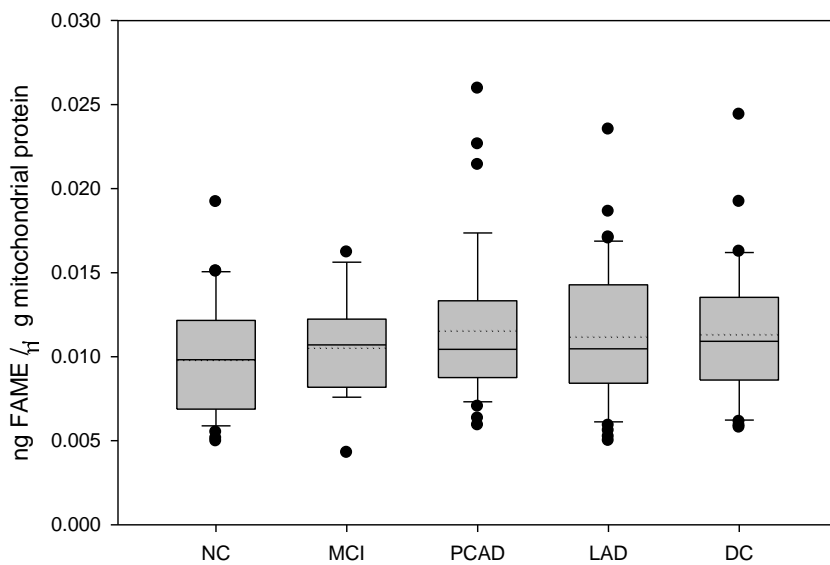
Figure 4.39. Distribution of 17:0 between disease states for combined neurological regions (normal control (NC), mild cognitive impairment (MCI), preclinical AD (PCAD) late-stage AD (LAD) and disease control (DC)). Significant differences (p<0.05) between disease states, compared to NC, are depicted by *.
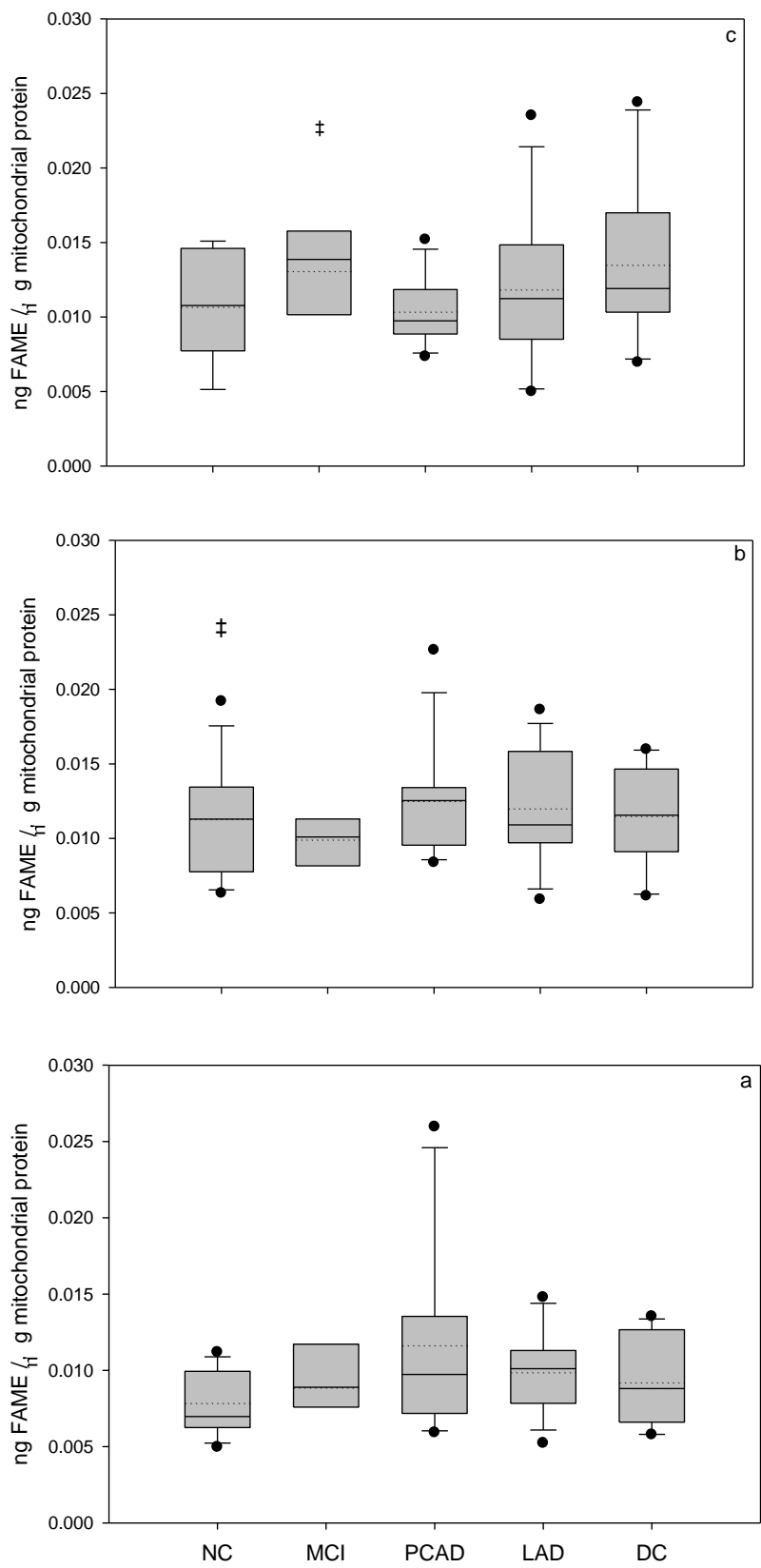
Figure 4.40. Distribution of 17:0 between disease states and regions (normal control (NC), mild cognitive impairment (MCI), preclinical AD (PCAD) late-stage AD (LAD) and disease control (DC), for cerebellum (a), inferior parietal lobule (b) and superior and middle temporal gyri (c)). Significant differences (p<0.05) between disease states, within the same region, compared to NC are depicted by *. Significant differences (p<0.05), within equivalent disease states, across regions are depicted by ‡.

Figure 4.41. Distribution of 18:2Δ9,12 between disease states for combined neurological regions (normal control (NC), mild cognitive impairment (MCI), preclinical AD (PCAD) late-stage AD (LAD) and disease control (DC)). Significant differences (p<0.05) between disease states, compared to NC, are depicted by *.

Figure 4.42. Distribution of 18:2Δ9,12 between disease states and regions (normal control (NC), mild cognitive impairment (MCI), preclinical AD (PCAD) late-stage AD (LAD) and disease control (DC), for cerebellum (a), inferior parietal lobule (b) and superior and middle temporal gyri (c)). Significant differences (p<0.05) between disease states, within the same region, compared to NC are depicted by *. Significant differences (p<0.05), within equivalent disease states, across regions are depicted by ‡.
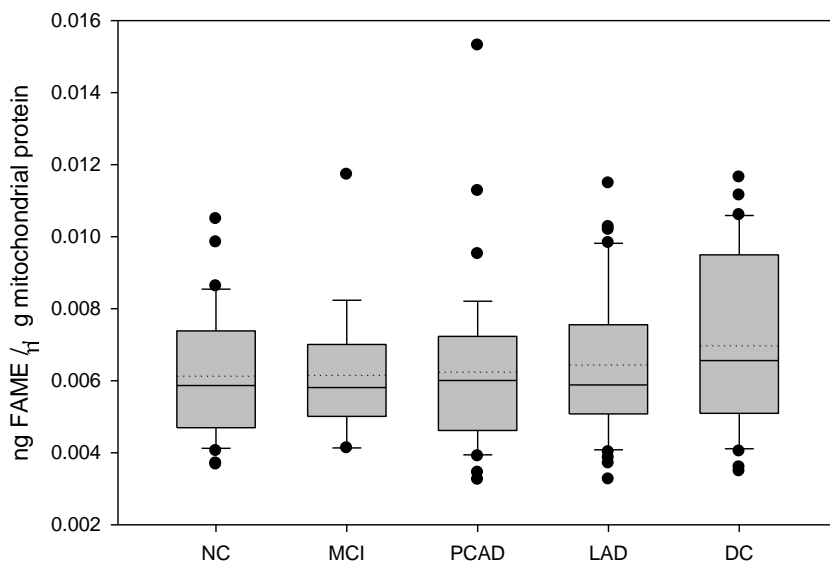
206

Figure 4.43. Distribution of 18:1Δ9 between disease states for combined neurological regions (normal control (NC), mild cognitive impairment (MCI), preclinical AD (PCAD) late-stage AD (LAD) and disease control (DC)). Significant differences (p<0.05) between disease states, compared to NC, are depicted by *.
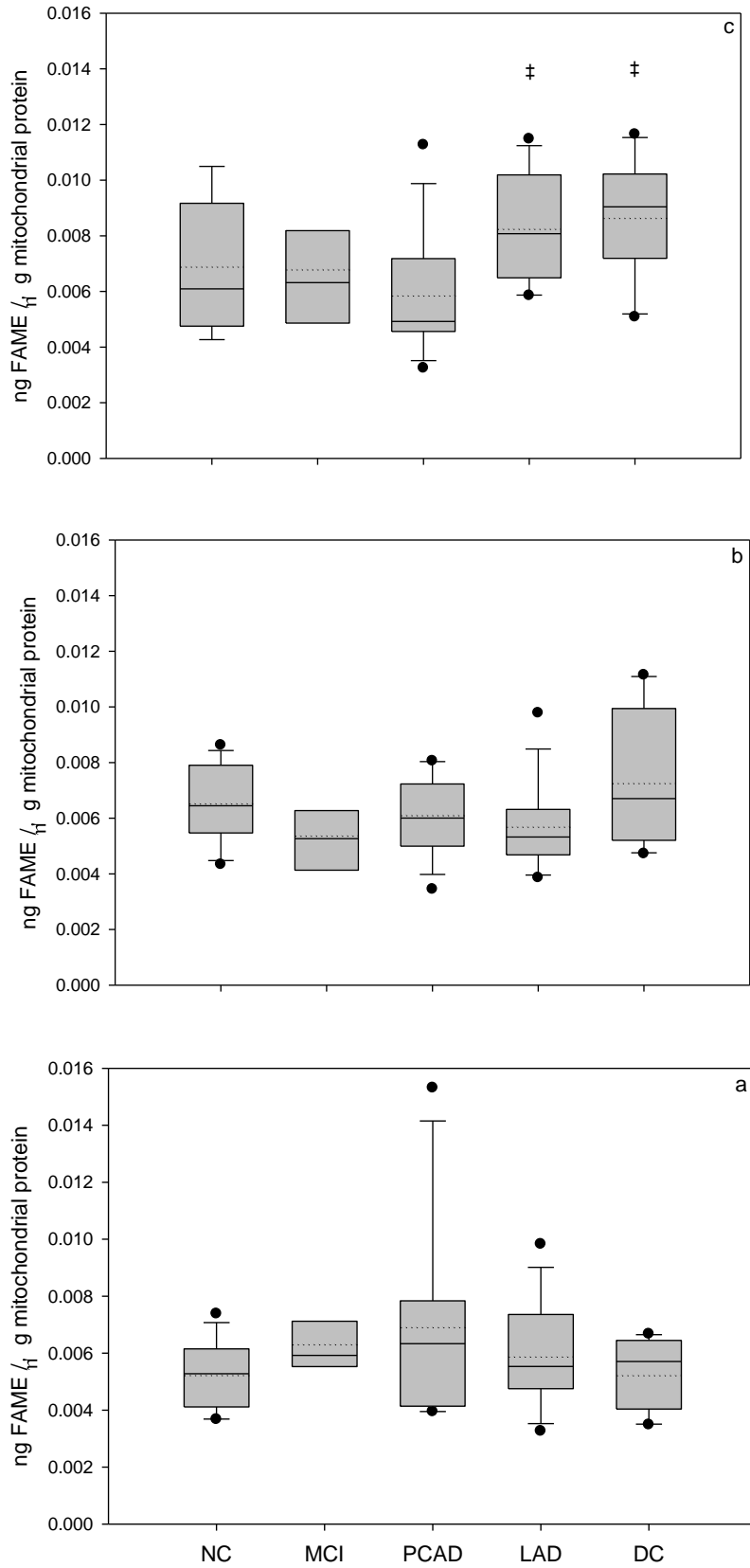
Figure 4.44. Distribution of 18:1Δ9 between disease states and regions (normal control (NC), mild cognitive impairment (MCI), preclinical AD (PCAD) late-stage AD (LAD) and disease control (DC), for cerebellum (a), inferior parietal lobule (b) and superior and middle temporal gyri (c)). Significant differences (p<0.05) between disease states, within the same region, compared to NC are depicted by *. Significant differences (p<0.05), within equivalent disease states, across regions are depicted by ‡.
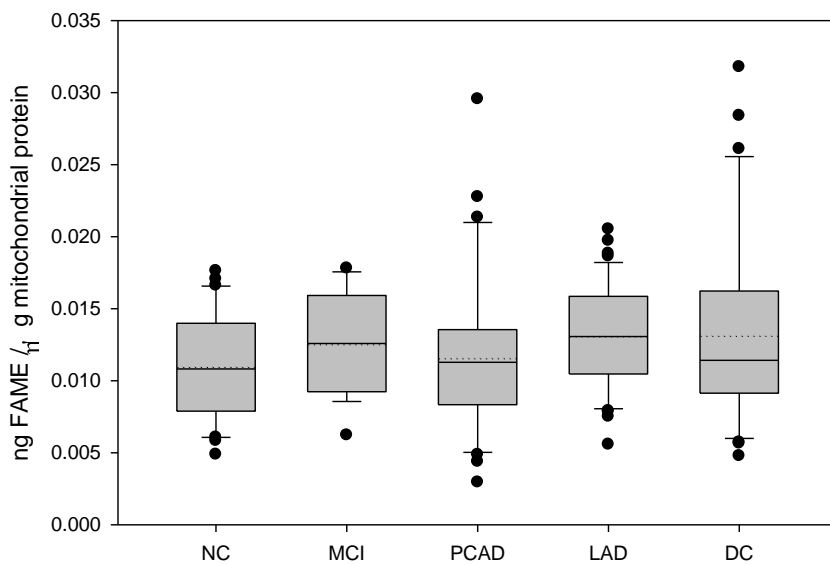
Figure 4.45. Distribution of 18:1Δ10 between disease states for combined neurological regions (normal control (NC), mild cognitive impairment (MCI), preclinical AD (PCAD) late-stage AD (LAD) and disease control (DC)). Significant differences (p<0.05) between disease states, compared to NC, are depicted by *.
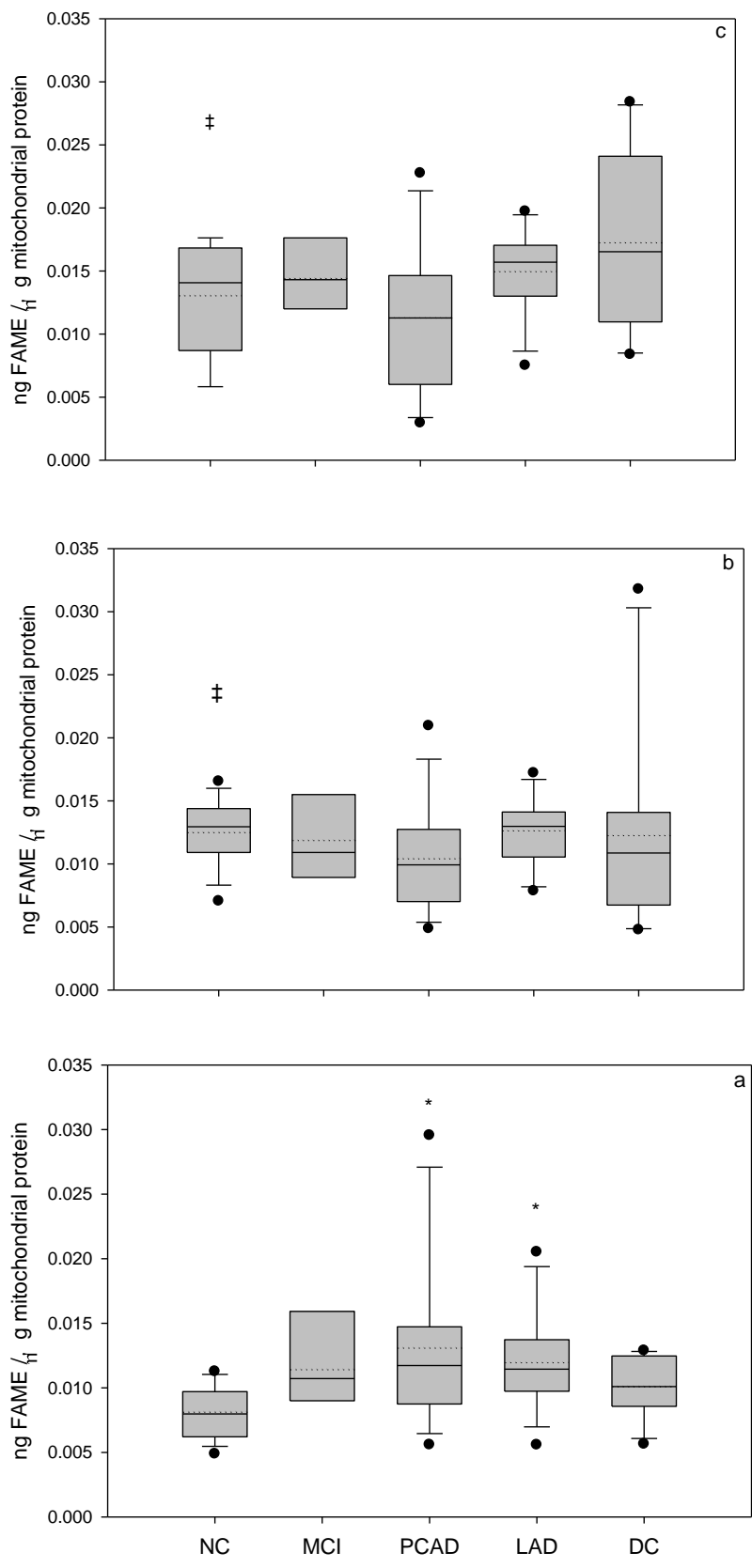
Figure 4.46. Distribution of 18:1Δ10 between disease states and regions (normal control (NC), mild cognitive impairment (MCI), preclinical AD (PCAD) late-stage AD (LAD) and disease control (DC), for cerebellum (a), inferior parietal lobule (b) and superior and middle temporal gyri (c)). Significant differences (p<0.05) between disease states, within the same region, compared to NC are depicted by *. Significant differences (p<0.05), within equivalent disease states, across regions are depicted by ‡.
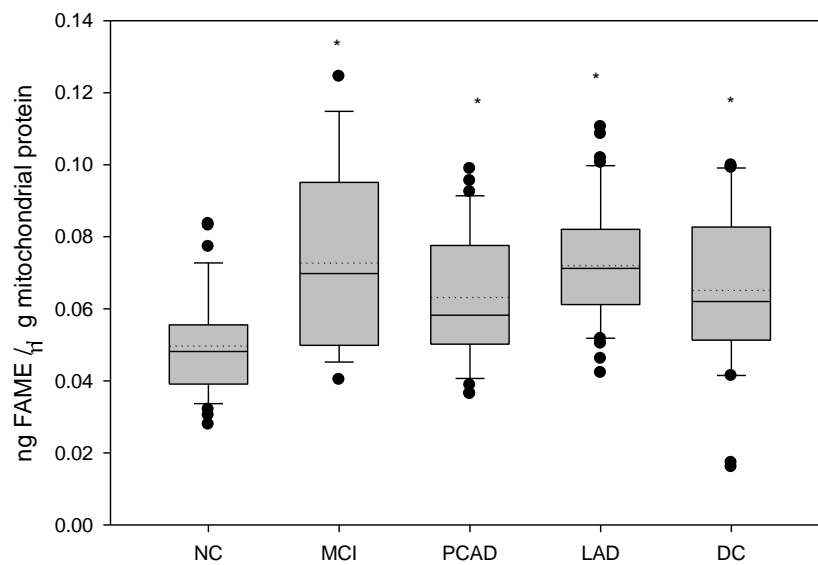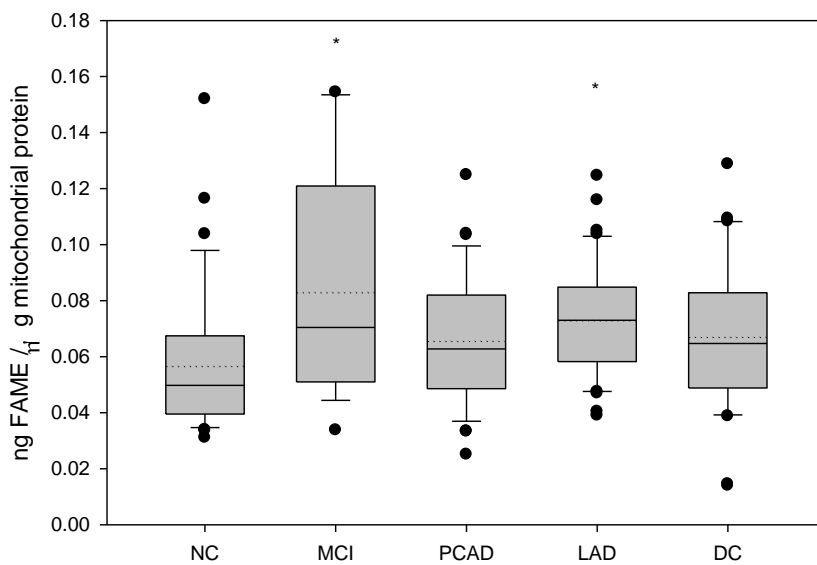
Figure 4.47. Distribution of 18:0 between disease states for combined neurological regions (normal control (NC), mild cognitive impairment (MCI), preclinical AD (PCAD) late-stage AD (LAD) and disease control (DC)). Significant differences ($p<0.05$) between disease states, compared to NC, are depicted by *.
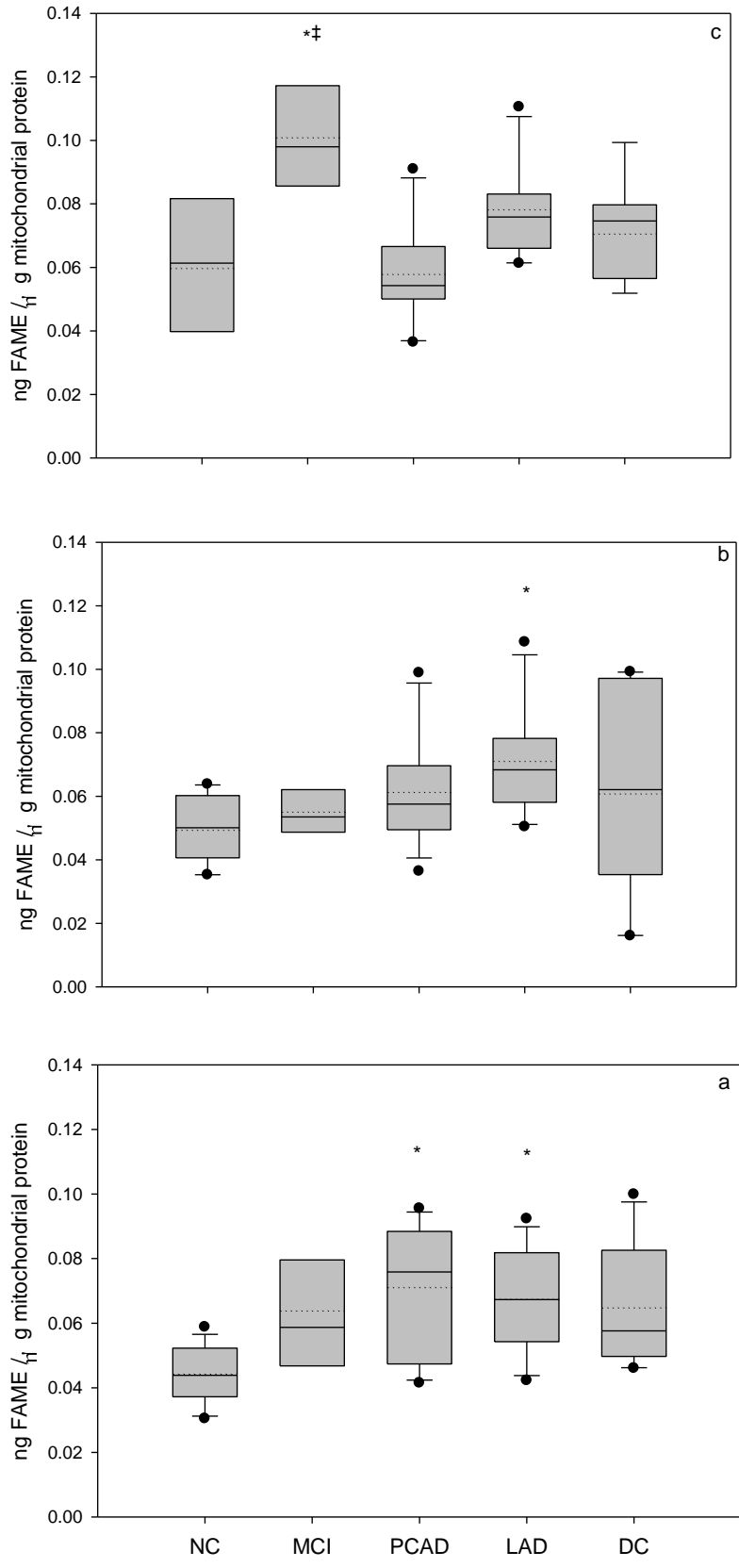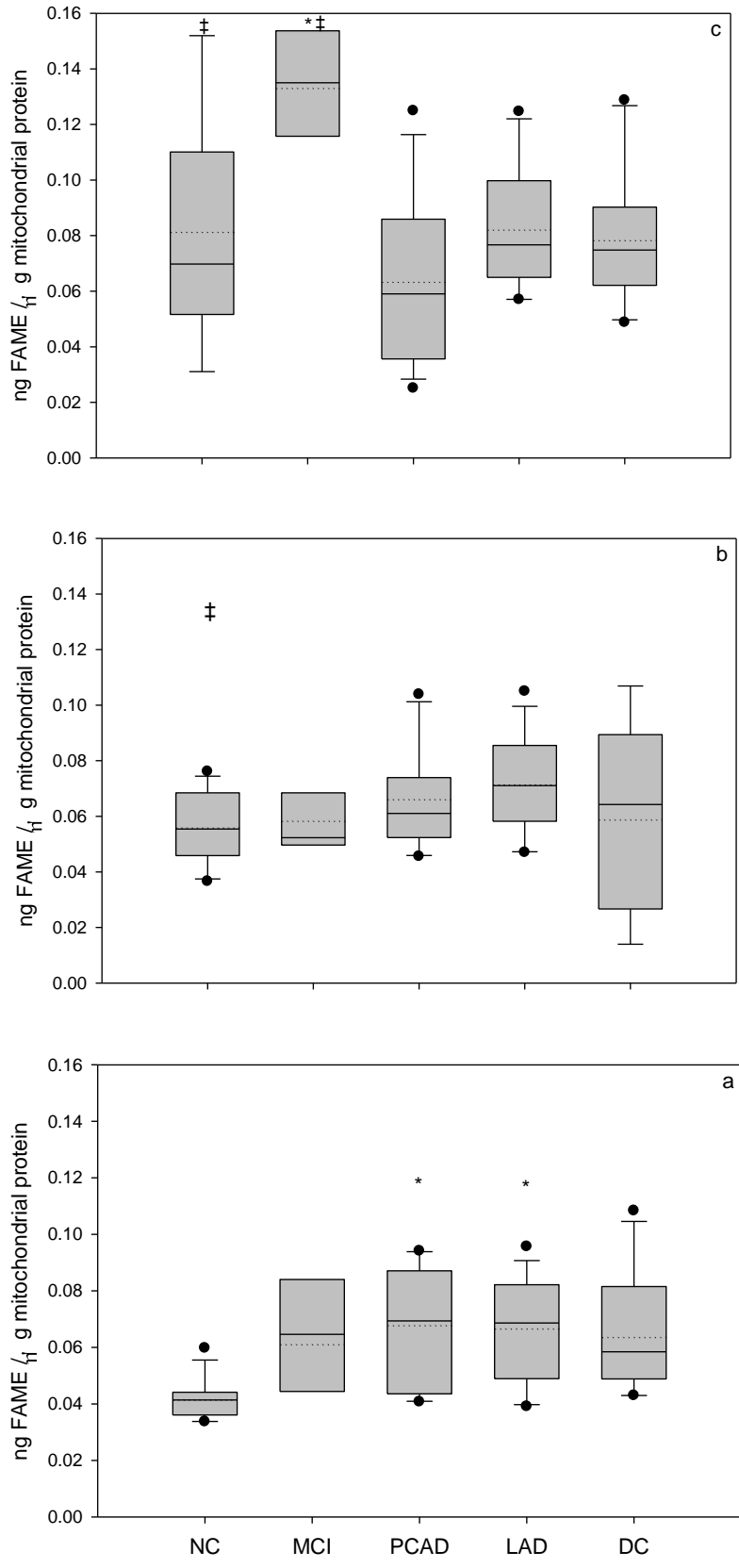
Figure 4.48. Distribution of 18:0 between disease states and regions (normal control (NC), mild cognitive impairment (MCI), preclinical AD (PCAD) late-stage AD (LAD) and disease control (DC), for cerebellum (a), inferior parietal lobule (b) and superior and middle temporal gyri (c)). Significant differences (p<0.05) between disease states, within the same region, compared to NC are depicted by *. Significant differences (p<0.05), within equivalent disease states, across regions are depicted by ‡.
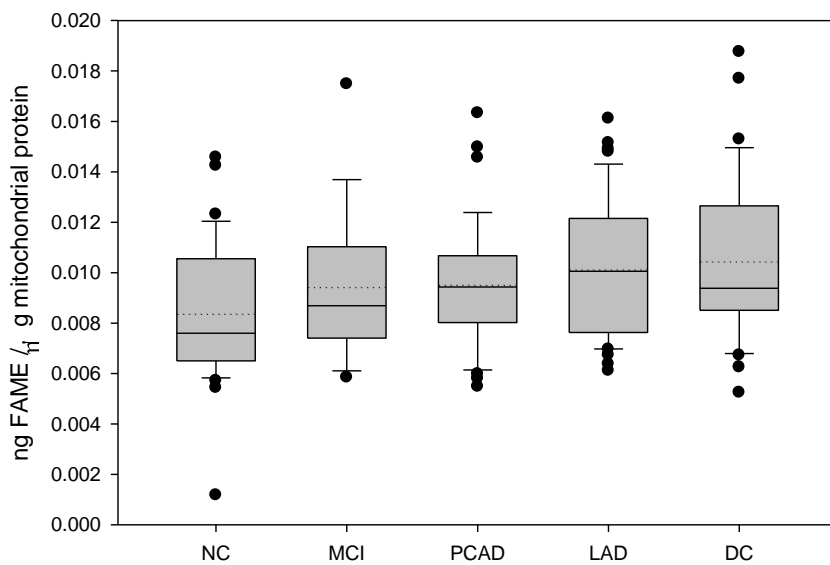
212
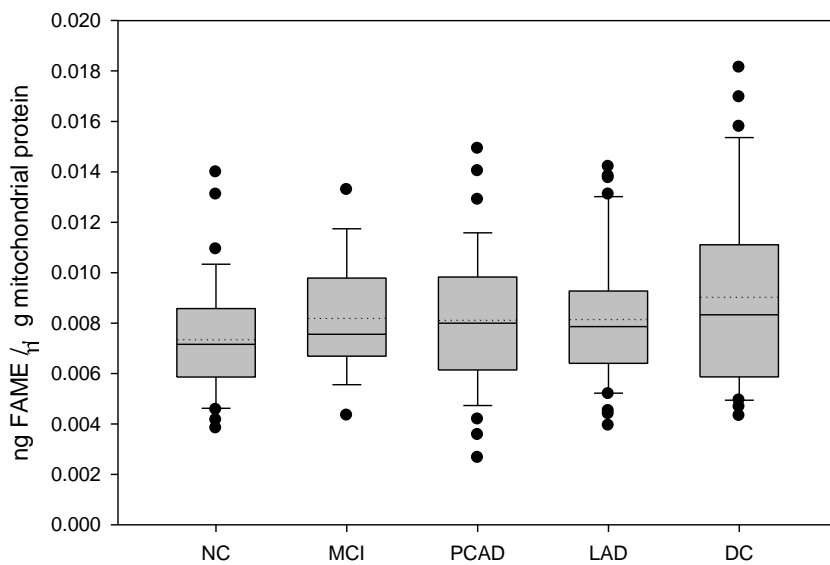
Figure 4.49. Distribution of P 18:1a between disease states for combined neurological regions (normal control (NC), mild cognitive impairment (MCI), preclinical AD (PCAD) late-stage AD (LAD) and disease control (DC)). Significant differences ($p<0.05$) between disease states, compared to NC, are depicted by *.
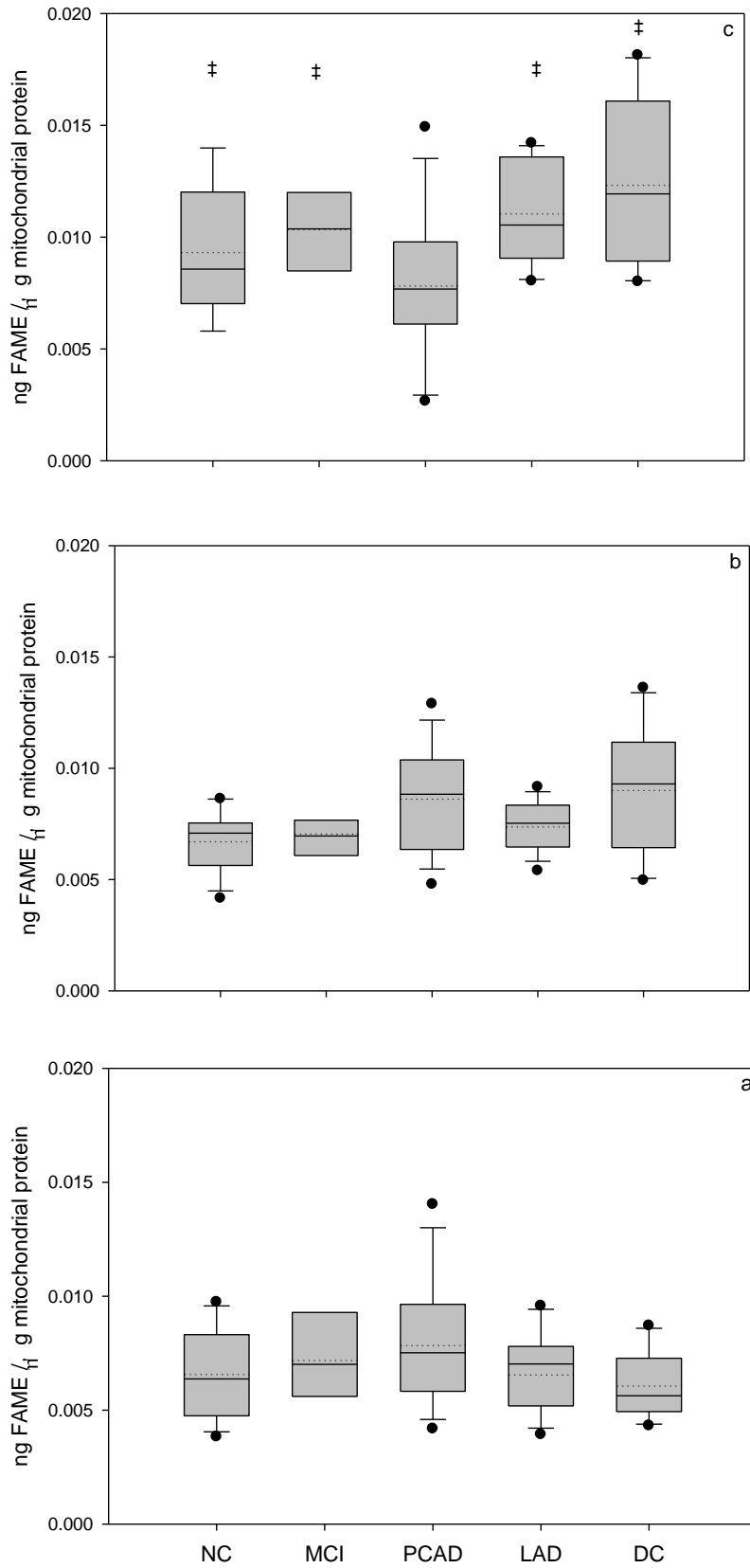
Figure 4.50. Distribution of P 18:1a between disease states and regions (normal control (NC), mild cognitive impairment (MCI), preclinical AD (PCAD) late-stage AD (LAD) and disease control (DC), for cerebellum (a), inferior parietal lobule (b) and superior and middle temporal gyri (c)). Significant differences ($p < 0.05$) between disease states, within the same region, compared to NC are depicted by *. Significant differences ($p < 0.05$), within equivalent disease states, across regions are depicted by ‡.
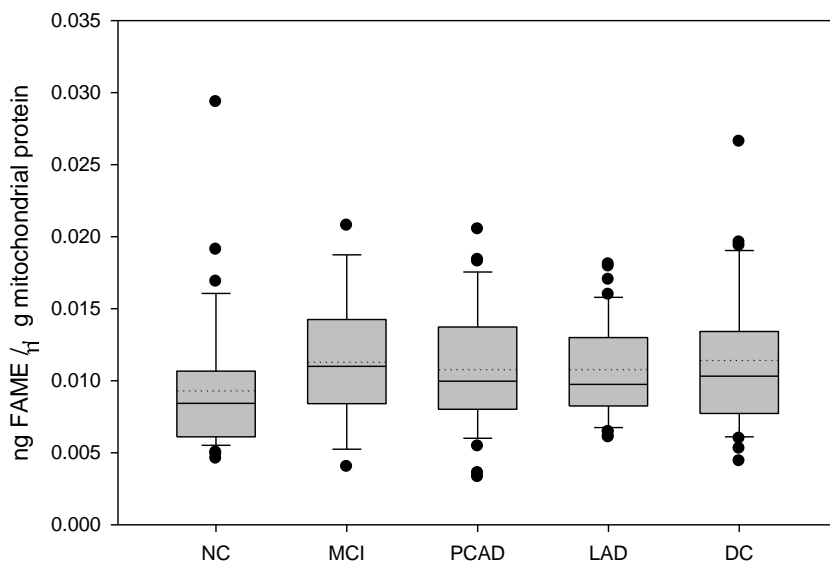
Figure 4.51. Distribution of P 18:1b between disease states for combined neurological regions (normal control (NC), mild cognitive impairment (MCI), preclinical AD (PCAD) late-stage AD (LAD) and disease control (DC)). Significant differences (p<0.05) between disease states, compared to NC, are depicted by *.

215
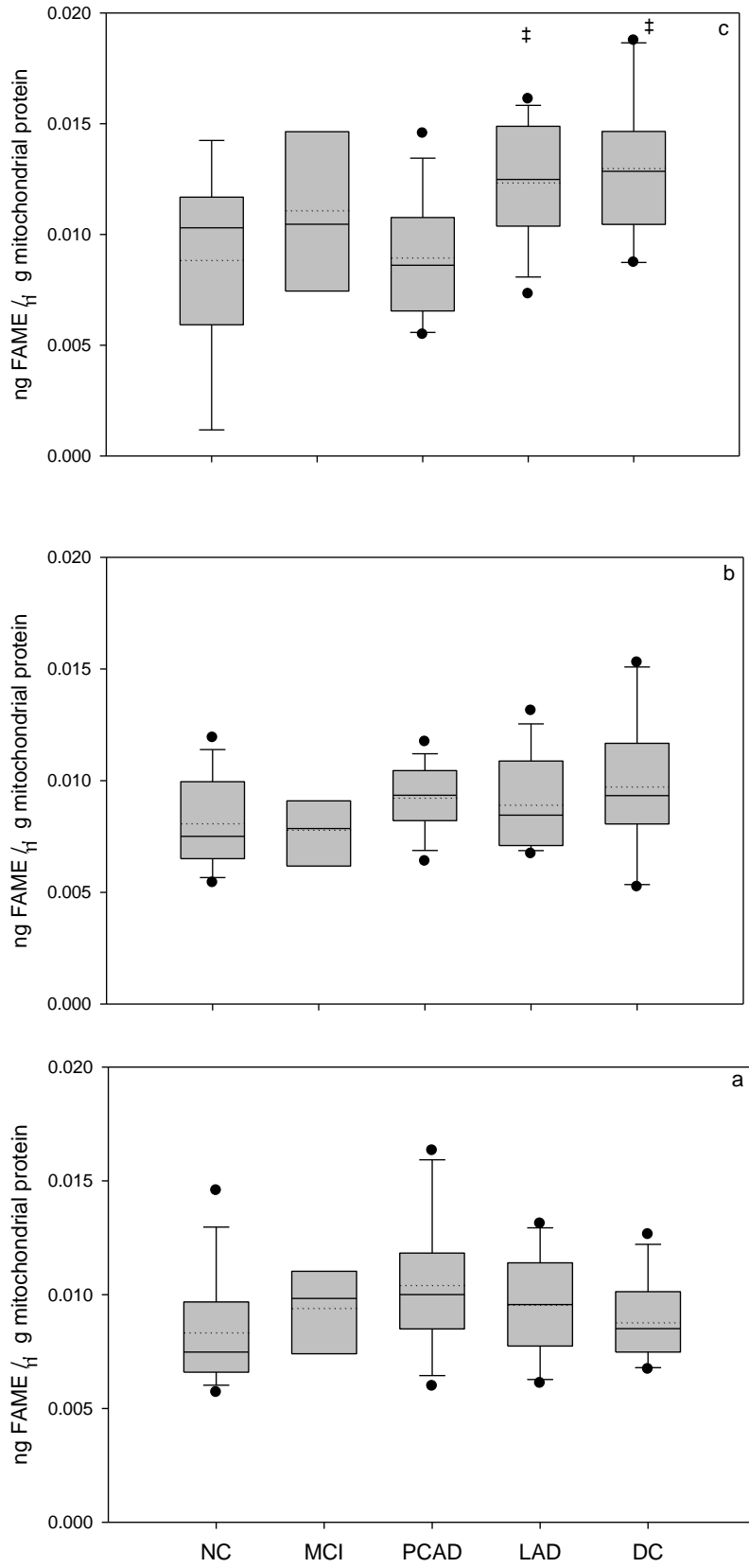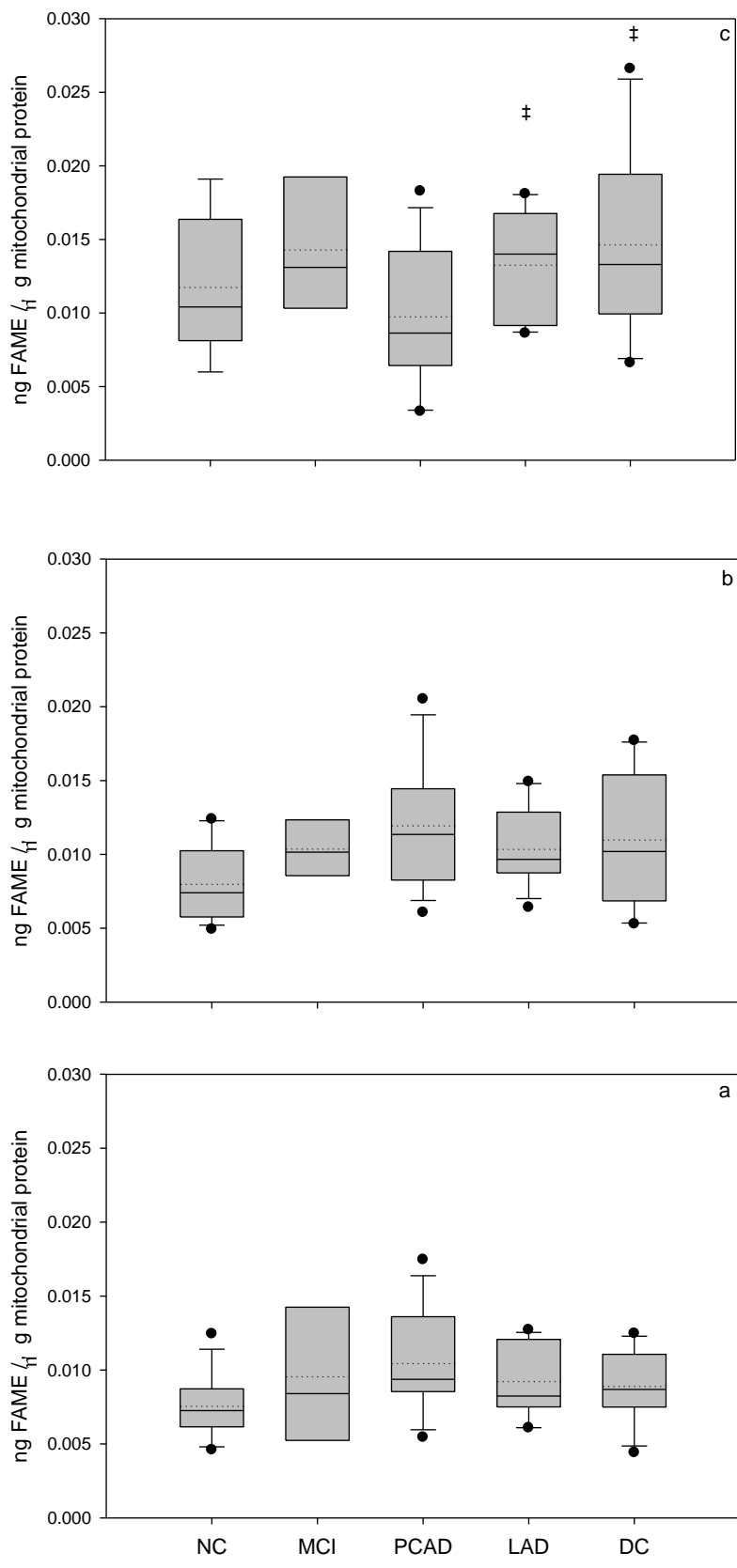
Figure 4.52. Distribution of P 18:1b between disease states and regions (normal control (NC), mild cognitive impairment (MCI), preclinical AD (PCAD) late-stage AD (LAD) and disease control (DC), for cerebellum (a), inferior parietal lobule (b) and superior and middle temporal gyri (c)). Significant differences (p<0.05) between disease states, within the same region, compared to NC are depicted by *. Significant differences (p<0.05), within equivalent disease states, across regions are depicted by ‡.
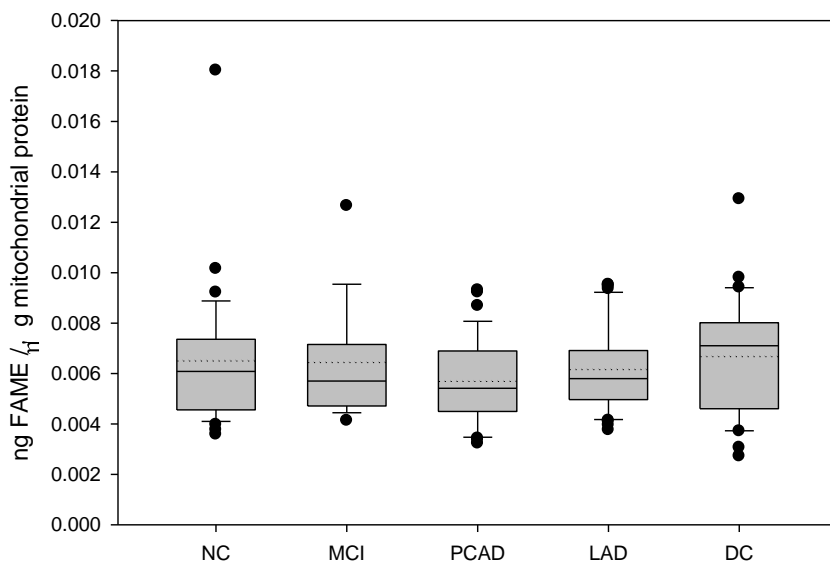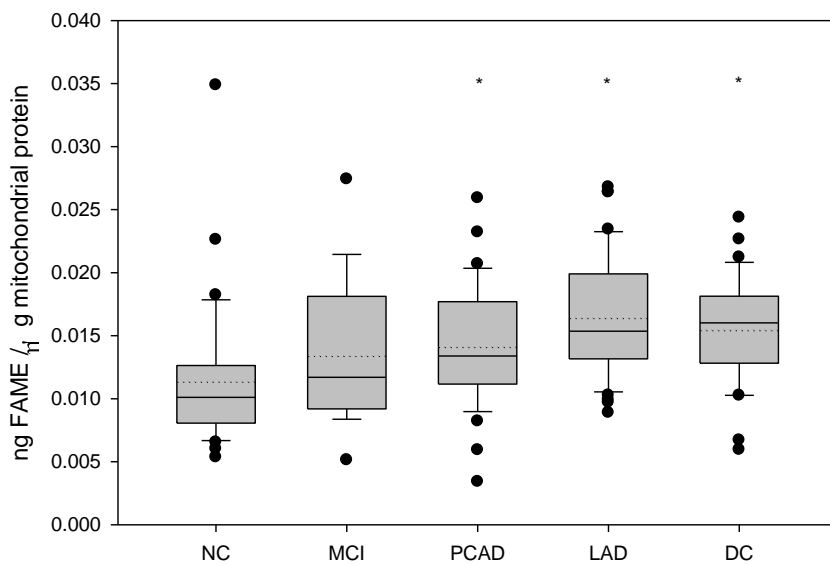
Figure 4.53. Distribution of P 18:0 between disease states for combined neurological regions (normal control (NC), mild cognitive impairment (MCI), preclinical AD (PCAD) late-stage AD (LAD) and disease control (DC)). Significant differences ($p<0.05$) between disease states, compared to NC, are depicted by *.
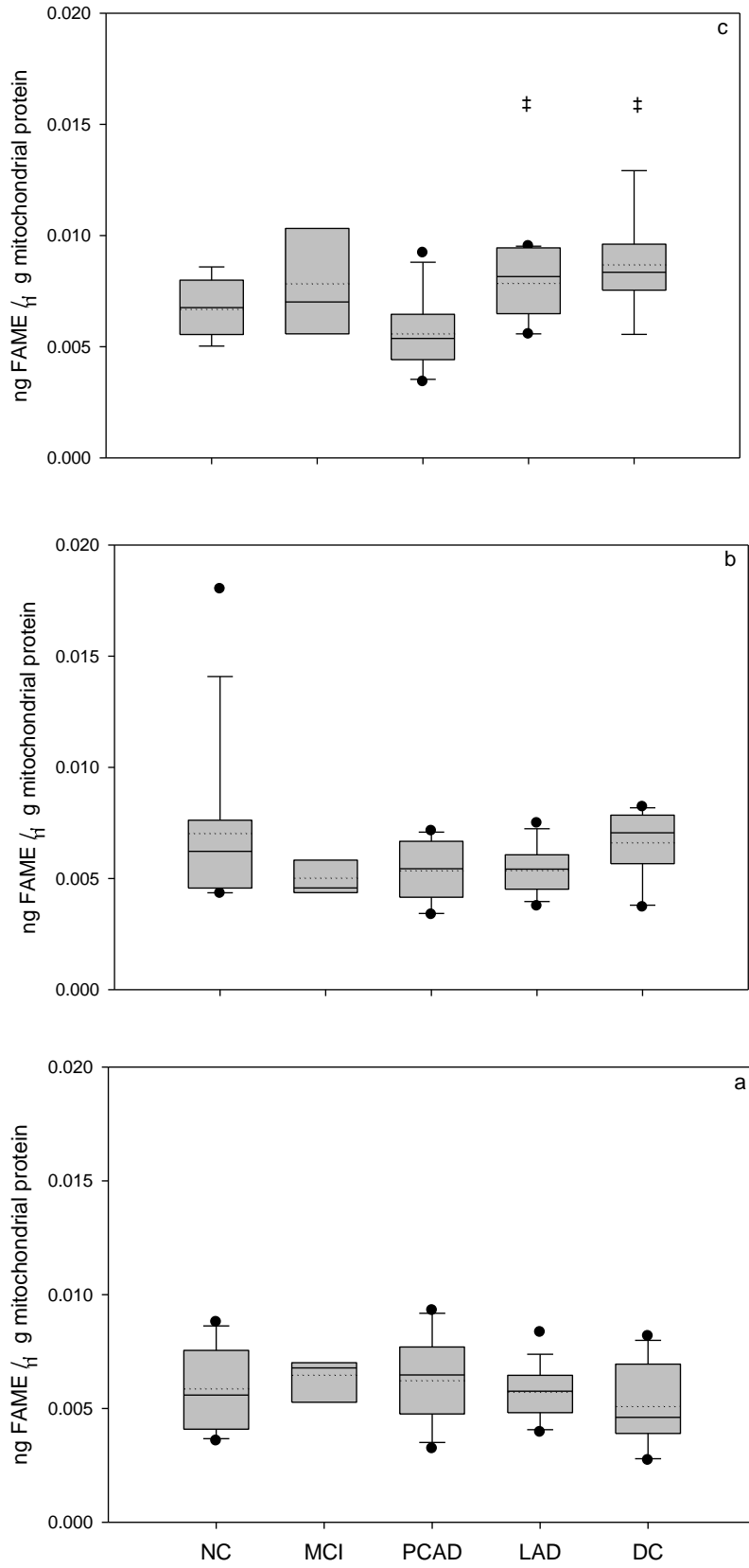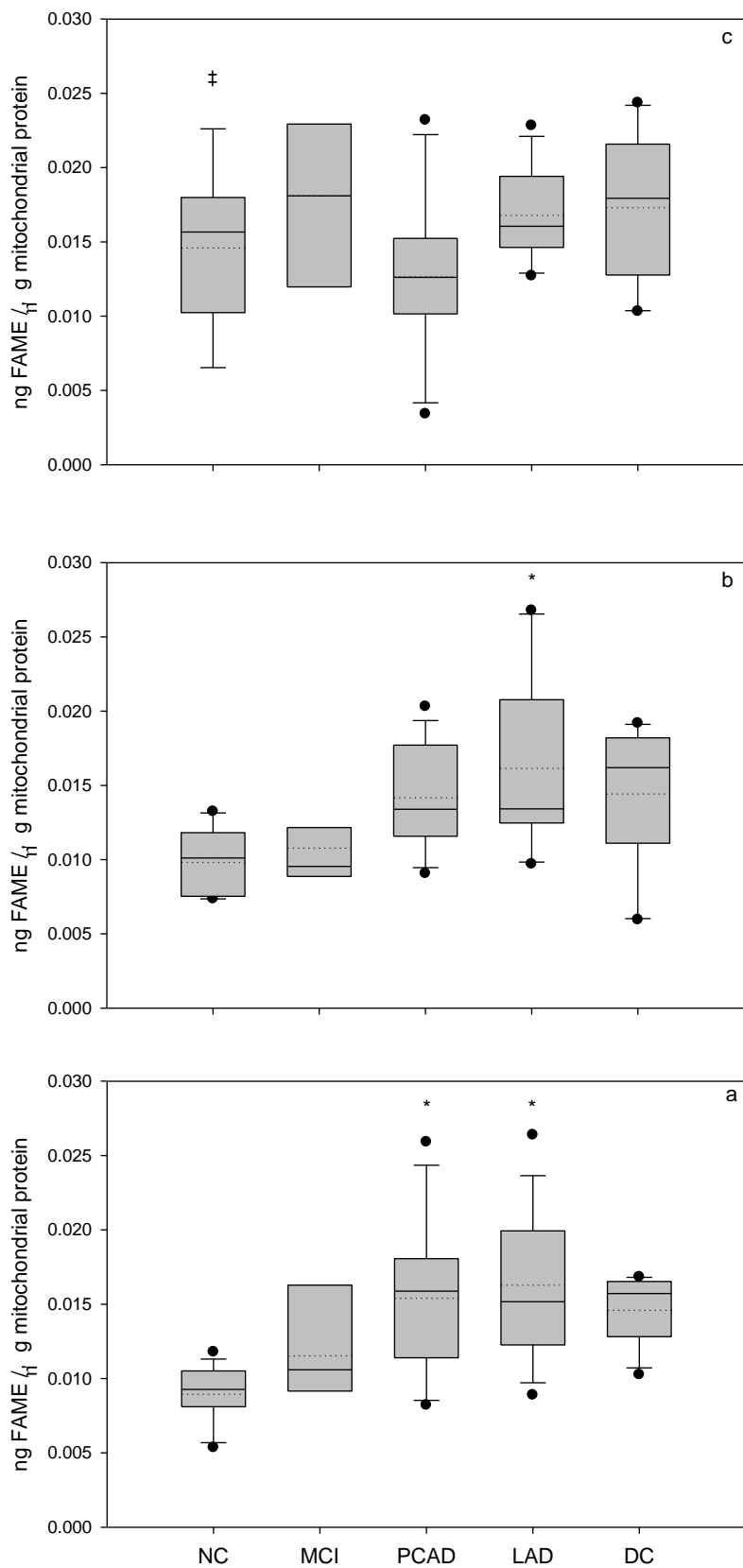
Figure 4.54. Distribution of P 18:0 between disease states and regions (normal control (NC), mild cognitive impairment (MCI), preclinical AD (PCAD) late-stage AD (LAD) and disease control (DC), for cerebellum (a), inferior parietal lobule (b) and superior and middle temporal gyri (c)). Significant differences (p<0.05) between disease states, within the same region, compared to NC are depicted by *. Significant differences (p<0.05), within equivalent disease states, across regions are depicted by ‡.
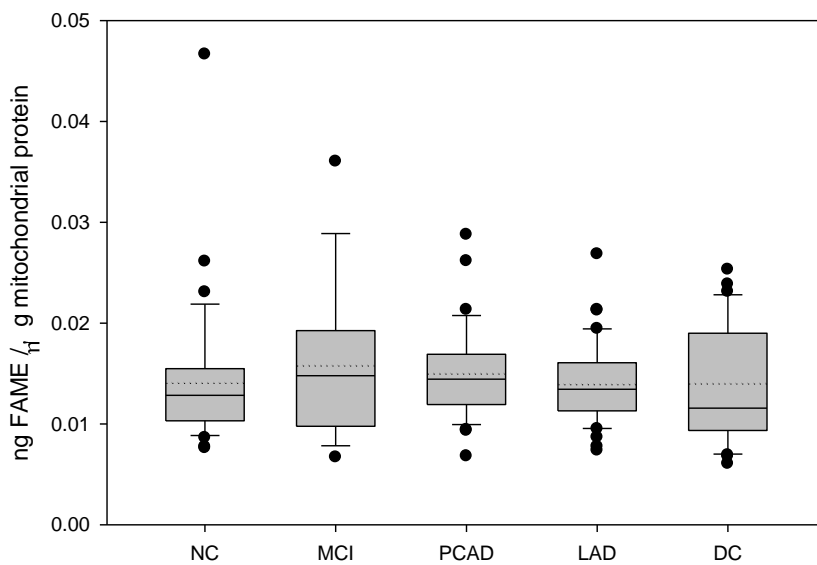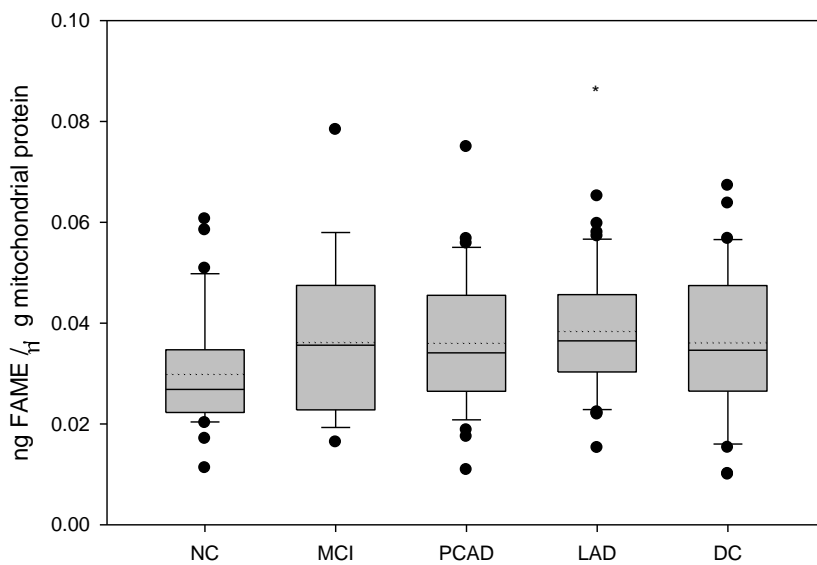
Figure 4.55. Distribution of 20:4Δ5,8,11,14 between disease states for combined neurological regions (normal control (NC), mild cognitive impairment (MCI), preclinical AD (PCAD) late-stage AD (LAD) and disease control (DC)). Significant differences (p<0.05) between disease states, compared to NC, are depicted by *.
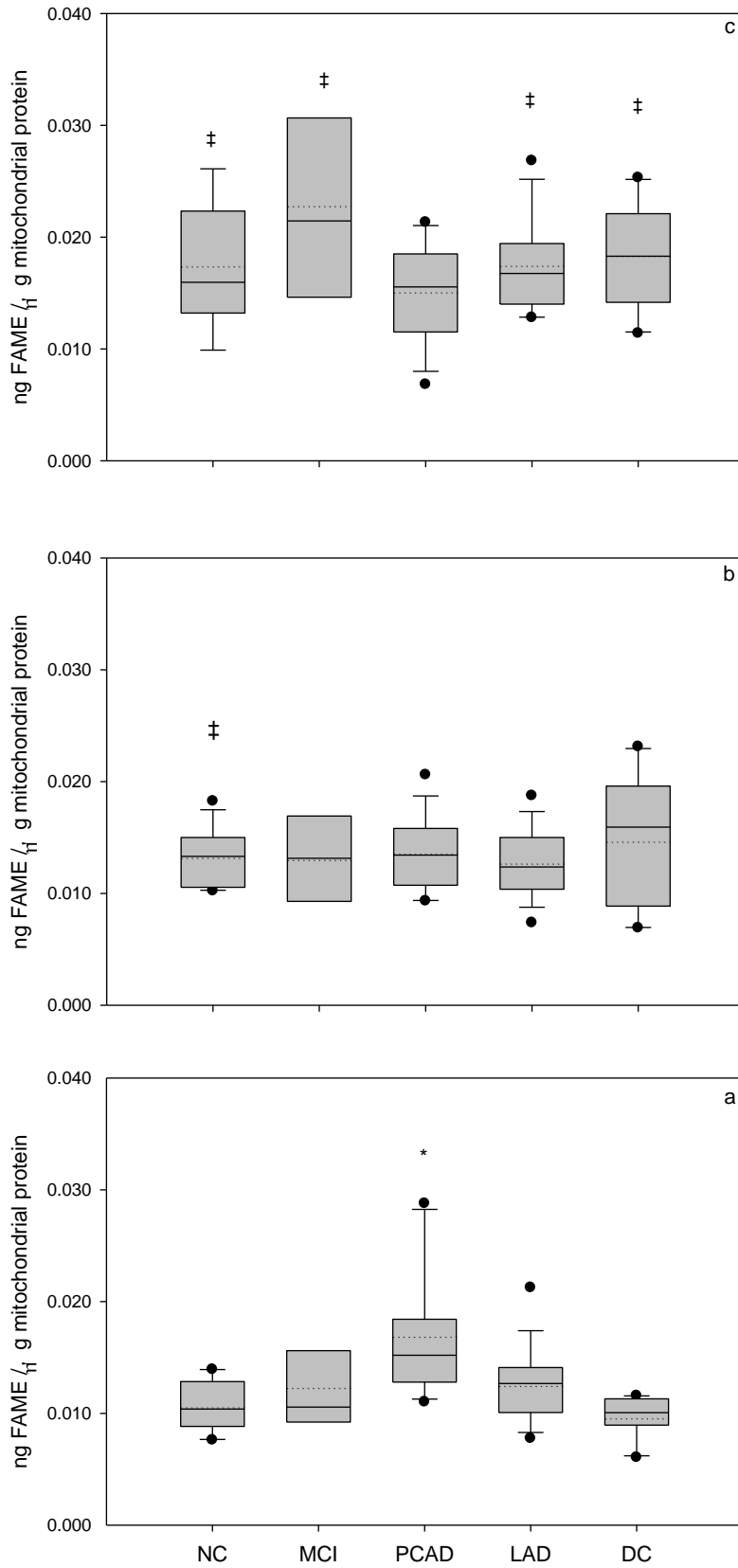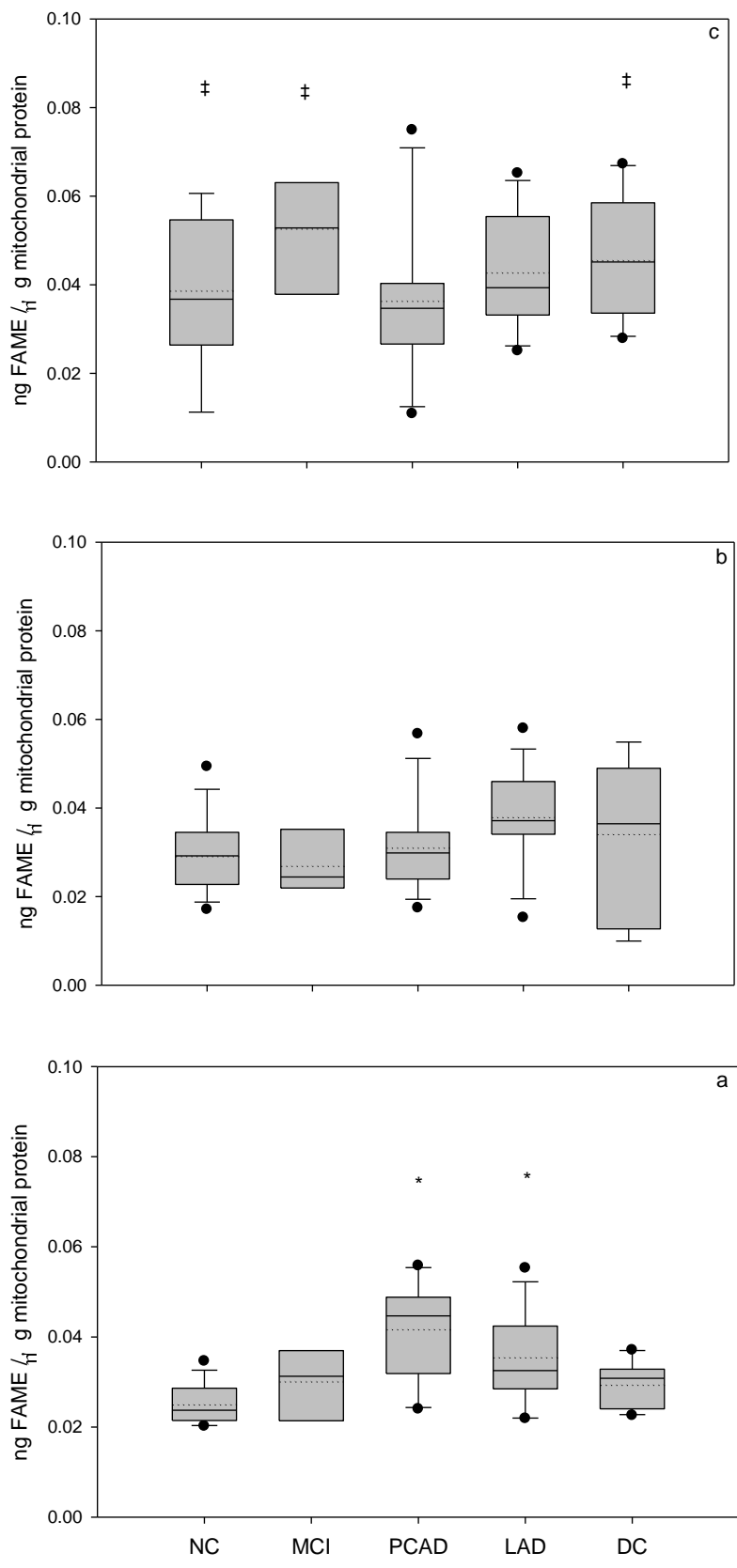
Figure 4.56. Distribution of 20:4Δ5,8,11,14 between disease states and regions (normal control (NC), mild cognitive impairment (MCI), preclinical AD (PCAD) late-stage AD (LAD) and disease control (DC), for cerebellum (a), inferior parietal lobule (b) and superior and middle temporal gyri (c)). Significant differences (p<0.05) between disease states, within the same region, compared to NC are depicted by *. Significant differences (p<0.05), within equivalent disease states, across regions are depicted by ‡.
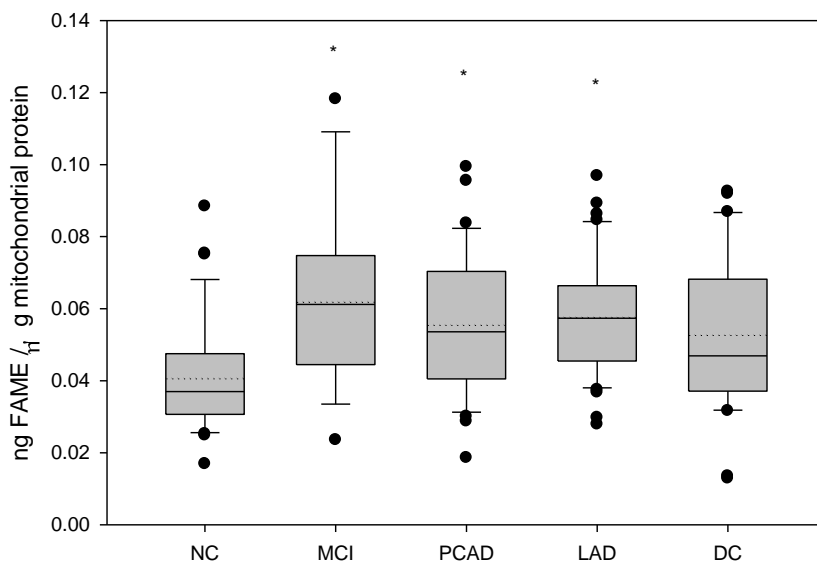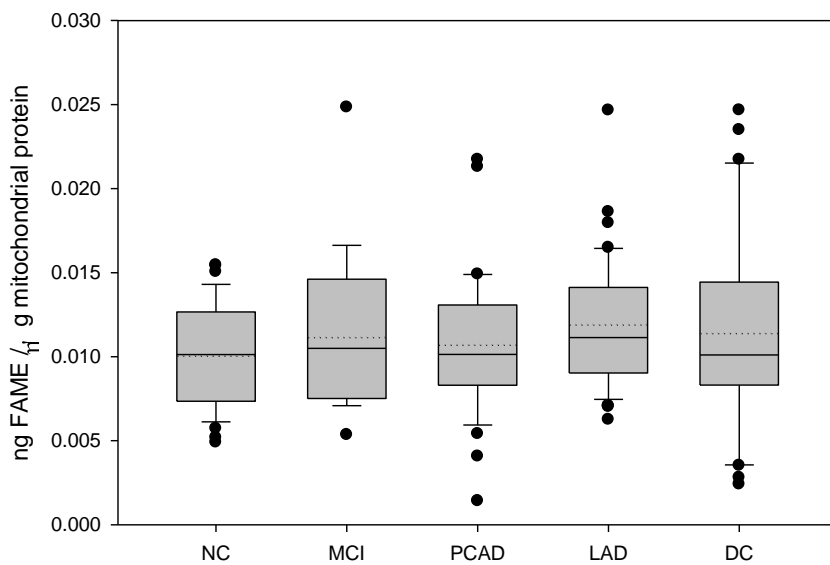
Figure 4.57. Distribution of 20:3Δ8,11,14 between disease states for combined neurological regions (normal control (NC), mild cognitive impairment (MCI), preclinical AD (PCAD) late-stage AD (LAD) and disease control (DC)). Significant differences (p<0.05) between disease states, compared to NC, are depicted by *.
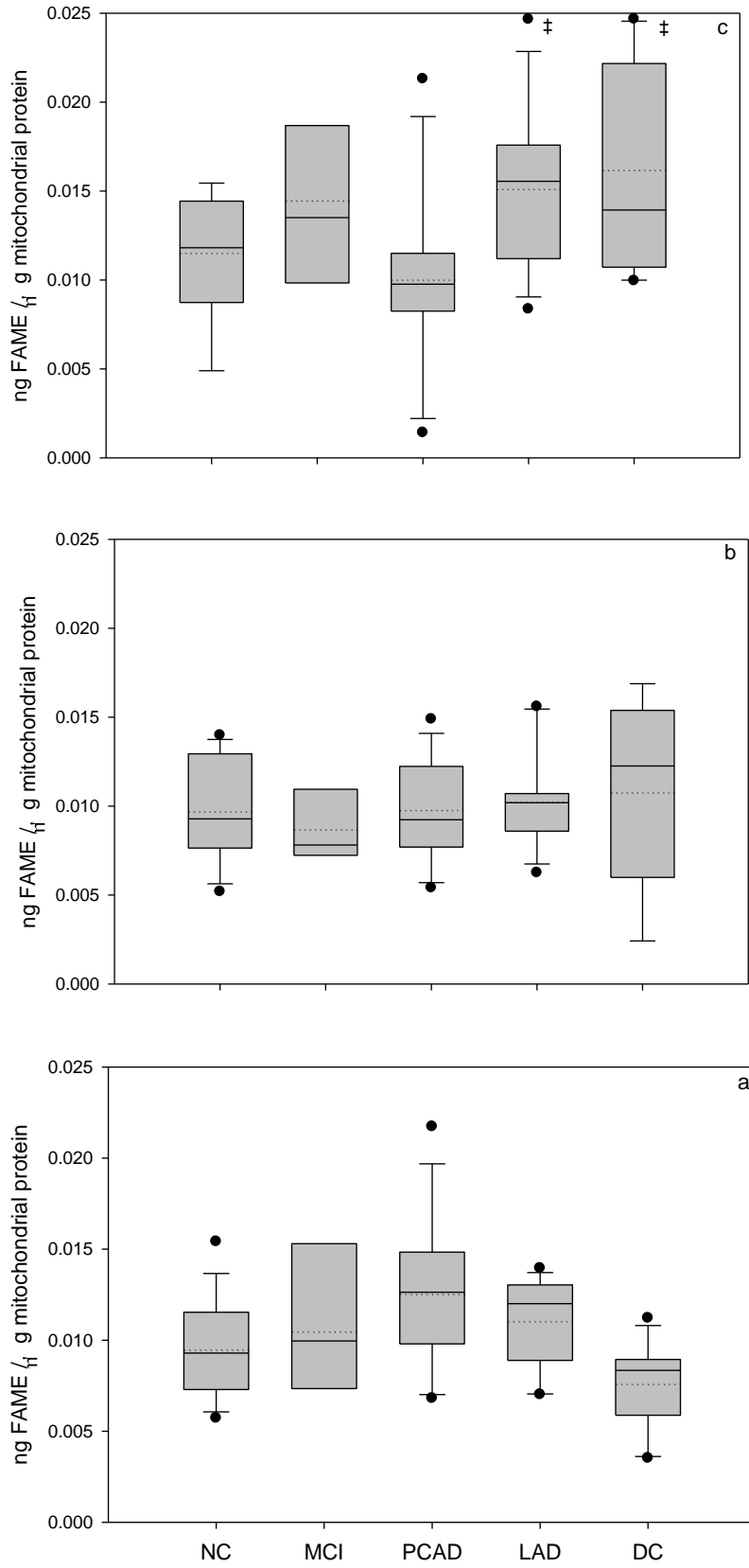
Figure 4.58. Distribution of 20:3Δ8,11,14 between disease states and regions (normal control (NC), mild cognitive impairment (MCI), preclinical AD (PCAD) late-stage AD (LAD) and disease control (DC), for cerebellum (a), inferior parietal lobule (b) and superior and middle temporal gyri (c)). Significant differences (p<0.05) between disease states, within the same region, compared to NC are depicted by *. Significant differences (p<0.05), within equivalent disease states, across regions are depicted by ‡.
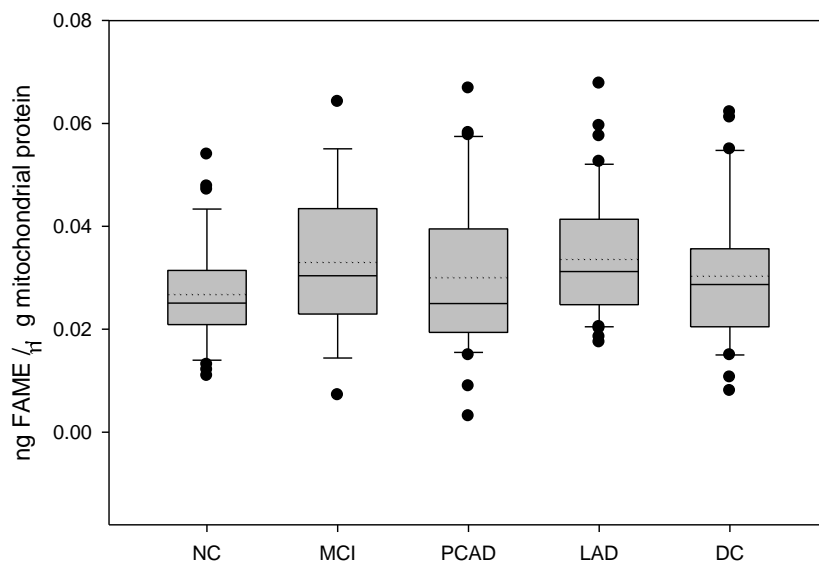
Figure 4.59. Distribution of 22:6Δ4,7,10,13,16,19
between disease states for combined neurological regions
(normal control (NC), mild cognitive impairment (MCI),
preclinical AD (PCAD) late-stage AD (LAD) and disease
control (DC)). Significant differences (p<0.05) between
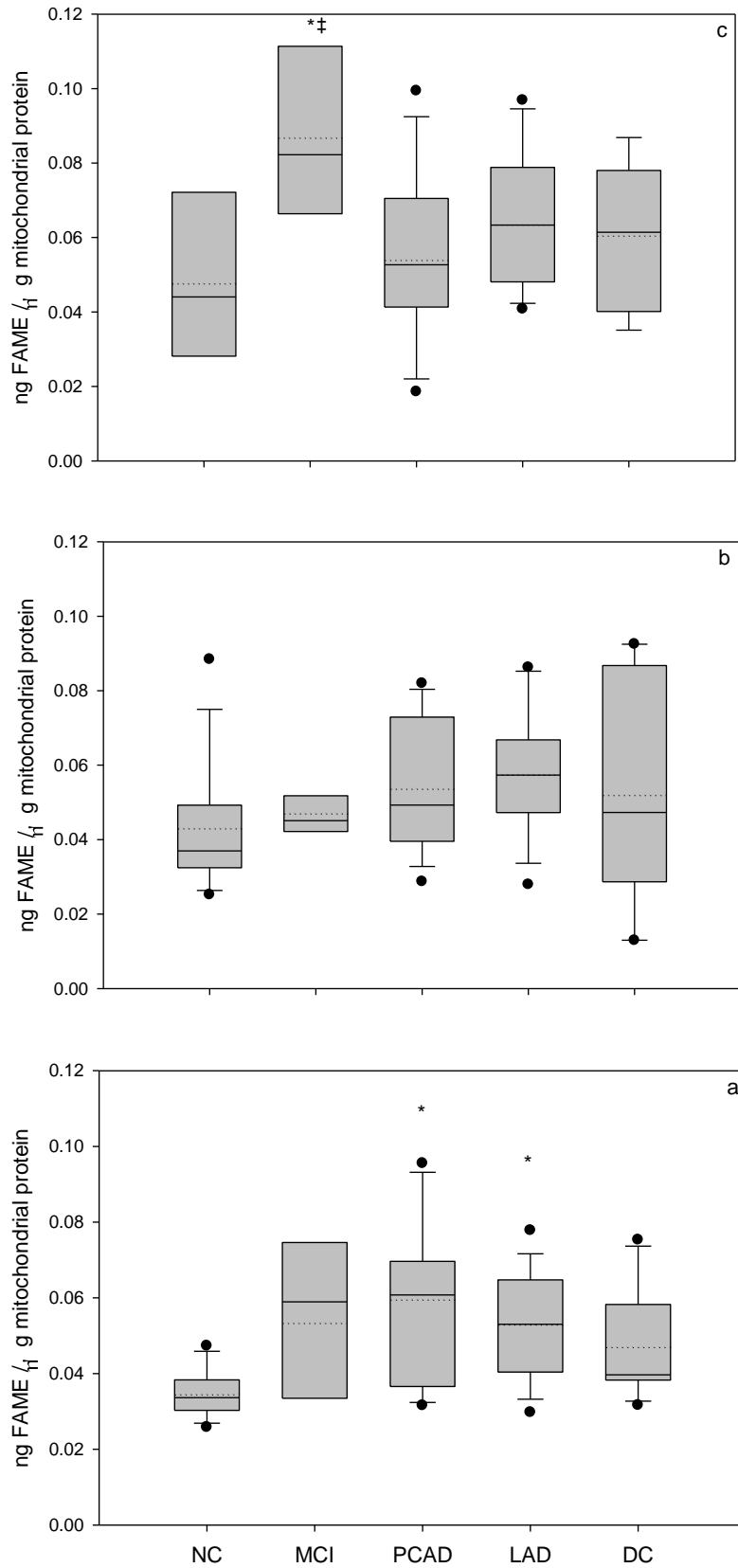disease states, compared to NC, are depicted by *.
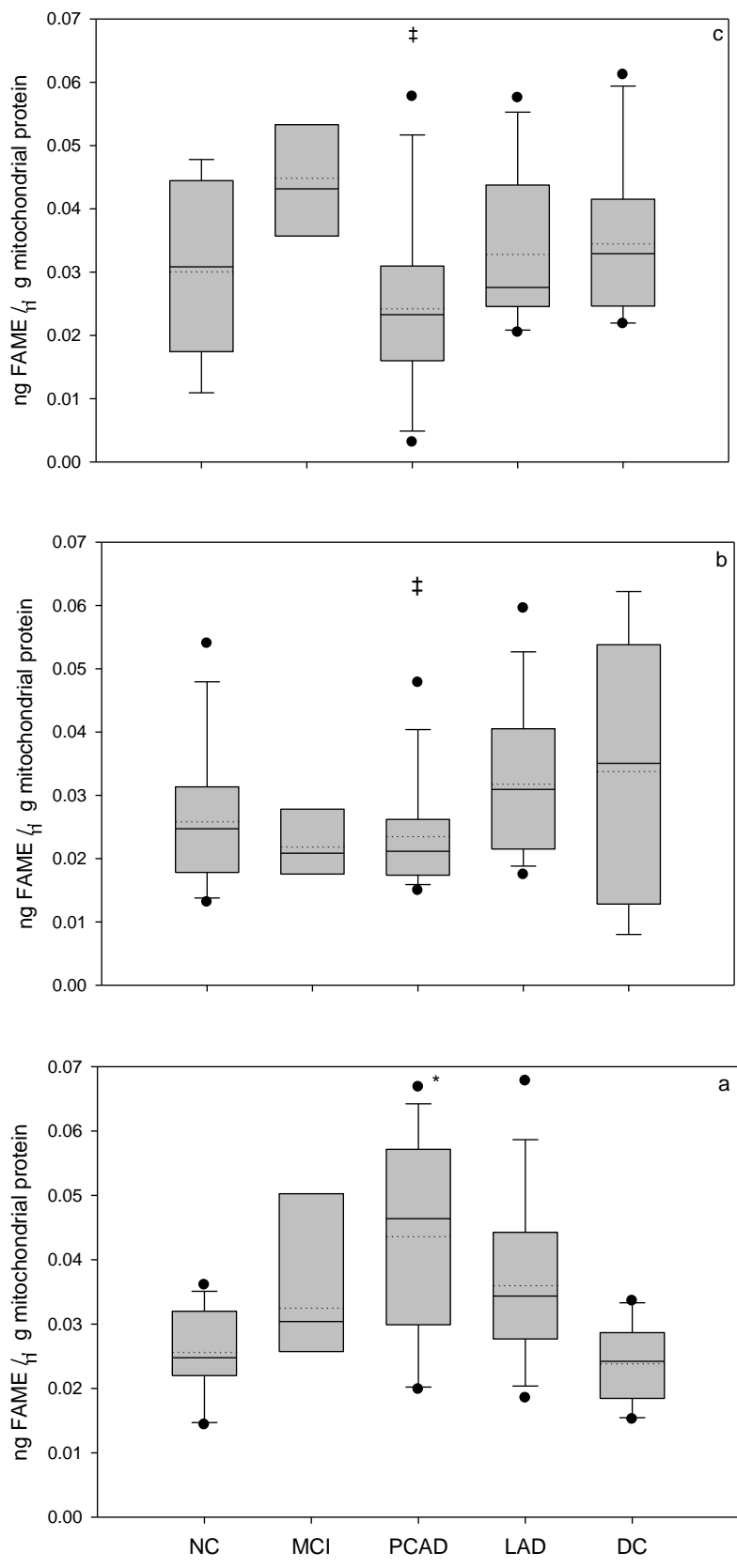
Figure 4.60. Distribution of 22:6Δ4,7,10,13,16,19 between disease states and regions (normal control (NC), mild cognitive impairment (MCI), preclinical AD (PCAD) late-stage AD (LAD) and disease control (DC), for cerebellum (a), inferior parietal lobule (b) and superior and middle temporal gyri (c)). Significant differences (p<0.05) between disease states, within the same region, compared to NC are depicted by *. Significant differences (p<0.05), within equivalent disease states, across regions are depicted by ‡.
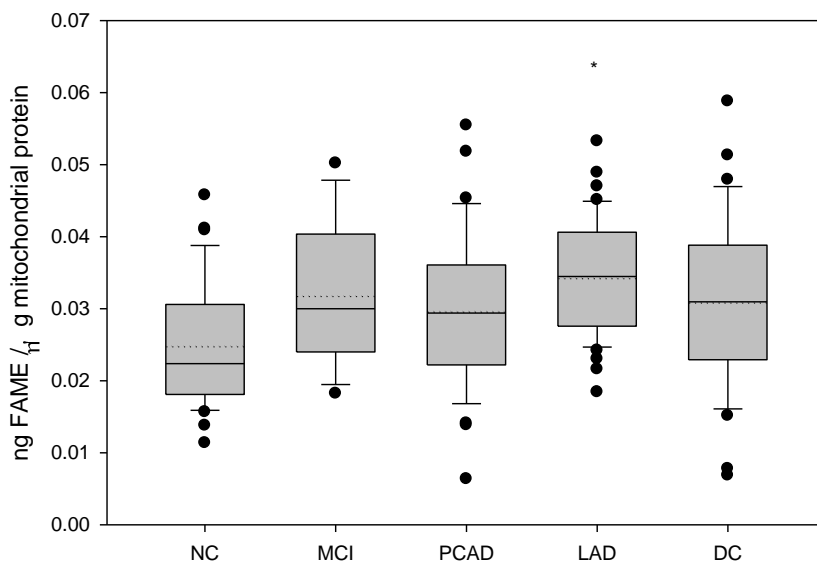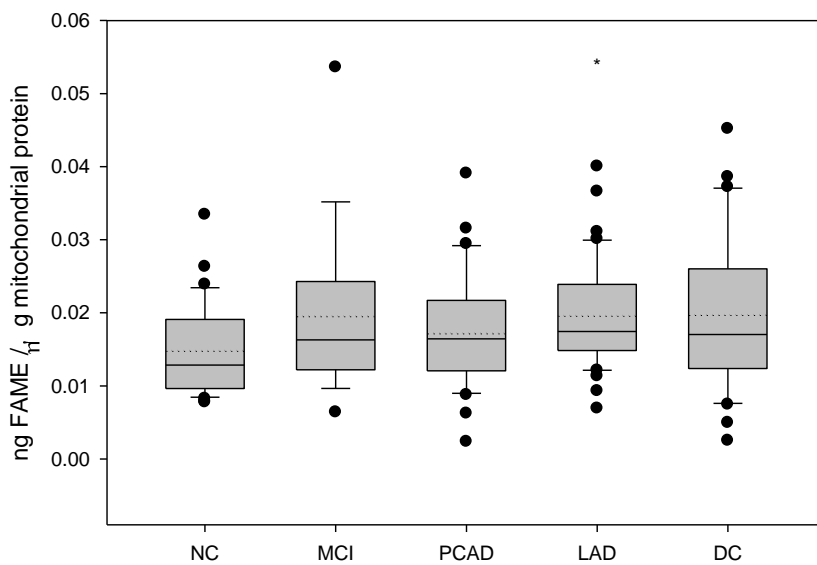
Figure 4.61. Distribution of 22:4Δ7,10,13,16 between disease states for combined neurological regions (normal control (NC), mild cognitive impairment (MCI), preclinical AD (PCAD) late-stage AD (LAD) and disease control (DC)). Significant differences (p<0.05) between disease states, compared to NC, are depicted by *.
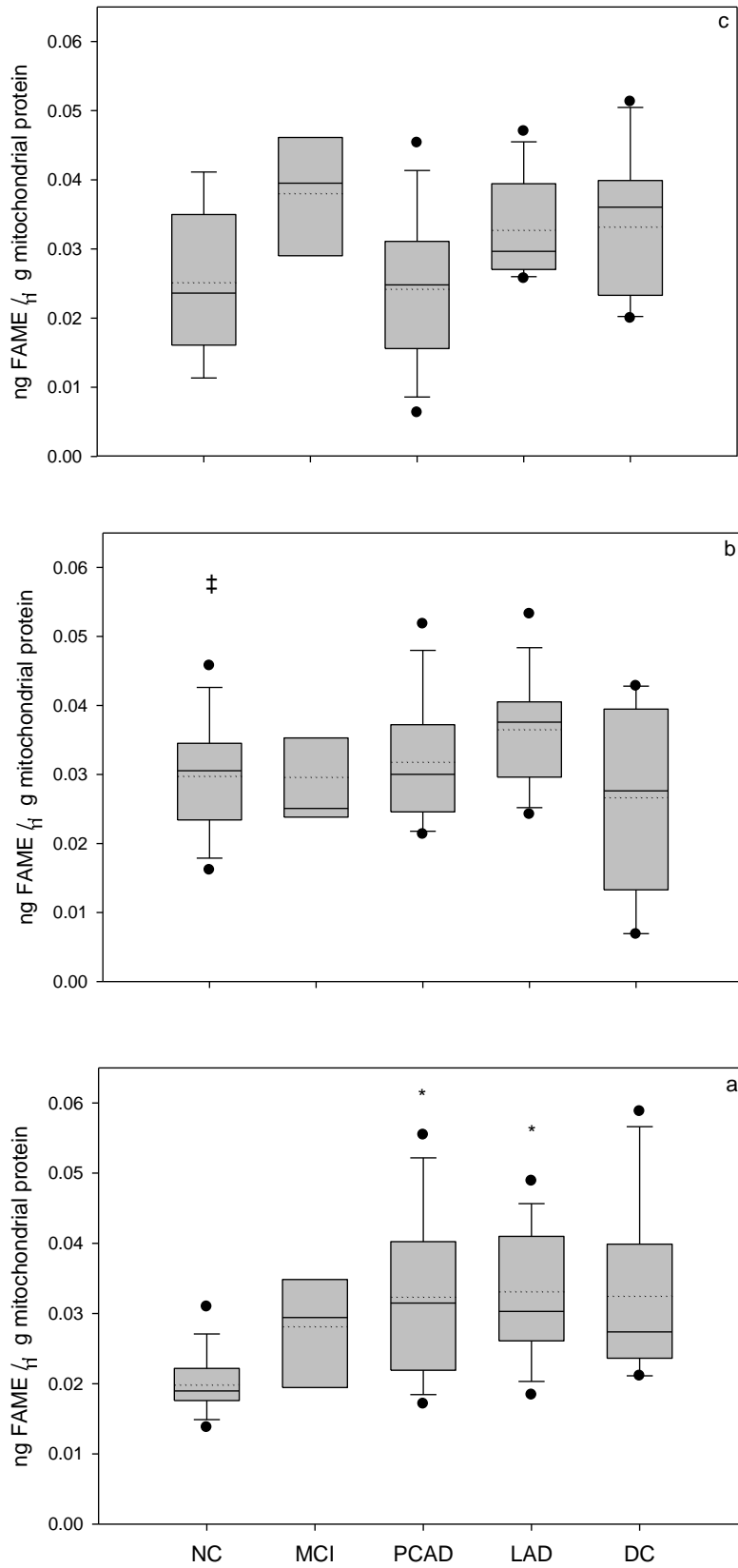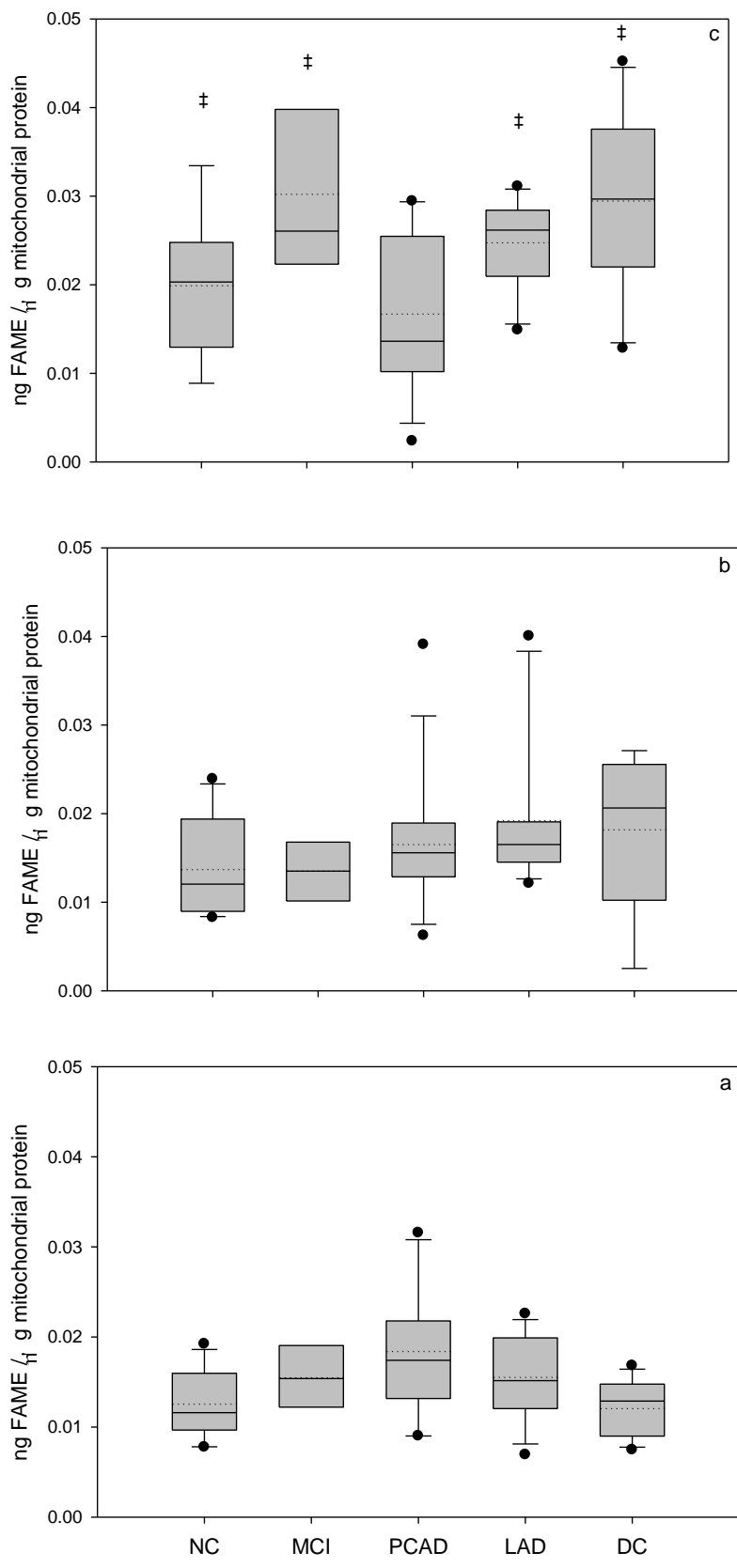
Figure 4.62. Distribution of 22:4Δ7,10,13,16 between disease states and regions (normal control (NC), mild cognitive impairment (MCI), preclinical AD (PCAD) late-stage AD (LAD) and disease control (DC), for cerebellum (a), inferior parietal lobule (b) and superior and middle temporal gyri (c)). Significant differences (p<0.05) between disease states, within the same region, compared to NC are depicted by *. Significant differences (p<0.05), within equivalent disease states, across regions are depicted by ‡.

way ANOVA on ranks, for non-normally distributed data. Significance was established by a Tukey post hoc test or Dunn's test, if treatment groups were unequal in number.

Comparisons were limited to equivalent fatty acids between brain regions and/or disease states, i.e. 12:0 NC (CER) vs. 12:0 NC (IPL) or 12:0 NC (CER) vs. 12:0 MCI (CER). Significant differences ($p<0.05$) across disease states, within a particular or combined brain region, compared to NC for that region are depicted by *. Significant differences ($p<0.05$) within equivalent disease states, across distinct brain regions compared to CER, are depicted by ‡. Results of statistical analysis from each lipid species will be discussed in the subsequent paragraphs.

Dodecanic acid (12:0) from disease control (DC) patients exhibited a significantly higher abundance within CER compared to other neuropathological demographics and regions (Figure 4.28). The overall distribution of 12:0 for DC patients was dominated by the CER region (Figure 4.27). Because of this disparity in 12:0, the three regional graphs are presented with different y-axes (Figure 4.28). Dodecanic acid did not differ significantly from NC for the other two regions: IPL or SMTG.

In contrast, tetradecanoic acid (14:0) and pentadecanoic acid (15:0) showed no statistical differences among disease states for combined regions (Figures 4.29 & 4.31). There were however a number of outliers across disease states for each FA species. Tetradecanoic acid demonstrated significant increases for NC patients in IPL and MCI subjects in SMTG, compared to CER levels (Figure 4.30). Pentadecanoic acid displayed significant increases for LAD and DC in SMTG (Figure 4.32). In addition pentadecanoic acid exhibited a negative correlation to Braak score, although no correlation was found for NP (Table 4.13).

Overall, results for 9-hexadecenoic acid (16:1Δ9) were not significantly different for disease states when evaluated for the combined regions (Figure 4.33). As with the two species prior, data from the combined regions yielded a number of outliers. Results from individual regions for 9-hexadecenoic acid, both PCAD and LAD showed a significant increase compared to NC for CER (Figure 4.33). In addition, CER quantities of 16:1Δ9 from NC subjects were appreciably lower than SMTG and IPL data.

The global profile of hexadecanoic acid revealed that NC had a significantly lower abundance than all other disease states (Figure 4.35). When the data was arranged

by region NC mitochondria were significantly lower in 16:0 than PCAD and LAD in CER, PCAD in IPL and MCI subjects from SMTG (Figure 4.36). Data from MCI patients indicate a significant increase for 16:0 in SMTG.

Quantitation of the dimethyl acetal of hexadecan-1-al, the product of 1-enyl-hexadecenoic acid (P 16:0) from the combined mitochondrial pool was nearly uniform across disease states (Figure 4.37). The regional analysis was similar with only LAD and DC exhibiting a significant increase in SMTG over CER (Figure 4.38). Also, worth noting is that NC patients displayed a lower abundance of P 16:0 in each region, with the only exception of PCAD in SMTG.

Results for heptadecanoic acid (17:0), appear almost identical to P 16:0. The combined profile was nearly even across patient demographics (Figure 4.39). Only significant increases in SMTG for late-stage AD and disease control patients over their corresponding CER levels were found (Figure 4.40).

The overall abundance of 9,12-octadecadienoic or linoleic acid (18:2Δ9,12) did not change throughout the disease profile (Figure 4.41). However, when data were analyzed by region, differences were present. A significant difference was established for preclinical AD patients in cerebellum compared to normal control. Also, normal control, mild cognitive impairment, late-stage AD and disease control subjects displayed a significant increase in SMTG linoleic abundance over their corresponding CER abundances (Figure 4.42). Overall, PCAD subjects displayed higher levels of 18:2Δ9,12 in CER and lower in SMTG than all other sample groups.

Data from the two octadecanoic unsaturated fatty acids (18:1Δ9 & 18:1Δ10) displayed similar profiles amongst disease states and regions. Normal control patients exhibited a lower combined regional abundance of both 9-octadecenoic (18:1Δ9) and 10-octadenoic (18:1Δ10) than all other states (Figures 4.43 & 4.45). This overall decreased abundance was statistically significant for MCI, PCAD and LAD subjects for 18:1Δ9 (Figure 4.43) and for LAD patients for 18:1Δ10 (Figure 4.45). Within CER 18:1Δ9 and 18:1Δ10 were significantly lower for NC compared to PCAD and LAD (Figure 4.44). Mild cognitive impairment subjects had a significant increase in abundance within SMTG (Figure 4.44). Normal control 10-octadenoic acid was also significantly increased in IPL compared to CER.

Octadecanoic acid (18:0) was found to be significantly higher with SMTG of MCI subjects compared to NC and other regions (Figure 4.48). Mitochondria from NC patients had significantly lower amounts of 18:0 than IPL or SMTG, in addition to PCAD and LAD within CER. The combined mitochondrial profile for 18:0 displayed significant increases from NC levels for MCI and LAD (Figure 4.47).

The two unsaturated plasmalogen species, 1-enyl-1,-octadecadienoic acids (P 18:1 a&b) exhibited similar profiles with neurological mitochondria. Both were equally distributed among disease states when compared as a composite of regions (Figures 4.49 & 4.51). However, data from individual regions provided slight distinction. Plasmalogen 18:1a (P 18:1a) displayed significant differences in SMTG compared to CER for NC, MCI, LAD and DC patients (Figure 4.50). Likewise, plasmalogen 18:1b (P 18:1b) had increases within SMTG for LAD and DC samples (Figure 4.52). No significant changes were found in CER or IPL across disease states.

The long-chain saturated plasmalogen species 1-enyl-octadecenoic acid (P 18:0) global expression found significant increases in PCAD, LAD and DC mitochondria compared to NC quantities (Figure 4.53). The regional distribution revealed significant increases in PCAD and LAD mitochondria in cerebellum and LAD samples from inferior parietal lobule (Figure 4.54). Superior and middle temporal gyri contained significantly higher quantities of P 18:0 for NC compared to CER.

Arachidonic acid (ARA) or 5,8,11,14-eicosatetraenoic ($20:4\Delta5,8,11,14$) globally had a significant increase for LAD mitochondria compared to NC (Figure 4.55). The regional distribution of arachidonic acid found that SMTG contained a significant increase in 20:4 abundance for NC, MCI and DC over their respective CER quantities (Figure 4.56). In addition PCAD and LAD subjects had a significant increase in ARA within CER tissue.

The comprehensive distribution of 8,11,14-eicosatrienoic acid ($20:3\Delta8,11,14$) within neurological mitochondria was consistant over disease states (Figure 4.57). Significant increases within the SMTG were found for LAD and DC patients compared to CER levels (Figure 4.58).

As a whole the allocation of 4,7,10,13,16,19-docosahexaenoic acid or DHA ($22:6\Delta4,7,10,13,16,19$) between disease states was uniform for combined regions (Figure

4.59). Comparison of the areas led to several interesting observations (Figure 4.60). Within the cerebellum NC and DC mitochondria had the lowest DHA levels. Among the three AD disease stages, MCI was slightly lower than LAD and both of these were less than preclinical AD subjects, which was significantly higher than NC. The CER graph shape gives the appearance of a broad bell-curve. Data from SMTG was nearly the inverse of the CER profile. Preclinical subjects had the lowest detected DHA which was significantly lower than respective CER levels, followed closely by LAD, then DC and NC. The MCI cases contained greater amounts of DHA than expected by this trend, however the increase was not significant.

Finally, 7,10,13,16-docosatetraenoic or adrenic acid (22:4Δ7,10,13,16) was detected in lower quantities, for each disease state, within the CER and IPL than in SMTG (Figure 4.62). In fact, with the exception of PCAD all other states had significantly higher adrenic acid quantities in SMTG compared to their analogous CER levels. The inclusive comparison of the three regions found that only LAD patients were significantly different, lower, than NC (Figure 4.61).

Chapter 4.4. Discussion

The electron transport chain (ETC), housed in the mitochondrial membrane, is vital for cellular energy production. Electrons leaking from mitochondria are the greatest source of ROS within a cell, thus mitochondria are the suspected cause and a potential target of oxidative stress. Oxidative stress, a hallmark of many neurodegenerative diseases, leads to the development of ROS. Common targets for ROS are lipid components, namely polyunsaturated fatty acids (PUFAs). The high oxygen consumption rate of neurological cells and comparatively low levels of antioxidant capacity would be expected to cause compensatory changes to the fatty acid profile in order to minimize susceptibility to oxidative damage. Neurological tissue has been reported to have an increased abundance of polyunsaturated fatty acids, namely docosahexaenoic acid (DHA) [118, 120, 132, 145].

Diversity in the mitochondrial fatty acid (FA) profile, could lead to a variety of innate responses as a consequence of detrimental ROS generated in vivo. The previously conducted study with Sprague Dawley rats focused on a comparison of the mitochondrial membrane composition between tissues provided evidence of increased neurological susceptibly to ROS. The appearance of unique PUFAs species in brain mitochondria provided greater potential susceptibility to ROS.

This project was designed to explore the variation in the mitochondrial fatty acid profile as a function of both disease progression and neurological region. Subjects were chosen to represent four distinct groupings of AD pathology as determined by the University of Kentucky Alzheimer's Disease Center (UK-ADC). Demographics for AD samples consisted of mild cognitive impairment (MCI), preclinical Alzheimer's disease (PCAD) and late-stage Alzheimer's disease (LAD) patients. Two additional sample populations, age-matched normal control (NC) and diseased control (DC) were added. Disease control were comprised of dementia with Lewy body disease (DLB) and frontotemporal dementia (FTD) patients. The rationale for the DC demographic was to provide further confirmation that changes to the mitochondrial FA profile were specific to AD pathology.

Tissue specimens from the superior and middle temporal gyri (SMTG), inferior parietal lobule (IPL), and cerebellum (CER) were collected from each patient employed

in the study. The three regions were selected to provide distinct locales with differing neurological function that displayed various degrees of AD pathology during disease progression. Cerebellum is the region that regulates the integration of sensory perception, coordination and motor control. It displays minimal pathology throughout the AD pathology spectrum. Data from the CER provides a comparison of lipid composition in an unaffected region across disease states and affected regions. The inferior parietal lobule is involved in integration of sensory information functions. Typically the IPL shows little pathology, except during late-stage disease profiles. Lastly, the superior and middle temporal gyri are the most affected regions of the three studied. The SMTG contains subdivisions involved in processing sound and visual cognition. It displays pathology early in AD progression, frequently during the MCI stage.

Subject neuropathological demographics

Statistical comparison of subject demographic data provided a basis for distintion between the populations (Table 4.1). Results from the one way ANOVA on the average age of subjects determined that no statistical differences existed between AD states compared to NC. Age matching was carried out to eliminate age as a potential variable, thus isolating differences to disease state or region. The diseased control subjects were found to be significantly younger (p<0.001) than the other neuropathological states studied. This result is not entirely unanticipated, since on set of Lewy body disease (DLB) and frontotemporal dementia (FTD) occurs at a younger age than AD [154, 159].

The post-mortem interval (PMI) data from each subject group showed no statistical differences between any of the samples, as determined by one way ANOVA. The PMI is critical because as the time interval between demise and autopsy increases degradation of biological analytes would be expected to occur. As with age, eliminating differences in PMI assists in isolating justification for differences between subjects.

Statistical comparison of the median Braak scores and neuritic plaques (NP) counts among the disease states, imparted the main distinction between the subjects. Both features are used in the neuropathological classification of patients within the disease spectrum. Therefore, it would be expected that both Braak scores and NP counts would be statistically different between disease states. Braak scores are a measure of

intraneuronal neurofibrillary tangles (NFT) which are enriched in hyperphosphorylated tau [103]. Due to Braak scores being presented as median values, statistical analysis required the non-parametric Kruskal-Wallis one way ANOVA on ranks with a Dunn's method post hoc test to establish significance. Both NC and DC groups were significantly lower ($p < 0.05$) than MCI, PCAD and LAD states. This reaffirms that NC and DC contained less NFT pathology than later states.

Average neuritic plague (NP), or senile plaque (SP), counts were compared across disease states for IPL and SMTG regions, data for NP from CER were not available. Plaques are extracellular aggregates composed mainly of amyloid beta peptide (Aβ) resulting from the proteolytic cleavage of amyloid precursor protein (APP) [103]. Plaque counts were compared statistically, across disease states for SMTG and IPL, by one way ANOVA with a Tukey post hoc test to establish significance. The inferior parietal lobule had a significant increase ($p < 0.001$) in NP for LAD compared to all other disease states. This result confirms the notion that the IPL typically only displays AD pathology in late-stage patients. For SMTG the LAD samples had a significant increase ($p < 0.001$) in NP compared to NC, PCAD and DC; however, comparison to MCI samples resulted in only a $p < 0.05$ significant increase. The results from SMTG confirm that this area is affected earlier in the pathogenesis of AD. The highly significant difference ($p < 0.001$) for NC and DC reinforces the concept that these demographics display minimal pathology associated with AD. A lower level of significance found for MCI patients substantiates the idea that this stage is a critical marker between normal aging and rapid disease onset.

Correlation tests

Pearson product-moment correlation tests conducted on subject demographics compares the linear relationship between two variables. The Pearson product-moment test allows a statistical measure of correlation between two variables without regard to variable dependence. The advantage with this approach is that any relationship of correlation is symmetrical with regard to the axis. In other words, establishment of variable dependence and independence is not required or calculated. The disadvantage is that correlation statistics cannot determine the cause-and-effect of two variables. Even though cause-and-effect statistics, through regression analysis, would be advantageous it

requires prior knowledge of variable dependence. This would require further testing, such as with oxidative insults resulting in a subsequent change in fatty acid profile.

Pearson product-moment correlation tests were performed on the subject population as a whole, segmented by region (Tables 4.10-4.12). Calculations compared the variables of age, Braak score and neuritic plaques (NP). For all three regions (CER, IPL and SMTG) no correlations were found between age and Braak score or NP. Note, no data was available on NP from CER, therefore only Braak score was tested for this region. No relationship was found between age and the two AD pathology markers is the result of age-matched normal control subjects. As determined previously, the NC patients displayed no statistical difference in age between other patient demographics, but were statistically different (at least $p<0.05$) in Braak score and NP counts.

Patient data concerning Braak score and NP, from SMTG and IPL, found a strong positive correlation ($p<3\times10^{-9}$) between these two variables. Being markers of AD progression, it is reasonable that these two variables would show a positive correlation.

Pearson product-moment correlation tests were also conducted on individual mitochondrial fatty acid methyl esters isolated from each region (Tables 4.13-4.15). Lipid species were tested for possible correlations to age, Braak score and NP (SMTG and IPL only) variables. Results from these statistical tests will be discussed later alongside results from fatty acid distribution and disease state analyses.

Mitochondria isolation

To conduct studies of mitochondrial lipidomics from human tissue, required the development of an isolation procedure resulting in high-purity mitochondria in considerable yields. There are numerous procedures for the isolation of mitochondria from tissue, which are mainly built around a foundation of mitochondrial isolation through differential centrifugation [109, 111-112, 114, 160-161]. The predominant differences between these procedures are generally variations to the isolation buffer, centrifugation times/speeds, and the type/percentages of density gradients utilized. The majority of these techniques utilize a rapid isolation of mitochondria for enzymatic studies, sacrificing purity for viability needed for respiration based studies. However, lipidomic based studies for this particular project required purity over viability. Therefore, the initial focus of the project was to adapt several previously established

isolation methods, maintaining the yields, while improving the purity, of mitochondria from a single neurological tissue section [109, 111-112, 114, 160].

The tissue to buffer ratio employed during the initial homogenization was found to be important for maximizing mitochondria recoveries and minimizing contamination. A weight-to-volume ratio of less than 10% led to lower than expected recoveries, primarily believed to be the result of insufficient tissue homogenization or loses during the initial low-speed centrifugation steps. Following the first low-speed centrifugation, re-homogenization of the nuclear pellet and a subsequent second low-speed centrifugation minimized possible mitochondrial loses. Contamination of the mitochondria isolate, due to residual nuclear material, was ultimately removed by means of a third low-speed spin following crude mitochondrial isolation.

The use of two separate Percoll solutions, as opposed to a single discontinuous Percoll gradient traditional used in other procedures [109, 111-112, 114], provided a mitochondrial pellet instead of bands. Formation of discrete Percoll interfaces by layering various percentage solutions can be problematic. Failure to form sharp boundaries will ultimately reduce yields due to diffusion of bands. The advantages of the proposed method and using two separate centrifugation steps each with a single Percoll concentration are that recoveries are not dependent on generation of sharp interfaces and formation of a mitochondrial pellet aids in the removal of excess Percoll which may hinder subsequent washing steps. This approach was thought to aid in mitochondria recoveries, as formation of and removal of mitochondrial bands from between discrete Percoll interfaces can be problematic.

The proposed method does not segregate synaptic and non-synaptic mitochondria isolation, however the procedure can easily be modified to accommodate this necessity. A 28% Percoll gradient can be run instead of a 19% to separate the two mitochondria species. Upon centrifugation (19,600xg, 10 min) the non-synaptic mitochondria will form a pellet, while the synaptic mitochondria will remain in suspension, immediately below the myelin layer. Synaptic mitochondrial isolation would proceed from the digitonin treatment step; whereas non-synaptic mitochondrial isolation could be finalized by washing with PBS.

Instead of necessitating different procedures based on the tissue wet weight, the developed method is directly applicable to a variety of tissue quantities [109, 114]. An additional advantage is the formation of a mitochondrial pellet during the Percoll steps that facilitate the utilization of smaller tissue quantities without incurring losses due to diffusion within a band. Although the developed method herein may require additional centrifugation steps, over previously described separation procedures the increased isolation purity was necessary for lipidomic based studies [109, 111-112, 114, 160-161].

Fatty acid structure analysis

Elucidation of unsaturation sites along the fatty acid backbone through transesterification to picolinyl esters was critical to understanding changes to mitochondrial fatty acids with AD progression. The oxidative stress model of neurodegenerative disease correlates the generation of reactive oxygen species (ROS) and subsequent ROS mediated oxidative damage to the degradation of cellular biomacromolecules, especially lipids, during disease pathogenesis. Current research has indicated that products of lipid peroxidation are dependent upon the sites of unsaturation [153]. The principal unsaturation site critical to determining the reactive aldehyde species generated from lipid peroxidation appears to be the omega (ω) double bond [119, 131, 162]. The omega (ω) designation signifies the position of the furthermost double bond relative to the carbonyl group, or the most terminal site.

Derivatization reactions to fatty acid picolinyl ester were successful in allowing the full elucidation of unsaturation sites from the mitochondrial fatty acid profile. As previously determined the lipid profile of neurological mitochondria from Sprague Dawley rats, human mitochondria displayed an analogous lipid profile. This is most apparent when comparing the relative distributions among the oleic acid series. Neurological mitochondria displayed a lower ratio of 9,12-octadecadienoic acid (18:2Δ9,12) to 9-octadecenoic acid (18:1Δ9) compared to other tissues.

More relevant to the oxidative stress model of lipid peroxidation were data acquired on the unsaturation sites from polyunsaturated fatty acids (PUFAs). Due to the increased functionality imparted from the double bond, these sites have increased vulnerability to ROS mediated oxidative damage. The increase in unsaturation index for PUFAs, as a result of multiple double bonds, designates examination these species

236

critical to understanding the relationship between lipids, oxidative damage and products of oxidative stress.

The mass spectrum for the picolinyl ester of 5,8,11,14-eicosatetraenoic acid (arachidonic acid, 20:4Δ5,8,11,14) illustrates a typical spectrum for an ω-6 fatty acid (Figure 4.12). Interpretation of the spectrum reveals that the first gap of -26 amu from the molecular ion occurs at m/z 324. The mass difference between the molecular ion and m/z 324 is 71 amu, which translates to loss of the terminal methyl group (15 amu) and 4 methylene groups (14 amu). Thus the ω-6 family of PUFAs has an unsaturation site beginning six carbons from the terminal methyl group.

As with picolinyl arachidonate, the spectra from the picolinyl esters of 8,11,14-eicosatrienoic acid (20:3Δ8,11,14) and 7,10,13,16-docosatetraenoic acid (22:4Δ7,10,13,16) provide fragmentation indicative of ω-6 fatty acids. For eicosatrienoic acid the ω-6 double bond is revealed with the -26 amu gap between m/z 326 to m/z 300 (Figure 4.13). In actuality, the spectrum from picolinyl 8,11,14-eicosatrienoate is very similar to the spectrum from picolinyl arachidonate, the mass units are just shifted up two mass units to account for the lack of a double bond at the 5 position. The spectrum for picolinyl 7,10,13,16-docosatetraenoate again displays an ω-6 pattern through loss -40 amu from m/z 352 to m/z 312 (Figure 4.15).

In total, three of the four mitochondrial long-chain PUFAs are comprised of three ω-6 fatty acids, with the only differing lipid being 4,7,10,13,16,19-docosahexaenoic acid (22:6Δ4,7,10,13,16,19). The picolinyl docosahexaenoate spectrum indicates that the farthest double bond on carbon 19 results in the loss of 26 amu from m/z 390 to m/z 364 (Figure 4.14). Docosahexaenoic acid, a member of the ω-3 fatty acid family, is a chief component of neurological cellular membranes. The increased proximity of the furthest double bond to the terminal methyl group imparts unique physical properties compared to ω-6 fatty acids.

Fatty acid profile analysis

Normality test

The distribution of lipid species amongst each disease demographic was subjected to Shapiro-Wilk's normality statistical test to analyze if the data diverges appreciably from a population with a normal Gaussian distribution. Shapiro-Wilk's normality tests

were conducted as a function of disease state for each individual neurological region: CER (Table 4.3), IPL (Table 4.4) and SMTG (Table 4.5).

The distribution of short-chain FAs, 12:0-16:1Δ9, within the cerebellum for PCAD patients was overwhelming non-normally distributed (Table 4.3). The analyte distributions of other disease states from cerebellum mitochondria exhibited only sporadic non-normal populations. These data indicate that the lipid compositions of CER mitochondria PCAD subjects displayed a wide distribution of shorter chain FAs. Analytical reasons for these non-normal distributions might be due to minor variations in peak area between low abundant FA species. These minor differences in area counts result in an exaggerated relative distribution. A biological explanation for the non-normal distribution might be rooted in the disease state designation of PCAD subjects. With proposed theory that PCAD might represent a prodromal stage in disease progression the PCAD population would be expected to exhibit a range of lipid variation.

The inferior parietal lobule (IPL) displayed the greatest number of non-normally distributed fatty acids across each of the disease states (Table 4.4). The rationale for this might be that patient-to-patient variability of mitochondrial lipid composition is greater for this particular region, in contrast to CER. The homogeneity found in CER FAs could possibly be the basis for the CER being largely immune from AD pathology.

Lastly, data from superior and middle temporal gyri exhibits the greatest degree of normally distributed FAs throughout each of the disease states, when compared to the other two regions (Table 4.5). Analytically these results might be explained that most FA species displayed greater abundance in the SMTG that the other regions. Therefore, minor differences in peak areas would not create large relative deviations between samples. Of course a biological rational might be that the lipid composition of the SMTG is conserved compared to CER or IPL.

Mitochondrial fatty acid compositions were also analyzed for normality as a composite of neurological areas (CER, SMTG and IPL) divided by the various disease states (Table 4.2). The principle reason for presenting the data in this manner was to examine the distribution of FAs across the three regions within each disease state. Among this data there are two unique situations that deserve note. The first being, FAs that were found to be non-normally distributed across the three regions, however data

238

from the individual regions indicated a normal distribution. These data suggests that the region-to-region variability is great enough to create a multimodal distribution. These lipid species are designated by † (Table 4.2). The second unique situation, FAs that were normally distributed across the combined three regions, however regional data indicates that one or more regions were non-normally distributed. This would imply that normality was unbalanced among the regions by outliers, and distributions from the additional regions fostered unification of the data. Species falling into this category are denoted by # (Table 4.2).

The inconsistent results from the Shapiro-Wilk's normality tests indicate that this statistical treatment is best suited as a test for population distributions that would determine the use of non-parametric or parametric during further statistical analysis. Unfortunately, the results of normality testing does not indicate designation of disease state, proliferation of AD or degree of disease pathology by oxidative damage.

Skewness test

The interpretation of skewness data for the combined regions means that NC subjects contained higher-value outliers. A change in positive to negative skewness, across the disease profile, implies that the outlier population is shifting causing it to occur above or below the mean, respectively.

Data for IPL from each disease grouping was compared to CER data from the equivalent disease state. As might be expected the two states with the most pronounced disease pathology, PCAD and LAD, exhibit the majority of deviations from the CER. The FA profile from the superior and middle temporal gyri (SMTG) exhibited a shift in skewness, especially because it occurs between NC and later disease stages might indicate a change in the mean for the disease population.

Overall the statistical importance of skewness provides a measure of symmetry around a population mean. A dramatic change in skewness polarity when compared across the disease states does indicate a shifting population mean. As with normality, the skewness value does not impart evidence of lipid peroxidation or degradation. Therefore, care must be taken not to over interpret the data as a diagnostic tool of disease progression. The importance of the test however, allows evaluation of the sample population as a whole.

Fatty acid distribution and disease state analysis

Methyl derivatizied species were treated as individual analytes, 18 in total, and subjected to a variety of statistically treatments. The purpose of evaluating the lipid species by exhaustive statistics was an attempt to determine differences between disease groups or neurological regions. In addition correlation tests were conducted in an effort to rationalize changes in relation to neuropathology markers. The culmination of the project comes down to the comparison of fatty acids regionally and between disease states. The statistical treatments employed either a parametric one way ANOVA, for normally distributed data as established by Shapiro-Wilk normality test; or a non-parametric Kruskal-Wallis one way ANOVA on ranks, for non-normally distributed data. Significance was established by a Tukey post hoc test when comparing regional distributions for a particular disease state. Dunn's test established significance was used when comparing disease states within a region because treatment groups were unequal in number. Discussion of regional, distribution and correlation statistical results from select lipid species analyzed will be covered in the subsequent paragraphs.

The overwhelming abundance of dodecanoic acid (12:0) in CER of DC patients imparted a unique mitochondrial FA profile. The lack of outliers within this particular sample set designates that patients, at least from this sample population, exhibiting Lewy body pathology have a significantly different mitochondrial FA profile than found with any demographic or region contained in this study. This disproportion in CER resulted in a negative correlation between 12:0 vs. age and Braak score. This correlation is likely due to DC patients having a slightly lower age than other subjects and lower Braak score than subjects with AD pathology.

9-Hexadecenoic acid (16:1Δ9) is the shortest-chain unsaturated fatty acid detected in mitochondria. A positive correlation was found in CER between 16:1Δ9 and Braak score, in addition to a negative correlation in SMTG with age. These random, albeit statistically significant, correlations are probably the consequence of minor fluctuations within the sample population.

Hexadecanoic or palmitic acid (16:0) is one of the most abundance lipids in the mitochondrial membrane. It is the primary substrate used during desaturation and elongation reactions in the synthesis of other fatty acids [15]. Correlation statistics

established a positive link between 16:0 and Braak score in CER in addition to Braak score and NP in IPL. These correlations are likely to be the result of significant increases in 16:0 from MCI, PCAD and LAD patients within various regions. It is interesting that both 16:0 and 16:1Δ9 were in lower abundance for CER mitochondria from NC subjects.

Linoleic or 9,12-octadecadienoic acid (18:2Δ9,12) is a precursor for synthesis of long chain PUFAs. As shown in the previous study (Chapter 3) neurological mitochondria contain a lower percentage of this particular fatty acid than other tissues studied. The significant increase in 18:2Δ9,12 with SMTG mitochondria for every population demographic, except PCAD, is worth noting. This is important because it relates to the potential for PUFAs synthesis. An increase in 18:2Δ9,12 substrate could signify an alteration in the need for PUFAs within this region. Preclinical AD subjects were found to have a significant increase in CER mitochondria, and a non-statistically significant decrease in SMTG mitochondria. It is interesting that the two regions (CER and SMTG) at opposite ends of the AD pathology scale exhibited such dissimilarity in 18:2Δ9,12 content, whereas IPL levels were seemingly unchanged. However, if a reduction in 18:2Δ9,12 was linked to AD pathology in SMTG, presumably LAD patients would be expected to display similar results to PCAD. The only correlation calculated was within CER between Braak score.

The two octadecenoic fatty acids (18:1Δ9 and 18:1Δ10) exhibited similar distributions among disease populations within equivalent regions. This might not be too surprising as a shift in one carbon for the double bond wouldn't be expected to impart drastically different physical characteristic to the membrane. The importance of 18:1 fatty acids within the mitochondrial membrane is due to their association as fatty acids found in the cardiolipin backbone [163-167]. Cardiolipin is a class of lipid exclusively synthesized in the inner mitochondrial membrane and is believed to be involved in stabilizing membrane bound proteins involved in the ETP [168-170]. In addition, proteomic studies conducted on phospholipases, which function to directly regulate phospholipid concentrations, have documented an increased expression in mitochondrial fractions with progression of AD [171-174]. Furthermore, activity of phospholipase D has been implemented in being linked to amyloid precursor protein, which is the progenitor to amyloid beta (Aβ) [172-173, 175]. Current research has reported a

connection with lipid expression that indicates phospholipase D activity is in part regulated by oleic acid (18:1Δ9) [174]. An interesting distinction between the two is that 10-octadecenoic acid was found to have a positive correlation to both Braak score and NP within the IPL.

Results from the analysis of octadecanoic or stearic acid (18:0) were similar to those from the 18:1 fatty acids. Again, this might not be entirely surprising due to the fact that 18:0 is substrate for both 18:1Δ9 and 18:1Δ10 syntheses. As with the other 18-length carbon fatty acids, stearic acid showed a positive correlation with Braak score within CER. This is probably the consequence of CER levels for NC which were significantly lower than IPL and SMTG measurements and lower than PCAD and LAD CER samples.

Finally, the two groups of lipid species to be discussed are the plasmalogens and polyunsaturated fatty acids (PUFAs). These two groups represented a great deal of the literature concerned with the intersection of lipids and health. Plasmalogens are of interest because they are considered to be inherent anti-oxidants of biological membranes, providing protection for PUFAs [16, 121-122, 136, 176]. Polyunsaturated fatty acids are of equal interest because of their susceptibility to ROS and the deleterious products formed from subsequent reactions [116-117, 119, 162, 177-178]. Because of PUFAs and plasmalogens presumed roles within the reactions oxidative damage comparison of these species across disease states and neurological regions is central to understanding changes in mitochondrial membrane components.

First, a discussion of the various plasmalogen species results. With regard to CER and IPL plasmalogens 16:0 and 18:1 a&b exhibited similar distributions among the disease states. No statistically significant changes were found between the regions or compared to NC quantities within a region. These results when viewed from the standpoint of plasmalogens role as anti-oxidants are not surprising being in two regions of limited pathology. The last plasmalogen species, P 18:0, had a slightly different profile. On the whole quantities of 1-enyl-octadecenoic acid (P 18:0) were greater in SMTG for each population compared to CER and IPL mitochondria. In contrast to the other plasmalogens there was a slight increase of P 18:0 from NC to LAD subjects. This increase was found to be significant for PCAD and LAD in CER and LAD in IPL. A

242

positive correlation to Braak score within CER was probably a consequence of this increase. As far as P 18:0 is concerned the increased abundance for later AD stages within pathology limited regions might provide anti-oxidant protection controlling the disease proliferation.

Overall, all plasmalogen species displayed greater mean abundance in SMTG mitochondria when compared to CER and IPL. For each plasmalogen in SMTG mitochondria the population distribution displayed a similar profile. Normal control was slightly lower than MCI, followed by a drop in abundance for PCAD, then an increase for both LAD and DC patients. For P 16:0 and P 18:1 a&b this increase was significant for LAD and DC, in addition to NC and MCI for P 18:1a. As for P 18:0 mean abundances for disease populations were noticeable higher in SMTG, although the increase was not statistically significant, with the exception of NC patients. The increased quantity of each plasmalogen species within SMTG mitochondrial membrane raises questions about their role with regards to oxidative stress.

The imperative question is whether these species are synthesized as a response to an oxidative stress environment [143, 179]. An increased synthesis within an oxidative stress environment would make sense following the concept of homeoviscous adaptation. However, if increased synthesis was a consequence of oxidative stress then NC patients would be expected to contain consistent quantities across the three regions. Of course the regional increase might be a preemptive modification to a potential oxidative stress environment. The population outlier with both of these theories are data from PCAD subjects. The statistically insignificant decrease of plasmalogen species for PCAD subjects in SMTG, compared to other regions, might make sense with the connection to increase AD pathology given the proposed mechanism of plasmalogens acting as antioxidants, [121-122, 134]. However, LAD data would be expected to display a similar if not greater reduction, and not a significant increase over CER levels [122-123, 134, 176].

The last set of lipid species to be discussed are arguably the most central to research on neurodegenerative disease, these are the long-chain polyunsaturation fatty acids. These PUFAs will be divided into two groups for discussion purposes. The first group will be the ω-6 fatty acid family. To begin with 5,8,11,14-eicosatetraenoic or

arachidonic acid (20:4) is one of the most abundant PUFAs found in neurological tissue. The cleavage and subsequent oxidation of arachidonic acid (ARA) from the phosphoglycerol background leads to the generation of isoprostanes and ensuing biomarkers of oxidative damage [119]. The expression of ARA is interesting being significantly higher in CER and reduced in SMTG, whereas the other disease populations were significantly higher within SMTG, compared to equivalent CER quantities. It is notable that a lipid species associated with oxidative damage would be less prominent during the two later disease states within a region abundant in disease pathology. These data implies that disease progression is associated with reduced ARA abundance within SMTG. However, no statistically significant correlation was found between Braak score or NP with SMTG.

The two FA, 8,11,14-eicosatrienoic (20:3) and 7,10,13,16-docosatetraenoic (22:4) exhibited comparable regional and disease state distributions, which are remarkable similar to ARA patterns. The quantities between disease populations were relatively unchanged within IPL. For mitochondria from CER both FAs were most abundant in PCAD patients, dropping in abundance for MCI and LAD, then again for NC and DC. Again, as seen with ARA the population expression was nearly opposite that of CER. Each of the three ω-6 FAs yielded a significant positive correlation in CER between Braak score and concentration. This implies that a greater abundance of PUFAs are associated with a known biomarker of oxidative damage, at least within a region deficient disease pathology.

The second set of PUFAs is the ω-3 family, 4,7,10,13,16,19-docosahexaenoic acid (22:6, DHA), which is unique being the only ω-3 FA detected in the mitochondrial membrane. Docosahexaenoic acid is widely acknowledged as the most abundant PUFA in neurological gray matter, the source for all tissue used in this study [180]. As with arachidonic acid, the cleavage of DHA from the glycerol backbone and consequently oxidation leads to the development of biomarkers of oxidative stress. These products, otherwise known as neuroprostanes, are the focus of research concerned with the products of oxidative stress from lipids [118, 120, 131-132, 145, 178, 181-184]. Overall, the regional and subject population distribution of DHA was nearly equivalent to each of the ω-6 FAs. The difference for DHA was a general higher abundance in CER and

SMTG for most disease states. In addition the disparity between higher PCAD and lower NC or DC abundances were more distinct. Along the same lines the significant drop in SMTG abundance for PCAD patients was greater with DHA in comparison to ARA. As with the ω-6 FAs DHA correlated positively with increasing Braak score.

As mentioned earlier because of their proximity to the generation of, and the consequential formation of reactive products with, ROS lipids are a fundamental aspect to research of neurodegenerative disease [107, 116-117, 119-120, 162, 185]. Studies conducted on plasma membrane lipids have found regional differences during the progression of Alzheimer's disease [140]. Further studies have detected regional differences in the form of biomarkers of lipid peroxidation when comparing AD patients to controls [120]. Literature such as these documenting variations of the lipid profile and/or products of lipid peroxidation on a regional scale within neurological tissue provided the basis for investigations for mitochondrial fatty acid regional dissimilarity, in addition to distinction among disease state.

Regional and AD disease progression data established that differences are present in mitochondria fatty acid profiles which are consistent with the current literature and the principle of oxidized products in pathology affected regions [120, 177]. Proteomic studies conducted on phospholipases, which function to directly regulate phospholipid concentrations, have documented an increased expression in mitochondrial fractions with progression of AD [171-174]. Furthermore, activity of phospholipase D has been implemented in being linked to amyloid precursor protein, which is the progenitor to amyloid beta (Aβ) [172-173, 175]. In other words, lipids have the potential to have an affect on the activity of proteins. The activated proteins, in turn, have the potential to employ lipids as substrates for the generation of further metabolic products [171, 174-175].

As a whole, the goal of the project was to elucidate possible changes to mitochondrial FAs as a reflection of advanced AD stages, in addition to being more prevalent in regions displaying greater pathology. When viewing the data of individual methyl derivatizied species, intra-regional changes were found among disease populations and inter-regional changes were found within equivalent disease populations.

Statistical evaluation of the data in this two-dimensional manner provided a substantial number of comparisons between associated groups.

The lack of an overwhelming trend concerning the change in methyl derivatizied species across disease states can possibly be explained by population noise. Variation in the sample population is natural and should be expected to occur for biological subjects. For evaluation of a human population some variables relating to a subject's history can not be controlled and therefore greater differences should be expected to arise. In addition, the designation of a subject's disease state mostly likely increased sample variation. Braak and Braak noted that pathology differences for classification were difficult to discern during transitional stages in disease progression [149]. The seemingly subjective nature of stage classification would contribute to variation within a disease state. The range of disease expression within each classification state could be the cause of non-normally distributed data. The ramifications of the non-normally distributions were the use of non-parametric statistical tests. Non-parametric tests compare differences in the medians between to groups, thus they lack the statistical power to differentiate between minor variations.

It is interesting to note that statistical differences appeared to be greater across neurological regions than found between disease states for a particular region. Further studies would have to be conducted to examine the response of lipid expression in response to oxidative stress agents. Although the current was successful in finding significant differences between disease states and regions, it was not possible to indicate whether changes were the result or cause of oxidative stress.

The current project applied the concept of homeoviscous adaptation, adjusting the traditional perception of environmental stimuli in exchange for neurological region and disease state. Overall, various FA and plasmalogen changes were found between disease states in both pathology affected and limited regions. Correlation statistics conducted between methylated species and disease markers provided random associations, however no definite connections were possible to link particular lipid species with plaques or tangles. Several of the changes, such as with PUFAs in SMTG, were unpredicted when considered in the context of disease progression and pathology. Further studies are being developed to discern possible changes to the mitochondrial membrane as a result to

246

specific oxidative insults. The data obtained from future studies and those obtained herein will hopefully provide further evidence for a link between mitochondrial lipid composition and AD pathology.

PART IV. CONCLUSIONS

Chapter 5.1. Conclusions

The concept of homeoviscous adaptation was a unifying theme between each of the research projects within this dissertation. This theory was developed by Michael Sinensky (circa 1974) as a means to characterize the influence that changes in fatty acid (FA) composition have on membrane viscosity. Sinensky's experiments with *Escherichia coli* found that cultures grown at various temperatures modified their FA content which resulted in maintenance of membrane viscosities [1]. Being as the membrane provides protection from extracellular environmental contaminates and as structure for membrane-bound proteins, regulation of membrane integrity is critical for cellular function [1, 41, 70, 186]. This phenomenon is not relegated to *E. coli*, as temperature induced membrane modification of fatty acids has been documented across a range of microorganisms [71-74, 77-78, 187]. The concept of microorganism membrane adaptation has since expanded to include a variety of environmental insults, including cultures grown in the presence of organic solvents [35, 37, 76, 188].

The initial research project (Chapter 2) was a multidisciplinary bio-fuels study concerned with FA analysis of *Clostridium thermocellum* strains [138]. The project centered on the comparison of membranes from wild-type and ethanol-adapted *C. thermocellum* strains. A hypothesis was developed that ethanol adaptation could lead to modifications in the FA profile, as established by the concept of homeoviscous adaptation. This hypothesis was tested by comparing the relative composition of FA between both strains. Further analysis compared the change in physical properties of the membrane induced by ethanol exposure through steady-state fluorescence anisotropy. The combination of FA and anisotropy data, proved the hypothesis to be correct, that changes in FA profile had occurred as a result of ethanol exposure. These data necessitated development of a model of ethanol adaptation for *C. thermocellum* cells [138].

The homeoviscous adaptation concept as employed by prokaryotic organisms was utilized as a foundation to explore FA variations occurring as a result of non-traditional "environmental" factors [1, 39]. Factors such as growth temperature [36, 38, 42, 71-74,

77-78], pressure [47, 69, 189] and solvent insults [35, 37, 42, 76, 188] have been recognized to affect not only the lipid composition, but also metabolic pathways of microorganisms [79-80, 190]. The central concept of homeoviscous adaptation through FA modification was expanded beyond unicellular systems and the traditional perception of environmental factors (i.e. temperature) to include changes in the intracellular environment.

Previous work from the Lynn group has involved research on mitochondrial based projects [191-193]. Mitochondria are of interest because of their involvement in an assortment of biomedical research endeavors including respiratory chain deficiencies [128, 194-196], age-related diseases [197-198], cancer [100, 196, 198] and neurodegenerative diseases [105, 154, 158, 199-200]. The role of mitochondria within cellular energy generating pathways, associates them with the development of ROS, which have been proposed as casual in the theories of oxidative stress and aging [103, 141, 198]. With prior group experience and the proposed evolutionary link between bacteria and mitochondria, allowed for a logical transition from prokaryotic to eukaryotic systems [151].

The concept of homeoviscous adaptation is generally applied to unicellular organisms, and not thought of on the scale of multicellular systems or subcellular organelles. Research conducted in the field of proteomics has documented variations in the protein expression between tissues within the same animal [99, 174, 201]. This provided motivation to investigate possible differences in the mitochondrial fatty acid profiles from various tissues within Sprague Dawley rats (Chapter 3). A hypothesis was formulated that changes in the extracellular environment could cause intracellular changes affecting the lipid composition of subcellular organelles. In order to test the hypothesis, mitochondria were isolated from kidney, liver, heart and brain of Sprague Dawley rats and derivatizied FAs were compared as a function of tissue. These results confirmed the hypothesis that variations in FA species and relative distributions existed between mitochondria isolated from various tissues. These data indicated that FAs within neurological mitochondria provide the potential for increased vulnerability to oxidative damage.

Data identifying the unique FA profile of neurological mitochondria generated interest in investigation of mitochondrial fatty acid modification in human brain regions during progression of neurological disease (Chapter 4). A hypothesis was developed that changes to mitochondrial FAs will be reflected during advanced stages of Alzheimer's disease (AD), in addition to being more prevalent in regions displaying greater pathology. To test this theory mitochondria were isolated from three regions of neurological tissue representing AD progression and compared to control samples. Although, the hypothesis was technically proven by observing statistically significant differences in the mitochondrial FA profile among regions and disease populations, the results did not provide distinctions as originally predicted. Therefore, the original hypothesis should be revised to more accurately identify dissimilarity between mitochondria. In keeping with advances in instrumental development further testing could be conducted to increase the volume of data obtained from mitochondria samples and fine-tune the hypothesis.

With the advent of electrospray ionization (ESI) the study of lipids has undergone a radical change in recent years [202-203]. The traditional method of derivatization prior to analysis has in large part been replaced by direct lipid analysis following a Folch style extraction [204]. The coupling of ESI to a mass analyzer allows the analysis of intact phospholipids following membrane extraction [9-10, 205-207]. The advantage with this technique is the ability to discern fatty acid acyl chain pairings and bonding geometries along the glycerol backbone in addition to phosphate polar head group determination [205, 208]. Data on glycerol associated fatty acid species are valuable to understanding the relationship of plasmalogens and PUFAs in an oxidative stress environment [177, 179, 209]. Analysis of polar head group designation is equally important for studying variations among phospholipids with respect to disease expression as these groups are involved in signal regulation [93, 97, 140].

The advantages afforded by ESI allow the acquisition of phospholipid data not possible with methyl derivatization techniques. However, data on individual FA species, such as sites of unsaturation are typically lost. Therefore, to get a complete lipidomics representation of a system and changes that occur in response to environmental stimuli both types of analysis would be necessary.

In keeping with current trends in lipid research and in an effort to acquire data lost during the derivatization process, method development for the analysis of neurological mitochondria phospholipid profiles were initiated using ESI techniques. The goal is to analyze mitochondria isolated during Chapter 4. Therefore, data can be obtained on FAs and phospholipids on the exactly the same sample set. The expectation is that intact phospholipid data will provide further differentiation between region and disease state mitochondria.

For the application of lipidomics and their involvement in neurodegenerative health, I would propose additional future experiments. With the current study isolated mitochondria were obtained from tissues obtained during autopsy. This means that both mitochondria and disease state classification represent the comparison of end-points. Data obtained do not provide an indication of whether the lipid profile influences disease progression or vise-versa. Obviously, isolation of tissue samples from living patients is not possible; however studies with cell cultures would alleviate this hurdle. Experiments with neurological cell cultures and the exposure to oxidative insults would provide data on the potential mitochondrial, or cellular, lipid response to a simulated disease state environment.

Going further with mitochondrial lipidomics, current research has proposed a link between disease and phospholipid expression along the outer-layer of the lipid bilayer [210-211]. Although the separation of inner and outer mitochondrial membranes has been documented, the method is probably not amendable to high-throughput analysis [212]. An alternative procedure would be to react intact mitochondria with a ligand that specifically binds to the phosphotidyl head group. Phospholipid isolation could then precede by established isolation methods following by ESI analysis. Phospholipids tagged with the ligand can be identified by mass shifts and the neutral loss of the tagged head-group through MS/MS spectra would be known to originate from the external layer of the outer membrane. The advantage with this technique is that it can be used in conjunction with established instrumental methods, complimenting acquisition by supplying additional information alongside previously acquired data.

The concept of homeoviscous adaptation was shown to be integral to each research project within this dissertation. The catalyst for environmental adaptation

evolved from an organic solvent to changes in extracellular environment, such as tissue and regional origin, and finally to neurodegenerative pathology. Adaptation of lipids at its best can be a process for cellular survival, as in the case with *C. thermocellum*, or at its worst create the potential for propagation of deleterious products resulting in macrocellular repercussions.

The field of lipid research has evolved over the years keeping pace with current trends in instrument development, facilitating research into biological systems. Still considerable challenges remain for the progression of lipidomics into high-throughput research endeavors [213-214]. The future of lipidomics seems boundless as chromatographic and mass spectral method developments are pushing the scientific envelope and allowing application into countless aspects of cellular and systems biology [4-5, 11, 13, 97, 129, 215-217].

REFERENCES

1. Sinensky, M., *Homeoviscous Adaptation - Homeostatic Process That Regulates Viscosity of Membrane Lipids in Escherichia-Coli.* Proceedings of the National Academy of Sciences of the United States of America, 1974. **71**(2): p. 522-525.
2. Rilfors, L. and G. Lindblom, *Regulation of lipid composition in biological membranes--biophysical studies of lipids and lipid synthesizing enzymes.* Colloids and Surfaces B: Biointerfaces, 2002. **26**(1-2): p. 112-124.
3. Han, X. and R.W. Gross, *Global analyses of cellular lipidomes directly from crude extracts of biological samples by ESI mass spectrometry: a bridge to lipidomics.* J. Lipid Res., 2003. **44**(6): p. 1071-1079.
4. Lagarde, M., et al., *Lipidomics is emerging.* Biochimica et Biophysica Acta (BBA) - Molecular and Cell Biology of Lipids, 2003. **1634**(3): p. 61-61.
5. Spener, F., et al., *Editorial: What is lipidomics?* European Journal of Lipid Science and Technology, 2003. **105**(9): p. 481-482.
6. Lee, S.H., et al., *Targeted lipidomics using electron capture atmospheric pressure chemical ionization mass spectrometry.* Rapid Commun Mass Spectrom, 2003. **17**(19): p. 2168-76.
7. Carvalho, A.P. and F.X. Malcata, *Preparation of fatty acid methyl esters for gas-chromatographic analysis of marine lipids: insight studies.* J Agric Food Chem, 2005. **53**(13): p. 5049-59.
8. Lepage, G. and C.C. Roy, *Direct transesterification of all classes of lipids in a one-step reaction.* J Lipid Res, 1986. **27**(1): p. 114-20.
9. Ingvardsen, L., S. Michaelsen, and H. Sorensen, *Analysis of Individual Phospholipids by High-Performance Capillary Electrophoresis.* Journal of the American Oil Chemists Society, 1994. **71**(2): p. 183-188.
10. Kim, H.Y., T.C.L. Wang, and Y.C. Ma, *Liquid-Chromatography Mass-Spectrometry of Phospholipids Using Electrospray-Ionization.* Analytical Chemistry, 1994. **66**(22): p. 3977-3982.
11. Wenk, M.R., *The emerging field of lipidomics.* Nature Reviews Drug Discovery, 2005. **4**(7): p. 594-610.
12. Carrasco-Pancorbo, A., N. Navas-Iglesias, and L. Cuadros-Rodríguez, *From lipid analysis towards lipidomics, a new challenge for the analytical chemistry of the 21st century. Part I: Modern lipid analysis.* TrAC Trends in Analytical Chemistry, 2009. **28**(3): p. 263-278.
13. Navas-Iglesias, N., A. Carrasco-Pancorbo, and L. Cuadros-Rodríguez, *From lipids analysis towards lipidomics, a new challenge for the analytical chemistry of the 21st century. Part II: Analytical lipidomics.* TrAC Trends in Analytical Chemistry, 2009. **28**(4): p. 393-403.
14. Voet, D. and J.G. Voet, *Biochemistry: Biomolecules, Mechanisms of Enzyme Action and Metabolism.* 3rd ed. Vol. One. 2004: Wiley.
15. Daum, G., *Lipids of Mitochondria.* Biochimica Et Biophysica Acta, 1985. **822**(1): p. 1-42.
16. Nagan, N. and R.A. Zoeller, *Plasmalogens: biosynthesis and functions.* Progress in Lipid Research, 2001. **40**(3): p. 199-229.
17. Stryer, L., *Biochemistry.* 2nd ed. 1981: W.H. Freeman and Company.

18. *The nomenclature of lipids (recommendations 1976). IUPAC-IUB Commission on Biochemical Nomenclature.* J. Lipid Res., 1978. **19**(1): p. 114-128.

19. Wade Jr., L.G., *Organic Chemistry*. 2nd ed. 1991: Prentice Hall.

20. Christie, W.W. *The Lipid Library*. http://www.lipidlibrary.co.uk/ 2010 [cited (accessed 2010); Available from: http://www.lipidlibrary.co.uk/.

21. Rood, D., *A Practical Guide to the Care, Maintenance, and Troubleshooting of Capillary Gas Chromatographic Systems*. 3rd ed. 1999: Wiley-VCH.

22. McMaster, M., *LC/MS: A Practical User's Guide*. 2005: Wiley-Interscience.

23. Watson, J.T. and O.D. Sparkman, *Introduction to Mass Spectrometry*. 4th ed. 2007: Wiley.

24. Gross, J.H., *Mass Spectrometry: A Textbook*. 2004: Springer.

25. Harrison, A.G., *Chemical Ionization Mass Spectrometry*. 2nd ed. 1992: CRC Press.

26. March, R.E., *An introduction to quadrupole ion trap mass spectrometry.* Journal of Mass Spectrometry, 1997. **32**(4): p. 351-369.

27. March, R.E., *Quadrupole ion trap mass spectrometry: Theory, simulation, recent developments and applications.* Rapid Communications in Mass Spectrometry, 1998. **12**(20): p. 1543-1554.

28. March, R.E. and J.F. Todd, *Practical Aspects of Ion Trap Mass Spectrometry: Volume 1: Fundamentals of Ion Trap Mass Spectrometry (Modern MS)*. 1995: CRC-Press.

29. March, R.E. and J.F. Todd, *Quadrupole Ion Trap Mass Spectrometry*. 2005: Wiley-Interscience.

30. Lynd, L.R., et al., *Microbial cellulose utilization: Fundamentals and biotechnology.* Microbiology and Molecular Biology Reviews, 2002. **66**(3): p. 506-+.

31. Demain, A.L., M. Newcomb, and J.H. Wu, *Cellulase, clostridia, and ethanol.* Microbiol Mol Biol Rev, 2005. **69**(1): p. 124-54.

32. Alexandre, H., I. Rousseaux, and C. Charpentier, *Relationship between Ethanol Tolerance, Lipid-Composition and Plasma-Membrane Fluidity in Saccharomyces-Cerevisiae and Kloeckera-Apiculata.* Fems Microbiology Letters, 1994. **124**(1): p. 17-22.

33. Jones, R.P., *Biological principles for the effects of ethanol.* Enzyme and Microbial Technology, 1989. **11**(3): p. 130-153.

34. Herrero, A.A., R.F. Gomez, and M.F. Roberts, *Ethanol-induced changes in the membrane lipid composition of Clostridium thermocellum.* Biochim Biophys Acta, 1982. **693**(1): p. 195-204.

35. Weber, F.J. and J.A.M. de Bont, *Adaptation mechanisms of microorganisms to the toxic effects of organic solvents on membranes.* Biochimica et Biophysica Acta (BBA) - Reviews on Biomembranes, 1996. **1286**(3): p. 225-245.

36. Russell, N.J. and N. Fukunaga, *A comparison of thermal adaptation of membrane lipids in psychrophilic and thermophilic bacteria.* FEMS Microbiology Letters, 1990. **75**(2-3): p. 171-182.

37. Ingram, L.O., *Adaptation of membrane lipids to alcohols.* J. Bacteriol., 1976. **125**(2): p. 670-678.

38. Russell, N.J., *Mechanisms of thermal adaptation in bacteria; blueprints for survival.* Trends in Biochemical Sciences, 1984. **9**(3): p. 108-112.

39. Silvius, J.R., N. Mak, and R.N. McElhaney, *Why do prokaryotes regulate membrane lipid fluidity?*, in *Membrane Fluidity: Biophysical Techniques and Cellular Regulation*, H. Kates and A. Kuksis, Editors. 1980, Humana Press: Clifton, N.J. p. 213-222.

40. Alexandre, H., J.P. Berlot, and C. Charpentier, *Effect of Ethanol on Membrane Fluidity of Protoplasts from Saccharomyces-Cerevisiae and Kloeckera-Apiculata Grown with or without Ethanol, Measured by Fluorescence Anisotropy.* Biotechnology Techniques, 1994. **8**(5): p. 295-300.

41. Yun, I., et al., *Bulk Vs Transbilayer Effects of Ethanol on the Fluidity of the Plasma-Membrane Vesicles of Cultured Chinese-Hamster Ovary Cells.* Asia Pacific Journal of Pharmacology, 1993. **8**(1): p. 9-16.

42. Chu-Ky, S., et al., *Combined cold, acid, ethanol shocks in Oenococcus oeni: Effects on membrane fluidity and cell viability.* Biochimica et Biophysica Acta (BBA) - Biomembranes, 2005. **1717**(2): p. 118-124.

43. Hu, C., F.-W. Bai, and L.-J. An, *Protein Amino Acid Composition of Plasma Membranes Affects Membrane Fluidity and Thereby Ethanol Tolerance in a Self-flocculating Fusant of Schizosaccharomyces pombe and Saccharomyces cerevisiae.* Chinese Journal of Biotechnology, 2005. **21**(5): p. 809-813.

44. Aricha, B., et al., *Differences in membrane fluidity and fatty acid composition between phenotypic variants of Streptococcus pneumoniae.* Journal of Bacteriology, 2004. **186**(14): p. 4638-4644.

45. Morein, S., et al., *Wild-type Escherichia coli Cells Regulate the Membrane Lipid Composition in a ``Window" between Gel and Non-lamellar Structures.* J. Biol. Chem., 1996. **271**(12): p. 6801-6809.

46. Shinitzky, M. and Y. Barenholz, *Fluidity Parameters of Lipid Regions Determined by Fluorescence Polarization.* Biochimica Et Biophysica Acta, 1978. **515**(4): p. 367-394.

47. Lopez, C.A., H.A. Garda, and E.A. Rivas, *The effect of osmotic stress on the biophysical behavior of the Bacillus subtilis membrane studied by dynamic and steady-state fluorescence anisotropy.* Archives of Biochemistry and Biophysics, 2002. **408**(2): p. 220-228.

48. Williams, T.I., et al., *Proteomic profile changes in membranes of ethanol-tolerant Clostridium thermocellum.* Applied Microbiology and Biotechnology, 2007. **74**(2): p. 422-432.

49. Kurkiewicz, S., et al., *GC/MS determination of fatty acid picolinyl esters by direct Curie-point pyrolysis of whole bacterial cells.* Journal of the American Society for Mass Spectrometry, 2003. **14**(1): p. 58.

50. Lepage, G. and C.C. Roy, *Specific methylation of plasma nonesterified fatty acids in a one-step reaction.* J Lipid Res, 1988. **29**(2): p. 227-35.

51. Destaillats, F. and P. Angers, *One-step methodology for the synthesis of FA picolinyl esters from intact lipids.* Journal of the American Oil Chemists Society, 2002. **79**(3): p. 253-256.

52. Bouchonnet, S., S. Kinani, and M. Sablier, *Letter: Does the reagent gas influence collisional activation when performing in situ chemical ionization with an ion*

trap mass spectrometer? European Journal of Mass Spectrometry, 2007. **13**(3): p. 223-226.

53.   Bothun, G.D., *Thesis (M.S. Ch. E.) University of Kentucky.* Thesis (M.S. Ch. E.) University of Kentucky, 2001.

54.   Bothun, G.D., et al., *Liposome fluidization and melting point depression by pressurized CO2 determined by fluorescence anisotropy.* Langmuir, 2005. **21**(2): p. 530-536.

55.   Masood, A., K.D. Stark, and N. Salem, Jr., *A simplified and efficient method for the analysis of fatty acid methyl esters suitable for large clinical studies.* J Lipid Res, 2005. **46**(10): p. 2299-305.

56.   Mjos, S.A. and O. Grahl-Nielsen, *Prediction of gas chromatographic retention of polyunsaturated fatty acid methyl esters.* J Chromatogr A, 2006. **1110**(1-2): p. 171-80.

57.   Thurnhofer, S. and W. Vetter, *A gas chromatography/electron ionization-mass spectrometry-selected ion monitoring method for determining the fatty acid pattern in food after formation of fatty acid methyl esters.* J Agric Food Chem, 2005. **53**(23): p. 8896-903.

58.   AOCS, A.O.C.S. *American Oil Chemists' Society (AOCS).* http://www.aocs.org/ 2010 [cited 2010.

59.   Christie, W.W., et al., *A Comparison of Pyrrolidide and Picolinyl Ester Derivatives for the Identification of Fatty-Acids in Natural Samples by Gas Chromatography-Mass Spectrometry.* Lipids, 1986. **21**(10): p. 657-661.

60.   Dobson, G. and W.W. Christie, *Structural analysis of fatty acids by mass spectrometry of picolinyl esters and dimethyloxazoline derivatives.* TrAC Trends in Analytical Chemistry, 1996. **15**(3): p. 130-137.

61.   Dubois, N., C. Barthomeuf, and J.P. Berge, *Convenient preparation of picolinyl derivatives from fatty acid esters.* European Journal of Lipid Science and Technology, 2006. **108**(1): p. 28-32.

62.   Hamilton, J.T.G. and W.W. Christie, *Mechanisms for ion formation during the electron impact-mass spectrometry of picolinyl ester and 4,4-dimethyloxazoline derivatives of fatty acids.* Chemistry and Physics of Lipids, 2000. **105**(1): p. 93-104.

63.   Harvey, D.J., *Mass spectrometry of picolinyl esters and other nitrogen-containing derivatives of lipids.* Advances in Lipid Methodology, 1992. **1**: p. 19-80.

64.   Christie, W.W., *The Lipid Library.* http://www.lipidlibrary.co.uk/, 2007. **(accessed 2007)**.

65.   Brenna, J.T., *Structural analysis of unsaturated fatty acid methyl ester isomers with acetonitrile covalent-adduct chemical ionization (CACI) tandem mass spectrometry.* Lipid analysis and lipidomics : new techniques and applications, 2006: p. 157-172.

66.   Lawrence, P. and J.T. Brenna, *Acetonitrile covalent adduct chemical ionization mass spectrometry for double bond localization in non-methylene-interrupted polyene fatty acid methyl esters.* Anal Chem, 2006. **78**(4): p. 1312-17.

67.   Michaud, A.L., et al., *On the formation of conjugated linoleic acid diagnostic ions with acetonitrile chemical ionization tandem mass spectrometry.* Rapid Communications in Mass Spectrometry, 2005. **19**(3): p. 363-368.

68. Michaud, A.L. and J.T. Brenna, *Structural characterization of conjugated linoleic acid methyl esters with acetonitrile chemical ionization tandem mass spectrometry.* Advances in Conjugated Linoleic Acid Research, 2006. **3**: p. 119-138.

69. Tymczyszyn, E.E., A. Gomez-Zavaglia, and E.A. Disalvo, *Influence of the growth at high osmolality on the lipid composition, water permeability and osmotic response of Lactobacillus bulgaricus.* Archives of Biochemistry and Biophysics, 2005. **443**(1-2): p. 66-73.

70. Konings, W.N., et al., *The cell membrane plays a crucial role in survival of bacteria and archaea in extreme environments.* Antonie Van Leeuwenhoek International Journal of General and Molecular Microbiology, 2002. **81**(1-4): p. 61-72.

71. Evans, R.I., et al., *The effect of growth temperature on the phospholipid and fatty acyl compositions of non-proteolytic Clostridium botulinum.* International Journal of Food Microbiology, 1998. **40**(3): p. 159-167.

72. Kropinski, A.M.B., V. Lewis, and D. Berry, *Effect of Growth Temperature on the Lipids, Outer-Membrane Proteins, and Lipopolysaccharides of Pseudomonas-Aeruginosa Pao.* Journal of Bacteriology, 1987. **169**(5): p. 1960-1966.

73. Gill, C.O. and J.R. Suisted, *Effects of Temperature and Growth-Rate on Proportion of Unsaturated Fatty-Acids in Bacterial Lipids.* Journal of General Microbiology, 1978. **104**(Jan): p. 31-36.

74. Hazeleger, W.C., et al., *Temperature-dependent membrane fatty acid and cell physiology changes in coccoid forms of Campylobacter jejuni.* Appl. Environ. Microbiol., 1995. **61**(7): p. 2713-2719.

75. Herrero, A.A. and R.F. Gomez, *Development of ethanol tolerance in Clostridium thermocellum: effect of growth temperature.* Appl Environ Microbiol, 1980. **40**(3): p. 571-7.

76. MacDonald, D.L. and H. Goldfine, *Effects of solvents and alcohols on the polar lipid composition of Clostridium butyricum under conditions of controlled lipid chain composition.* Appl. Environ. Microbiol., 1991. **57**(12): p. 3517-3521.

77. Suutari, M. and S. Laakso, *Changes in fatty acid branching and unsaturation of Streptomyces griseus and Brevibacterium fermentans as a response to growth temperature.* Appl. Environ. Microbiol., 1992. **58**(7): p. 2338-2340.

78. Suutari, M. and S. Laakso, *Unsaturated and Branched-Chain Fatty-Acids in Temperature Adaptation of Bacillus-Subtilis and Bacillus-Megaterium.* Biochimica Et Biophysica Acta, 1992. **1126**(2): p. 119-124.

79. Berberich, J.A., et al., *Product selectivity shifts in Clostridium thermocellum in the presence of compressed solvents.* Industrial & Engineering Chemistry Research, 2000. **39**(12): p. 4500-4505.

80. Bothun, G.D., et al., *Metabolic selectivity and growth of Clostridium thermocellum in continuous culture under elevated hydrostatic pressure.* Appl Microbiol Biotechnol, 2004. **65**(2): p. 149-57.

81. Tailliez, P., et al., *Cellulose Fermentation by an Asporogenous Mutant and an Ethanol-Tolerant Mutant of Clostridium-Thermocellum.* Applied and Environmental Microbiology, 1989. **55**(1): p. 203-206.

82. Tailliez, P., et al., *Enhanced Cellulose Fermentation by an Asporogenous and Ethanol-Tolerant Mutant of Clostridium-Thermocellum.* Applied and Environmental Microbiology, 1989. **55**(1): p. 207-211.

83. Johnston, N.C. and H. Goldfine, *Isolation and characterization of new phosphatidylglycerol acetals of plasmalogens: A family of ether lipids in clostridia.* European Journal of Biochemistry, 1994. **223**(3): p. 957-963.

84. Elsden, S.R., et al., *The Lipid Fatty-Acids of Proteolytic Clostridia.* Journal of General Microbiology, 1980. **118**(May): p. 115-123.

85. Berberich, J.A., et al., *Toxicity effects of compressed and supercritical solvents on thermophilic microbial metabolism.* Biotechnology and Bioengineering, 2000. **70**(5): p. 491-497.

86. Bothun, G.D., et al., *Molecular and phase toxicity of compressed and supercritical fluids in biphasic continuous cultures of Clostridium thermocellum.* Biotechnology and Bioengineering, 2005. **89**(1): p. 32-41.

87. Gutierrezruiz, M.C., et al., *Chronic and Acute Ethanol Treatment Modifies Fluidity and Composition in Plasma-Membranes of a Human Hepatic Cell-Line (Wrl-68).* Cell Biology and Toxicology, 1995. **11**(2): p. 69-78.

88. Kikukawa, T., et al., *Restricted motion of photoexcited bacteriorhodopsin in purple membrane containing ethanol.* Biophysical Journal, 1997. **73**(1): p. 357-366.

89. Jain, M.K. and L.V. Wray, *Partition coefficients of alkanols in lipid bilayer/water.* Biochemical Pharmacology, 1978. **27**(8): p. 1294-1295.

90. Denich, T.J., et al., *Effect of selected environmental and physico-chemical factors on bacterial cytoplasmic membranes.* J Microbiol Methods, 2003. **52**(2): p. 149-82.

91. Ingram, L.O., *Ethanol Tolerance in Bacteria.* Critical Reviews in Biotechnology, 1990. **9**(4): p. 305-319.

92. Cocco, T., et al., *Tissue-specific changes of mitochondrial functions in aged rats: Effect of a long-term dietary treatment with N-acetylcysteine.* Free Radical Biology and Medicine, 2005. **38**(6): p. 796-805.

93. Hicks, A.M., et al., *Unique molecular signatures of glycerophospholipid species in different rat tissues analyzed by tandem mass spectrometry.* Biochimica Et Biophysica Acta-Molecular and Cell Biology of Lipids, 2006. **1761**(9): p. 1022-1029.

94. Rossignol, R., et al., *Tissue variation in the control of oxidative phosphorylation: implication for mitochondrial diseases.* Biochemical Journal, 2000. **347**: p. 45-53.

95. Wood, R., G.C. Upreti, and R.J. Deantueno, *A Comparison of Lipids from Liver and Hepatoma Subcellular Membranes.* Lipids, 1986. **21**(4): p. 292-300.

96. Barzanti, V., et al., *Effect of Lipids Having Different N-6 and N-3 Fatty-Acid Contents on Some Organs and Subcellular Structures of the Rat.* Progress in Lipid Research, 1986. **25**: p. 221-224.

97. Postle, A.D., *Phospholipid lipidomics in health and disease.* European Journal of Lipid Science and Technology, 2009. **111**(1): p. 2-13.

98. Lohner, K., *Is the high propensity of ethanolamine plasmalogens to form non-lamellar lipid structures manifested in the properties of biomembranes?* Chemistry and Physics of Lipids, 1996. **81**(2): p. 167-184.

99. Reifschneider, N.H., et al., *Defining the mitochondrial proteomes from five rat organs in a physiologically significant context using 2D blue-native/SDS-PAGE.* Journal of Proteome Research, 2006. **5**(5): p. 1117-1132.

100. Kiebish, M.A., et al., *Brain mitochondrial lipid abnormalities in mice susceptible to spontaneous gliomas.* Lipids, 2008. **43**(10): p. 951-959.

101. Almeida, A.M., et al., *Mitochondrial DNA damage associated with lipid peroxidation of the mitochondrial membrane induced by Fe2+-citrate.* Anais Da Academia Brasileira De Ciencias, 2006. **78**(3): p. 505-514.

102. Lovell, M.A. and W.R. Markesbery, *Oxidative damage in mild cognitive impairment and early Alzhelimer's disease.* Journal of Neuroscience Research, 2007. **85**(14): p. 3036-3040.

103. Markesbery, W.R., *Oxidative stress hypothesis in Alzheimer's disease.* Free Radical Biology and Medicine, 1997. **23**(1): p. 134-147.

104. Perry, G., et al., *Is oxidative damage the fundamental pathogenic mechanism of Alzheimer's and other neurodegenerative diseases?* Free Radical Biology and Medicine, 2002. **33**(11): p. 1475-1479.

105. Wang, J., et al., *Increased oxidative damage in nuclear and mitochondrial DNA in Alzheimer's disease.* Journal of Neurochemistry, 2005. **93**(4): p. 953-962.

106. Polidori, M.C., et al., *Hallmarks of protein oxidative damage in neurodegenerative diseases: focus on Alzheimer's disease.* Amino Acids, 2007. **32**(4): p. 553-559.

107. Uchida, K., *4-Hydroxy-2-nonenal: a product and mediator of oxidative stress.* Progress in Lipid Research, 2003.

108. Watson, A.D., *Thematic review series: Systems Biology Approaches to Metabolic and Cardiovascular Disorders. Lipidomics: a global approach to lipid analysis in biological systems.* J. Lipid Res., 2006. **47**(10): p. 2101-2111.

109. Sims, N.R. and M.F. Anderson, *Isolation of mitochondria from rat brain using Percoll density gradient centrifugation.* Nature Protocols, 2008. **3**(7): p. 1228-1238.

110. Dunkley, P.R., et al., *A rapid method for isolation of synaptosomes on Percoll gradients.* Brain Research, 1986. **372**(1): p. 115-129.

111. Lai, J.C.K., et al., *Preparation of synaptic and nonsynaptic mitochondria from mammalian brain*, in *Methods in Enzymology*. 1979, Academic Press. p. 51-60.

112. Lai, J.C.K., et al., *Synaptic and Non-Synaptic Mitochondria from Rat-Brain - Isolation and Characterization.* Journal of Neurochemistry, 1977. **28**(3): p. 625-631.

113. Millar, A.H., et al., *Isolation and Subfractionation of Mitochondria from Plants*, in *Methods in Cell Biology*. 2007, Academic Press. p. 65-90.

114. Sims, N.R., *Rapid Isolation of Metabolically Active Mitochondria from Rat-Brain and Subregions Using Percoll Density Gradient Centrifugation.* Journal of Neurochemistry, 1990. **55**(2): p. 698-707.

115. Shao, C., et al., *Altered 8-oxoguanine glycosylase in mild cognitive impairment and late-stage Alzheimer's disease brain.* Free Radical Biology and Medicine, 2008. **45**(6): p. 813-819.

116. Montuschi, P., P.J. Barnes, and L.J. Roberts, II, *Isoprostanes: markers and mediators of oxidative stress.* FASEB J., 2004. **18**(15): p. 1791-1800.

117. Yin, H., E.S. Musiek, and J.D. Morrow, *Quantification of isoprostanes as an index of oxidative stress: a update.* Journal of Biological Sciences (Faisalabad, Pakistan), 2006. **6**(3): p. 469-479.

118. Reich, E.E., et al., *Formation of novel D-ring and E-ring isoprostane-like compounds (D4/E4-neuroprostanes) in vivo from docosahexaenoic acid.* Biochemistry, 2000. **39**(9): p. 2376-83.

119. Morrow, J.D., *The isoprostanes - unique products of arachidonate peroxidation: their role as mediators of oxidant stress.* Current Pharmaceutical Design, 2006. **12**(8): p. 895-902.

120. Reich, E.E., et al., *Brain regional quantification of F-ring and D-/E-ring isoprostanes and neuroprostanes in Alzheimer's disease.* Am J Pathol, 2001. **158**(1): p. 293-7.

121. Brosche, T. and D. Platt, *Mini-review - The biological significance of plasmalogens in defense against oxidative damage.* Experimental Gerontology, 1998. **33**(5): p. 363-369.

122. Engelmann, B., *Plasmalogens: targets for oxidants and major lipophilic antioxidants.* Biochemical Society Transactions, 2004. **32**: p. 147-150.

123. Maeba, R. and N. Ueta, *A novel antioxidant action of ethanolamine plasmalogens in lowering the oxidizability of membranes.* Biochemical Society Transactions, 2004. **32**: p. 141-143.

124. Mitchell, T.W., R. Buffenstein, and A.J. Hulbert, *Membrane phospholipid composition may contribute to exceptional longevity of the naked mole-rat (Heterocephalus glaber): A comparative study using shotgun lipidomics.* Experimental Gerontology, 2007. **42**(11): p. 1053-1062.

125. Pamplona, R., et al., *Low fatty acid unsaturation protects against lipid peroxidation in liver mitochondria from long-lived species: The pigeon and human case.* Mechanisms of Ageing and Development, 1996. **86**(1): p. 53-66.

126. Tahin, Q.S., M. Blum, and E. Carafoli, *The Fatty Acid Composition of Subcellular Membranes of Rat Liver, Heart, and Brain: Diet-Induced Modifications.* European Journal of Biochemistry, 1981. **121**(1): p. 5-13.

127. Valianpour, F., et al., *Quantitative and Compositional Study of Cardiolipin in Platelets by Electrospray Ionization Mass Spectrometry: Application for the Identification of Barth Syndrome Patients.* Clin Chem, 2002. **48**(9): p. 1390-1397.

128. Kiebish, M.A., et al., *Lipidomic analysis and electron transport chain activities in C57BL/6J mouse brain mitochondria.* Journal of Neurochemistry, 2008. **106**(1): p. 299-312.

129. Adibhatla, R.M., J.F. Hatcher, and R.J. Dempsey, *Lipids and lipidomics in brain injury and diseases.* Aaps Journal, 2006. **8**(2): p. E314-E321.

130. Hoffman, D.R., et al., *Docosahexaenoic acid in red blood cells of term infants receiving two levels of long-chain polyunsaturated fatty acids.* J Pediatr Gastroenterol Nutr, 2006. **42**(3): p. 287-92.

131. Musiek, E.S., et al., *Quantification of F-ring isoprostane-like compounds (F4-neuroprostanes) derived from docosahexaenoic acid in vivo in humans by a stable isotope dilution mass spectrometric assay.* J Chromatogr B Analyt Technol Biomed Life Sci, 2004. **799**(1): p. 95-102.

132. Roberts, L.J., 2nd, et al., *Formation of isoprostane-like compounds (neuroprostanes) in vivo from docosahexaenoic acid.* J Biol Chem, 1998. **273**(22): p. 13605-12.

133. Gorgas, K., et al., *The ether lipid-deficient mouse: Tracking down plasmalogen functions.* Biochimica et Biophysica Acta (BBA) - Molecular Cell Research, 2006. **1763**(12): p. 1511-1526.

134. Kuczynski, B. and N.V. Reo, *Evidence that plasmalogen is protective against oxidative stress in the rat brain.* Neurochemical Research, 2006. **31**(5): p. 639-656.

135. Stadelmann-Ingrand, S., R. Pontcharraud, and B. Fauconneau, *Evidence for the reactivity of fatty aldehydes released from oxidized plasmalogens with phosphatidylethanolamine to form Schiff base adducts in rat brain homogenates.* Chemistry and Physics of Lipids, 2004. **131**(1): p. 93-105.

136. Brites, P., H.R. Waterham, and R.J.A. Wanders, *Functions and biosynthesis of plasmalogens in health and disease.* Biochimica et Biophysica Acta (BBA) - Molecular and Cell Biology of Lipids, 2004. **1636**(2-3): p. 219-231.

137. Byrdwell, W.C., *Atmospheric pressure chemical ionization mass spectrometry for analysis of lipids.* Lipids, 2001. **36**(4): p. 327-346.

138. Timmons, M.D., et al., *Analysis of composition and structure of Clostridium thermocellum membranes from wild-type and ethanol-adapted strains.* Appl Microbiol Biotechnol, 2009. **82**(5): p. 929-39.

139. Cuzner, M.L., A.N. Davison, and N.A. Gregson, *Turnover of Brain Mitochondrial Membrane Lipids.* Biochemical Journal, 1966. **101**(3): p. 618-&.

140. Prasad, M.R., et al., *Regional membrane phospholipid alterations in Alzheimer's disease.* Neurochemical Research, 1998. **23**(1): p. 81-88.

141. Finkel, T. and N.J. Holbrook, *Oxidants, oxidative stress and the biology of ageing.* Nature, 2000. **408**(6809): p. 239-247.

142. Anandatheerthavarada, H.K. and L. Devi, *Amyloid Precursor Protein and Mitochondrial Dysfunction in Alzheimer's Disease.* Neuroscientist, 2007. **13**(6): p. 626-638.

143. Ginsberg, L., J.H. Xuereb, and N.L. Gershfeld, *Membrane instability, plasmalogen content, and Alzheimer's disease.* Journal of Neurochemistry, 1998. **70**(6): p. 2533-2538.

144. Montine, T.J. and J.D. Morrow, *Fatty acid oxidation in the pathogenesis of Alzheimer's disease.* Am J Pathol, 2005. **166**(5): p. 1283-9.

145. Youssef, J.A., et al., *Age-independent, gray matter-localized, brain-enhanced oxidative stress in male fischer 344 rats: brain levels of F2-isoprostanes and F4-neuroprostanes.* Free Radical Biology and Medicine, 2003. **34**(12): p. 1631.

146. Stadelmann-Ingrand, S., et al., *Plasmalogen degradation by oxidative stress: production and disappearance of specific fatty aldehydes and fatty [alpha]-hydroxyaldehydes.* Free Radical Biology and Medicine, 2001. **31**(10): p. 1263-1271.

147. Folstein, M.F., S.E. Folstein, and P.R. McHugh, *"Mini-mental state" : A practical method for grading the cognitive state of patients for the clinician.* Journal of Psychiatric Research, 1975. **12**(3): p. 189-198.

148. Yaari, R. and J. Corey-Bloom, *Alzheimer's disease.* Seminars in Neurology, 2007. **27**(1): p. 32-41.

149. Braak, H. and E. Braak, *Neuropathological Staging of Alzheimer-Related Changes.* Acta Neuropathologica, 1991. **82**(4): p. 239-259.

150. Priller, C., et al., *Synapse Formation and Function Is Modulated by the Amyloid Precursor Protein.* J. Neurosci., 2006. **26**(27): p. 7212-7221.

151. Marieb, E.N., *Human Anatomy & Physiology*. 4th ed. 1998: Benjamin/Cummings.

152. Clower, D.M., et al., *The Inferior Parietal Lobule Is the Target of Output from the Superior Colliculus, Hippocampus, and Cerebellum.* J. Neurosci., 2001. **21**(16): p. 6283-6291.

153. Bradley, M.A., W.R. Markesbery, and M.A. Lovell, *Increased levels of 4-hydroxynonenal and acrolein in the brain in preclinical Alzheimer disease.* Free Radical Biology and Medicine, 2010. **48**(12): p. 1570-1576.

154. Dalfo, E.P., et al., *Evidence of Oxidative Stress in the Neocortex in Incidental Lewy Body Disease.* Journal of Neuropathology & Experimental Neurology, 2005. **64**(9): p. 816-830.

155. Kalaitzakis, M.E., R.K.B. Pearce, and S.M. Gentleman, *Clinical correlates of pathology in the claustrum in Parkinson's disease and dementia with Lewy bodies.* Neuroscience Letters, 2009. **461**(1): p. 12-15.

156. Noguchi-Shinohara, M., et al., *CSF [alpha]-synuclein levels in dementia with Lewy bodies and Alzheimer's disease.* Brain Research, 2009. **1251**: p. 1-6.

157. Öhrfelt, A., et al., *Cerebrospinal fluid [alpha]-synuclein in neurodegenerative disorders--A marker of synapse loss?* Neuroscience Letters, 2009. **450**(3): p. 332-335.

158. Fessel, J.P., et al., *Isofurans, but not F2-isoprostanes, are increased in the substantia nigra of patients with Parkinson's disease and with dementia with Lewy body disease.* J Neurochem, 2003. **85**(3): p. 645-50.

159. Parnetti, L., et al., *Cerebrospinal fluid biomarkers in Parkinson's disease with dementia and dementia with Lewy bodies.* Biol Psychiatry, 2008. **64**(10): p. 850-5.

160. Anderson, M.F. and N.R. Sims, *Improved recovery of highly enriched mitochondrial fractions from small brain tissue samples.* Brain Research Protocols, 2000. **5**(1): p. 95-101.

161. Pallotti, F. and G. Lenaz, *Isolation and Subfractionation of Mitochondria from Animal Cells and Tissue Culture Lines*. Methods in Cell Biology. Vol. 80. 2007: Elsevier Inc.

162. Musiek, E.S., et al., *Cyclopentenone isoprostanes are novel bioactive products of lipid oxidation which enhance neurodegeneration.* Journal of Neurochemistry, 2006. **97**(5): p. 1301-1313.

163. Schlame, M. and D. Haldar, *Cardiolipin is synthesized on the matrix side of the inner membrane in rat liver mitochondria.* Journal of Biological Chemistry, 1993. **268**(1): p. 74-79.

164. Schlame, M. and K.Y. Hostetler, *Cardiolipin synthase from mammalian mitochondria.* Biochimica et Biophysica Acta (BBA) - Lipids and Lipid Metabolism, 1997. **1348**(1-2): p. 207-213.

165. Schlame, M. and M. Ren, *The role of cardiolipin in the structural organization of mitochondrial membranes.* Biochimica et Biophysica Acta (BBA) - Biomembranes, 2009. **1788**(10): p. 2080-2083.

166. Schlame, M., D. Rua, and M.L. Greenberg, *The biosynthesis and functional role of cardiolipin.* Progress in Lipid Research, 2000. **39**(3): p. 257-288.

167. Xu, Y., et al., *Remodeling of Cardiolipin by Phospholipid Transacylation.* Journal of Biological Chemistry, 2003. **278**(51): p. 51380-51385.

168. Gohil, V.M., et al., *Cardiolipin Biosynthesis and Mitochondrial Respiratory Chain Function Are Interdependent.* Journal of Biological Chemistry, 2004. **279**(41): p. 42612-42618.

169. Kiebish, M.A., et al., *Cardiolipin and electron transport chain abnormalities in mouse brain tumor mitochondria: lipidomic evidence supporting the Warburg theory of cancer.* J. Lipid Res., 2008. **49**(12): p. 2545-2556.

170. Sen, T., et al., *Lipid peroxidation associated cardiolipin loss and membrane depolarization in rat brain mitochondria.* Neurochemistry International, 2006. **49**(1): p. 20-27.

171. Humeau, Y., et al., *A role for phospholipase D1 in neurotransmitter release.* Proceedings of the National Academy of Sciences of the United States of America, 2001. **98**(26): p. 15300-15305.

172. Jin, J.K., et al., *Phospholipase D1 is associated with amyloid precursor protein in Alzheimer's disease.* Neurobiology of Aging, 2007. **28**(7): p. 1015-1027.

173. Jin, J.K., et al., *Phospholipase D1 is up-regulated in the mitochondrial fraction from the brains of Alzheimer's disease patients.* Neuroscience Letters, 2006. **407**(3): p. 263-267.

174. Kim, J.H., et al., *Selective activation of phospholipase D-2 by unsaturated fatty acid.* Febs Letters, 1999. **454**(1-2): p. 42-46.

175. Cai, D.M., et al., *Presenilin-1 uses phospholipase D1 as a negative regulator of beta-amyloid formation.* Proceedings of the National Academy of Sciences of the United States of America, 2006. **103**(6): p. 1941-1946.

176. Morandat, S., et al., *Plasmalogens protect unsaturated lipids against UV-induced oxidation in monolayer.* Biochimica et Biophysica Acta (BBA) - Biomembranes, 2003. **1616**(2): p. 137-146.

177. Spiteller, G., *Peroxyl radicals: Inductors of neurodegenerative and other inflammatory diseases. Their origin and how they transform cholesterol, phospholipids, plasmalogens, polyunsaturated fatty acids, sugars, and proteins into deleterious products.* Free Radical Biology and Medicine, 2006. **41**(3): p. 362-387.

178. Fam, S.S., et al., *Formation of Highly Reactive A-ring and J-ring Isoprostane-like Compounds (A4/J4-neuroprostanes) in Vivo from Docosahexaenoic Acid.* J. Biol. Chem., 2002. **277**(39): p. 36076-36084.

179. Brosche, T., *Plasmalogen phospholipids - Facts and theses to their antioxidative qualities.* Archives of Gerontology and Geriatrics, 1997. **25**(1): p. 73-81.

180. Woods, A.S. and S.N. Jackson, *Brain tissue lipidomics: Direct probing using matrix-assisted laser desorption/ionization mass spectrometry.* Aaps Journal, 2006. **8**(2): p. E391-E395.

181. Quan, L.G. and J.K. Cha, *Preparation of Isoprostanes and Neuroprostanes.* J. Am. Chem. Soc., 2002. **124**(42): p. 12424-12425.

182. Quan, L.G. and J.K. Cha, *Recent advances in the stereoselective synthesis of isoprostanes and neuroprostanes.* Chemistry and Physics of Lipids, 2004. **128**(1-2): p. 3.

183. Taber, D.F. and L. Jackson Roberts Ii, *Nomenclature systems for the neuroprostanes and for the neurofurans.* Prostaglandins &Other Lipid Mediators, 2005. **78**(1-4): p. 14.

184. Yin, H., et al., *Regiochemistry of Neuroprostanes Generated from the Peroxidation of Docosahexaenoic Acid in Vitro and in Vivo.* J. Biol. Chem., 2005. **280**(28): p. 26600-26611.

185. Greco, A. and L. Minghetti, *Isoprostanes as biomarkers and mediators of oxidative injury in infant and adult central nervous system diseases.* Curr Neurovasc Res, 2004. **1**(4): p. 341-54.

186. Lindblom, G. and L. Rilfors, *Nonlamellar Phases Formed by Membrane-Lipids.* Advances in Colloid and Interface Science, 1992. **41**: p. 101-125.

187. Khuller, G.K. and H. Goldfine, *Phospholipids of Clostridium-Butyricum .5. Effects of Growth Temperature on Fatty-Acid, Alk-1-Enyl Ether Group, and Phospholipid Composition.* Journal of Lipid Research, 1974. **15**(5): p. 500-507.

188. Konopasek, I., K. Strzalka, and J. Svobodova, *Cold shock in Bacillus subtilis: different effects of benzyl alcohol and ethanol on the membrane organisation and cell adaptation.* Biochimica et Biophysica Acta (BBA) - Biomembranes, 2000. **1464**(1): p. 18-26.

189. Mangelsdorf, K., et al., *A quantitative assessment of pressure dependent adaptive changes in the membrane lipids of piezosensitive deep sub-seafloor bacterium.* Organic Geochemistry, 2005. **36**(11): p. 1459-1479.

190. Knutson, B.L., et al., *Effect of pressurized solvents on ethanol production by the thermophilic bacterium Clostridium thermocellum.* Journal of Supercritical Fluids, 1999. **16**(2): p. 149-156.

191. Fu, Y.J., et al., *Quantitative proteomic analysis of mitochondria in aging PS-1 transgenic mice.* Cell Mol Neurobiol, 2009. **29**(5): p. 649-64.

192. Lynn, B.C., et al., *Quantitative Changes in the Mitochondrial Proteome from Subjects with Mild Cognitive Impairment, Early Stage, and Late Stage Alzheimer's Disease.* J Alzheimers Dis, 2009.

193. Lynn, B.C., et al., *Quantitative changes in the mitochondrial proteome from subjects with mild cognitive impairment, early stage, and late stage Alzheimer's disease.* J Alzheimers Dis, 2010. **19**(1): p. 325-39.

194. Birch-Machin, M.A., D.M. Turnbull, and E.A.S. Liza A. Pon, *Chapter 5 Assaying mitochondrial respiratory complex activity in mitochondria isolated from human cells and tissues*, in *Methods in Cell Biology*. 2001, Academic Press. p. 97-117.

195. Chretien, D., et al., *Assay of mitochondrial respiratory chain complex I in human lymphocytes and cultured skin fibroblasts.* Biochemical and Biophysical Research Communications, 2003. **301**(1): p. 222-224.

196. Kiebish, M.A., et al., *In vitro growth environment produces lipidomic and electron transport chain abnormalities in mitochondria from non-tumorigenic astrocytes and brain tumours.* ASN NEURO, 2009. **1**(3): p. e00011.

197. Cowell, C.F., et al., *Mitochondrial diacylglycerol initiates protein-kinase-D1-mediated ROS signaling.* Journal of Cell Science, 2009. **122**(7): p. 919-928.

198. Ruggiero, F.M., et al., *Lipid-Composition in Synaptic and Nonsynaptic Mitochondria from Rat Brains and Effect of Aging.* Journal of Neurochemistry, 1992. **59**(2): p. 487-491.

199. Alikhani, N., M. Ankarcrona, and E. Glaser, *Mitochondria and Alzheimer's disease: amyloid-beta peptide uptake and degradation by the presequence protease, hPreP.* J Bioenerg Biomembr, 2009. **41**(5): p. 447-51.

200. Geddes, J.W. and P.G. Sullivan, *Special Issue: Mitochondria and neurodegeneration.* Experimental Neurology, 2009. **218**(2): p. 169-170.

201. Kim, H., et al., *Differential expression of phospholipases D1 and D2 in mouse tissues.* Cell Biology International, 2007. **31**(2): p. 148-155.

202. Whitehouse, C.M., et al., *Electrospray Interface for Liquid Chromatographs and Mass Spectrometers.* Analytical Chemistry, 1985. **57**(3): p. 675-679.

203. Yamashita, M. and J.B. Fenn, *Electrospray Ion-Source - Another Variation on the Free-Jet Theme.* Journal of Physical Chemistry, 1984. **88**(20): p. 4451-4459.

204. Folch, J., M. Lees, and G.H.S. Stanley, *A Simple Method For The Isolation and Purification of Total Lipides From Animal Tissues.* J. Biol. Chem., 1957. **226**(1): p. 497-509.

205. Buyukpamukcu, E., et al., *Analysis of phospholipids using electrospray ionisation tandem mass spectrometry.* Lipid Technology, 2007. **19**(6): p. 136-138.

206. Jackson, S.N., et al., *A Study of Phospholipids by Ion Mobility TOFMS.* Journal of the American Society for Mass Spectrometry, 2008. **19**(11): p. 1655-1662.

207. Pulfer, M. and R.C. Murphy, *Electrospray mass spectrometry of phospholipids.* Mass Spectrometry Reviews, 2003. **22**(5): p. 332-364.

208. Vernooij, E.A.A.M., et al., *RP-hPLC/ESI MS determination of acyl chain positions in phospholipids.* Journal of Separation Science, 2002. **25**(5-6): p. 285-289.

209. Mawatari, S., Y. Okuma, and T. Fujino, *Separation of intact plasmalogens and all other phospholipids by a single run of high-performance liquid chromatography.* Analytical Biochemistry, 2007. **370**(1): p. 54-59.

210. Simakova, O. and N.J. Arispe, *The Cell-Selective Neurotoxicity of the Alzheimer's A Peptide Is Determined by Surface Phosphatidylserine and Cytosolic ATP Levels. Membrane Binding Is Required for A Toxicity.* J. Neurosci., 2007. **27**(50): p. 13719-13729.

211. Zhao, H., E.K.J. Tuominen, and P.K.J. Kinnunen, *Formation of Amyloid Fibers Triggered by Phosphatidylserine-Containing Membranes†.* Biochemistry, 2004. **43**(32): p. 10302-10307.

212. Greenawalt, J.W., F. Sidney, and P. Lester, *[30] The isolation of outer and inner mitochondrial membranes*, in *Methods in Enzymology*. 1974, Academic Press. p. 310-323.

213. Fahy, E., et al., *A comprehensive classification system for lipids.* J. Lipid Res., 2005. **46**(5): p. 839-862.

214. Oresic, M., *Bioinformatics and computational approaches applicable to lipidomics.* European Journal of Lipid Science and Technology, 2009. **111**(1): p. 99-106.

215.   Piomelli, D., G. Astarita, and R. Rapaka, *A neuroscientist's guide to lipidomics.* Nature Reviews Neuroscience, 2007. **8**(10): p. 743-754.
216.   Van Meer, G., *Cellular Lipidomics.* The EMBO Journal, 2005. **24**: p. 3159-3165.
217.   Vidal, M., *A Biological Atlas of Functional Maps.* Cell, 2001. **104**(3): p. 333-339.

VITA

The author was born in Rockford, IL on July 10, 1973. He graduated from Terre Haute North Vigo High School in May of 1991. He enrolled at Western Kentucky University, where he double majored in recombinant genetics and chemistry. He graduated with a B.S. from Western Kentucky University in May 1996. He then enrolled in the graduate program for chemistry at Western Kentucky University in August of 1991 under the study of Dr. Don Slocum. While enrolled at in the graduate program he studied the directed ortho-metalation of dimethylarylamines. He graduated with a M.S. from Western Kentucky University in May 2002. Upon graduation Michael soon began working at Martek Biosciences in Winchester, KY. Following a brief stint in industry, Michael enrolled in the graduate program for chemistry at the University of Kentucky under the study of Dr. Bert Lynn. While enrolled at UK, Michael married Jilliann Marissa Wiese whom he meant while working at Martek Biosciences. He is a member of the American Chemical Society (ACS), American Oil Chemists Society (AOCS) and American Society for Mass Spectrometry (ASMS).

Presentations:

Lipidomic analysis of neurological mitochondria isolated from various lobes as a function of Alzheimer's disease progression. Michael D. Timmons; Melissa A. Bradley; Mark A. Lovell; Bert C. Lynn, 58th ASMS Conference on Mass Spectrometry, Salt Lake City, UT, May 23-27, 2010, Section MP; Lipids I, poster 282.

Changes in the Mitochondrial Lipidome as a Function of Alzheimer's Disease Progression. Michael D. Timmons; Melissa Bradley; Jianquan Wang; Mark A. Lovell; Bert C. Lynn, 57th ASMS Conference on Mass Spectrometry, Philadelphia, PA, May 30-June 4, 2009, Section MPI; Lipids: Biochem & Steroid, poster 225.

Lipidomic Analysis and Comparison of Mitochondrial and Plasma Membrane Fatty Acid Profiles Isolated From Various Tissues. Michael D. Timmons; Shuling Xiong; Mark A. Lovell; Bert C. Lynn, 56th ASMS Conference on Mass Spectrometry, Denver, CO, June 1-5, 2008, Section TPHH; Lipids, poster 223.

Lipid Composition Comparison and Structural Analysis from *Clostridium thermocellum* Wild-type and Ethanol-adapted Strains. Michael D. Timmons; Herbert J. Strobel; Barbara L. Knutson; Sue E. Nokes; Bert C. Lynn, 55th ASMS Conference on Mass Spectrometry, Indianapolis, IN, June 3-7, 2007, Section WPZ; Lipids, poster 422.

Publications:

Method for the Isolation of Mitochondria from Neuronal Tissue. Timmons, M. D., Bradley, M. A., Lovell, M. A., Lynn, B. C. In Preparation (2010).

Comparison of rat mitochondrial fatty acid profiles isolated from various tissues. Timmons, M. D., Bradley, M. A., Lovell, M. A., Lynn, B. C. Submitted (2010).

Analysis of composition and structure of *Clostridium thermocellum* membranes from wild-type and ethanol-adapted strains. Timmons, M. D., Knutson, B. L., Nokes, S. E., Strobel, H. J., Lynn, B. C. Appl. Microbiol. Biotechnol. (2009), 82, 929-939.